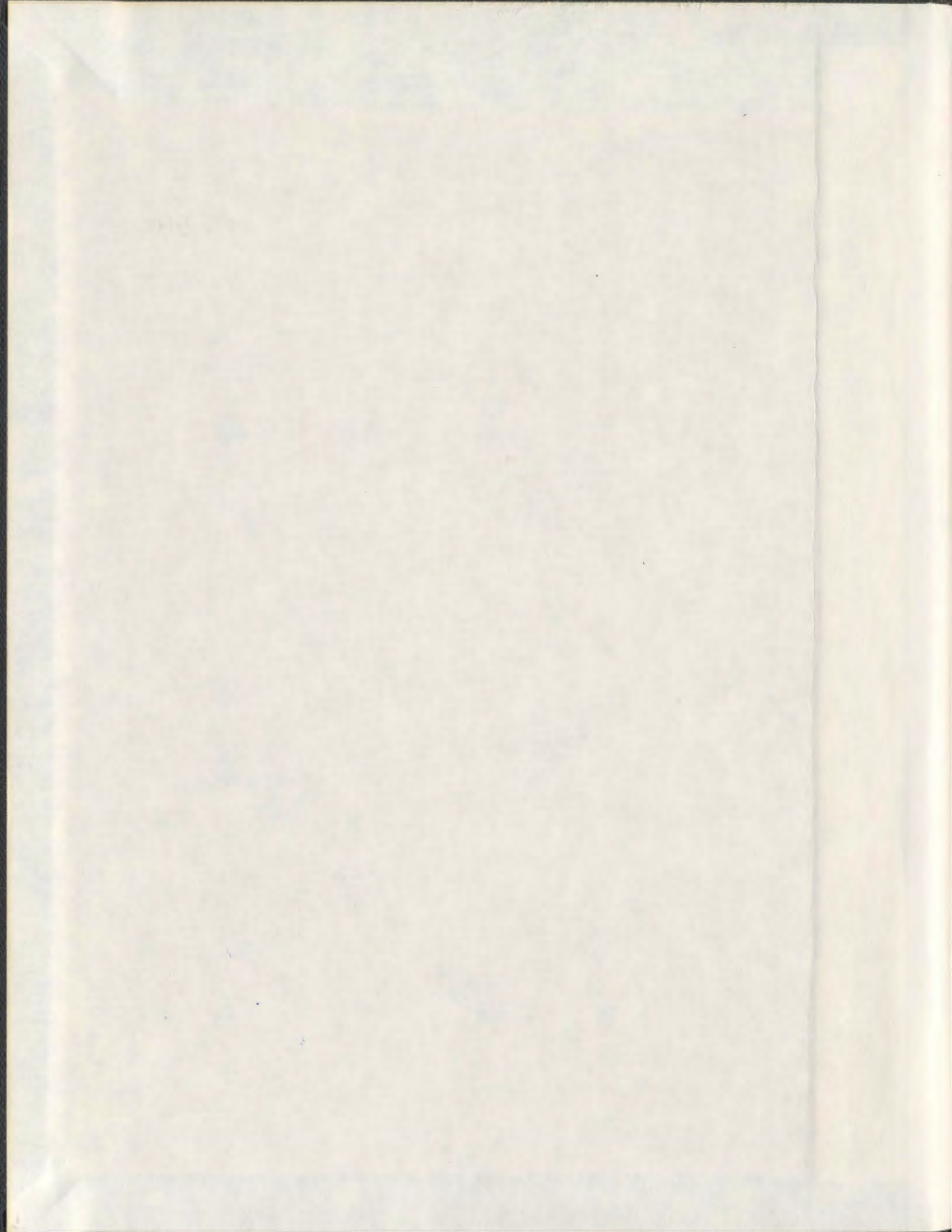
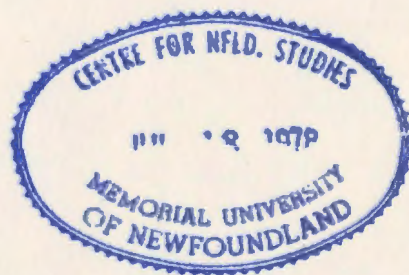


PERFORMANCE STUDY OF PODED PROPULSORS
WITH VARIED GEOMETRY AND AZIMUTHING CONDITIONS

MOHAMMED FAKHRUL ISLAM



001311



Performance Study of Podded Propulsors with Varied Geometry and Azimuthing Conditions

By

© Mohammed Fakhrol Islam, B. Eng., B. Sc., M. Eng.

**A thesis submitted to the School of Graduate Studies in
partial fulfilment of the requirements for the degree of
Doctor of Philosophy**

**Ocean and Naval Architectural Engineering
Faculty of Engineering & Applied Science
Memorial University of Newfoundland**

March 2009

St. John's

Newfoundland

Canada

Abstract

The current research investigates the performance of podded propulsors with varied geometry at different azimuthing conditions for pusher and puller configurations in open water.

In order to determine the prominent geometric parameters and to establish their effects on the hydrodynamic performance, the first part of the research concentrated on the geometry of pusher- and puller-podded propulsors. This experimental study consisted of investigating five geometrical parameters and their effects on propeller thrust, torque and efficiency, unit thrust and efficiency of podded propulsors. The work used a factorial design (a design of experiment technique) and analysis approach to study these effects.

The second part of the research focussed on the hydrodynamic properties of the podded propulsors in static and dynamic azimuthing conditions. This study implemented two investigations using two separate experimental apparatus. In the first investigation, two podded propulsors were tested to measure the forces and moments on the propeller and on the unit at different static azimuthing angles within the range of -30° to 30° . In the second investigation, a separate dynamometer system was used to measure forces and moments of a model pod unit at different static and dynamic azimuthing conditions within the range of 0° to 360° . An additional study evaluated the effects of azimuthing

rate and propeller shaft speed on the performance parameters under consideration at dynamic azimuthing conditions.

The study of pods with varied geometry showed that the geometric parameters have noticeable effect on propulsive characteristics of the propulsor. The analysis provided valuable information to the podded propulsor designers. In static azimuthing conditions in the range of $+30^\circ$ to -30° , the propeller and unit performance coefficients changed with the change of propeller loading and azimuthing angles. In the dynamic azimuthing study, the coefficients of the propeller and the pod unit showed a strong dependence on the propeller loading and azimuthing angle. Further, these results can be used as a base for validation of numerical modelling.

The uncertainty analysis of the measurements provided strong evidence that the presented results revealed the true performance characteristics of the model scale podded propulsors under consideration.

Acknowledgements

The author extends his gratitude to his supervisor and mentor, Dr. Brian Veitch for the opportunity to pursue this research, the wisdom and guidance of whom made this thesis possible. I will never forget his encouragement, understanding and support during the course of my Ph.D. Thanks are extended to the co-supervisors: Dr. Pengfei Liu, Dr. Neil Bose and Dr. Ayhan Akinturk for their patient support and guidance. Their leadership and mentorship have been very much appreciated.

I am grateful to the members of the PhD Examination board, Professors William B. Morgan and Mahmoud R. Haddara and Dr. Dan Walker, for their instructions and comments on my thesis. I found their comments extremely constructive and useful, which certainly upgrade the academic standard of the thesis.

I also wish to thank the Institute of Ocean Technology of the National Research Council for providing much needed workspace, equipment, and technical services to take this research work from idea to implementation. I also thank the staff in IOT for their sincere cooperation and cordiality throughout my stay there.

Financial support from the Natural Sciences and Engineering Research Council (NSERC) Canada, the National Research Council (NRC), Oceanic Consulting Corp., Thordon Bearings Inc., and Memorial University is greatly appreciated.

Acknowledgements

Special thanks to Andrew MacNeill of Oceanic Consulting Corp. for designing the NSERC dynamometer system and helping with the set-up. Thanks are also extended to Jim Gosse and other technical service staff of Memorial University.

Finally, I would like to dedicate this thesis to my parents, brothers and sister for their love, patience, encouragement and moral support throughout my life. I am deeply indebted to my sister, Nasreen, for her endless love and continual moral support. My friends are also thanked for their moral support and encouragement.

Table of Contents

Abstract	ii
Acknowledgements	iv
Table of Contents	vi
List of Tables	x
List of Figures	xiv
Nomenclature	xxi
Chapter 1: Introduction	1
1.1 Chapter Objectives	2
1.2 Background and Motivation	2
1.3 Scope of the Research	5
1.4 Literature Review on Pods	8
<i>1.4.1 Study on Pod Technology</i>	<i>8</i>
<i>1.4.2 Study on Pod Geometry</i>	<i>12</i>
<i>1.4.3 Study of Pod in Azimuthing Conditions</i>	<i>14</i>
1.5 Layout of thesis	21
Chapter 2: Methods, Models and Instruments	24
2.1 Chapter Objectives	25
2.2 Methods	25
<i>2.2.1 DOE Methodology to Study Pod Geometry</i>	<i>26</i>

2.2.2	<i>Physical Model Tests</i>	30
2.3	Propeller and Pod Models	34
2.3.1	<i>Propeller Geometry</i>	34
2.3.2	<i>Pod Geometry</i>	36
2.4	Experimental Set-up	40
2.4.1	<i>NSERC Pod Dynamometer System</i>	40
2.4.2	<i>IOT Pod Dynamometer System</i>	44
2.5	Experimental Facilities	46
2.6	Coordinate System	49
2.7	Data Reduction Equations	50
2.8	Study of <i>Reynolds Number</i> Effects	52
2.9	Summary	57
3	Uncertainty Analysis	58
3.1	Chapter Objectives	59
3.2	Components of Measurement Uncertainty	59
3.2.1	<i>Bias Error</i>	60
3.2.2	<i>Precision Error</i>	61
3.3	The Uncertainty Expressions	63
3.3.1	<i>Uncertainty in the Six-Component Global Dynamometer</i>	65
3.4	Uncertainty Estimates for NSERC Pod Measurements	70
3.5	Uncertainty Estimates for IOT Pod Measurements	73
3.6	Discussion on Uncertainty	76
3.7	Summary	78
Chapter 4:	Study of Pod with Varied Geometry	80

4.1 Chapter Objectives	81
4.2 Test Results	81
<i>4.2.1 Pod Series in Puller Configurations</i>	81
<i>4.2.2 Pod Series in Pusher Configurations</i>	86
4.3 DOE Analyses and Discussions	91
<i>4.3.1 Discussion on Puller Configuration</i>	92
<i>4.4.2 Discussion on Pusher Configuration</i>	99
4.5 Summary	106
Chapter 5: Study of Pod at Static Azimuthing Conditions	108
5.1 Chapter Objectives	109
5.2 Test Results	109
<i>5.2.1 Puller Configuration</i>	110
<i>5.2.2 Pusher Configuration</i>	117
5.3 Discussion on Effects of Static Azimuthing Angles	123
<i>5.3.1 Propeller Shaft Local Thrust and Torque Coefficients</i>	127
<i>5.3.2 Unit Thrust Coefficients</i>	132
<i>5.3.3 Transverse Force Coefficients</i>	136
<i>5.3.4 Vertical Force Coefficients</i>	138
<i>5.3.5 Axial Moment Coefficients</i>	140
<i>5.3.6 Transverse Moment Coefficients</i>	141
<i>5.3.7 Steering Moment Coefficients</i>	143
5.4 Summary	146
Chapter 6: Study of pod at dynamic azimuthing	147

conditions	
6.1 Chapter Objectives	148
6.2 Static Azimuthing Conditions	148
6.2.1 <i>Propeller Thrust and Torque</i>	149
6.2.2 <i>Unit Forces and Moments</i>	152
6.3 Dynamic Azimuthing Conditions	161
6.3.1 <i>Effects of Dynamic Azimuthing</i>	163
6.3.2 <i>Effects of Azimuthing Rate</i>	170
6.3.3 <i>Effects of Propeller Shaft rps</i>	174
6.4 Summary	178
Chapter 7: Conclusions	179
7.1 Chapter Objectives	180
7.2 Summary of the Objectives	180
7.3 Summary of the Results	182
7.3.1 <i>Pods with Varied Geometry</i>	182
7.3.2 <i>Pods at Static Azimuthing Conditions</i>	185
7.3.3 <i>Pods at Dynamic Azimuthing Conditions</i>	189
7.3.4 <i>Uncertainty Analysis</i>	193
7.4 Main Findings	194
7.5 Recommendations for Further Study	196
References	199
Appendix A: Data Tables	210
Appendix B: Uncertainty Data	230
Appendix C: DOE Technique	241

List of Tables

Table 1.1: Interaction coefficients for the Roddy Pods (Karafiath & Lyons, 1998).	13
Table 2.1: Series and average design of podded propulsors (Molloy, 2003).	28
Table 2.2: Test matrix for systematic geometric pod series tests.	31
Table 2.3: Test matrix for systematic static azimuthing podded propulsors' tests.	32
Table 2.4: Test matrix for systematic dynamic azimuthing podded propulsors' tests.	34
Table 2.5: Basic geometric particulars of the model propellers.	35
Table 2.6: Combinations of dimensions of the 16 pods in the series.	37
Table 2.7: Geometric particulars of the two average pod models.	38
Table 2.8: Propeller and pod dimensions used in dynamic azimuthing study.	39
Table 2.9: Particulars of the (OERC) MUN towing tank.	47
Table 2.10: Particulars of the IOT towing tank.	48
Table 2.11: Data reduction equations and definitions of different parameters used to present the experimental data.	51
Table 2.12: A List of <i>Reynolds Number</i> and the operating condition used to study the <i>Reynolds Number</i> effects for propeller only cases.	53
Table 3.1: Overall uncertainty estimates for podded propulsor variables (NSERC pod).	70
Table 3.2: Overall uncertainties in advance coefficients, propeller thrust and torque coefficients and unit thrust coefficients (NSERC pod).	71
Table 3.3: Overall uncertainties in global forces and moments in the three orthogonal directions for the podded propulsors (NSERC pod).	71
Table 3.4: Overall uncertainty estimates for podded propulsor variables (IOT pod).	73
Table 3.5: Overall uncertainties in advance coefficients, propeller thrust and torque coefficients and unit thrust coefficients (IOT pod).	74
Table 3.6: Overall uncertainties in global forces and moments in the three orthogonal directions for the podded propulsors (IOT pod).	74

List of Tables

<p>Table 4.1: Fractional factorial design results: List of significant factors and interaction of factors for puller propulsors. Here, A is the ratio of pod diameter to propeller diameter, D_{Pod}/D_{Prop}, B is the ratio of pod length to propeller diameter, L_{Pod}/D_{Prop}, C is the ratio of pod taper length to propeller diameter, TL/D_{Prop}, D is the ratio of strut distance to propeller diameter, S_{Dist}/D_{Prop}, and E is the propeller hub taper angle, H_{Angle}.</p>	93
<p>Table 4.2: Fractional factorial design results: List of significant factors and interaction of factors for pusher propulsors. Here, A is the ratio of pod diameter to propeller diameter, D_{Pod}/D_{Prop}, B is the ratio of pod length to propeller diameter, L_{Pod}/D_{Prop}, C is the ratio of pod taper length to propeller diameter, TL/D_{Prop}, D is the ratio of strut distance to propeller diameter, S_{Dist}/D_{Prop}, and E is the propeller hub taper angle, H_{Angle}.</p>	101
<p>Table A.1: Pod series data in straight-ahead puller configuration: propeller thrust coefficient, K_{Tprop}.</p>	211
<p>Table A.2 : Pod series data in straight-ahead puller configuration: propeller torque coefficient, $10K_Q$.</p>	211
<p>Table A-3: Pod series data in straight-ahead puller configuration: propulsor (unit) thrust coefficient, K_{Tunit}.</p>	212
<p>Table A.4: Pod series data in straight-ahead pusher configuration: propeller thrust coefficient, K_{Tprop}.</p>	212
<p>Table A.5: Pod series data in straight-ahead pusher configuration: propeller torque coefficient, $10K_Q$.</p>	213
<p>Table A.6: Pod series data in straight-ahead pusher configuration: propulsor (unit) thrust coefficient, K_{Tunit}.</p>	213
<p>Table A.7: Performance coefficient of average pod 01 at azimuthing conditions and in puller configuration: propeller thrust coefficient, K_{Tprop}.</p>	214
<p>Table A.8: Performance coefficient of average pod 01 at azimuthing conditions and in puller configuration: propeller torque coefficient, $10K_Q$.</p>	214
<p>Table A.9: Performance coefficient of average pod 01 at azimuthing conditions and in puller configuration: propulsor (unit) thrust coefficient, K_{Tunit}.</p>	215
<p>Table A.10: Performance coefficient of average pod 01 at azimuthing conditions and in puller configuration: propulsor (unit) transverse force coefficient, K_{FY}.</p>	215
<p>Table A.11: Performance coefficient of average pod 01 at azimuthing conditions and in puller configuration: propulsor (unit) vertical force coefficient, K_{FZ}.</p>	216
<p>Table A.12: Performance coefficient of average pod 01 at azimuthing conditions and in puller configuration: propulsor (unit) axial moment coefficient, K_{MX}.</p>	216
<p>Table A.13: Performance coefficient of average pod 01 at azimuthing conditions and in puller configuration: propulsor (unit) transverse moment coefficient, K_{MY}.</p>	217

List of Tables

Table A.14: Performance coefficient of average pod 01 at azimuthing conditions and in puller configuration: propulsor (unit) steering moment coefficient, K_{MZ} .	217
Table A.15: Performance coefficient of average pod 01 at azimuthing conditions and in pusher configuration: propeller thrust coefficient, K_{TProp} .	218
Table A.16: Performance coefficient of average pod 01 at azimuthing conditions and in pusher configuration: propeller torque coefficient, $10K_Q$.	218
Table A.17: Performance coefficient of average pod 01 at azimuthing conditions and in pusher configuration: propulsor (unit) thrust coefficient, K_{TUnit} .	219
Table A.18: Performance coefficient of average pod 01 at azimuthing conditions and in pusher configuration: propulsor (unit) transverse force coefficient, K_{FY} .	219
Table A.19: Performance coefficient of average pod 01 at azimuthing conditions and in pusher configuration: propulsor (unit) vertical force coefficient, K_{FZ} .	220
Table A.20: Performance coefficient of average pod 01 at azimuthing conditions and in pusher configuration: propulsor (unit) axial moment coefficient, K_{MX} .	220
Table A.21: Performance coefficient of average pod 01 at azimuthing conditions and in pusher configuration: propulsor (unit) transverse moment coefficient, K_{MY} .	221
Table A.22: Performance coefficient of average pod 01 at azimuthing conditions and in pusher configuration: propulsor (unit) steering moment coefficient, K_{MZ} .	221
Table A.23: Performance coefficient of the pod with 200 mm diameter propeller at static azimuthing angles and in puller configuration: propeller thrust coefficient, K_{TProp} .	222
Table A.24: Performance coefficient of the pod with 200 mm diameter propeller at static azimuthing angles and in puller configuration: propeller torque coefficient, $10K_Q$.	223
Table A.25: Performance coefficient of the pod with 200 mm diameter propeller at static azimuthing angles and in puller configuration: propulsor (unit) thrust coefficient, K_{TUnit} .	224
Table A.26: Performance coefficient of the pod with 200 mm diameter propeller at static azimuthing angles and in puller configuration: propulsor (unit) transverse force coefficient, K_{FY} .	225
Table A.27: Performance coefficient of the pod with 200 mm diameter propeller at static azimuthing angles and in puller configuration: propulsor (unit) vertical force coefficient, K_{FZ} .	226
Table A.28: Performance coefficient of the pod with 200 mm diameter propeller at static azimuthing angles and in puller configuration: propulsor (unit) axial moment coefficient, K_{MX} .	227
Table A.29: Performance coefficient of the pod with 200 mm diameter propeller at static azimuthing angles and in puller configuration: propulsor (unit) transverse moment coefficient, K_{MY} .	228

List of Tables

Table A.30: Performance coefficient of the pod with 200 mm diameter propeller at static azimuthing angles and in puller configuration: propulsor (unit) vertical force coefficient, K_{MZ} .	229
Table B.1: Bias and precision limits for a list of performance coefficients for the NSERC podded propulsor unit.	231
Table B.2: Bias and precision limits of a list of performance coefficients for the IOT podded propulsor unit.	236
Table C-1. Factorial effect aliases in the 16 pods series design (used in fractional factorial design).	246

List of Figures

Figure 2.1: Geometric parameters used to define pod-strut geometry.	27
Figure 2.2: Podded propulsors in open water test set-up (Atlar <i>et al.</i> 2005).	30
Figure 2.3: Four model propellers (Left hand side - rendered numerical model; Right hand side - physical model): a, b, c, d are the propellers with hub taper angles of +15° (push), +20° (pull), -15° (pull), -20° (pull), respectively.	35
Figure 2.4: Geometric models of the pod series.	37
Figure 2.5: Two pod models (top - rendered model; bottom - physical model): left – Pod 01 and right – Pod02, respectively.	39
Figure 2.6: Different parts of the experimental apparatus used in the podded propulsor tests. The picture shows the apparatus installed in the OERC (MUN) towing tank.	42
Figure 2.7: Pod and the global dynamometer system designed and fabricated at IOT.	45
Figure 2.8: The open boat to tests the podded propulsors at static and dynamic azimuthing conditions, designed and fabricated at IOT.	46
Figure 2.9: NSERC pod dynamometer system installed at the OERC towing tank facility.	47
Figure 2.10: IOT pod dynamometer system installed at the IOT towing tank facility.	48
Figure 2.11: Definitions of forces, moments, coordinate of the puller azimuthing podded propulsors.	49
Figure 2.12: Open water coefficients of the podded propellers (large propeller with diameter 270 mm and small propeller with diameter 200 mm).	54
Figure 2.13a: <i>Reynolds Number</i> effects tests on propeller thrust coefficient in puller configuration podded propulsors.	55
Figure 2.14a: <i>Reynolds Number</i> effects tests on propeller thrust coefficient in pusher configuration podded propulsors.	55
Figure 2.13b: <i>Reynolds Number</i> effects tests on propeller torque coefficient in puller configuration podded propulsors.	56

List of Figures

Figure 2.14b: <i>Reynolds Number</i> effects tests on propeller torque coefficient in pusher configuration podded propulsors.	56
Figure 2.13c: <i>Reynolds Number</i> effects tests on unit thrust coefficient in puller configuration podded propulsors.	56
Figure 2.14c: <i>Reynolds Number</i> effects tests on unit thrust coefficient in pusher configuration podded propulsors.	56
Figure 3.1: Block diagram for podded propulsor open water tests and uncertainty analysis.	63
Figure 3.2: Performance curves for NSERC pod 01 (270 mm propeller diameter) in straight-course puller configuration with uncertainty (error) bars.	72
Figure 3.3: Performance curves for IOT pod 01 (270 mm propeller diameter) in straight-course puller configuration with uncertainty (error) bars.	75
Figure 4.1: Experimental results: Propeller thrust coefficient of the pods in the series in puller configuration.	83
Figure 4.2: Experimental results: Propeller torque coefficient of the pods in the series in puller configuration.	83
Figure 4.3: Experimental results: propeller efficiency of the pods in the series in puller configuration.	84
Figure 4.4: Experimental results: unit thrust or axial force coefficient of the pods in the series in puller configuration.	85
Figure 4.5: Experimental results: unit efficiency of the pods in the series in puller configuration.	86
Figure 4.6: Experimental results: Propeller thrust coefficient of the pods in the series in pusher configuration.	88
Figure 4.7: Experimental results: Propeller torque coefficient of the pods in the series in pusher configuration.	88
Figure 4.8: Experimental results: Propeller efficiency of the pods in the series in pusher configuration.	89
Figure 4.9: Experimental results: unit thrust or axial force coefficient of the pods in the series in pusher configuration.	90
Figure 4.10: Experimental results: unit efficiency of the pods in the series in puller configuration.	91
Figure 4.11: DOE Analysis: The effect of D_{Pod}/D_{Prop} (A) on propeller thrust at	94

List of Figures

$J=0.0$ for puller propulsors.	
Figure 4.12: DOE Analysis: The effect of D_{Pod}/D_{Prop} (A) on propeller thrust at $J=0.8$ for puller propulsors.	94
Figure 4.13: DOE Analysis: The effect of significant factors, S_{Dist}/D_{Prop} (D) on propeller thrust at $J=0.6$ for puller propulsors.	95
Figure 4.14: DOE Analysis: The effect of significant factors, S_{Dist}/D_{Prop} (D) on propeller thrust at $J=0.8$ for puller propulsors.	95
Figure 4.15: DOE Analysis: The effect of significant factor, H_{Angle} (E) on propeller thrust at $J=0.0$ for puller propulsors.	97
Figure 4.16: DOE Analysis: The effect of significant factor, H_{Angle} (E) on propeller thrust at $J=0.8$ for puller propulsors.	97
Figure 4.17: DOE Analysis: The effect of significant factor, H_{Angle} (E) on propeller torque at $J=0$ for puller propulsors.	98
Figure 4.18: DOE Analysis: The effect of significant factor, H_{Angle} (E) on propeller torque at $J=0.8$ for puller propulsors.	98
Figure 4.19: DOE Analysis: The interaction effect of significant factors, D_{Pod}/D_{Prop} (A) and H_{Angle} (E) on propeller thrust at $J=0.8$ for puller propulsors.	99
Figure 4.20: DOE Analysis: The interaction effect of significant factors, L_{Pod}/D_{Prop} (B) and S_{Dist}/D_{Prop} (D) on unit thrust at $J=0.8$ for puller propulsors.	99
Figure 4.21: DOE Analysis: The effect of D_{Pod}/D_{Prop} (A) on propeller thrust at $J=0.8$ for pusher propulsors.	102
Figure 4.22: DOE Analysis: The effect of D_{Pod}/D_{Prop} (A) on unit thrust at $J=0.8$ for pusher propulsors.	102
Figure 4.23: DOE Analysis: The effect of TL/D_{Prop} (C) on unit thrust at $J=0.0$ for pusher propulsors.	103
Figure 4.24: DOE Analysis: The effect of TL/D_{Prop} (C) on unit thrust at $J=0.8$ for pusher propulsors.	103
Figure 4.25: DOE Analysis: The effect of L_{Pod}/D_{Prop} (B) on unit thrust at $J=0.9$ for pusher propulsors.	104
Figure 4.26: DOE Analysis: The effect of S_{Dist}/D_{Prop} (D) on propeller thrust at $J=0.8$ for pusher propulsors.	104
Figure 4.27: DOE Analysis: The effect of H_{Angle} (E) on propeller thrust at $J=0.0$ for pusher propulsors.	105
Figure 4.28: DOE Analysis: The effect of H_{Angle} (E) on propeller thrust at $J=0.8$ for pusher propulsors.	105
Figure 4.29: DOE Analysis: The interaction effect of L_{Pod}/D_{Prop} (B) and TL/D_{Prop}	106

List of Figures

(C) on propeller thrust at $J=0$ for pusher propulsors.

Figure 4.30: DOE Analysis: The interaction effect of D_{Pod}/D_{Prop} (A) and L_{Pod}/D_{Prop} (B) on unit thrust at $J=0$ for pusher propulsors. 106

Figure 5.1: Propeller thrust coefficient vs. advance coefficient at constant values of azimuthing angles in the puller configuration. 111

Figure 5.2: Propeller torque coefficient vs. advance coefficient at constant values of azimuthing angles in the puller configuration. 111

Figure 5.3: Unit thrust coefficient vs. advance coefficient at constant values of azimuthing angles in the puller configuration. 113

Figure 5.4: Transverse force coefficient vs. advance coefficient at constant values of azimuthing angles in the puller configuration. 113

Figure 5.5: Vertical force coefficient vs. advance coefficient at constant values of azimuthing angles in the puller configuration. 114

Figure 5.6: Axial moment coefficient vs. advance coefficient at constant values of azimuthing angles in the puller configuration. 115

Figure 5.7: Transverse moment coefficient vs. advance coefficient at constant values of azimuthing angles in the puller configuration. 116

Figure 5.8: Steering moment coefficient vs. advance coefficient at constant values of azimuthing angles in the puller configuration. 116

Figure 5.9: Propeller thrust coefficient vs. advance coefficient at constant values of azimuthing angles in the pusher configuration. 117

Figure 5.10: Propeller torque coefficient vs. advance coefficient at constant values of azimuthing angles in the pusher configuration. 118

Figure 5.11: Unit thrust coefficient vs. advance coefficient at constant values of azimuthing angles in the pusher configuration. 119

Figure 5.12: Transverse force coefficient vs. advance coefficient at constant values of azimuthing angles in the pusher configuration. 120

Figure 5.13: Vertical force coefficient vs. advance coefficient at constant values of azimuthing angles in the pusher configuration. 120

Figure 5.14: Axial moment coefficient vs. advance coefficient at constant values of azimuthing angles in the pusher configuration. 122

Figure 5.15: Transverse moment coefficient vs. advance coefficient at constant values of azimuthing angles in the pusher configuration. 122

Figure 5.16: Steering moment coefficient vs. advance coefficient at constant 123

List of Figures

values of azimuthing angles in the pusher configuration.

Figure 5.17: Conceptual propeller and pod wake at static azimuthing angles with: left for puller configuration and right for pusher configuration.	125
Figure 5.18: Propeller thrust coefficient vs. azimuthing angle at constant values of advance coefficient in the puller configuration (left handed propeller).	130
Figure 5.19: Propeller thrust coefficient vs. azimuthing angle at constant values of advance coefficient in the pusher configuration (right handed propeller).	130
Figure 5.20: Propeller torque coefficient vs. azimuthing angle at constant values of advance coefficient in the puller configuration (left handed propeller).	131
Figure 5.21: Propeller torque coefficient vs. azimuthing angle at constant values of advance coefficient in the pusher configuration (right handed propeller).	132
Figure 5.22: Unit thrust coefficient vs. azimuthing angle at constant values of advance coefficient in the puller configuration (left handed propeller).	134
Figure 5.23: Unit thrust coefficient vs. azimuthing angle at constant values of advance coefficient in the pusher configuration (right handed propeller).	135
Figure 5.24: Unit transverse force coefficient vs. azimuthing angle at constant values of advance coefficient in the puller configuration (left handed propeller).	136
Figure 5.25: Unit transverse force coefficient vs. azimuthing angle at constant values of advance coefficient in the pusher configuration (right handed propeller).	137
Figure 5.26: Unit vertical force coefficient vs. azimuthing angle at constant values of advance coefficient in the puller configuration (left handed propeller).	139
Figure 5.27: Unit vertical force coefficient vs. azimuthing angle at constant values of advance coefficient in the pusher configuration (right handed propeller).	139
Figure 5.28: Unit axial moment coefficient vs. azimuthing angle at constant values of advance coefficient in the puller configuration (left handed propeller).	140
Figure 5.29: Unit axial moment coefficient vs. azimuthing angle at constant values of advance coefficient in the pusher configuration (right handed propeller).	141
Figure 5.30: Unit transverse moment coefficient vs. azimuthing angle at constant values of advance coefficient in the puller configuration (left handed propeller).	142
Figure 5.31: Unit transverse moment coefficient vs. azimuthing angle at constant values of advance coefficient in the pusher configuration (right handed propeller).	143
Figure 5.32: Unit steering moment coefficient vs. azimuthing angle at constant values of advance coefficient in the puller configuration (left handed propeller).	145
Figure 5.33: Unit steering moment coefficient vs. azimuthing angle at constant values of advance coefficient in the pusher configuration (right handed propeller).	145

List of Figures

Figure 6.1: Experimental results: propeller thrust coefficient of the model pod unit in puller configuration (left-handed propeller in static azimuthing conditions).	151
Figure 6.2: Experimental results: propeller torque coefficient of the model pod unit in puller configuration (left-handed propeller in static azimuthing conditions).	151
Figure 6.3: Experimental results: unit thrust coefficient of the model pod unit in puller configuration (left-handed propeller in static azimuthing conditions).	153
Figure 6.4: Experimental results: transverse force coefficient of the model pod unit in puller configuration (left-handed propeller in static azimuthing conditions).	154
Figure 6.5: Experimental results: unit horizontal resultant force coefficient of the model pod unit in puller configuration (left-handed propeller in static azimuthing conditions).	155
Figure 6.6: Experimental results: vertical force coefficient of the model pod unit in puller configuration (left-handed propeller in static azimuthing conditions).	157
Figure 6.7: Experimental results: axial moment coefficient of the model pod unit in puller configuration (left-handed propeller in static azimuthing conditions).	158
Figure 6.8: Experimental results: transverse moment coefficient of the model pod unit in puller configuration (left-handed propeller in static azimuthing conditions).	159
Figure 6.9: Experimental results: steering moment coefficient of the model pod unit in puller configuration (left-handed propeller in static azimuthing conditions).	160
Figure 6.10: Conceptual propeller and pod wake at dynamic azimuthing conditions for a right-handed propeller: from top left clockwise, clockwise azimuthing at the 1 st quadrant (Port), counter-clockwise azimuthing in the 4 th quadrant (Starboard), counter-clockwise azimuthing in the 1 st quadrant (Port) and clockwise azimuthing in the 4 th quadrant (Starboard).	162
Figure 6.11: Experimental results: comparison of propeller thrust coefficient of the model pod unit at static (black solid circle) and dynamic azimuthing conditions (black dots for raw unfiltered data and red line for 10 th order polynomial fit to the raw data).	165
Figure 6.12: Experimental results: comparison of propeller torque coefficient of the model pod unit at static (black solid circle) and dynamic azimuthing conditions (black dots for raw unfiltered data and red line for 10 th order polynomial fit to the raw data).	165
Figure 6.13: Experimental results: comparison of unit thrust coefficient of the model pod unit at static (black solid circle) and dynamic azimuthing conditions (black dots for raw unfiltered data and red line for 10 th order polynomial fit to the raw data).	166
Figure 5-14: Experimental results: comparison of transverse force coefficient of the model pod unit at static (black solid circle) and dynamic azimuthing conditions (black dots for raw unfiltered data and red line for 10 th order	166

List of Figures

polynomial fit to the raw data).	
Figure 6.15: Experimental results: comparison of resultant horizontal force coefficient of the model pod unit at static (black solid circle) and dynamic azimuthing conditions (black dots for raw unfiltered data and red line for 10 th order polynomial fit to the raw data).	167
Figure 6.16: Experimental results: comparison of steering moment coefficient of the model pod unit at static (black solid circle) and dynamic azimuthing conditions (black dots for raw unfiltered data and red line for 10 th order polynomial fit to the raw data).	168
Figure 6.17: Experimental results: comparison of propeller thrust coefficient of the model pod unit at static (black solid circle) and dynamic azimuthing conditions (black dots for raw unfiltered data and black solid line for 10 th order polynomial fit to the raw data).	169
Figure 6.18: Experimental results: Original unfiltered data showing the variation of propeller thrust coefficient of the model pod unit with azimuthing rate in dynamic conditions.	171
Figure 6.19: Experimental results: Variation of propeller thrust coefficient of the model pod unit with azimuthing rate in dynamic conditions.	172
Figure 6.20: Experimental results: Variation of propeller torque coefficient of the model pod unit with azimuthing rate in dynamic conditions.	172
Figure 6.21: Experimental results: Variation of unit thrust coefficient of the model pod unit with azimuthing rate in dynamic conditions.	173
Figure 6.22: Experimental results: Variation of transverse force coefficient of the model pod unit with azimuthing rate in dynamic conditions.	173
Figure 6.23: Experimental results: Variation of steering moment coefficient of the model pod unit with azimuthing rate in dynamic conditions.	173
Figure 6.24: Experimental results: Variation of propeller thrust coefficient of the model pod unit with shaft speed and azimuthing rate in dynamic conditions.	175
Figure 6.25: Experimental results: Variation of propeller torque coefficient of the model pod unit with shaft speed and azimuthing rate in dynamic conditions.	176
Figure 6.26: Experimental results: Variation of unit thrust coefficient of the model pod unit with shaft speed and azimuthing rate in dynamic conditions.	176
Figure 6.27: Experimental results: Variation of transverse force coefficient of the model pod unit with shaft speed and azimuthing rate in dynamic conditions.	177
Figure 6.28: Experimental results: Variation of steering moment coefficient of the model pod unit with shaft speed and azimuthing rate in dynamic conditions.	177

Nomenclature

ITTC Symbol	Name	Definition or Explanation	SI Unit
D	Propeller diameter		m
R	Propeller radius		m
$C_{0.7R}$	Propeller blade chord length at 0.7R		m
n	Propeller shaft rps (rotation per second)		rps
T_{Prop}	Propeller thrust		N
Q	Propeller torque		N-m
V_A	Advance speed of propeller		m/s
ρ	Fresh water density		Kg/m ³
ν	Kinematic viscosity of fresh water		m ² /s
T_{Unit} or F_X	Unit thrust or Unit axial force		N
F_Y	Unit transverse force		N
F_Z	Unit vertical force		N
M_X	Unit axial moment		N-m
M_Y	Unit transverse moment		N-m
M_Z	Unit steering moment		N-m
w_T	Wake fraction		
t	Thrust deduction fraction		
J	Propeller advance coefficient	V_A/nD	
K_{TProp}	Propeller thrust coefficient	$T_{Prop}/(\rho n^2 D^4)$	
K_Q	Propeller torque coefficient	$Q/(\rho n^2 D^5)$	
K_{Tunit} or K_{FX}	Unit thrust coefficient or Unit axial force coefficient	$T_{Unit}/(\rho n^2 D^4)$ or $F_X/(\rho n^2 D^4)$	
K_{FY}	Unit transverse force coefficient	$F_Y/(\rho n^2 D^4)$	

Nomenclature

ITTC Symbol	Name	Definition or Explanation	SI Unit
K_{FZ}	Unit vertical force coefficient	$F_Z/(\rho n^2 D^4)$	
K_{MX}	Unit axial moment coefficient	$M_X/(\rho n^2 D^5)$	
K_{MY}	Unit transverse moment coefficient	$M_Y/(\rho n^2 D^5)$	
K_{MZ}	Unit steering moment coefficient	$M_Z/(\rho n^2 D^5)$	
η_{Prop}	Propeller efficiency	$(J/2\pi) \times (K_{TProp}/K_Q)$	
η_{Unit}	Unit efficiency	$(J/2\pi) \times (K_{TUnit}/K_Q)$	
R_N	<i>Reynolds Number</i>	$R_N = C_{0.7R} \sqrt{V_A^2 + 0.7\pi n D^2} / \nu$	
LE	Leading Edge of Propeller Blade		
DOE	Design of Experiments		
FFD	Fractional Factorial Design		
OERC	Ocean Engineering Research Centre		
IOT	Institute for Ocean Technology		
NRC	National Research Council		
MUN	Memorial University of Newfoundland		
NSERC	Natural Sciences and Engineering Research Council		

CHAPTER

1

INTRODUCTION

1 Introduction

1.1 Chapter Objectives

This chapter provides the background and motivation of this doctoral research work. It describes the research problems that are addressed as well as the approaches followed are described. In addition, the scope of the current research is presented in the context of other relevant work. Finally, this chapter presents a layout of this thesis.

1.2 Background and Motivation

For the last eighteen years, the marine industry has witnessed a rapid growth of integral electric-driven pod propulsors in the cruise, ferry and other shipping sectors. The application of this propulsor has outpaced the understanding of the hydrodynamics. There are similarities between a conventional propeller-rudder propulsion system and an azimuthing podded propulsion system in terms of hydrodynamic behaviour. Roughly, an azimuthing-podded propulsor may be thought of as an integrated propulsion unit entirely replacing the actions of a separate propeller and rudder. However, the podded propulsor is not merely a replacement of a propeller and a rudder. In this system, the propeller accelerates flow over the strut body and the propeller induced flow stays parallel to the strut for all azimuthing angles, which is not true for a conventional rudder at steering (azimuthing) angles. Again, the propeller in this system receives asymmetric inflow at azimuthing positions and the resulting forces and moments are very different from a

Introduction

conventional propeller-rudder system. The technology is relatively new, and as of present, there is little scientific information available in the public domain to assist in understanding the hydrodynamics.

In a study on podded propulsor optimization, Goubault and P  r  e (2004) concluded that the pod motor parameters are not as influential on the hydrodynamic performance as the external geometric (hydrodynamic) parameters. This emphasizes the need for further research on pod-strut outer shape to better understand the effect of geometry on podded propulsors' hydrodynamic performance. Also, while there are claims of improved flow to the propeller, hence improved cavitation behaviour, this has only been shown in the puller or tractor pod (where the propeller is fitted on the forward end of the pod body), and not in the pusher pod (where the propeller is fitted on the aft end of the pod body, Karafiath and Lyons, 1998 and 1999). It is thus important that the study of geometry of the propulsors is done in pusher and puller configurations separately because of different flow conditions. Again, there has been no clear evidence that shows how the pod, strut and propeller combination can be optimized to improve hydrodynamic performance. In this doctoral research work, five geometric parameters of the pod, strut and propeller were studied to evaluate the relative importance of the parameters and combinations of the parameters on the thrust, torque and propulsive efficiency of podded propulsors.

In 2005, during the 24th International Towing Tank Conference, the Specialist Committee on Azimuthing Podded Propulsion provided a final report and recommendations for

Introduction

procedures for podded propulsor tests and extrapolation, procedures for carrying out podded propulsor cavitation and open water experiments, and procedures to study the impact of off-design conditions on loads at steady and dynamic azimuthing conditions (Atlar *et al.* 2005). The report emphasized the requirement of performing extensive experimental and numerical investigations on podded propulsors' hydrodynamic performance in cavitating and non-cavitating open water conditions both in regular straight course and off-design loading conditions. This is primarily because of inadequate knowledge about the hydrodynamics of the propulsors at different operating conditions.

One of the most attractive features of a podded propulsor is its ability to direct its thrust toward any direction in a 360° horizon. However, this feature also raised a number of concerns such as the nature of forces and moments on the unit that result from the hydrodynamic interactions between its components at different loading conditions. Bearing forces, transverse force, and steering moment are particularly important in conditions such as manoeuvring, steering at high speed, and sailing in a seaway. Failures on early pod units led to a study about the sources of failure of podded propulsors (Carlton, 2002). This showed that bearings and seals were the sources of over one-half of the failures, thus highlighting the importance of predicting bearing and other propulsion forces accurately. Moreover, the propeller forces and moments are by no means stationary and important contributions to the vibration excitation may arise from the propeller working in an irregular hull wake. A thorough investigation of the hydrodynamics of the fluctuation of these forces and moments while operating in straight

course and azimuthing conditions is required for a proper understanding of the issue. This doctoral study focuses on the experimental measurement of propeller shaft thrust and torque as well as the forces and moments on the entire pod unit of several model podded propulsors in static and dynamic azimuthing conditions.

1.3 Scope of the Research

The doctoral research work is focussed on podded propulsors. Primarily, the work addresses two research questions regarding the performance evaluation of podded propulsors as outlined below:

First: How do the performance coefficients of a podded propulsor change with the change of a number of geometric parameters in pusher and puller configurations in open water?

In answering the first question, the current work concentrates on the hydrodynamic performance evaluation for varied geometry of pusher- and puller-podded propulsors. Three geometric parameters of the pod namely, length, diameter and taper length, as well as propeller hub taper angle and lateral strut distance from the propeller plane were selected for the experimental study. Karafiath and Lyons (1998) offer the first report that presents a study on the effect of variation in pod geometry on the performance of podded propulsors (details in section 1.4.2.). This study offers some opportunity for comparison

Introduction

with the current research work. To date, there are no other published results showing the effects of geometric parameters on podded propulsors' performance.

The work used a Design of Experiment (DOE) technique, namely, fractional factorial design and analysis approach (Montgomery 2005) to produce a systematic series of physical pod models to study the five geometric parameters of pusher and puller propulsors. This study dealt with the effects of both individual geometric parameters and their interaction on the thrust and efficiency of both the propeller and the whole unit, and on the torque on propeller shaft. The outcome of this study was a quantification of the most significant geometric parameters of podded propulsors in defining thrust, torque and efficiency. The results also provide guidelines to designers to design podded propulsors with a geometric shape suitable for a specific configuration.

Second: How do the performance coefficients of a podded propulsor change with different static and dynamic azimuthing conditions in open water?

For the second question, the research work focuses on hydrodynamic properties of the podded propulsors in static and dynamic azimuthing conditions. There are a few recently published works that address the behaviour of podded propulsors at static and dynamic azimuthing angles. The following did the most relevant research: Szantyr (2001a and 2001b), Grygorowicz and Szantyr (2004), Woodward *et al.* (2004), Heinke (2004), Stettler (2004), and Woodward (2006) are the most relevant ones (details in section

Introduction

1.4.3). These papers discuss different aspects of pushing and pulling podded propulsors operating at different static and dynamic azimuthing conditions. Atlar *et al.* 2005 encouraged further experimental and numerical studies to evaluate the nature of the forces and moments that act on the propulsors at different static and dynamic azimuthing conditions for a better understanding of the hydrodynamics.

To address the research question, two separate experimental studies were carried out. In the first study, two podded propulsors were tested to measure the forces and moments on the propeller and the unit at different static azimuthing angles within the range from -30° to 30° . The tests were performed both with puller and pusher configurations. The results facilitated an evaluation of the variations of the pod performance coefficients at different loading conditions and configurations at static azimuthing positions. In the second study, another dynamometer system was used to measure forces and moments of a pod unit at different dynamic azimuthing conditions in the range of 0° to 360° azimuthing positions. The results helped to evaluate the variation of the forces and moments on the pod unit as the propulsor azimuthed dynamically, providing some fundamental information with respect to manoeuvring loads from the pod as well as providing a base for the validation of numerical modeling. An additional study was carried out to evaluate the effects of azimuthing rate and propeller shaft rps on the performance coefficients at dynamic azimuthing conditions.

1.4 Literature Review on Pods

Podded propulsors are considered as an alternative propulsion system for most commercial vessels. Among the claimed benefits are better manoeuvrability, enhanced propeller location, flexibility in the layout of the ship, freedom in hull-form design, potentially reduced vibrations and noise, novel propeller arrangements such as contra-rotating propellers, and improved cavitation properties because of more uniform inflow (Pakaste *et al.* 1999). A further discussion on the advantages and disadvantages of podded propulsion technology is provided in Islam (2004). Section 1.4.1 provides a general literature review on the experimental work on pod technology. Section 1.4.2 and 1.4.3 provide a comprehensive literature review on the previous experimental work, the scope of which is limited to work of direct relevance to this doctoral work.

1.4.1 Study on Pod Technology

Podded propulsors were first used on harbour tugs and then introduced to the cruise and shipping industries in 1990 by ABB and Kvaerner Masa (Anon, 2000). Arctic tankers were retrofitted with ABB's Azipod[®] to prove the concept, and their pods have subsequently been used to power a range of vessels including cruise ships, tankers and icebreakers (Anon, 2001). Since the introduction of the ABB Azipod[®], other companies have introduced similar systems. Podded propulsion systems have been installed on tankers, military vessels, oceanographic vessels and seismic survey vessels, to name a few. The commercial pods now being produced are the ABB's Azipod[®], the Mermaid

Introduction

from Rolls-Royce, the SSP from Schottel and Siemens, the Dolphin from STN Atlas, and the French DCN pod.

An early but detailed investigation into some hydrodynamic issues such as pod-strut total drag and full-scale power prediction of vessels fitted with podded propulsors (not azimuthing) was done by Rains and Vanlandingham (1981). Halstensen and Leivdal (1990) discussed various hydrodynamic and mechanical aspects of a tractor type podded propulsion system, *SpeedZ*. Several model tests and full-scale measurements of this high-speed craft propulsion system were discussed and the system was recommended as a promising alternative for speeds up to 50 knots. Chen and Tseng (1995) presented a design procedure of a contra-rotating propeller with a tractor pod for a high-speed patrol boat and measurements of power and cavitation behaviour. Laukia (1996) discussed various hydrodynamic issues related to the design and use of a commercial azimuthing podded drive Azipod[®]. Niini (1997) performed a similar study and discussed various hydrodynamic aspects of Azipod[®], especially from efficiency and manoeuvrability points of view as applied to large cruise ships. Kurimo (1998) presented sea trial results on general hydrodynamic issues such as speed trials, cavitation observation, pressure pulse measurement and manoeuvring tests. Raynor (1998) discussed the prospects, design issues and some manoeuvring characteristics of podded propulsion in the offshore market especially for monohull and semi-submersibles. Kanerva (1999) discussed various aspects of *Ro-Ro* passenger ferries and the prospects of podded propulsion as the primary propulsion unit. Bose *et al.* (1999) briefly discussed general power extrapolation methods

Introduction

and test procedures for podded propulsors. Karafiath and Lyons (1999) presented detailed measurements and analyses of tests conducted with a view to have better understanding on the hydrodynamic characteristics of podded propeller concepts as applied to fast naval vessels.

Backlund and Kuuskoski (2000) discussed various design features and benefits of using a contra-rotating propeller with a podded drive, demonstrated with a case study. Lepeix (2001) discussed different hydrodynamic issues such as power/speed curve, ship wake and pressure fluctuation and manoeuvring performance of large cruise ships with podded propulsors and discussed the new trends in hull lines of large podded driven cruise ships. In the paper by Terwisga *et al.* (2001), the authors discussed some critical hydrodynamic issues and design consequences of several steerable thrusters and podded propulsors and put them in an historic perspective.

Mewis (2001) described model test procedures and presented the results obtained on podded propulsors giving the effects of the presence of pods and propeller gap pressure on the propulsive efficiency of the pod unit. Tozer and Penfold (2002) discussed various design features of an ultra-large container ship and applicability of podded propulsors as the main propulsion unit for those vessels. Kim and Choi (2002) investigated powering performance of three different propulsion systems for ultra-large container vessels through various model tests and concluded that the contra-rotating azimuthing podded propulsor is a serious alternative. Toxopeus and Loeff (2002) presented various aspects

Introduction

of application of pods from a manoeuvring viewpoint, comparing the manoeuvrability between a ship designed with conventional propulsion and pod propulsion and highlighted the benefits and points of attention of using pod propulsion. Trägårdh *et al.* (2004) presented the results of model tests and sea trials done on Double Acting Tankers (DAT) showing good propulsive, manoeuvring and cavitation performance. Sasaki *et al.* (2004) presented the scale effects on open sea performance and the ice breaking capacity of the double acting tankers, *Tempera* and *Mastera* based on extensive model tests and full-scale trials.

Several research projects on podded propulsors have been done on various aspects of the propulsors. OPTIPOD, PODs-in-service and FASTPOD are some of the projects carried out under the EU framework program (FP5). These projects basically looked into various design and operation aspects of the propulsors (Atlar *et al.* 2005).

A five-year research programme, entitled “Systematic Investigation of Azimuthing Podded Propeller Performance”, was started in 2002 in Canada with the collaboration of Memorial University of Newfoundland (MUN), the Institute for Ocean Technology (IOT) of National Research Council (NRC), Oceanic Consulting Corporation Inc., and Thordon Bearings Inc. This research program aimed to quantify the effects of podded propulsor configuration on its performance; develop computational methods for performance prediction; develop an extrapolation method for power prediction; quantify the blade-loading effects in open water and in ice at off-design conditions and develop

new instrumentation for performance evaluation. Amongst the hydrodynamic issues that have been identified and addressed are questions regarding the effects of hub taper angle (Islam 2004, Islam *et al.* 2004, Islam *et al.* 2005, Islam *et al.* 2006a, Taylor 2006, Taylor *et al.* 2005), pod-strut configuration (Islam 2004, Islam *et al.* 2006c, and Taylor 2006), pod-strut interactions (He *et al.* 2005a, He *et al.* 2005b, He 2006), gap pressure (MacNeill *et al.* 2004), pod-strut geometry (Molly *et al.* 2005, Islam *et al.* 2006b and Islam *et al.* 2008a), pod gap effect (Islam *et al.* 2007a), static azimuthing conditions (Islam *et al.* 2008b) and dynamic azimuthing conditions (Islam *et al.* 2007b) on podded propulsor performance. A technical overview of the numerical and experimental investigations done to study various hydrodynamic aspects of podded propulsors in open water conditions are presented in Islam *et al.* 2008c and 2008d.

1.4.2 Study on Pod Geometry

As mentioned in section 1.3, Karafiath and Lyons (1998) offered the first report that presents a study on the effect of variation in pod geometry. Pod length and strut position were varied using four pods to study their effects on pod drag and pod-propeller interactions.

The study by Karafiath and Lyons (1998) involved a number of different experiments performed over the past 30 years. Each set of tests was limited in its scope. In the first set of pods, four non-azimuthing pods were tested in pusher and puller configurations and the pod drag and pod-propeller interactions were studied. The pods varied in their body

Introduction

length and strut position. The first two pods, 1 and 2, were pusher pods with a centre strut and different pod body lengths. The remaining two, 3 and 4, were the same length and had significantly shorter pod lengths; about half the length of the smaller of 1 and 2, with a forward strut. Pods 3 and 4 were tested in pushing and tractor configurations, respectively. The propeller diameter for pods 3 and 4 was 406.4 mm. The distance from the top of the pod to the groundboard was not kept constant. The drag of the pod and strut was measured by a block gauge system mounted at the top of the strut. The thrust of the pod unit, T_{Unit} , was also measured at the top of the strut. The propulsion tests on these pods were conducted in a manner similar to the conduct of propeller open water tests. Table 1.1 shows the summary of propeller to pod-strut interaction coefficients as measured for the configurations with 25% propeller clearance and at an advance coefficient of $J=1.20$. At this advance coefficient, both the pusher and puller propellers were operating at or very near the maximum efficiency. The results (see Table 1.1) show that the largest pod, 1, had the largest wake (w_T) and thrust deduction fraction (t) and the smallest thrust ratio (thrust of the unit compared to the thrust of the propeller, $T_{\text{Unit}}/T_{\text{Prop}}$). Here the wake fraction and thrust deduction fraction were calculated using the traditional naval architectural approach (self propulsion tests, Lewis 1990). The smallest pusher pod, pod 3, had the highest thrust ratio and the highest efficiency. The propeller wash on the strut increased the drag of the tractor pod 4. This is shown by an increased thrust deduction fraction and the decreased thrust ratio of pod 4 compared to the equivalent pusher pod, pod 3. The inflow to the propeller for pod 4 was very uniform.

Table 1.1: Interaction coefficients for the Roddy Pods (Karafiath & Lyons, 1998)

Pod Type	$I-w_T$	$I-t$	T_{Unit}/T_{Prop}	$I-t/I-w_T$
Roddy 1 pusher	0.932	0.921	0.78	0.988
Roddy 2 pusher	0.957	0.928	0.82	0.969
Roddy 3 pusher	0.973	0.975	0.89	1.002
Roddy 4 tractor	0.988	0.939	0.85	0.950

The test series looked at two geometric parameters and the tests were done in a fashion that the effects of individual parameters were assessed. It is required to study how other prominent geometric parameters affect the performance coefficients. It is also essential to study the effects of individual parameters as well as their interaction. It was thought that a more comprehensive study on the geometry of the propulsor that evaluates the individual, as well as interaction effect of the parameters, would help in enhancing the knowledge on the propulsive effect of the geometry of the propulsor and hence this led to the work done here.

1.4.3 Study of Pod in Azimuthing Conditions

There is very little information in the literature regarding hydrodynamic performance of podded propulsors in static and dynamic azimuthing conditions. Prior to 2001, there have been only general literature notes regarding the effectiveness of podded propulsion in terms of manoeuvring, and slow speed manoeuvrability with low-power thrusters. Van Terwisga *et al.* (2001) provided a general overview of the history of mechanical and electrical steerable propulsion units, and address general hydrodynamic issues associated with their design and use. Toxopeus and Loeff (2002) discussed recent applications of

Introduction

podded propulsion from a manoeuvring perspective, comparing manoeuvrability between specific ship designs with conventional propulsion and podded propulsion, and highlighting the general benefits and points of attention. Additional comparative manoeuvring testing has been conducted under the auspices of the OPTIPOD and FASTPOD research programs funded by the European Union, with some results published in the first international conference on technological advances in podded propulsion held in 2004.

Szantyr (2001a and 2001b) published one of the first sets of systematic experimental data on podded propulsors as the main propulsion unit with static azimuthing angles. This test series was performed to provide data to validate a numerical hydrodynamic analysis program. The tests measured the axial and transverse loads and used traditional non-dimensional coefficients to analyze the data. Szantyr (2001a and 2001b) tested a twin-screw pod with propellers fitted at both ends and puller and pusher type pods in a cavitation tunnel. The pods were tested at straight courses and at $\pm 15^\circ$ static azimuthing angles. It was concluded that the azimuth angle had a pronounced effect upon the axial hydrodynamic force on the twin-screw podded unit and a similar, though smaller effect, upon the system with a single puller-type propulsor. Additional investigation revealed that the direction of propeller rotation influenced the axial and transversal hydrodynamic force with the azimuth angle; the force increase was greater with turns coinciding with the propeller rotation direction (the pod azimuths in clockwise direction i.e. starboard looking from behind, with a right hand screw propeller). Hydrodynamic characteristics of

Introduction

the podded drive were found to be asymmetric with respect to the static azimuth angle. The study was limited to $\pm 15^\circ$ angles and the effect of an azimuthing angle on propeller torque was not studied.

Grygorowicz and Szantyr (2004) presented open-water measurements of podded propulsors both in puller and pusher configurations in a circulating water channel. A complete pod was mounted on a six-component dynamometer and measurements were made of the resulting forces and moments in a range of advance coefficients combined with a range of azimuthing angles $\pm 30^\circ$ for puller- and pusher-type podded propulsors. The published results show that with both puller and pusher units, axial and transverse forces and vertical moments were complex functions of the azimuth angle, propeller loading, and of the external flow velocity, but in a completely different manner (different functional relationship between the forces and moments with the azimuth angle). This emphasizes that the puller and pusher propulsors should be studied separately. The complete range of loading condition was not presented in the study.

Heinke (2004) reported on comprehensive and systematic model test results, with 4- and 5-bladed propellers fitted to a generic pod housing in pull- and push-mode. In the report, Heinke presented systematic data for forces and moments on the propeller and pod body at different static azimuthing angles. The study also included the effect of cavitation at conditions for a blocked propeller (no propeller rotation), low number of revolutions (simulating crash stop) and at the design speed and revolutions with dynamically turning

Introduction

pod. Both push and pull modes of the propulsors were tested. The forces and moments of the propeller and podded drive showed a strong dependency on the propeller loading and azimuthing angle. The results showed that the open water characteristics were mostly irregular for the astern thrust conditions in the azimuthing angle range 90° to 270° due to flow separation at the propeller blades and pod housing. It was also claimed that the maximum forces and moments observed in the dynamic azimuthing conditions were slightly higher than those obtained in tests at fixed azimuthing angles. The increase of the azimuthing rate led to a small increase in the maximum forces and moments. Nevertheless, the obtained results demonstrated that the pseudo-steady approach is quite acceptable for predicting forces and moments on propellers and podded drive systems.

Stettler (2004) in his doctoral work investigated steady and unsteady dynamic manoeuvring forces associated with an azimuthing podded propulsor, and also provided supporting theoretical insight toward understanding their mechanisms and prediction. The work included quasi-steady vectored manoeuvring forces, of importance to all manoeuvring vehicles or ships, as well as unsteady or transient manoeuvring forces, which have more significance to the manoeuvrability of smaller vehicles, particularly for precision control applications. Stettler also published part of his doctoral work in the first international conference on technological advances in podded propulsion conference (Stettler *et al.*, 2004).

Stettler's (2004) efforts were focused in four main areas. Firstly, a number of relevant dynamic models for the manoeuvring of a surface vehicle with an azimuthing propulsor

Introduction

were developed. Secondly, an extensive test program measured and characterized the nature of quasi-steady vectored manoeuvring forces associated with a podded propulsor in azimuth to $\pm 180^\circ$ for the entire range of forward propeller speeds, as well as unsteady or transient manoeuvring forces due to rapid changes in azimuth angle or propeller rate. Stettler's test program was aimed at quantifying the steady and unsteady parameters associated with the developed dynamic models. Thirdly, two flow visualization techniques were utilized to visualize, document, and correlate the helical wake characteristics, velocities and forces for both quasi-steady and unsteady propulsor states. A new fluorescent paint flow visualization technique was developed and applied for small, moderate and large propulsor azimuth angles, and a laser particle image velocimetry (PIV) technique was adapted for small and moderate propulsor azimuth angles. Finally, a set of comprehensive physics-based models were developed to foster the understanding of the mechanisms associated with the steady and unsteady force dynamics. The quasi-steady models were based upon a combination of momentum-based, blade-element, and vortex wake propeller theories, as applied to an azimuthing podded propulsor. The unsteady force models were based upon unsteady wake or "dynamic inflow" methods. Additionally, an interesting phenomenon associated with the formation of a vortex ring during rapid propeller rate increase was presented and discussed.

In the study by Stettler, the steady and unsteady test results, flow visualizations, and theoretical models, were shown to be consistent in terms of the magnitudes and character of the azimuthing manoeuvring forces. Limited comparisons of quasi-steady propulsor

Introduction

forces at small, moderate and large azimuth angles were also made with forces predicted by a modified combined blade-element-momentum method, as well as the unsteady vortex-lattice propeller code MPUF-3A, with and without modified inflows to account for propulsor pod wake. The results illustrated inherent complexities related to use of existing computational fluid dynamics tools with azimuthing-podded propulsors. The study was carried out only for a pod unit in pusher configuration and a very basic pod-strut shape was used.

Woodward (2006) identified a few new methods for modelling the hydrodynamic reaction for both the ship hull and pod drive. A dedicated numerical simulation study was conducted exploring systematic variation of applied helm angles and comparison of time- and frequency-domain response. The study reached the definitive conclusion that the IMO manoeuvring criteria provide equivalent information about the manoeuvring response of pod-driven ships as for conventionally propelled ships; and can thus be applied directly. Woodward's study identified that hull-forms suited to the application of pods can have poor course stability characteristics. It was also identified that pod drives experience significant spike loads that are in origin related to dynamic manoeuvring. The loads did not impact directly on the manoeuvring response assessment; however they had significant implications for the structural design and may also impact on the roll stability of the vessel.

Introduction

Reichel (2007) presented the preliminary part of comprehensive maneuvering open-water tests of a gas carrier model primarily focusing on open water experiments with an azimuthing podded propulsor. The test program was carried out in the cavitation tunnel and the large towing tank of Ship Hydromechanics Division, Ship Design and Research Centre, Gdańsk. Steering forces were measured in the range of advance coefficient from 0.0 to 0.8 combined with the range of deflection angles from -45° up to $+45^\circ$. Measurements on the pod without propeller were also performed. Reichel concluded that the asymmetries in values of the force coefficients for positive and negative deflection angles are due to the influence of the direction of propeller rotation. It was also concluded that with positive azimuthing angle (counter clockwise rotation of the unit looking from top) a negative normal force is produced and vice versa, which results in a destabilizing moment tending to increase the turn rate. Reichel (2007) also found that for azimuthing angles larger than 15° the thrust and normal force coefficients are from 10% to 30% smaller than for the corresponding positive azimuthing angles, which is caused due to the interaction between right – handed propeller and podded drive. The pod was only tested in pusher configuration. The detailed account of the forces and moments of the pod unit in three coordinate directions are not presented in the paper.

Wang (2007) performed a study to understand propeller-ice interaction phenomena and developed a numerical method to predict the interaction ice loads at different azimuthing conditions. A model podded propulsor was tested in an ice tank with scaled model ice. Three six-component dynamometers and six single-axis dynamometers measured the ice

loads acting on various azimuthing positions of the experimental model. In order to achieve the desired numerical simulations, both a panel method and empirical formulae were used. Numerical results were compared and validated with the experimental results. The numerical model was valid for the first quadrant operating conditions with various azimuthing (yaw) angles.

1.5 Layout of thesis

This thesis documents the work done to characterize and understand the effects of five geometric parameters of podded propulsors on the propulsive performance of puller and pusher configurations. Also, this thesis reports a detailed quantitative study on the nature of forces and moments of podded propulsors at various static and dynamic azimuthing conditions.

The overall goal of this research work is to investigate two aspects of a podded propulsor's hydrodynamics: geometric variations and azimuthing conditions. The first step in the research is to design, modify, model and construct an instrumentation system to test certain pod unit models at specified loading conditions. Chapter 2 provides a basic overview of the design and construction of two pod instrumentation systems, which have been utilized for this research. The chapter also includes details of the propulsor and propeller geometries, and a brief discussion of the experimental set-up and test matrices and the data reduction equations used to present the results. In addition, the chapter provides a brief discussion on the *Reynolds Number* effect in the measurement.

Introduction

Chapter 3 presents details of uncertainty analyses of the two dynamometer systems used to obtain the experimental data for the podded propulsor's study on pod geometry, and at static and dynamic azimuthing conditions. A brief overview of the analysis methodology has been provided, with a particular focus on specific elements that are unique to the experiments. Also, the chapter presents a general discussion on the uncertainty data, followed by a few recommendations of possible ways to reduce the overall uncertainty levels.

Chapter 4 deals with the experimental results and the subsequent analysis to evaluate the most significant geometric parameters in the study of podded propulsor's performance with varied geometry. The experimental results in the pod geometry study at different loading conditions and two pod configurations are presented first. An interpretation of the analyzed data using a design of experiment technique is then described for each of the five geometric parameters. A general discussion on the significant parameters and interaction of parameters in the two configurations is presented at the end of the chapter.

Chapter 5 deals with the results and analyses of the experimental study into the variations of propulsive characteristics of puller and pusher podded propulsors in static azimuthing open water conditions. The variations in forces and moments of the pod unit tested with change of azimuthing angle and advance speed are presented in non-dimensional forms.

Introduction

A general discussion of the comparison of the performance coefficients of the two configurations is also presented.

Chapter 6 presents results and analyses of the experimental study into the effects of dynamic azimuthing conditions on the propulsive characteristics of a puller-podded unit in open water conditions. A comparative study of static and dynamic azimuthing conditions is presented first followed by studies into the effect of azimuthing rate and shaft rps in dynamic azimuthing conditions.

Chapter 7 summarizes the objectives of this thesis. A summary of the experimental results with the trends observed is given. Specific conclusions based on the results and the subsequent analysis on the podded propulsor's study with varied geometry and azimuthing conditions are presented. A few recommendations for future research in this area are also provided.

Next, a list of references is provided that covers the citations in the thesis. Appendices A and B present the relevant supplementary data tables, and the detailed uncertainty data, respectively. Appendix C provides a brief discussion of the use of Fractional Factorial Design (FFD).

CHAPTER

2

**METHODS, MODELS
and INSTRUMENTS**

2 Methods, Models and Instruments

2.1 Chapter Objectives

The objective of this chapter is to describe in detail the methods and equipment utilized to conduct experiments in this investigation. The chapter presents the details of the propeller geometry as well as the pod and strut particulars. In addition, it presents a brief description of the test facilities used in conducting the experiments. Lastly, a brief account of the *Reynolds Number* effect on the measurements is presented.

2.2 Methods

The experimental study of the research work is divided into two parts.

1. The first part focuses on the hydrodynamic performance of podded propulsors with varied geometry and configurations. In this part, a systematic investigation was done to test the effect of geometric parameters of pod-strut-propeller combinations on the propulsive performance of a series of pusher and puller podded propulsors. Five geometric parameters were selected and a fractional factorial design of experiment technique (see section 2.2.1) was used to combine these parameters to obtain a series of 16 pods.
2. The second part focuses on the hydrodynamic performance of podded propulsors at static and dynamic azimuthing conditions. This part has two sections.

2.1. In the first section, two pod models were tested at different static azimuth angles ranging from -30° to 30° at increments of 5° and 10° both in pusher and puller configurations (using a custom-designed pod dynamometer system, see section 2.4.1).

2.2. In the second section, a pod model was tested at dynamic azimuthing angles ranging from 0° to 360° to measure the propeller and unit forces and moments of the propulsors at different azimuthing rate and shaft rps (using a second custom-designed pod dynamometer system, see section 2.4.2).

2.2.1 DOE Methodology to Study Pod Geometry

A brief introduction to the design of experiment technique can be found in Montgomery (2005), Lye (2002), Anderson and Whitcomb (1996), Hawkins and Lye (2006), Myers and Montgomery (2002) and Ryan (2007). The method has two main aspects: design and statistical analysis. This is a very structured approach to experimentation, especially involving large number of variables. The following steps were followed to study the performance of podded propulsors using the method.

- 1. Statement of the problem:** Consider five geometric particulars of the podded propulsors. Evaluate how the geometric parameters and interaction of the parameters affect the performance coefficients of the propulsors in open water conditions and in puller and pusher configurations.

2. **Choice of factors, levels, ranges and response variables:** Using existing commercial pods as a reference, the parameters were selected to study their effects on the performance. The selection of the parameters allowed the variations in the primary dimensions of the propulsor primarily focusing on pod-strut body. The pod length, diameter and taper length, as well as strut distance from the propeller plane, and propeller hub taper angle were chosen as defining parameters of the propulsor (Figure 2.1). The response variables under consideration were thrust and efficiency of both the propeller and the entire unit and the torque in the propeller shaft.

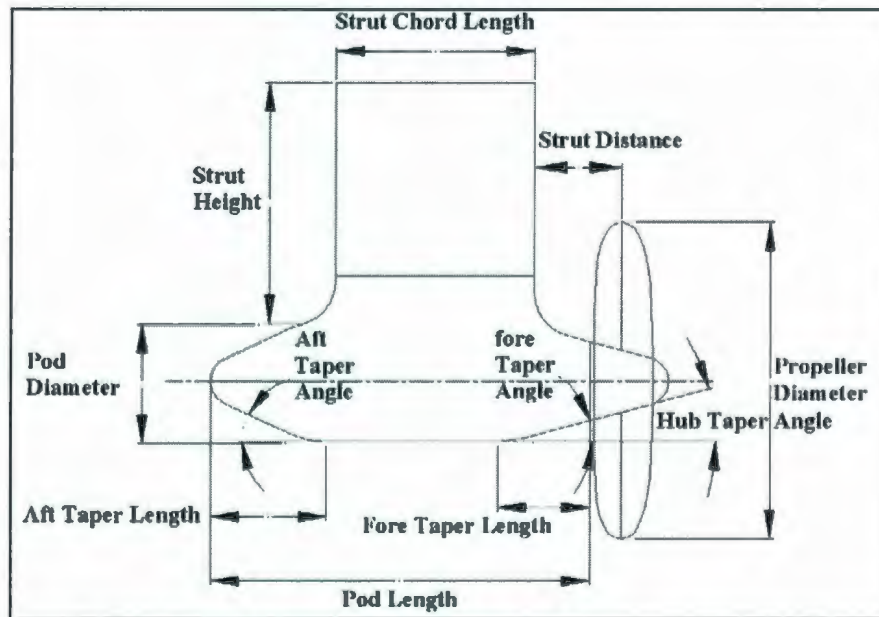


Figure 2.1: Geometric parameters used to define pod-strut geometry.

3. **Choice of experimental design:** Molloy (2003) first initiated a detailed study of the effects of geometric parameters on propulsive performance of podded propulsors using a factorial design of experiment (DOE) technique. A Fractional Factorial

Design (FFD) was used to design the experiments. Appendix C provides a brief discussion on the use of DOE. As mentioned in the appendix and in Montgomery (2005), the half fractional factorial design for the 5 factors resulted in 16 pods with the combination of the factors with the dimensions shown in Table 2.1. The high, low and the average values of the parameters were obtained from the existing commercial pod dimensions.

Table 2.1: Series and average design of podded propulsors (from Molloy, 2003).

External Dimensions of Model Pod	Average Values	Low Values	High Values
Propeller Diameter, D_{Prop} in mm	270	270	270
Pod Diameter, D_{Pod} in mm	139	128	166
Pod Length, L_{Pod} in mm	430	430	524
Strut Distance, S_{Dist} in mm	100	75	133
Aft Taper Length, L_{Taper} in mm	110	69	150
Hub Angle, H_{Angle} in degree	15° & 20°	15°	20°

- 4. Conduct the experiments:** Each of the pod models was tested individually in puller and pusher configurations, separately. Each pod was tested at 17 different advance coefficients as shown in Table 2.3. The tests were done at the fixed propeller shaft rps of 11 at various carriage speeds. The details of the experimental technique and the apparatus are provided in section 2.2.2 and 2.4.1, respectively. It is a standard practice that the series tests that use factorial design are done in a uniform manner and under similar test conditions; mainly the research team, temperature, and humidity should be same. This uniformity ensures that the experimental error (bias error) is minimized throughout the whole process. In most cases, this means running all of the tests in one session, if possible. However, with the size of podded

propulsion model tests and test facility limitations, this was not possible. A method of separating the test series into blocks of runs performed in a prescribed order, which balances the tests so that the experimental error is reduced, is discussed in Montgomery (2005). This method is called “confounding” and it essentially reduces the number of runs per day and gives provisions to repeat runs. The commercial software, Design Expert® (2005) can automate fractional factorial experimental design and analysis process and was used to design and analyze these experiments and the results.

5. **Statistical analysis of the data:** Statistical analysis of the experimental results is a major step in the design of experiment methods. The Analysis of Variance Approach (ANOVA, see Montgomery 2005) incorporating 95% confidence interval was used to examine the geometric parameters of the series that have the most significant impact on the performance of the podded propulsors. The significance of individual factors is ranked in an ascending order based on the estimate of their effects on the overall result of the experiments. A separate analysis was completed for each advance coefficient.

6. **Conclusion and recommendations:** The analysis of the data resulted in the identification of the most significant factors and interactions of factors that affect the propulsive performance of the podded propulsors both in puller and pusher configurations.

2.2.2 Physical Model Tests

The research work was primarily involved towing tank physical model tests in open water conditions. The tests of the pod series consisting of 16 pods, the static azimuthing conditions consisting of two pods and the dynamic azimuthing conditions consisting of one pod were performed in accordance with the ITTC recommended procedure (ITTC Recommended Procedure, 2002) using the test configurations shown in Figure 2.2. A custom-designed dynamometer system called NSERC dynamometer system (MacNeill *et al.* 2004) was used to test the pod units in the geometric series and static azimuthing conditions. Another custom-designed dynamometer system called IOT dynamometer system was used to test the pod units in dynamic azimuthing conditions. A brief description of the two apparatus is provided in section 2.4.1 and 2.4.2, respectively.

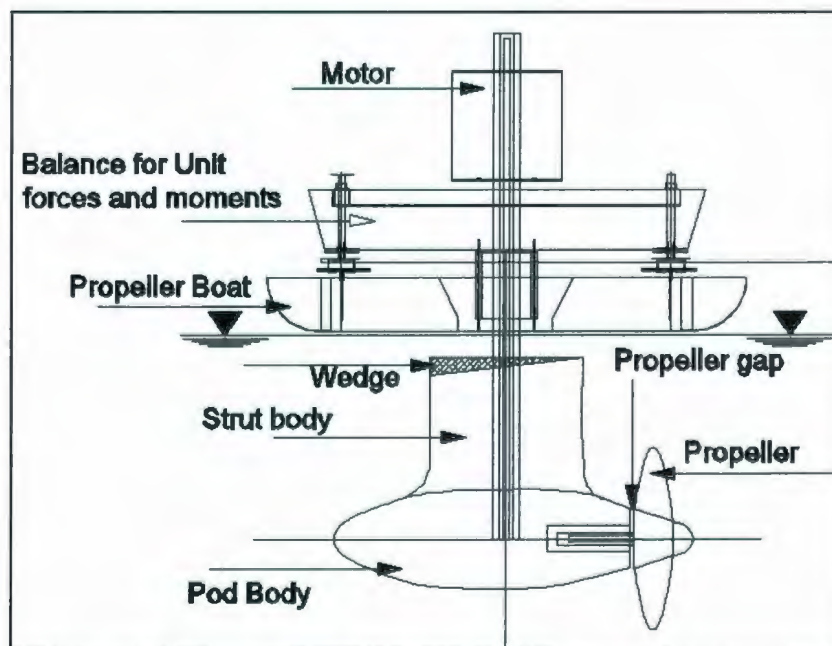


Figure 2.2: Podded propulsors in open water test set-up (Atlar *et al.* 2005).

Methods, Models and Instruments

For the pod series tests, a dynamometer was used to measure the following items:

- ✓ Propeller thrust (T_{Prop})
- ✓ Propeller torque (Q)
- ✓ Unit axial force (F_X) and moment (M_X)
- ✓ Unit transverse force (F_Y) and moment (M_Y)
- ✓ Unit vertical force (F_Z) and moment (M_Z)

Here the unit thrust was measured in these experiments as it is of particular relevance for powering predictions for podded propulsors. The unit thrust means the net available thrust for propelling the ship and includes not only the thrust of the propeller, but also the drag and other hydrodynamic forces acting on the pod-strut body. Also the water temperature, carriage speed, V_A and the propeller shaft rps, n , were measured.

Table 2.2 shows the test matrix for the geometric pod series tests. The test plan is for one pod configuration. All of the 16 pods in the pod series were tested at the same test points. This ensured a systematic test of the pod series and also facilitated the analysis process.

Table 2.2: Test matrix for systematic geometric pod series tests.

Configuration	Run Number	Shaft rps	Carriage speed (m/s)
Pusher Mode	17	11	0.0, 0.2, 0.4, 0.6, 0.8, 1.0, 1.2, 1.4, 1.6, 1.8, 2.0, 2.2, 2.4, 2.6, 2.8, 3.0, 3.2 (randomized)
Puller Mode	17	11	0.0, 0.2, 0.4, 0.6, 0.8, 1.0, 1.2, 1.4, 1.6, 1.8, 2.0, 2.2, 2.4, 2.6, 2.8, 3.0, 3.2 (randomized)

Methods, Models and Instruments

The open water static azimuthing angle tests were performed using the NSERC pod dynamometer system. The system (section 2.4.1) was modified to adapt it to different static azimuthing positions and was used to measure similar items, as done in case of the pod series tests.

Table 2.3 shows the test matrix for the static azimuthing tests performed using the two average pods. Both of the pods were tested at the same test points. This ensured a systematic test of the pods and facilitated the analysis process.

Table 2.3: Test matrix for systematic static azimuthing podded propulsors' tests.

Mode	Pod Name	Azimuthing Angle	Shaft rps	Carriage speed (m/s)
Pusher Mode	Average Pod 01	-30°, -20°, -15°, -10°, -5°, 0°, 5°	11	0.0, 0.2, 0.4, 0.6, 0.8, 1.0, 1.2, 1.4, 1.6, 1.8, 2.0, 2.2, 2.4, 2.6, 2.8, 3.0, 3.2 (randomized)
	Average Pod 02	10°, 15°, 20°, 30°		
Puller Mode	Average Pod 01	-30°, -20°, -15°, -10°, -5°, 0°, 5°	11	0.0, 0.2, 0.4, 0.6, 0.8, 1.0, 1.2, 1.4, 1.6, 1.8, 2.0, 2.2, 2.4, 2.6, 2.8, 3.0, 3.2 (randomized)
	Average Pod 02	10°, 15°, 20°, 30°		

The podded propulsor study in dynamic azimuthing conditions was performed using a custom-designed dynamometer and pod system designed and fabricated at National Research Council's Institute for Ocean Technology (IOT). The propeller and unit performance were measured and analyzed at dynamically varying azimuthing angles under different operating conditions. Firstly, a dynamically-azimuthing podded propulsor was tested in puller configurations in open water conditions with 0° to 360° azimuthing.

Methods, Models and Instruments

Secondly, the podded propulsor was tested at different static azimuthing angles for comparison purposes with the dynamic test results. The following measurements were taken:

- ✓ Propeller thrust (T_{Prop})
- ✓ Propeller torque (Q)
- ✓ Unit axial force (F_X) and moment (M_X)
- ✓ Unit transverse force (F_Y) and moment (M_Y)
- ✓ Unit vertical force (F_Z) and moment (M_Z)

In dynamic azimuthing tests, the pod unit with the propeller was rotated about the vertical axis passing through the centre of the strut in a continuous motion as the whole test unit moved forward with a specific advance speed, and the propeller rotated at a certain shaft rps. Measurements were taken for the forces and moments acting on the propeller and the whole pod unit at different advance coefficients, and at different dynamic azimuthing rates. For the dynamic azimuthing study, the tests were done for dynamic azimuthing angles ranging from 0° to 360° at different azimuthing (steering) rates (2° , 5° , 10° , 15° and 20° per second) in puller configurations. Measurements were taken at different advance coefficients ranging from $J=0.0$ to $J=1.20$ at propeller shaft rps of 15. Additional tests were conducted at propeller shaft rps of 8 at the mentioned azimuthing rate to investigate the effects of shaft rps on the performance coefficients at dynamic azimuthing conditions. The same pod unit was used to do the tests at different static azimuthing

angles for comparison purposes with the dynamic test results. Table 2.4 shows the test matrix for the experiments in dynamic azimuthing conditions.

Table 2.4: Test matrix for systematic dynamic azimuthing podded propulsors' tests.

Mode	Azimuth angle (degrees)	Shaft rps, n	Carriage speed (m/s)
Static Azimuth	0, ± 5 , ± 10 , ± 15 , ± 20 , ± 30 , ± 45 , ± 60 , ± 90 , ± 120 , ± 150 , ± 160 , ± 170 , ± 175 , 180	15	0.0, 0.3, 0.45, 0.6, 0.75, 1.05, 1.2, 1.8, 2.1, 2.4, 2.7, 3.0, 3.3, 3.6 (randomized)
Dynamic Azimuth	0 to 360 at different turning rates (2, 5, 10, 15, and 20 per seconds)	0, 8 and 15	0.0, 0.3, 0.45, 0.6, 0.75, 1.05, 1.2, 1.8, 2.1, 2.4, 2.7, 3.0, 3.3, 3.6 (randomized)

2.3 Propeller and Pod Models

2.3.1 Propeller Geometry

Four model propellers were used in the pod series and static azimuthing studies. Two of the propellers were used in the test for the puller configuration and the other two for the pusher configuration. The propellers had the same blade sections with different hub taper angles. The basic geometric particulars of the propellers are given in Table 2.5. Liu (2006) gives the details of the geometry of the model propellers. The four propellers had hub taper angles of 15° (right handed pusher configuration, *Push+15°*), 20° (right handed pusher configuration, *Push+20°*), -15° (left handed puller configuration, *Pull-15°*), -20° (right-handed puller configuration, *Pull-20°*). Following ITTC definition, a left-handed propeller is a propeller, which rotates in the counter clockwise direction when viewed

from astern. A right-handed propeller is a propeller which rotates in the clockwise direction when viewed from astern. Figure 2.3 shows a rendered view and a photograph of the model propellers.

Table 2.5: Basic geometric particulars of the model propellers.

Diameter	270 mm
Number of blade	4
Design advance coefficient, J	0.8
Hub-Diameter ratio, (H/D)	0.26 (based on regular straight hub)
Shaft rps, n	15
Section thickness form	NACA 66 (DTMB Modified)
Section meanline	NACA = 0.8
Blade planform shape	Blade planform shape was based on David Taylor Model Basin model P4119
Expanded area ratio, EAR	0.60
Pitch distribution	Constant, $P/D=1.0$
Skew distribution	Zero
Rake distribution	Zero

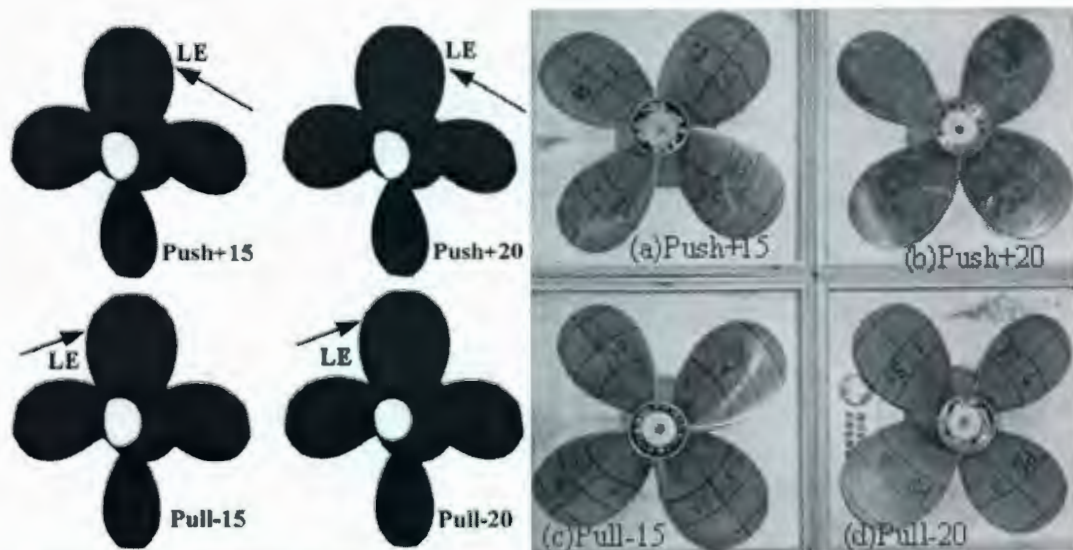


Figure 2.3: Four model propellers (Left hand side - rendered numerical model; Right hand side - physical model): a, b, c, d are the propellers with hub taper angles of $+15^\circ$ (push), $+20^\circ$ (push), -15° (pull), -20° (pull), respectively.

2.3.2 Pod Geometry

As mentioned in Section 2.2.1, 16 pods were manufactured and tested, which were combinations of the five geometric parameters. The combinations that were used in the series tests are listed in Table 2.6 and were selected to include one combination with all dimensions low and one with all dimensions high (Table 2.1). As shown in Table 2.6, propeller diameter was used to obtain non-dimensional forms of the geometrical parameters. The pod HiLo_1 has low values of all the parameters normalized by propeller diameter and the pod HiLo_16 has high values of all the parameters normalized by propeller diameter. This decision was made to allow further testing to compare two pods directly and compare these pods with a pod having intermediate dimensions (Molloy *et al.* 2005). The 16 model pods that were tested in the geometric series tests are shown in Figure 2.4.

Methods, Models and Instruments

Table 2.6: Combinations of dimensions of the 16 pods in the series.

Randomized Order	Factor A	Factor B	Factor C	Factor D	Factor E	Pod Name
	D_{Prop}/D_{Pod}	D_{Prop}/L_{Pod}	D_{Prop}/S_{Dist}	D_{Prop}/TL	H_{Angle}	
	Pod Diameter	Pod Length	Strut Distance	Aft Taper Length	Hub Angle	
Fixed Propeller Diameter, $D_{Prop}=270$ mm						
1	1.63	0.52	2.05	1.8	15	HiLo_1
2	2.11	0.63	2.05	1.8	15	HiLo_4
3	2.11	0.52	2.7	1.8	15	HiLo_10
4	1.63	0.63	2.7	1.8	15	HiLo_11
5	1.63	0.52	2.05	3.91	15	HiLo_5
6	2.11	0.63	2.05	3.91	15	HiLo_8
7	2.11	0.52	2.7	3.91	15	HiLo_14
8	1.63	0.63	2.7	3.91	15	HiLo_15
9	2.11	0.52	2.05	1.8	20	HiLo_2
10	1.63	0.63	2.05	1.8	20	HiLo_3
11	1.63	0.52	2.7	1.8	20	HiLo_9
12	2.11	0.63	2.7	1.8	20	HiLo_12
13	2.11	0.52	2.05	3.91	20	HiLo_6
14	1.63	0.63	2.05	3.91	20	HiLo_7
15	1.63	0.52	2.7	3.91	20	HiLo_13
16	2.11	0.63	2.7	3.91	20	HiLo_16

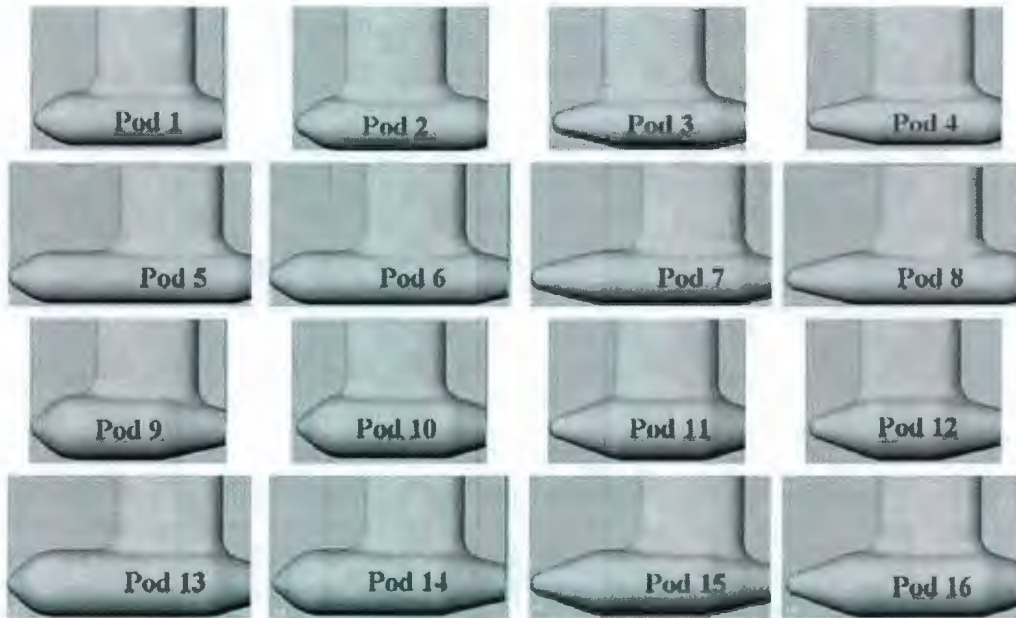


Figure 2.4: Geometric models of the pod series.

Methods, Models and Instruments

For the study of static azimuthing conditions, the two model pod units were used together with the four model propellers mentioned in section 2.3.1. The average values of the parameters (Table 2.1) excluding hub taper angle were used to create two pods (called pod 01 and pod 02, designed to fit the two propellers with hub angles of 15° and 20° , respectively). These two pods were used to perform tests at static azimuthing angles as discussed in section 2.2.2. Two propellers with hub taper angles of 15° and 20° (named as *Push+15°* and *Push+20°*, respectively) were used in combination with the pod series in pusher configurations, and two propellers with hub taper angles of -15° and -20° (named as *Pull-15°* and *Pull-20°*, respectively) were used in combination with the pod series in puller configurations. The pod models had the same geometrical particulars except the fore (propeller) ends, which had two different angles to provide smooth transition between the propeller hub and the subsequent sections of the units. The particulars of the pod-strut body tested are shown in Table 2.7. The geometric particulars of the pod-strut models were defined using the parameters depicted in Figure 2.1. Figure 2.5 shows the rendered and physical model of the two average pods.

Table 2.7. Geometric particulars of the two average pod models.

Geometric Parameters	Pod 01	Pod 02
Propeller Diameter, D_{Prop}	270 mm	270 mm
Pod Diameter, D_{Pod}	139 mm	139 mm
Pod Length, L_{Pod}	410 mm	410 mm
Strut Height, S_{Height}	300 mm	300 mm
Strut Chord Length	225 mm	225 mm
Strut Distance, S_{Dist}	100 mm	100 mm
Strut Width	60 mm	60 mm
Fore Taper Length	85 mm	85 mm
Fore Taper Angle	15°	20°
Aft Taper Length	110 mm	110 mm
Aft Taper Angle	25°	25°

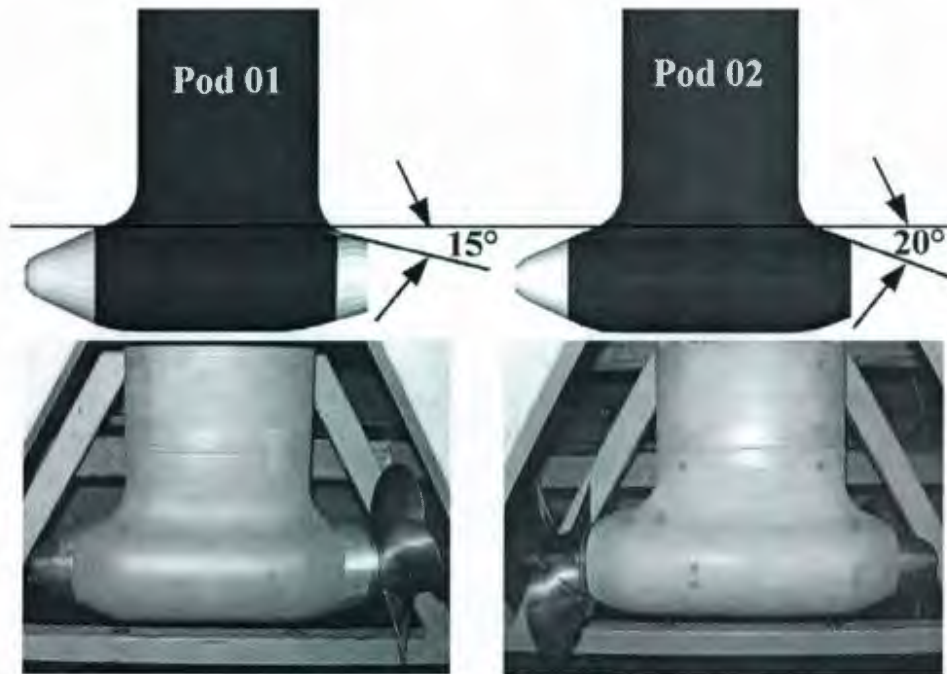


Figure 2.5: Two pod models (top - rendered model; bottom - physical model fitted with propeller): left – Pod 01 and right – Pod02, respectively.

The geometry of the pod unit (pod-strut and the propeller) used in the dynamic azimuthing tests was essentially the same as the dimensions of the *Pull-15°* (left-handed) propeller and the pod-strut body, Pod 01, as mentioned above, only on a reduced scale based on the propeller diameter. The principal dimensions of the pod and the propeller are provided in Table 2.8 below.

Table 2.8: Propeller and pod dimensions used in dynamic azimuthing study.

External Dimensions of Model Pod	Values (mm)
Propeller Diameter	200.0
Hub Angle (degrees)	15°
Pod Diameter	102.9
Pod Length	318.5
Strut Distance	74.1
Taper Length	81.5
Strut Length at Top	132.9
Strut Length at Pod	232.0

2.4 Experimental Set-up

The experimental study of the podded propulsors with varied geometry and static azimuthing conditions was performed using the modified version of the custom-designed dynamometer system called the NSERC pod dynamometer system. The performance study of podded propulsors under various dynamic azimuthing conditions were performed using a custom-designed dynamometer and pod system called the IOT pod dynamometer system. A brief discussion of the two systems is provided in the following sections.

2.4.1 NSERC Pod Dynamometer System

Figure 2.6 is a picture of the experimental apparatus, which has the following major components. For more details, refer to MacNeill *et al.* (2004).

1. Lift System Drive Train: Consists of the electric drive motor, timing pulleys and drive belts to operate lead screws. Each lead screw has a timing pulley to allow for synchronous operation of all four screws to raise or lower the pod unit.
2. Lift System Frameworks: Supporting structure for lift system.
3. Fixed Frame: Frame that rests on the towing carriage rails and provides stability for the rest of the instrumentation package.
4. Live Frame: This frame houses the global dynamometer instrumentation package (which measures the unit forces and moments). This first major part of the NSERC system is mounted on four lead screws that allow the entire pod unit to be raised out

of the water. This frame moves with the pod unit during lifting and it secured to the fixed frame during testing.

5. Main Drive Train: Consists of a 3hp electric motor coupled to a 90° gearbox. This gearbox is connected to the main pulley, which drives the belt that rotates the propeller shaft.
6. Instrumented Pod Unit: This second major part of the NSERC system houses the propeller and pod geometry and contains the sensors for thrust, torque, drag and gap pressure. With the exception of torque, all forces are measured with off the shelf load cells. Torque is measured using strain gauges.

In the instrumentation, a boat shaped body called a wave shroud was attached to the frame of the test equipment and placed just above the water surface. The bottom of the shroud stayed 3 mm to 5 mm above the water surface to suppress waves caused by the strut piercing the surface. A motor fitted above the shroud drove the propeller via a belt system. The centre of the propeller shaft was $1.5D$ below the water surface. The part of the shaft above the strut (the shaft connected the pod unit to the main drive) went through the shroud. Water temperature, carriage speed, V_A , and the propeller shaft rps, n , were also measured.

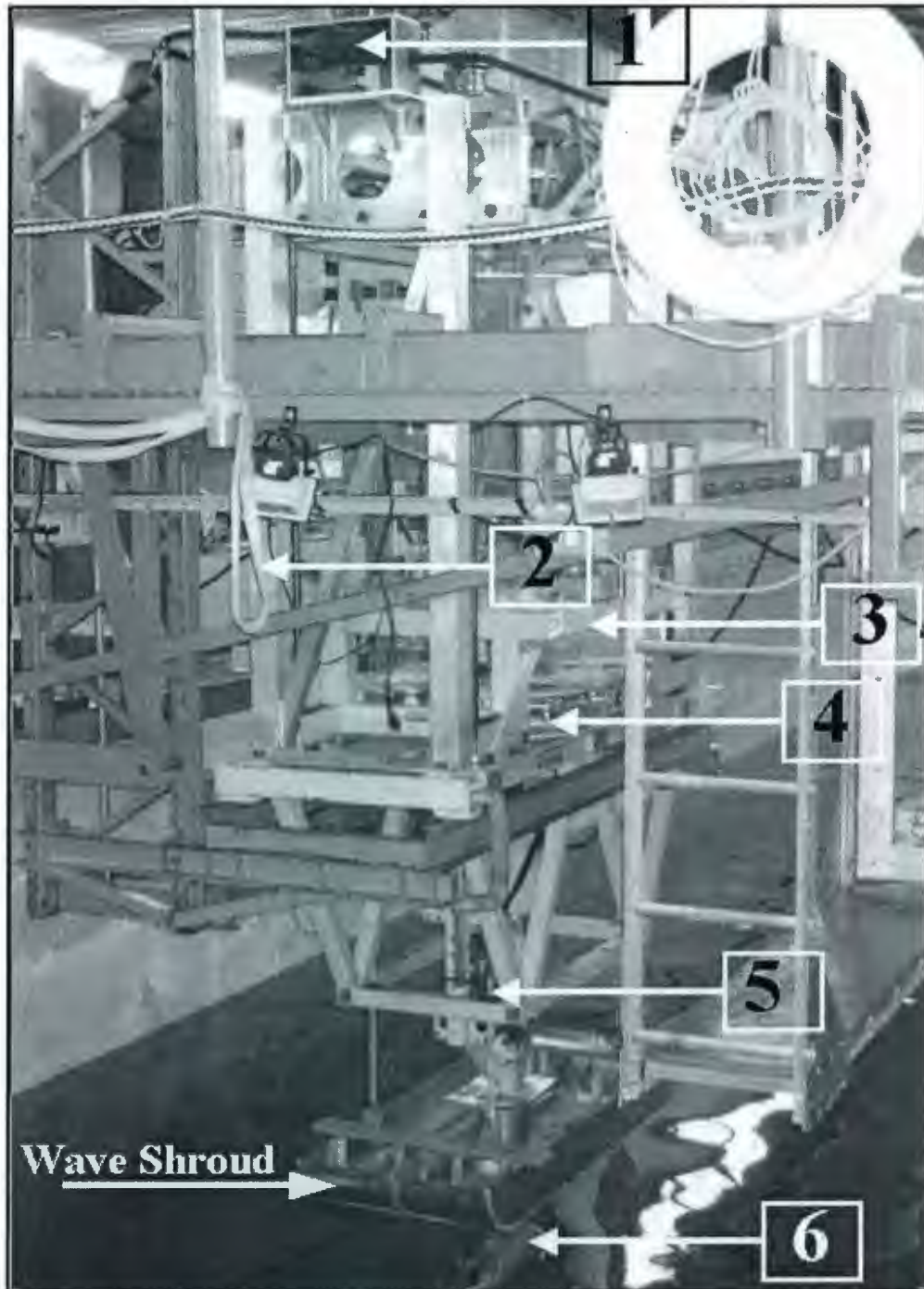


Figure 2.6: Different parts of the experimental apparatus used in the podded propulsor tests. The picture shows the apparatus installed in the OERC (MUN) towing tank.

As shown in Figure 2.6, the dynamometer system has two major parts. The first part is the pod dynamometer, which measures the thrust and torque of the propeller at the propeller shaft. The second part of the system is the global dynamometer, which measures the unit forces in three coordinate directions at a location vertically 1.68m above the pod centre. The moments at the same location about the three coordinate directions are calculated based on the forces at the load cell centre and their relative distance from the pod centre using force and moment balance. The entire lower part hung on a round plate, which had machined marks that defined the azimuth angles. The propulsor was placed at different static azimuthing conditions by rotating the entire lower part of the instrumentation (instrumented pod unit and the main drive as shown in Figure 2.6). In the study of the pod geometry, the 16 model pod units were tested only in straight-ahead conditions. In the static azimuthing tests, the two average pod units were tested at different static azimuthing conditions (from 30° on the port side to -30° on the starboard side at increments of 5° and 10°). At each of the 11 static azimuthing angular positions, the unit was tested at a fixed propeller shaft rps of 11 with varying carriage advance speeds from 0 to 3.56 m/s - a total of 17 speeds. The tests were conducted in the puller configuration first. The propellers, *Pull-15°* and *Pull-20°* were used in these tests. The entire instrumentation was then set up in reverse position to obtain the pusher configuration propulsor by replacing the *Pull-15°* and *Pull-20°* propellers with the *Push+15°* and *Push+20°*, respectively. Similar experiments were carried out in this configuration.

2.4.2 IOT Pod Dynamometer System

The IOT pod dynamometer system, Figure 2.7, the equipment has two major parts. The pod dynamometer measures the thrust and the torque of the propeller at the propeller shaft very close to the hub. The global dynamometer measures the unit forces and moments in three coordinate directions. A motor mounted at the top of the global dynamometer drives the propeller shaft through internal gear arrangement. Another motor arrangement mounted at the top of the seal plate turns the whole pod arrangement in a continuous motion over the horizontal plane (thus providing dynamic azimuthing). The six-component global dynamometer has three load cells measuring forces in the Z (vertically downward) direction; one load cell measuring forces in the X direction (in the direction of propeller advance) and two load cells measuring forces in the Y direction (across the propeller advance direction).

Figure 2.8 shows the propeller boat that was used to hold the dynamometer system. The boat protected the global unit and the data acquisition system from the water spray created by the pod unit. The boat was designed to be round so that it could be installed in any orientation and facilitate the installation of the pod units at any direction in the 360° horizon.

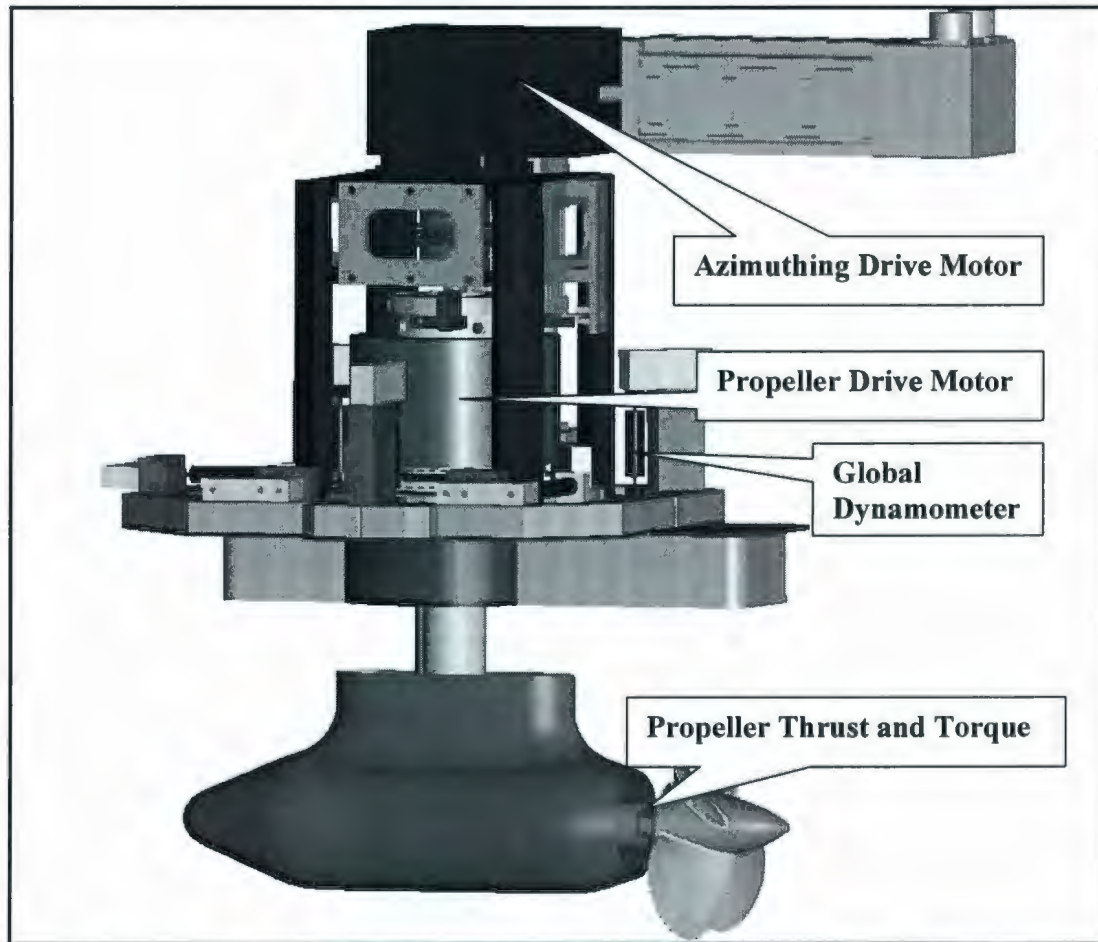


Figure 2.7: Pod and the global dynamometer system designed and fabricated at IOT.

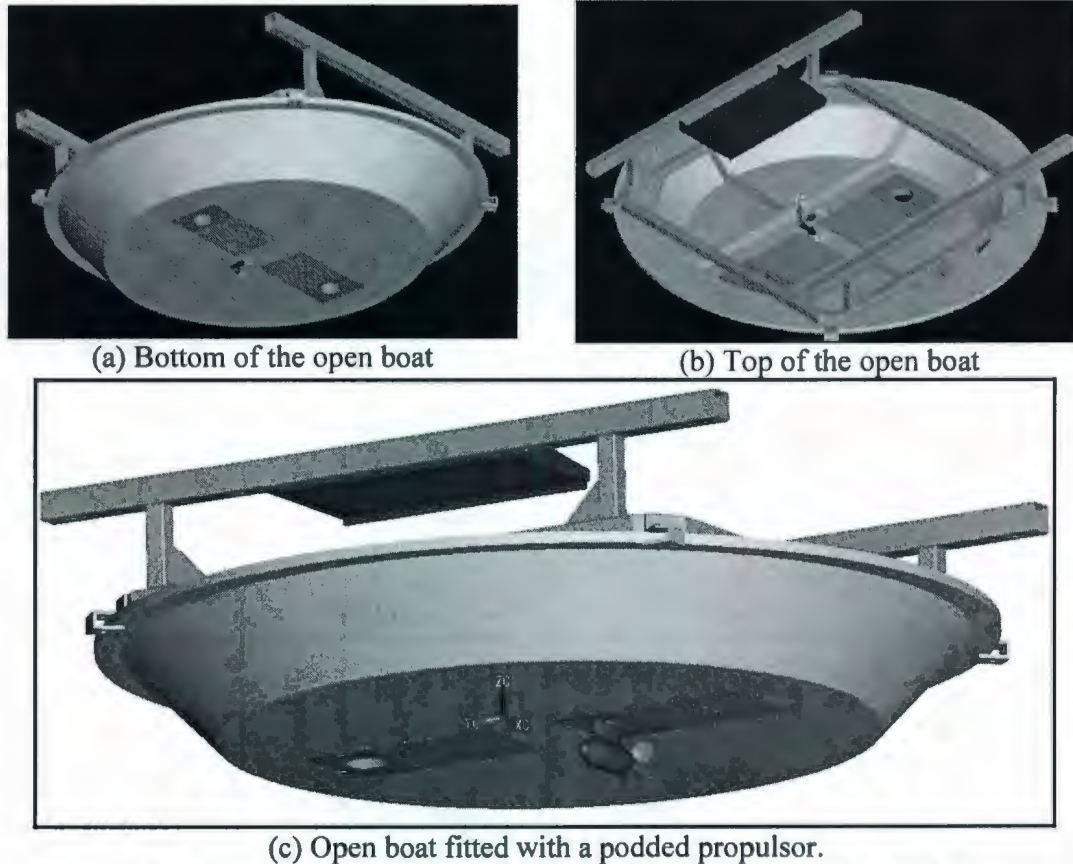


Figure 2.8: The open boat to tests the podded propulsors at static and dynamic azimuthing conditions, designed and fabricated at IOT.

2.5 Experimental Facilities

The open water experiments were performed in the Ocean Engineering Research Centre's (OERC) towing tank at Memorial University of Newfoundland (MUN) and in the large towing tank at the Institute for Ocean Technology (IOT), National Research Council (NRC) Canada.

Memorial University has a testing facility with the following parameters (Table 2.9) (www.engr.mun.ca/naval):

Table 2.9: Particulars of the (OERC) MUN towing tank.

Parameters	Dimensions
Length	58 m
Width	4.5 m
Water Depth	2.2 m
Tow Carriage Speed	5 m/sec
Max. Wave Height (Regular Waves)	0.7 m
Max. Sig. Wave Height (Irregular Waves)	0.2 m
Range of Wavelengths	0.9 m to 17 m

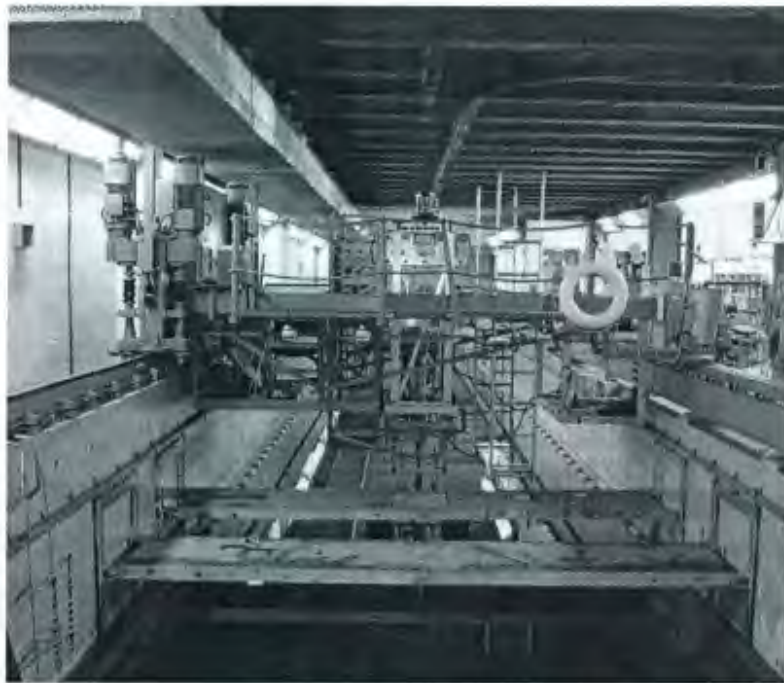


Figure 2.9: NSERC pod dynamometer system installed in the OERC towing tank facility.

The test facilities at MUN were used to perform the systematic geometric series tests in puller and pusher configurations and the static azimuthing angle tests of two average pods in pusher and puller configurations using NSERC pod dynamometer system. Figure 2.9 shows the NSERC pod dynamometer system installed in the OERC towing tank.

Methods, Models and Instruments

IOT has a long towing tank where open water tests with a pod in dynamic azimuthing conditions were performed. The carriage is designed with a central testing area where a test frame, mounted to the carriage frame, allows the experimental setup to move transversely across the entire width of the tank. The parameters of the test facility are given in Table 2.10. Figure 2.10 shows the IOT pod dynamometer system installed in the IOT towing tank.

Table 2.10: Particulars of the IOT Towing Tank.

Parameters	Dimensions
Length	200 m
Width	12 m
Still Water Depth	7 m
Tow Carriage Speed	10 m/sec.
Max. Wave Height	(Regular Waves) 1.0 m
Max. Sig. Wave Height	(Irregular Waves) .50 m
Range of Wavelengths at 7 m Depth	0.50 m – 40 m
Max. Wind Speed 1 m from Fans	11 m/sec.
Max. Wind Speed 5 m from Fan	5 m/sec



Figure 2.10: IOT pod dynamometer system installed in the IOT towing tank facility.

2.6 Coordinate System

The definitions of the forces, moments and co-ordinates that were used to analyze the data and present the results in the study of pod geometry, static and dynamic azimuthing conditions are shown in Figure 2.11. For the NSERC pod instrumentation, the coordinate centre situated vertically 1.68m above the pod centre, which is the intersection of the horizontal axis through the propeller shaft centre and the vertical axis through the strut shaft centre. However, for the IOT pod instrumentation, the coordinate centre was located vertically 0.5m above the pod centre.

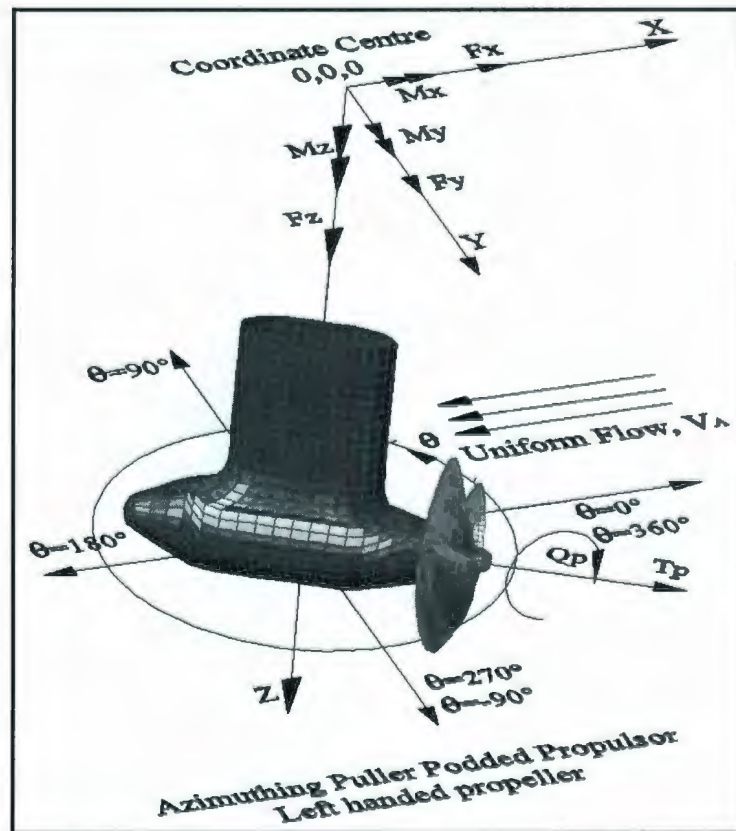


Figure 2.11: Definitions of forces, moments, coordinate of the puller azimuthing podded propulsors.

2.7 Data Reduction Equations

In the current study, both pod dynamometer systems measured propeller and pod forces and moments, namely: propeller shaft thrust (T_{Prop}), propeller shaft torque (Q), unit thrust (T_{Unit}) or unit axial force (F_X) and moment (M_X), unit transverse force (F_Y) and moment (M_Y), and unit vertical force (F_Z) and moment (M_Z).

In both cases, the global dynamometer was calibrated using the method as described by Hess *et al.* (2000) and Galway (1980). The method takes into account cross-talk between the six load cells and produces an interaction matrix to convert the voltage output into the forces and moments in the three coordinate directions. The propeller thrust and torque, unit forces and moments are presented in the form of traditional non-dimensional coefficients as defined in Table 2.11.

Table 2.11: Data reduction equations and definitions of different parameters used to present the experimental data.

Performance Characteristics	Data Reduction Equation
K_{TProp} – propeller thrust coefficient	$T_{Prop} / \rho n^2 D^4$
K_{TUnit} – unit thrust coefficient, or unit axial force coefficient, K_{FX}	$T_{Unit} / \rho n^2 D^4$ or $F_X / \rho n^2 D^4$
$10K_Q$ – propeller torque coefficient	$10Q / \rho n^2 D^5$
J – propeller advance coefficient	V_A / nD
η_{Prop} – propeller efficiency	$J / 2\pi \times (K_{TProp} / K_Q)$
η_{Unit} – unit efficiency	$J / 2\pi \times (K_{TUnit} / K_Q)$
K_{FY} – transverse force coefficient	$F_Y / \rho n^2 D^4$
K_{FZ} – vertical force coefficient	$F_Z / \rho n^2 D^4$
K_{MX} – moment coefficient about x axis	$M_X / \rho n^2 D^5$
K_{MY} – moment coefficient about y axis	$M_Y / \rho n^2 D^5$
K_{MZ} – moment coefficient about z axis (steering moment)	$M_Z / \rho n^2 D^5$

General definitions

T_{Prop} - propeller thrust

ρ - water density

T_{Unit} - unit thrust

n - propeller shaft rps

Q - propeller torque

D - propeller diameter

V_A - propeller advance speed, in the direction of carriage motion

$F_{X,Y,Z}$ - components of the hydrodynamic force on the pod

$M_{X,Y,Z}$ - components of the hydrodynamic moment on the pod

It should be noted that propeller advance coefficient, J is defined using the propeller advance speed, V_A in the direction of carriage motion (in the direction of X in the inertia frame), not in the direction of propeller axis. The propeller thrust, T_{Prop} is defined in the direction of the propeller axis, and F_X is the projected forces on the X-axis in the inertia frame.

2.8 Study of *Reynolds Number* Effects

Testing done on model propellers must be at shaft rps that allows the propeller to operate in a flow regime that minimizes laminar flow on the suction side or flow separation on the trailing edge. In the case of open-water measurements, a convenient procedure is to perform tests at a shaft rps that allows operation in a flow regime where laminar flow on the blade suction side, or flow separation at the trailing edge are minimized. Hence, a closer similarity to full-scale conditions is achieved. For the present study, two separate scale effect tests were carried out, namely: the 'propeller only case' and the 'propeller with pod-strut or unit case'. Table 2.12 shows the combination of propeller shaft rps and advance speed used to study the *Reynolds Number* effect for the two propellers used in the experimentation of the podded propulsors in static and dynamic azimuthing conditions.

Table 2.12: A List of *Reynolds Number* and the operating condition used to study the *Reynolds Number* effects for propeller only cases.

<i>Reynolds Number</i> based on propeller chord length at 0.7R, $R_N = C_{0.7R} \times \sqrt{(V_A^2 + 0.7\pi n D^2)} / \nu, D=200 \text{ mm}$				<i>Reynolds Number</i> based on propeller chord length at 0.7R, $R_N = C_{0.7R} \times \sqrt{(V_A^2 + 0.7\pi n D^2)} / \nu, D=270 \text{ mm}$			
Shaft rps, <i>n</i>	Adv speed, V_A	Adv. coeff., <i>J</i>	R_N	Shaft rps, <i>n</i>	Adv speed, V_A	Adv. coeff., <i>J</i>	R_N
10	0.00	0.00	3.19E+05	10	0.00	0.00	5.81E+05
10	1.60	0.80	3.39E+05	10	2.16	0.80	6.19E+05
10	2.50	1.25	3.67E+05	10	3.38	1.25	6.69E+05
15	0.00	0.00	4.78E+05	15	0.00	0.00	8.72E+05
15	2.40	0.80	5.09E+05	15	3.24	0.80	9.28E+05
15	3.75	1.25	5.50E+05	15	5.06	1.25	1.00E+06
20	0.00	0.00	6.38E+05	20	0.00	0.00	1.16E+06
20	3.20	0.80	6.79E+05	20	4.32	0.80	1.24E+06
20	5.00	1.25	7.34E+05	20	6.75	1.25	1.34E+06
25	0.00	0.00	7.97E+05	25	0.00	0.00	1.45E+06
25	4.00	0.80	8.48E+05	25	5.40	0.80	1.55E+06
25	6.25	1.25	9.17E+05	25	8.44	1.25	1.67E+06
30	0.00	0.00	9.57E+05	30	0.00	0.00	1.74E+06
30	4.80	0.80	1.02E+06	30	6.48	0.80	1.86E+06
30	7.50	1.25	1.10E+06	30	10.13	1.25	2.01E+06
35	0.00	0.00	1.12E+06	35	0.00	0.00	2.03E+06
35	5.60	0.80	1.19E+06	35	7.56	0.80	2.17E+06
35	8.75	1.25	1.28E+06	35	11.81	1.25	2.34E+06
		Max R_N	1.28E+06			Max R_N	2.34E+06
		Min R_N	3.19E+05			Min R_N	5.81E+05

As shown in Table 2.12, for the larger propeller, the shaft rps and the speed of advance must be very high to reach the recommended value of the *Reynolds Number* of 1×10^6 (shaft rps of 15 and advance speed of 5.06 m/s is required). Again, for the smaller propeller, a shaft rps of 30 and advance speed of 4.8 m/s is required to obtain *Reynolds Number* of 1×10^6 .

The *Reynolds Number* effect study was carried out with the two propellers (propeller only case) using a *Kemph* and *Remmers* dynamometer. Figure 2.12 shows the curves of the propeller coefficients of the 270 mm diameter and 200 mm diameter propellers,

respectively for different *Reynolds Number* (by changing shaft rps and carriage advance speed) at fixed advance coefficients. It can be noticed that for the propeller with 270 mm diameter, for shaft rps 10 or higher (corresponding *Reynolds Number* of 5.81×10^5 or higher), the performance coefficients do not change significantly, which confirms minimized *Reynolds Number* effect. Again, for the 200 mm diameter propeller, for shaft rps 15 or higher (corresponding *Reynolds Number* of 4.78×10^5 or higher), the performance coefficients do not change significantly. It is also noticed that that the performance coefficients of the smaller propeller stabilized at lower *Reynolds Numbers* than expected as also observed by Jessup *et al.* (2002).

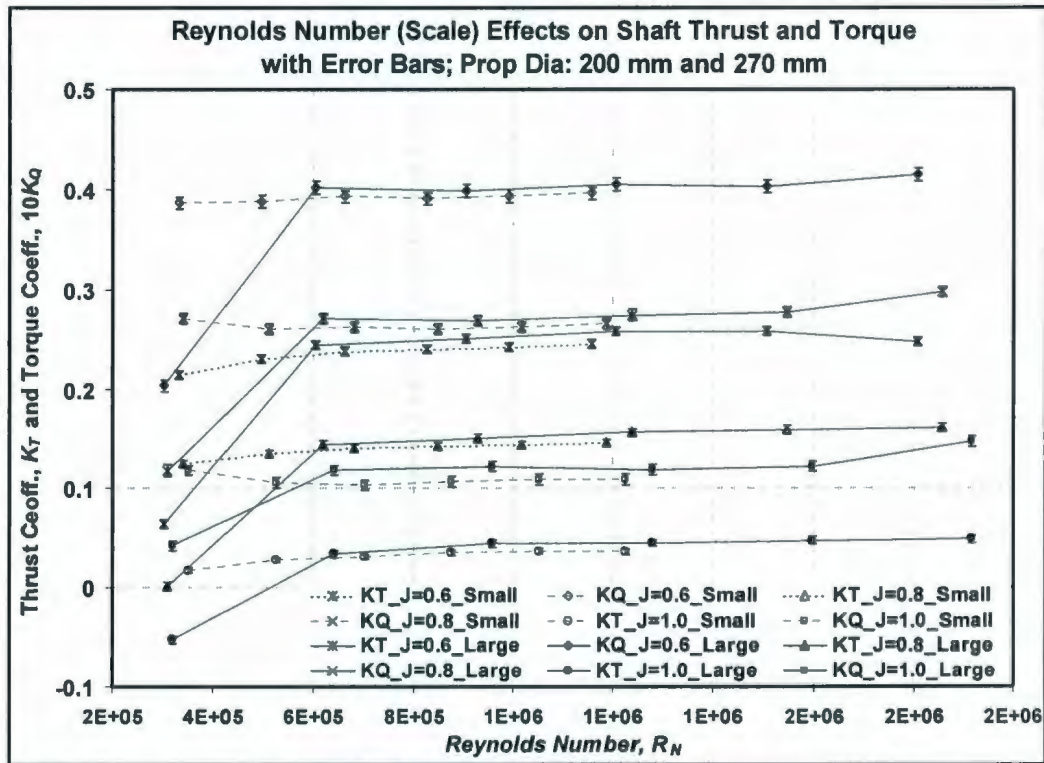


Figure 2.12: Open water coefficients of the podded propellers (large propeller with diameter 270 mm and small propeller with diameter 200 mm).

The NSERC dynamometer system was used to investigate the *Reynolds Number* effect of the pod model, average Pod 01. A various combinations of propeller shaft rps and carriage advance speed were used to study the performance of the model pod at various *Reynolds Numbers* both in puller and pusher configurations. In puller configuration, for the Pod 01, Figures 2.13a to 2.13c show the plots of propeller thrust, torque and unit thrust coefficients against *Reynolds Number* at different advance coefficients, respectively. It is observed that the value of the performance coefficients started to stabilize at *Reynolds Number* of 6.5×10^5 or above (equivalent to propeller shaft rps of 11 or more). This is approximately true for all other advance coefficients. This suggests that the propeller tested at shaft rps of 11 or above would be at minimized *Reynolds Number* effects. Figures 2.14a to 2.14c show the same performance coefficients in the same conditions for the pusher configurations.

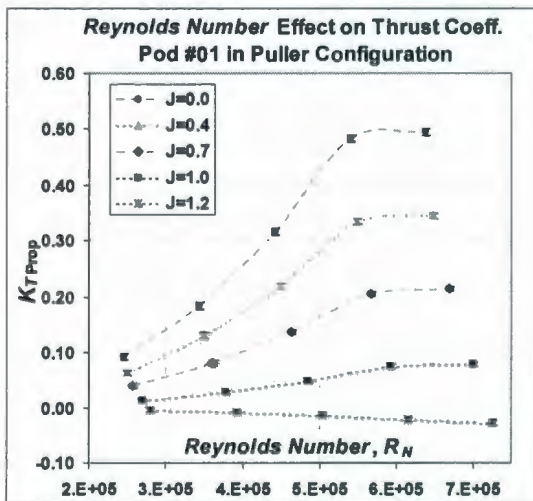


Figure 2.13a: *Reynolds Number* effect tests on propeller thrust coefficient in puller configuration podded propulsors.

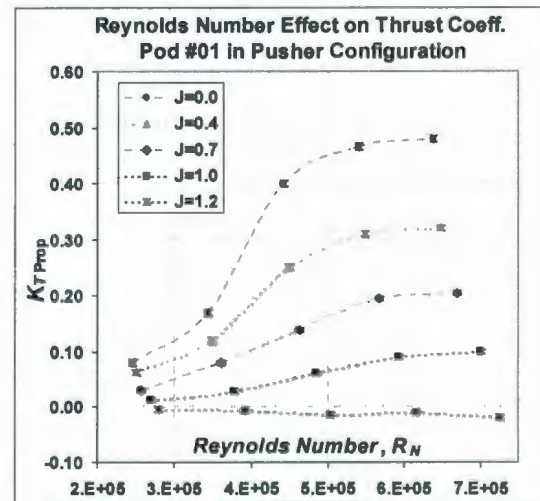


Figure 2.14a: *Reynolds Number* effect tests on propeller thrust coefficient in pusher configuration podded propulsors.

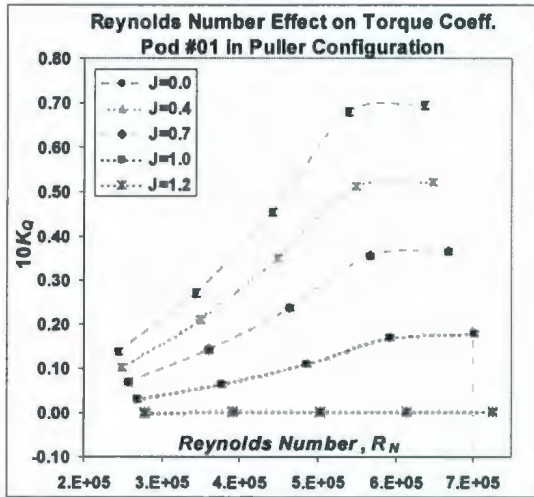


Figure 2.13b: *Reynolds Number* effect tests on propeller torque coefficient in puller configuration podded propulsors.

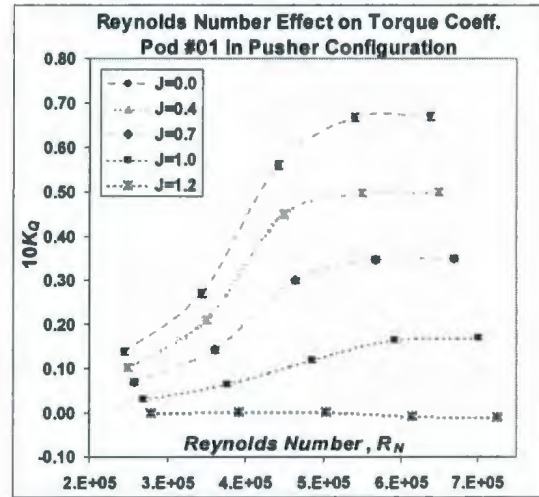


Figure 2.14b: *Reynolds Number* effect tests on propeller torque coefficient in pusher configuration podded propulsors.

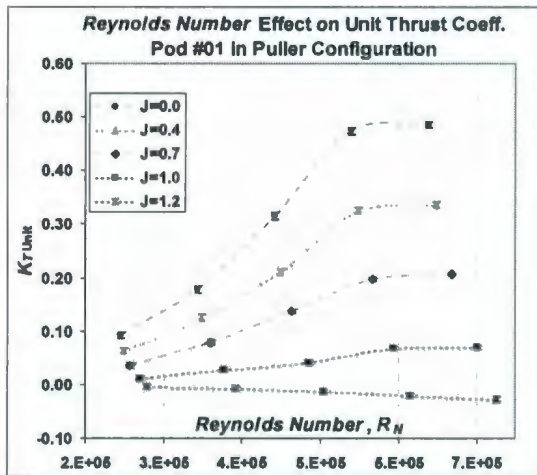


Figure 2.13c: *Reynolds Number* effect tests on unit thrust coefficient in puller configuration podded propulsors.

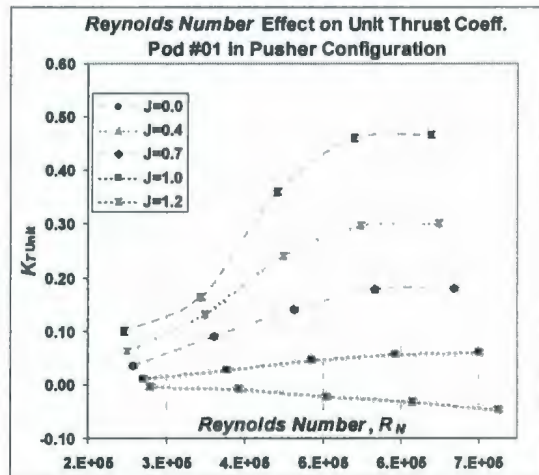


Figure 2.14c: *Reynolds Number* effect tests on unit thrust coefficient in pusher configuration podded propulsors.

2.9 Summary

This chapter has provided a presentation of the experimental methods, model geometry, test program and test facilities utilized in conducting the experimentation on the podded propulsor model units with a view to carry out quantitative investigations on the hydrodynamic performance with varied geometry and azimuthing conditions. The design of experiment technique used to obtain the pod series consisting of 16 pods with combinations of five geometrid parameters is detailed. The test program and technique to carry out the open water experiments at static and dynamic azimuthing conditions are presented. The geometric particulars of the propellers and pods used in the testing are also provided. The test equipment used to conduct the tests with the pods both in static and dynamic azimuthing tests are described. A brief description of the test facilities used for both static and dynamic azimuthing studies is presented. A brief discussion on the *Reynolds Number* effect study of the bare propellers and the pod unit is also provided.

CHAPTER

3

**UNCERTAINTY
ANALYSIS**

3 Uncertainty Analysis

3.1 Chapter Objectives

This chapter presents details of uncertainty analysis of the experimental data obtained for the podded propulsor's study on pod geometry, and at static and dynamic azimuthing conditions using the dynamometer systems (NSERC pod dynamometer system and IOT pod dynamometer system). The general recommendations and guidelines provided by the International Towing Tank Conference (ITTC) for uncertainty analysis for resistance and propulsion tests are most closely aligned with the testing techniques used to study the uncertainty in the dynamometers. The methodology used in the analysis of the uncertainty in the experimentation of puller and pusher podded propulsors follows the recommended guidelines set out by the ITTC in combination with approaches described by Bose and Luznik (1996), Coleman and Steele (1999), and Hess *et al.* (2000). A brief overview of the analysis methodology is provided, with a particular focus on specific elements that are unique to these experiments. A general discussion on the uncertainty data is provided, followed by a few recommendations of possible ways to reduce the overall uncertainty levels.

3.2 Components of Measurement Uncertainty

As described in Coleman and Steele (1999), uncertainty in a measurement consists of two major components: bias error and precision error. Bias error is a constant, systematic

error in the system or process, which may be reduced through calibration, whereas, precision error is the random contribution often referred to as repeatability error, which can be reduced through the use of multiple readings.

3.2.1 Bias Error

Considering the forces and moments applied to a dynamometer during calibration and testing, analysis of the sources of bias error depends upon the calibration as well as testing methods employed. For example, consider a calibration stand using weight pans connected to cables passing through pulleys to apply loading to a dynamometer. If the calibration stand has not been accurately levelled, applied forces and moments will not be as expected. If various geometrical distances associated with the calibration stand are inaccurately measured, applied forces and moments will be affected by this inaccuracy. If the weights used to load the pans have drifted such that their true weight is not their stated weight, additional bias errors will creep into the calibration. If the pulleys do not have ideal, frictionless bearings, the true applied forces and moments will be altered by pulley resistance. Variation in physical constants can lead to bias errors as well; this is often the case when thermal variations are present. Incorrect experimental methods can lead to bias errors. For example, application of forces and moments during calibration in ascending or descending order as opposed to a random order can lead to a bias uncertainty. Identification of elemental bias errors for other types of dynamometer calibration equipment, such as load cells, would proceed in a similar fashion.

Uncertainty Analysis

Sources of bias error are also present in the output from the dynamometer. For example, biases may be present in the A/D converter, the amplifier gain, and the applied excitation voltage. For example, a quantization bias error in the analog to digital converter is usually taken to be one half of the least significant bit. Biases from the amplifier and power supply should be identified from manufacturer's specifications and should include factors such as gain, linearity and zero errors. Hess *et al.* (2000) suggested that the biases in the output from the dynamometer be calculated using the following equation.

$$\frac{\mu V}{V_{ex}} = bits * \left(\frac{20}{4096} \frac{V}{bit} \right) * \left(1000000 \frac{\mu V}{V} \right) * \left(\frac{1}{Gain} \right) * \left(\frac{1}{V_{ex}} \right)$$

Where, V_{ex} is the excitation voltage used to power the dynamometer.

A detailed accounting of the sources of bias error is often difficult and requires a careful analysis of the calibration device, physical constants and geometrical data, associated experimental equipment and calibration procedures. Because of the expense that such a thorough examination may entail, one should perform a cursory investigation to estimate the order of magnitude of the biases. If all biases are negligible when compared to precision uncertainties, then clearly precision uncertainty will dominate, and setting the biases to zero will not significantly alter the calculation.

3.2.2 Precision Error

Precision error is determined by repetition. For the dynamometer calibration device, the ability to repeatedly apply a given force or moment must be quantified. If F_i is a force

Uncertainty Analysis

component applied by the calibration device during the i^{th} repetition, and N is the total number of measurements (spots) by an independent force gauge (calibration standard), then compute a mean and a standard deviation using:

$$\text{Mean of forces or moments, } \bar{F} = \frac{1}{N} \sum_{i=1}^N F_i$$

$$\text{Standard deviation of forces or moments, } S_F = \left[\frac{1}{N-1} \sum_{i=1}^N (F_i - \bar{F})^2 \right]^{1/2}$$

A 95% confidence estimate of the precision uncertainty at a specific magnitude of applied force is estimated as: $P_F = t S_F / \sqrt{N}$; where, t represents a value drawn from the Student's t distribution for a 95% confidence level and $N - 1$ degrees of freedom. It should be carefully noted that, if N is small, then a 95% confidence level estimate will be large due to the paucity of the data; 5 to 10 trials should be sufficient to characterize the uncertainty level for a given force magnitude. One must perform this computation for a selection of force magnitudes throughout the dynamic range of the device. Similarly, the precision uncertainty of the output from the dynamometer, expressed in $\mu V / V_{ex}$ (see equation 1.1), should be determined from repetitions with the same applied force or moment combination for a selection of force magnitudes throughout the dynamic range of the device. If all precision errors are negligible when compared to bias uncertainties, then clearly bias uncertainty will dominate, and setting the precision errors to zero will not significantly alter the calculation.

3.3 The Uncertainty Expressions

The overall uncertainty in the non-dimensional performance coefficients, as shown in Table 2.12 in section 2.6, of the podded propulsors require proper identification of all the variables contained within the data reduction expressions. Thus, the variables of interest in the podded propulsors uncertainty analysis were propeller thrust, unit thrust, propeller torque, forces and moments on the propulsor in the three orthogonal directions, propeller shaft rps, carriage advance speed, azimuthing angle, water density (function of water temperature) and propeller diameter. Figure 3.1 shows a block diagram for the podded propulsor open water tests including the individual measurement systems, measurement of individual variables, data reduction and experimental results.

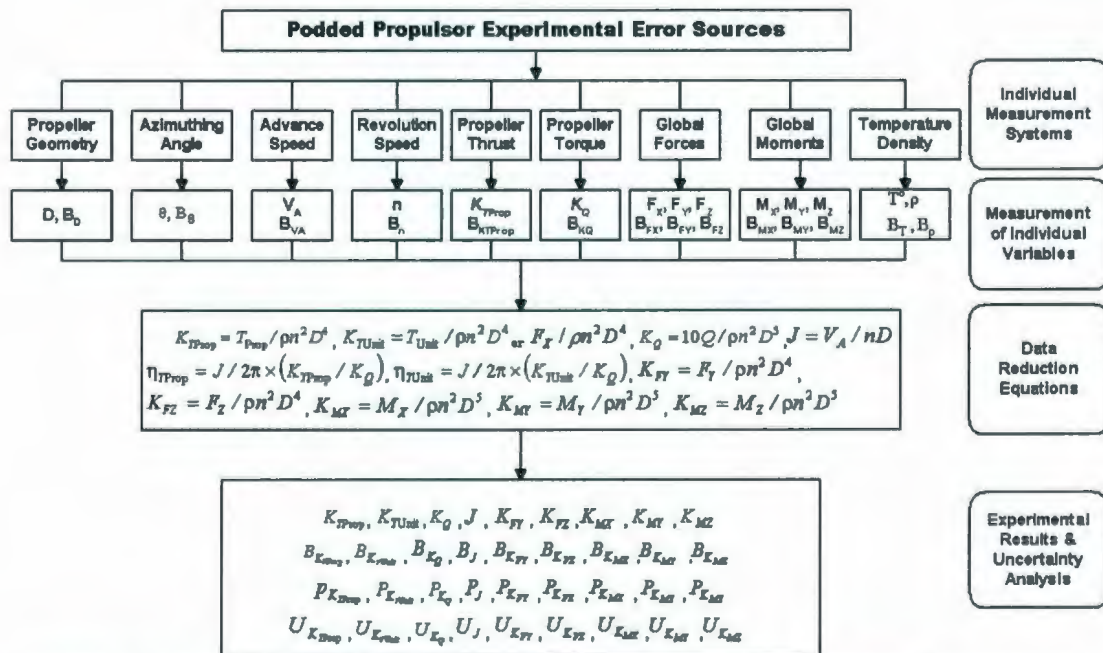


Figure 3.1: Block diagram for podded propulsor open water tests and uncertainty analysis.

Uncertainty Analysis

The experimental approaches used to obtain the data for each of these variables were influenced by a variety of elemental sources of error. These elemental sources were estimated, as detailed in Appendix B, and combined using the root sum square (RSS) method to give the bias and precision limits for each of the variables. The bias errors were consisted of many elemental sources of error, which depended on the approaches followed to measure the variables. However, for the precision error estimates of most variables, only one source of error (repeatability) was considered significant.

The error estimates used in the determination of the bias and precision errors in this study were considered to be a 95% coverage estimates. The bias uncertainty and the precision uncertainty were combined using the root sum square (RSS) method shown below to provide estimates of overall uncertainty levels in these variables. The overall uncertainty was thus considered to be a 95% coverage estimate.

$$U_v = \sqrt{B_v^2 + P_v^2}$$

The final step in the methodology of uncertainty analysis was to determine how uncertainties in each of the variables propagate through the data reduction equations (see Table 3.12). Using the approaches described by Bose and Luznik (1996), and Coleman and Steele (1999) the uncertainty expressions for each set of experiments were developed as shown in equation 3.1 to 3.9.

$$\left(\frac{U_{K_{TProp}}}{K_{TProp}}\right)^2 = \left(\frac{U_{TProp}}{T_{Prop}}\right)^2 + \left(\frac{U_{\rho}}{\rho}\right)^2 + 4\left(\frac{U_n}{n}\right)^2 + 16\left(\frac{U_{D_{Prop}}}{D_{Prop}}\right)^2 \quad (3.1)$$

$$\left(\frac{U_{K_Q}}{K_Q}\right)^2 = \left(\frac{U_Q}{Q}\right)^2 + \left(\frac{U_{\rho}}{\rho}\right)^2 + 4\left(\frac{U_n}{n}\right)^2 + 25\left(\frac{U_{D_{Prop}}}{D_{Prop}}\right)^2 \quad (3.2)$$

$$\left(\frac{U_{K_{TUnit}}}{K_{TUnit}}\right)^2 = \left(\frac{U_{TUnit}}{T_{Unit}}\right)^2 + \left(\frac{U_{\rho}}{\rho}\right)^2 + 4\left(\frac{U_n}{n}\right)^2 + 16\left(\frac{U_{D_{Pr op}}}{D_{Pr op}}\right)^2 \quad (3.3)$$

$$\left(\frac{U_{F_Y}}{K_{F_Y}}\right)^2 = \left(\frac{U_{F_Y}}{F_Y}\right)^2 + \left(\frac{U_{\rho}}{\rho}\right)^2 + 4\left(\frac{U_n}{n}\right)^2 + 16\left(\frac{U_{D_{Pr op}}}{D_{Pr op}}\right)^2 \quad (3.4)$$

$$\left(\frac{U_{F_Z}}{K_{F_Z}}\right)^2 = \left(\frac{U_{F_Z}}{F_Z}\right)^2 + \left(\frac{U_{\rho}}{\rho}\right)^2 + 4\left(\frac{U_n}{n}\right)^2 + 16\left(\frac{U_D}{D}\right)^2 \quad (3.5)$$

$$\left(\frac{U_{K_{M_X}}}{K_{M_X}}\right)^2 = \left(\frac{U_{M_X}}{M_X}\right)^2 + \left(\frac{U_{\rho}}{\rho}\right)^2 + 4\left(\frac{U_n}{n}\right)^2 + 25\left(\frac{U_{D_{Pr op}}}{D_{Pr op}}\right)^2 \quad (3.6)$$

$$\left(\frac{U_{K_{M_Y}}}{K_{M_Y}}\right)^2 = \left(\frac{U_{M_Y}}{M_Y}\right)^2 + \left(\frac{U_{\rho}}{\rho}\right)^2 + 4\left(\frac{U_n}{n}\right)^2 + 25\left(\frac{U_{D_{Pr op}}}{D_{Pr op}}\right)^2 \quad (3.7)$$

$$\left(\frac{U_{K_{M_Z}}}{K_{M_Z}}\right)^2 = \left(\frac{U_{M_Z}}{M_Z}\right)^2 + \left(\frac{U_{\rho}}{\rho}\right)^2 + 4\left(\frac{U_n}{n}\right)^2 + 25\left(\frac{U_{D_{Pr op}}}{D_{Pr op}}\right)^2 \quad (3.8)$$

$$\left(\frac{U_J}{J}\right)^2 = \left(\frac{U_{V_A}}{V_A}\right)^2 + \left(\frac{U_n}{n}\right)^2 + \left(\frac{U_{D_{Pr op}}}{D_{Pr op}}\right)^2 \quad (3.9)$$

In the expressions for the podded propulsors' tests, it should be noted that for thrust and torque coefficient uncertainties, the tare thrust and frictional torque were imbedded in the corresponding measurements. Since the tare thrust and frictional torque were part of the same data stream as the thrust and torque readings, it had not been treated as an independent contributor of error to the corresponding coefficients, but rather has been treated as a bias error on the static zero value of the thrust and the torque measurements.

3.3.1 Uncertainty in the Six-Component Global Dynamometer

The calibration of the six degree of freedom NSERC and IOT global dynamometer yielded an $N \times M$ array of applied force and moment components, \mathbf{F} , and an $N \times M$ array of corresponding output voltages, \mathbf{V} (Islam 2006c). To each element of the \mathbf{F} and \mathbf{V} arrays

there was a corresponding bias and precision uncertainty that had been determined as described in Appendix B.

In order to calculate uncertainty in a six-component dynamometer measurement, one must determine how the uncertainties in the calibration data propagates into each element of the interaction matrix and into future measured forces and moments. As described in Hess *et al.* (2000), the solution for interaction matrix is given as:

$$\mathbf{C} = (\mathbf{V}^T \mathbf{V})^{-1} \mathbf{V}^T \mathbf{F}$$

If we consider one dynamometer axis at a time (one column of \mathbf{C} and \mathbf{F}), then the equation can be rewritten as:

$$\mathbf{V}^T \mathbf{V} \mathbf{C}_i = \mathbf{V}^T \mathbf{F}_i$$

which is a classic form of the normal equations for a least squares fit problem. To determine the bias and precision uncertainty propagated into each column of the interaction matrix, one must determine how uncertainty in input data propagates into the coefficients of a least squares fit. Similarly, to determine the uncertainty present in future measured forces and moments from the fit ($\mathbf{F}=\mathbf{V}\mathbf{A}$), one must understand how uncertainty propagates through a least squares fit into the output.

As given in Hess *et al.* (2000), the uncertainty propagated into the slope, m , for a linear least square fit of the form, $y=mx+b$ is of the form:

$$U_m = \left[\begin{array}{l} \left(\frac{\partial m}{\partial x_1} U_{x_1} \right)^2 + \left(\frac{\partial m}{\partial x_2} U_{x_2} \right)^2 + \left(\frac{\partial m}{\partial x_3} U_{x_3} \right)^2 + \dots + \left(\frac{\partial m}{\partial x_N} U_{x_N} \right)^2 \\ + \left(\frac{\partial m}{\partial y_1} U_{y_1} \right)^2 + \left(\frac{\partial m}{\partial y_2} U_{y_2} \right)^2 + \left(\frac{\partial m}{\partial y_3} U_{y_3} \right)^2 + \dots + \left(\frac{\partial m}{\partial y_N} U_{y_N} \right)^2 \end{array} \right]^{1/2} \quad (3.10)$$

Uncertainty Analysis

Thus, the uncertainty in the slope depends upon the uncertainties in each of the abscissas and ordinates of the raw data used to construct the fit. Thus, one must determine the partial derivatives, $\partial m / \partial x_i$ and $\partial m / \partial y_i$, which are found to be of the form:

$$\frac{\partial m}{\partial x_i} = \frac{Ny_i - \sum y_i - 2m(Nx_i - \sum x_i)}{N \sum x_i^2 - (\sum x_i)^2}$$

and

$$\frac{\partial m}{\partial y_i} = \frac{Nx_i - \sum x_i}{N \sum x_i^2 - (\sum x_i)^2}$$

where,

$$m = \frac{N \sum_{i=1}^N x_i y_i - \sum_{i=1}^N x_i \sum_{i=1}^N y_i}{N \sum_{i=1}^N x_i^2 - \left(\sum_{i=1}^N x_i \right)^2}$$

For a six degree of freedom dynamometer system, the uncertainty in each of the element of the interaction matrix is obtained using equation 3.10 where U_x and U_y are the uncertainties in the voltage and applied load measurements for each of the N loading conditions.

In the present case, a total loading cases of $N=195$ was obtained. The applied loads to the calibration frame designed specifically for the dynamometer system (Islam 2006c) were converted to forces and moments in the three coordinate directions. In the matrix form, the forces and moments and the corresponding voltage output from the six-component dynamometer are expressed as:

Uncertainty Analysis

$$F = \begin{bmatrix} F_{1,1} & - & - & - & - & F_{1,6} \\ - & - & - & - & - & - \\ - & - & - & - & - & - \\ - & - & - & - & - & - \\ F_{195,1} & - & - & - & - & F_{195,6} \end{bmatrix} \text{ and } V = \begin{bmatrix} V_{1,1} & - & - & - & - & V_{1,6} \\ - & - & - & - & - & - \\ - & - & - & - & - & - \\ - & - & - & - & - & - \\ V_{195,1} & - & - & - & - & V_{195,6} \end{bmatrix}$$

The F and V matrices used to calculate the uncertainties in the global components of the dynamometer are given in Islam (2006c). The uncertainties in the interaction matrix were then obtained using the equation 3.10. Each of the 36 elements of the interaction matrix had corresponding uncertainties that were calculated using equation 3.10. It is to be noted that the uncertainties in each elements in the F and V matrix is assumed to be equal for simplicity.

The next thing to do in the uncertainty analysis of the dynamometer is to consider how the uncertainties in the calibration matrix propagate into a future calculation. A general formula for the uncertainty, U_R , which propagates into a results, R , from uncertainties in M different variables, X_i ; $i=1,2,\dots,M$, where $R=R(X_1, X_2,\dots,X_M)$ is given by equation 3.11 (Hess *et al.* 1999):

$$U_R = \left[\left(\frac{\partial R}{\partial X_1} U_{x_1} \right)^2 + \left(\frac{\partial R}{\partial X_2} U_{x_2} \right)^2 + \left(\frac{\partial R}{\partial X_3} U_{x_3} \right)^2 + \dots + \left(\frac{\partial R}{\partial X_n} U_{x_n} \right)^2 \right]^{1/2} \quad (3.11)$$

In the present case of the six component dynamometer, the defining equation, $F=VA$, where $F=F(F_x, F_y, F_z, M_x, M_y, M_z)$ gives us:

$$\begin{aligned} F_x &= C_{11}V_1 + C_{12}V_2 + C_{13}V_3 + C_{14}V_4 + C_{15}V_5 + C_{16}V_6 \\ F_y &= C_{21}V_1 + C_{22}V_2 + C_{23}V_3 + C_{24}V_4 + C_{25}V_5 + C_{26}V_6 \end{aligned}$$

Uncertainty Analysis

$$\begin{aligned}
 F_z &= C_{31}V_1 + C_{32}V_2 + C_{33}V_3 + C_{34}V_4 + C_{35}V_5 + C_{36}V_6 \\
 M_x &= C_{41}V_1 + C_{42}V_2 + C_{43}V_3 + C_{44}V_4 + C_{45}V_5 + C_{46}V_6 \\
 M_y &= C_{51}V_1 + C_{52}V_2 + C_{53}V_3 + C_{54}V_4 + C_{55}V_5 + C_{56}V_6 \\
 M_z &= C_{61}V_1 + C_{62}V_2 + C_{63}V_3 + C_{64}V_4 + C_{65}V_5 + C_{66}V_6
 \end{aligned}$$

Now applying equation 3.11 to these equations yielded:

$$U_{F_x} = \left[\begin{aligned} &\left(\frac{\partial F_x}{\partial C_{11}} U_{C_{11}}\right)^2 + \left(\frac{\partial F_x}{\partial C_{12}} U_{C_{12}}\right)^2 + \left(\frac{\partial F_x}{\partial C_{13}} U_{C_{13}}\right)^2 + \left(\frac{\partial F_x}{\partial C_{14}} U_{C_{14}}\right)^2 + \left(\frac{\partial F_x}{\partial C_{15}} U_{C_{15}}\right)^2 + \left(\frac{\partial F_x}{\partial C_{16}} U_{C_{16}}\right)^2 \\ &+ \left(\frac{\partial F_x}{\partial V_1} U_{V_1}\right)^2 + \left(\frac{\partial F_x}{\partial V_2} U_{V_2}\right)^2 + \left(\frac{\partial F_x}{\partial V_3} U_{V_3}\right)^2 + \left(\frac{\partial F_x}{\partial V_4} U_{V_4}\right)^2 + \left(\frac{\partial F_x}{\partial V_5} U_{V_5}\right)^2 + \left(\frac{\partial F_x}{\partial V_6} U_{V_6}\right)^2 \end{aligned} \right]^{1/2}$$

which reduces to:

$$U_{F_x} = \left[\begin{aligned} &(V_1 U_{C_{11}})^2 + (V_2 U_{C_{12}})^2 + (V_3 U_{C_{13}})^2 + (V_4 U_{C_{14}})^2 + (V_5 U_{C_{15}})^2 + (V_6 U_{C_{16}})^2 + \\ &(C_{11} U_{V_1})^2 + (C_{12} U_{V_2})^2 + (C_{13} U_{V_3})^2 + (C_{14} U_{V_4})^2 + (C_{15} U_{V_5})^2 + (C_{16} U_{V_6})^2 \end{aligned} \right]^{1/2}$$

In a similar fashion we get,

$$U_{F_y} = \left[\begin{aligned} &(V_1 U_{C_{21}})^2 + (V_2 U_{C_{22}})^2 + (V_3 U_{C_{23}})^2 + (V_4 U_{C_{24}})^2 + (V_5 U_{C_{25}})^2 + (V_6 U_{C_{26}})^2 + \\ &(C_{21} U_{V_1})^2 + (C_{22} U_{V_2})^2 + (C_{23} U_{V_3})^2 + (C_{24} U_{V_4})^2 + (C_{25} U_{V_5})^2 + (C_{26} U_{V_6})^2 \end{aligned} \right]^{1/2}$$

These equations and the rest four components when put into the matrix form yielded:

$$\begin{array}{l}
 \left. \begin{array}{l} U_{F_x} \\ U_{F_y} \\ U_{F_z} \\ U_{M_x} \\ U_{M_y} \\ U_{M_z} \end{array} \right| = \begin{array}{cccccccccccc}
 U_{C_{11}} & U_{C_{12}} & U_{C_{13}} & U_{C_{14}} & U_{C_{15}} & U_{C_{16}} & C_{11} & C_{12} & C_{13} & C_{14} & C_{15} & C_{16} \\
 U_{C_{21}} & U_{C_{22}} & - & - & - & U_{C_{26}} & C_{21} & - & - & - & - & C_{26} \\
 - & - & - & - & - & - & - & - & - & - & - & - \\
 - & - & - & - & - & - & - & - & - & - & - & - \\
 - & - & - & - & - & - & - & - & - & - & - & - \\
 U_{C_{61}} & U_{C_{62}} & - & - & - & U_{C_{66}} & C_{61} & - & - & - & - & C_{66}
 \end{array} \times \left. \begin{array}{l} V_1 \\ V_2 \\ V_3 \\ V_4 \\ V_5 \\ V_6 \\ U_{V_1} \\ U_{V_2} \\ U_{V_3} \\ U_{V_4} \\ U_{V_5} \\ U_{V_6} \end{array} \right|
 \end{array}$$

3.4 Uncertainty Estimates for NSERC Pod Measurements

The details of the uncertainty calculation for each component of the NSERC pod dynamometer are provided in Table B.1 in Appendix B. The table summarizes the bias and precision limit estimated for the podded propulsors obtained using the approach described in section 3.3. The biases and precision limits were combined using RSS to determine the overall uncertainty estimates for each of the variables of interests as shown in Table 3.1.

Table 3.1: Overall uncertainty estimates for the podded propulsor variables (NSERC pod).

<i>J</i>	U_{ρ}	U_D	U_{AA}	U_n	U_{VA}	U_{TProp}	U_Q	U_{TUnit}	U_{FY}	U_{FZ}	U_{MX}	U_{MY}	U_{MZ}
0.0	0.094	0.0001	0.695	0.0513	0.0154	2.3132	0.0728	2.7266	-1.7834	-4.1103	2.0086	6.3168	-1.1673
0.1	0.094	0.0001	0.695	0.0525	0.0154	2.2984	0.0768	2.8147	-1.5395	4.2045	1.7203	6.7964	-1.1824
0.2	0.094	0.0001	0.695	0.0525	0.0154	2.2910	0.0730	2.9994	-2.0219	4.1391	1.7305	7.5522	-1.1247
0.3	0.094	0.0001	0.695	0.0526	0.0154	2.3026	0.0714	3.2612	-1.8371	4.0256	1.8760	6.8058	-1.1113
0.4	0.094	0.0001	0.695	0.0531	0.0154	2.2622	0.0869	3.0933	-2.4209	4.1940	1.9230	6.4301	-1.1629
0.5	0.094	0.0001	0.695	0.0523	0.0154	2.2938	0.0742	3.0972	-1.9250	4.0775	2.2374	5.9553	1.1432
0.6	0.094	0.0001	0.695	0.0525	0.0154	2.2668	0.0800	2.3796	-1.6698	4.0351	1.6845	6.6246	1.1795
0.7	0.094	0.0001	0.695	0.0521	0.0154	2.2742	0.0824	2.1842	-1.7539	4.0231	1.6578	7.5308	1.2073
0.8	0.094	0.0001	0.695	0.0528	0.0154	2.2616	0.0838	2.4774	-1.7819	4.0912	1.8021	6.5109	1.2106
0.9	0.094	0.0001	0.695	0.0531	0.0154	2.2725	0.0779	2.4737	-1.8024	4.0289	1.5671	6.2548	1.1719
1.0	0.094	0.0001	0.695	0.0531	0.0154	2.2602	0.0802	2.3119	-1.5910	4.0468	1.8575	6.9945	1.1646
1.1	0.094	0.0001	0.695	0.0528	0.0154	2.2564	0.0793	-2.5187	-2.2933	4.0827	1.9865	-4.6496	1.2097
1.2	0.094	0.0001	0.695	0.0525	0.0154	-2.2435	-0.0841	-2.3048	-1.9824	3.9229	-1.9229	-4.8499	1.2382

Substitution of the uncertainty values from Table 3.1 into the appropriate uncertainty equations (equations 3.1 to 3.9) yielded the overall uncertainty levels for the propulsive performance coefficients of the podded propulsors as summarized in Table 3.2 and 3.3. The uncertainty estimates were based on the test and calibration data presented in the reports by Islam, (2006a, 2006b and 2006c).

Uncertainty Analysis

Table 3.2: Overall uncertainties in advance coefficients, propeller thrust and torque coefficients and unit thrust coefficients (NSERC pod).

Advance Coefficient J	Advance Coefficient $J (+/-)$	Advance Coefficient Error (+/-)	Propeller Thrust Coefficient $K_{TProp} (+/-)$	Propeller Thrust Coefficient Error (+/-)	Propeller Torque Coefficient $K_Q (+/-)$	Propeller Torque Coefficient Error (+/-)	Unit Thrust Coefficient $K_{TUnit} (+/-)$	Unit Thrust Coefficient Error (+/-)
0.00	-	-	0.0059	1.19	0.0008	1.16	0.0071	1.46
0.10	0.0052	5.21	0.0058	1.25	0.0008	1.18	0.0066	1.46
0.20	0.0053	2.63	0.0055	1.29	0.0007	1.22	0.0057	1.40
0.30	0.0054	1.79	0.0052	1.34	0.0007	1.24	0.0063	1.70
0.40	0.0056	1.41	0.0049	1.43	0.0007	1.42	0.0058	1.77
0.50	0.0058	1.16	0.0046	1.54	0.0006	1.37	0.0053	1.88
0.60	0.0060	1.00	0.0043	1.71	0.0006	1.48	0.0042	1.80
0.70	0.0063	0.90	0.0041	1.96	0.0006	1.65	0.0035	1.84
0.80	0.0065	0.81	0.0039	2.44	0.0006	1.89	0.0032	2.38
0.90	0.0068	0.75	0.0037	3.11	0.0005	2.24	0.0048	5.61
1.00	0.0071	0.71	0.0035	5.06	0.0005	2.71	0.0042	15.25
1.10	0.0074	0.68	0.0035	13.60	0.0004	4.91	-0.0051	2.80
1.20	0.0103	0.86	-0.0035	9.62	-0.0005	97.34	-0.0044	3.66

Table 3.3: Overall uncertainties in global forces and moments in the three orthogonal directions for the podded propulsors (NSERC pod).

Advance Coeff. J	Trans. Force Coeff. $K_{FY} (+/-)$	Trans. Force Coeff. Error (+/-)	Vertical Force Coeff. $K_{FZ} (+/-)$	Vertical Force Coeff. Error (+/-)	Axial Moment Coeff. $K_{MX} (+/-)$	Axial Moment Coeff. Error (+/-)	Vertical Moment Coeff. $K_{YX} (+/-)$	Vertical Moment Coeff. Error (+/-)	Steering Moment Coeff. $K_{ZX} (+/-)$	Steering Moment Coeff. Error (+/-)
0.00	-0.0031	19.66	-0.0052	221.33	0.0108	8.26	0.0498	1.40	-0.0069	42.30
0.10	-0.0031	17.34	0.0048	141.29	0.0087	8.31	0.0449	1.39	-0.0070	40.98
0.20	-0.0030	13.97	0.0052	38.44	0.0111	8.60	0.0466	1.56	-0.0068	56.58
0.30	-0.0034	13.90	0.0055	17.21	0.0074	5.67	0.0429	1.58	-0.0066	72.40
0.40	-0.0026	10.07	0.0048	12.69	0.0077	3.52	0.0428	1.79	-0.0065	3606.84
0.50	-0.0028	9.34	0.0047	9.48	0.0128	5.07	0.0464	2.25	0.0062	41.37
0.60	-0.0036	12.86	0.0048	8.16	0.0124	4.74	0.0438	2.58	0.0071	40.79
0.70	-0.0026	11.66	0.0049	7.46	0.0138	7.50	0.0323	2.36	0.0071	35.84
0.80	-0.0024	11.14	0.0052	6.41	0.0075	4.16	0.0426	4.36	0.0072	38.33
0.90	-0.0040	14.22	0.0048	6.15	0.0112	6.20	0.0402	6.59	0.0066	36.98
1.00	-0.0030	13.08	0.0047	7.06	0.0138	4.76	0.0387	17.07	0.0067	39.11
1.10	-0.0027	12.71	0.0050	9.85	0.0123	12.76	-0.0266	12.30	0.0070	25.05
1.20	-0.0034	25.35	0.0050	18.51	-0.0116	18.50	-0.0314	4.33	0.0073	25.92

Uncertainty Analysis

From Table 3.2 and 3.3, it can be seen that the uncertainty levels of the propeller thrust coefficient are higher than those of the unit thrust coefficient. However, the uncertainty in torque coefficient is comparable with that of the bare propeller test uncertainty presented in Bose and Luznik (1996). Applying the uncertainty limits to the performance curves of the average pod 01 in the form of error bars results in a plot as shown in Figure 3.2.

From Figure 3.2, it is observed that the curves fitted to the data lie inside the error bars. Therefore, the fitted curves provide a good representation of the trends indicated by the results.

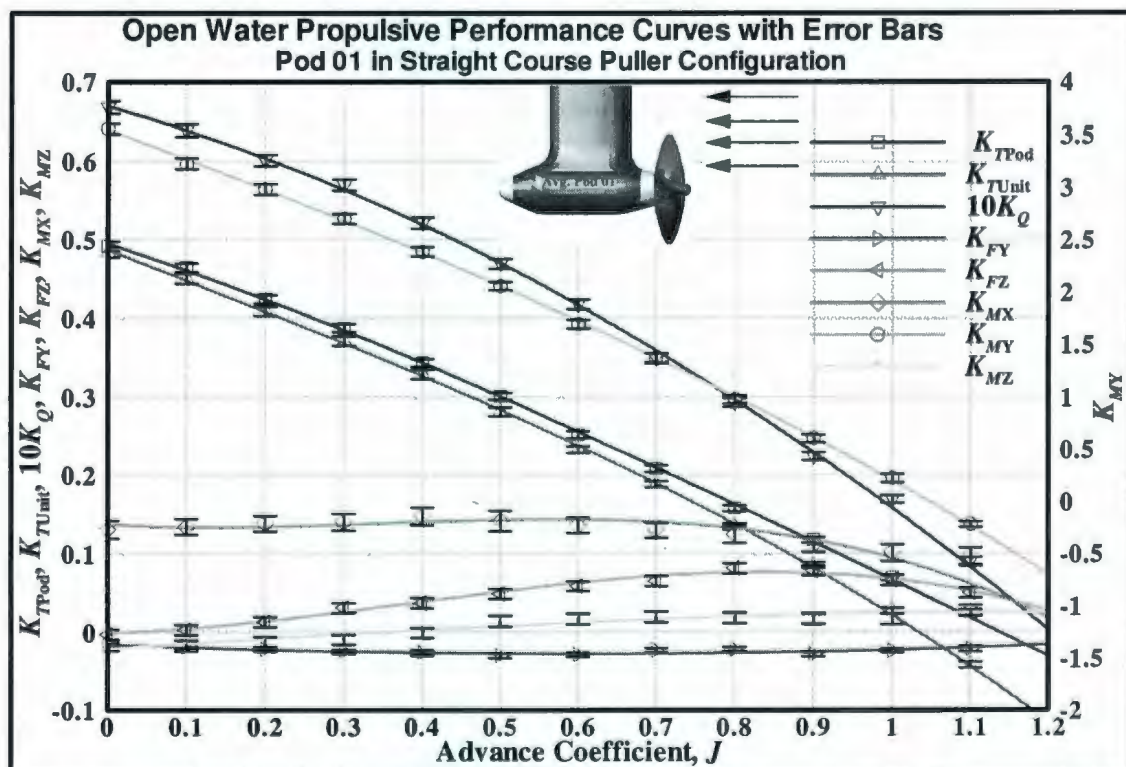


Figure 3.2: Performance curves for NSERC pod 01 (270 mm propeller diameter) in straight-course puller configuration with uncertainty (error) bars.

3.5 Uncertainty Estimates for IOT Pod Measurements

Table B.2 in Appendix B summarizes the bias and precision limit estimated for the measurements using IOT dynamometer system using the approach described in section 3.3. Similar to the NSERC Pod dynamometer system, the biases and precision limits were combined using RSS to determine the overall uncertainty estimates for each of the variables of interests as shown in Table 3.4.

Table 3.4: Overall uncertainty estimates for podded propulsor variables (IOT pod).

<i>J</i>	U_p	U_D	U_{AA}	U_n	U_{VA}	U_{TProp}	U_Q	U_{TUnit}	U_{FY}	U_{FZ}	U_{MX}	U_{MY}	U_{MZ}
0.0	0.0721	0.0001	0.692	0.0506	0.0154	4.2767	0.0711	0.9258	-1.5418	4.7359	0.0589	0.1901	-0.0611
0.2	0.0721	0.0001	0.692	0.0506	0.0058	4.2767	0.0711	0.8067	-1.3296	4.0243	0.0587	0.1644	-0.0611
0.4	0.0721	0.0001	0.692	0.0506	0.0058	4.2767	0.0711	0.6738	-1.0895	3.2018	0.0585	0.1355	-0.0610
0.6	0.0721	0.0001	0.692	0.0506	0.0058	4.2767	0.0711	0.5554	-0.8703	2.4200	0.0584	0.1092	-0.0610
0.7	0.0721	0.0001	0.692	0.0506	0.0058	4.2767	0.0711	0.4860	-0.7379	1.9176	0.0583	0.0935	-0.0610
0.8	0.0721	0.0001	0.692	0.0506	0.0058	4.2767	0.0711	0.4205	-0.6080	1.3737	0.0582	0.0783	-0.0610
0.9	0.0721	0.0001	0.692	0.0506	0.0058	4.2767	0.0711	0.3650	-0.4917	0.7590	0.0582	0.0650	-0.0610
1.0	0.0721	0.0001	0.692	0.0506	0.0058	4.2767	0.0711	0.3403	-0.4374	0.2397	0.0582	0.0588	-0.0610
1.1	0.0721	0.0001	0.692	0.0506	0.0058	4.2767	0.0711	-0.3737	-0.5132	0.8885	0.0582	-0.0673	-0.0610
1.2	0.0721	0.0001	0.692	0.0506	0.0058	-4.2767	-0.0711	-0.4675	0.7059	1.7853	-0.0583	-0.0896	-0.0610

Substitution of the uncertainty values from Table 3.4 into the appropriate uncertainty equations (equations 3.1 to 3.9) yielded the overall uncertainty levels for the propulsive performance coefficients of the podded propulsors as summarized in Table 3.5 and 3.6.

Uncertainty Analysis

Table 3.5: Overall uncertainties in advance coefficients, propeller thrust and torque coefficients and unit thrust coefficients (IOT pod).

Advance Coefficient, J	Advance Coefficient J (+/-)	Advance Coefficient Error (+/-)	Propeller Thrust Coefficient K_{TProp} (+/-)	Propeller Thrust Coefficient Error (+/-)	Propeller Torque Coefficient K_Q (+/-)	Propeller Torque Coefficient Error (+/-)	Unit Thrust Coefficient K_{TUnit} (+/-)	Unit Thrust Coefficient Error (+/-)
0.00	-	-	0.0069	2.54	0.0005	1.62	0.0023	0.90
0.20	0.0020	1.02	0.0069	2.90	0.0004	1.79	0.0020	0.91
0.40	0.0024	0.59	0.0068	3.53	0.0004	2.05	0.0016	0.94
0.60	0.0028	0.47	0.0067	4.68	0.0004	2.51	0.0012	1.00
0.70	0.0031	0.44	0.0067	5.61	0.0004	2.86	0.0010	1.05
0.80	0.0033	0.42	0.0067	7.16	0.0004	3.47	0.0008	1.16
0.90	0.0036	0.40	0.0067	9.96	0.0004	4.42	0.0006	1.47
1.00	0.0039	0.39	0.0067	16.93	0.0004	6.33	0.0005	3.50
1.10	0.0042	0.38	0.0067	72.98	0.0004	12.83	-0.0006	3.87
1.20	0.0045	0.38	-0.0067	28.16	-0.0004	82.33	-0.0008	1.65

Table 3.6: Overall uncertainties in global forces and moments in the three orthogonal directions for the podded propulsors (IOT pod).

Advance Coeff. J	Trans. Force Coeff. K_{FY} (+/-)	Trans. Force Coeff. Error (+/-)	Vertical Force Coeff. K_{FZ} (+/-)	Vertical Force Coeff. Error (+/-)	Axial Moment Coeff. K_{MX} (+/-)	Axial Moment Coeff. Error (+/-)	Vertical Moment Coeff. K_{YX} (+/-)	Vertical Moment Coeff. Error (+/-)	Steering Moment Coeff. K_{ZX} (+/-)	Steering Moment Coeff. Error (+/-)
0.00	-0.0024	110.94	0.0074	633.92	0.0004	1.34	0.0021	0.86	-0.0004	4.90
0.20	-0.0021	31.81	0.0063	100.09	0.0004	1.30	0.0018	0.86	-0.0004	4.79
0.40	-0.0017	15.01	0.0050	53.09	0.0004	1.28	0.0014	0.87	-0.0004	5.53
0.60	-0.0014	8.73	0.0038	37.10	0.0004	1.33	0.0010	0.91	-0.0004	5.80
0.70	-0.0012	7.00	0.0030	25.16	0.0004	1.39	0.0009	0.93	-0.0004	6.14
0.80	-0.0010	6.07	0.0021	14.76	0.0004	1.53	0.0007	0.99	-0.0004	6.65
0.90	-0.0008	5.75	0.0012	6.88	0.0004	1.82	0.0005	1.16	-0.0004	8.30
1.00	-0.0007	6.82	0.0004	1.98	0.0004	2.51	0.0004	2.47	-0.0004	10.44
1.10	-0.0008	30.32	0.0014	5.77	0.0003	7.14	-0.0004	2.77	-0.0004	20.06
1.20	0.0011	26.00	0.0028	9.95	-0.0003	6.90	-0.0006	1.34	-0.0004	1655.98

From Table 3.5 and 3.6, it can be seen that the uncertainty levels of the propeller thrust coefficient are higher than those of the unit thrust coefficient as observed for the case of NSERC pod measurement system. It is also observed that the uncertainty limit for the

Uncertainty Analysis

global unit for the IOT pod system were less than that of the NSERC system. This can be attributed to the compactness of the IOT pod system and due to the fact that the pod unit in the NSERC system was 1.68m vertically below the global unit system as compared to only 0.5m below for the IOT system. The uncertainty in torque coefficient was comparable with that of the bare propeller test uncertainty presented in Bose and Luznik (1996). Applying the uncertainty limits to the performance curves of pod unit used in the IOT system in the form of error bars results in a plot as shown in Figure 3.3.

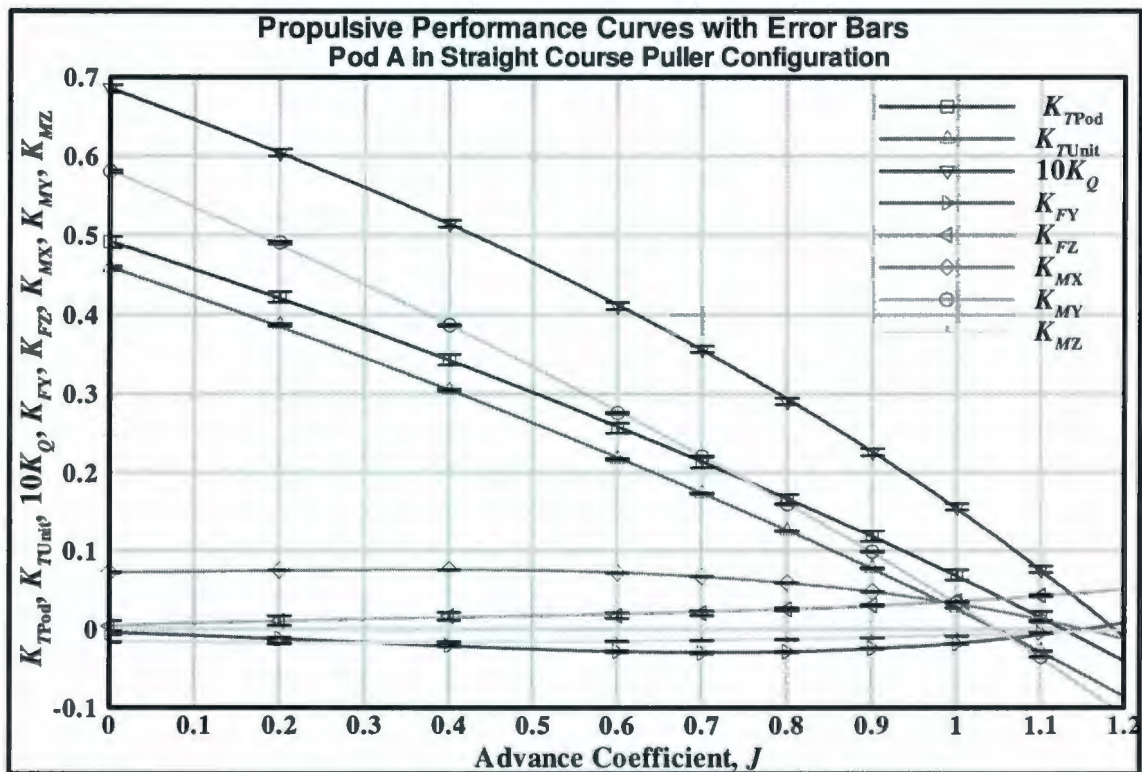


Figure 3.3: Performance curves for IOT pod 01 (200 mm propeller diameter) in straight-course puller configuration with uncertainty (error) bars.

From Figure 3.3, it is observed that the curves fitted to the data lie inside the error bars. Therefore, the fitted curves provide a good representation of the trends indicated by the results.

3.6 Discussion on Uncertainty

The podded propulsor tests to study the effect of pod geometry and static azimuthing conditions were conducted using the NSERC pod dynamometer system. The IOT pod dynamometer system was used to conduct pod unit tests at static and dynamic azimuthing conditions. The uncertainty analysis results of these systems were compared to that of a previous measurements (tests done in the IOT towing tank to measure the performance of some bare podded propellers and using the NSERC dynamometer to conduct podded propulsor tests, Taylor 2006) similar to the current experiments using the same equipment. The uncertainties of the bare propeller tests results were used as a benchmark to compare the uncertainty levels of the new dynamometer system. When the results provided in Table 3.1 were compared with the corresponding results given in Taylor (2006) for the bare propellers and the pod test results, it was seen that the podded propulsor tests using both the NSERC and IOT pod systems in the current phase of tests provided the level of accuracy comparable with the established equipment. The uncertainty levels observed in the propeller thrust and unit thrust in the podded propulsor tests using both pieces of equipment were found to be higher than the thrust uncertainty for the baseline tests, but less than the corresponding uncertainties in the pod tests as given in Taylor (2006).

It can be seen in Table B.1 and B.2 in Appendix B that for majority of the cases, the primary element of the uncertainty of the propeller performance coefficients was the bias error (60% or more on the total uncertainty for the NSERC pod system and 80% or more the IOT pod system). The high precision limit of the IOT pod system can be attributed to the compactness of the system. To reduce the overall uncertainty in the final results, the

Uncertainty Analysis

primary focus should be to reduce the bias error in the equipment. Each individual variable in Table B.1 and B.2 should be examined for possible ways to improve the bias errors.

Given the high degree of accuracy found in the temperature, density, propeller diameter, azimuthing angle, shaft rps and advance speed, these variables have not been given any further consideration for improvement. It can be seen from Table B.1 that the major component influencing the bias limits of propeller thrust and torque for the podded propulsor tests was the curve fit error. As suggested in Taylor (2006), the Sum of Square Error (SEE) analysis was incorporated into the calibration procedure and the error was reduced substantially (compare corresponding results in the uncertainty of the pod tests as given in Taylor, 2006). The calibration of the propeller thrust and torque measurement gauges were repeated 5 to 8 times and SEE analysis applied to the results determined whether or not a curve fit was acceptable and ascertained the functionality of the equipment. The uncertainty levels of the propeller torque were less than the baseline propellers or the pod tests as given in Taylor (2006). This is primarily because of smaller weight and curve fit errors. The uncertainty level of the unit thrust was less than the pod test results as given in Taylor (2006). This is primarily because of the different calibration approaches.

Another way to improve the calibration error is by selecting calibration weights so as to provide adequate resolution over the expected loading range. Selection of poor weight distribution over the expected loading range might contribute to the error in the calibration curve obtained for the propeller thrust or torque readings in the podded propulsor tests. For

the test series in the pod geometry and static azimuthing study, the NSERC dynamometer system had been calibrated to a maximum load of approximately 500N. From the test results, it was found that, for the selected shaft rps of 11, a maximum calibration load of 300N with a finer resolution of calibration data points would have likely produced a better set of calibration data.

One possible approach to improve accuracy of the uncertainties in propeller thrust and torque of the podded propulsor tests is to conduct tests at higher shaft rps. As identified in Table B.1, for the torque readings of the podded propeller experiments, there was not any single dominant factor influencing the overall uncertainty. Despite low error levels in the variables in the torque uncertainty expression, the magnitudes of the actual test measurements were small which resulted in larger overall error. At higher shaft rps, higher advance speeds will be required to achieve the desired advance coefficients. Under these conditions the magnitudes of the thrust and torque will be larger relative to the uncertainty levels. Correspondingly, the percent error for each of these measured variables would be reduced, which would result in less overall uncertainty in the thrust and torque coefficients.

3.7 Summary

The results of the uncertainty analysis for the NSERC and IOT pod dynamometer systems are presented. The uncertainty limits were comparable with those calculated for similar tests conducted by Bose and Luznik (1996) and Taylor (2006). It has been shown that both of the instrumentations were capable of providing levels of accuracy comparable with commercial standard equipment. In case of propeller thrust and torque, the uncertainty

Uncertainty Analysis

limits observed for the NSERC pod system were very close to that observed for the IOT pod system. For the global forces and moments, however, the uncertainty level of the IOT system was much less than that of the NSERC system.

CHAPTER

4

**STUDY of POD with
VARIED GEOMETRY**

4 Study of Pod with Varied Geometry

4.1 Chapter Objectives

This chapter presents results and analyses of the experimental study into the effects of geometric parameters on the propulsive characteristics of puller and pusher podded propulsors in straight course open water conditions. Test results on the 16 different pod-strut-propeller combinations in puller and pusher configurations are presented first. Details of the statistical analysis and the subsequent interpretation follow.

4.2 Test Results

The propeller thrust coefficient, K_{TProp} , propeller torque coefficient, $10K_Q$ and propulsive efficiency, η_{Prop} , unit thrust coefficient, K_{TUnit} , and unit efficiency, η_{Unit} values for each of the 16 pods in the pod series experiments (in the range of advance coefficient of $J=0.0-1.20$) in both puller and pusher configurations are presented in this section.

4.2.1 Pod Series in Puller Configurations

The propulsive performance coefficients (propeller thrust coefficient, K_{TProp} , propeller torque coefficient, $10K_Q$ and propulsive efficiency, η_{Prop}) for each of the pods in the puller pod series experiments are presented in Figures 4.1, 4.2 and 4.3, respectively. With reference to the Figures, for the puller propulsors in the series, the K_{TProp} values at $J = 0$ ranged from 0.464-0.495, an approximately 7% spread based on the lowest K_{TProp} given

Study of Pod with Varied Geometry

by pod HiLo_15. At $J = 0.8$, the K_{TProp} values covered 0.152-0.179 (approximately 17% spread based on the lowest K_{TProp}). At $J=0.8$, the highest K_{TProp} was given by pod HiLo_16 and the lowest K_{TProp} was given by pod HiLo_3. The torque coefficient ($10K_Q$) values of the different pods ranged from 0.679-0.692 (approximately 2% spread based on the lowest $10K_Q$ given by pod HiLo_3) at $J = 0$ and 0.275-0.312 (approximately 14% spread based on the lowest $10K_Q$ given by pod HiLo_4) at $J = 0.8$. The η_{Prop} values of the different pods ranged from 0.647-0.753 at $J = 0.8$ and 0.625-0.824 at $J = 1.0$. The trends showed that for puller configuration propulsors, there was significant variation in K_{TProp} , $10K_Q$ and η_{Prop} values with the change of the geometric parameters. At $J=0$, the thrust coefficients of the pods HiLo_1, HiLo_3, HiLo_6, HiLo_7, HiLo_12, HiLo_14 and HiLo_15 were lower than those of pod HiLo_9 and the thrust coefficients of the remaining pods were higher than those of pod HiLo_9. At $J=0.8$, the propulsive efficiencies of the pods HiLo_1, HiLo_3, HiLo_6, HiLo_7, HiLo_12, HiLo_14 and HiLo_15 were lower than those of pod HiLo_9 and the propulsive efficiencies of the remaining pods were higher than those of pod HiLo_9. This indicated that the efficiency of the propeller attached to pod HiLo_9 was approximately the average of all the other pods. Among the pods, pod HiLo_3 had the lowest efficiency ($\eta_{Prop} = 0.647$) and pod HiLo_16 had the highest efficiency ($\eta_{Prop} = 0.753$) at the design advance coefficient of $J=0.8$. Tables A.1 and A.2 present the K_{TProp} and $10K_Q$ values, respectively, for the pods in puller configuration.

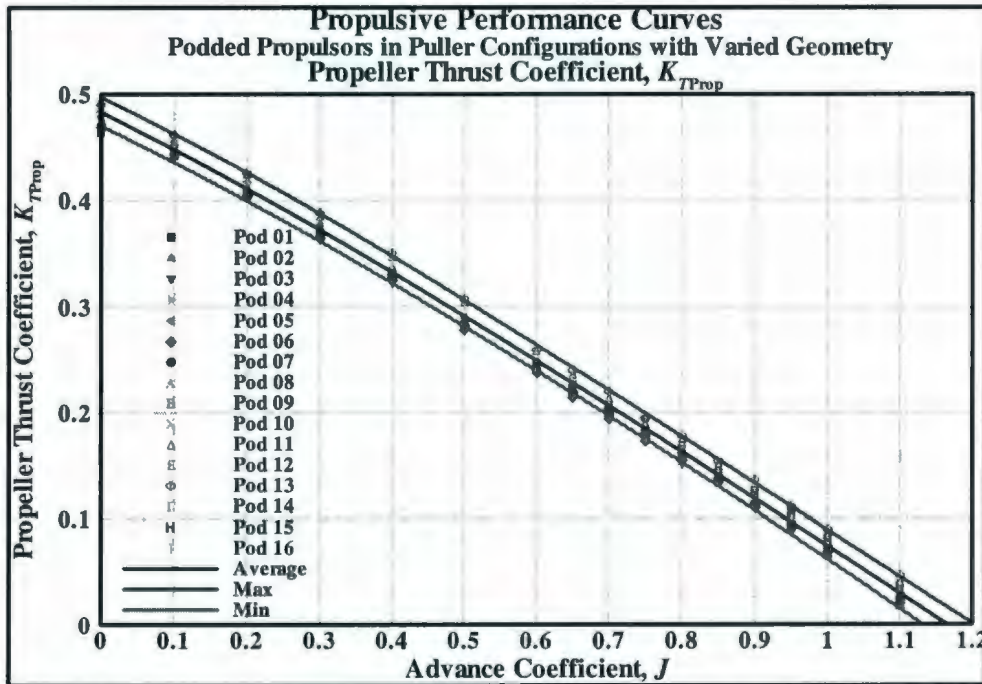


Figure 4.1: Experimental results: Propeller thrust coefficient of the pods in the series in puller configuration.

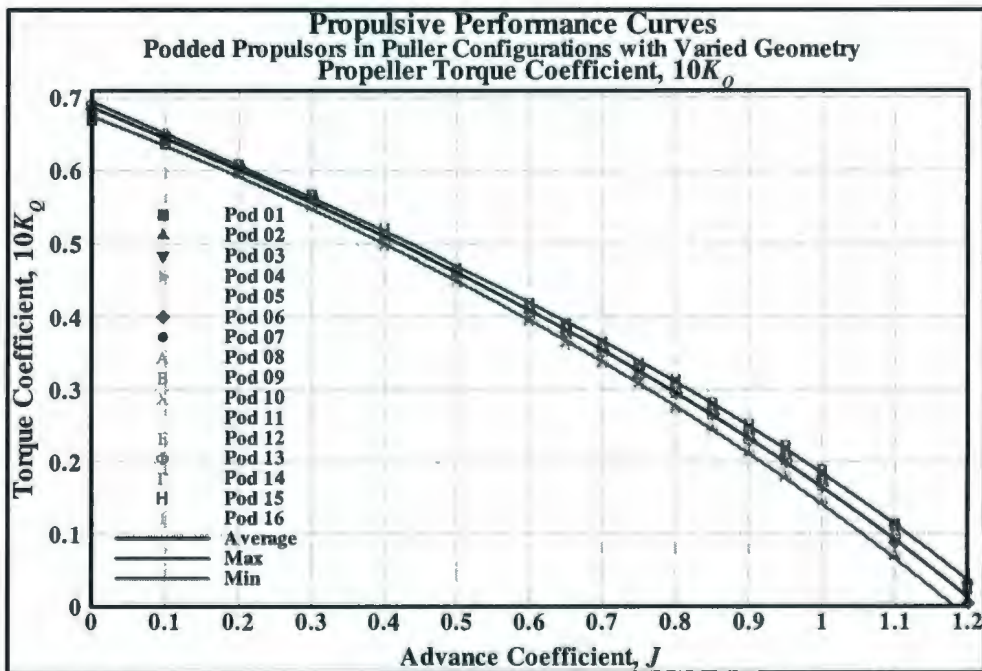


Figure 4.2: Experimental results: Propeller torque coefficient of the pods in the series in puller configuration.

Study of Pod with Varied Geometry

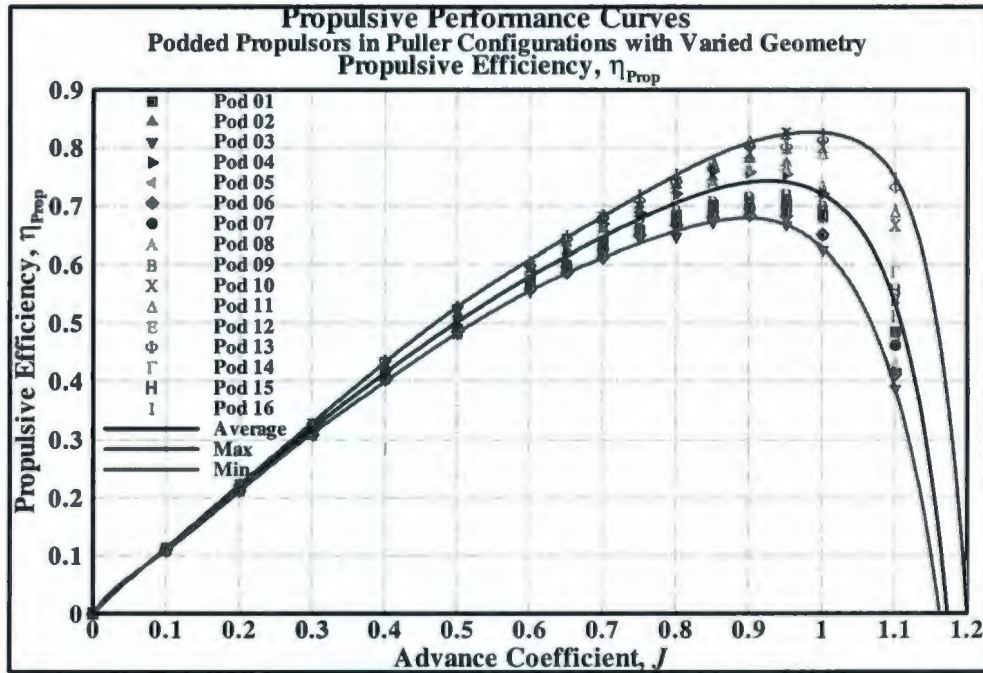


Figure 4.3: Experimental results: propeller efficiency of the pods in the series in puller configuration.

The unit thrust coefficient, K_{TUnit} and unit efficiency, η_{Unit} values for each of the pods in the pod series experiments (in the range of $J=0.0\sim 1.20$) are presented in Figures 4.4 and 4.5. The unit thrust coefficient values at $J = 0$ for the different pods ranged from 0.458 to 0.484, an approximately 6% spread based on the lowest K_{TUnit} given by pod HiLo_7. At $J = 0.8$, the K_{TUnit} values ranged from 0.13 and 0.153, an approximately 18% spread based on the lowest K_{TUnit} given by pod HiLo_4. The η_{Unit} values of the different pods ranged from 0.564 to 0.645 at $J = 0.8$ and from 0.366 to 0.565 at $J = 1.0$. The trends showed that there was significant variation in K_{TUnit} and η_{Unit} values with the change of the geometric parameters. At $J=0$, the unit thrust coefficients of the pods HiLo_1, HiLo_3, HiLo_6, HiLo_7, HiLo_12, HiLo_14 and HiLo_15 were lower than those of pod HiLo_9 and the thrust coefficients of the remaining pods were higher than those of pod

Study of Pod with Varied Geometry

HiLo_9. Among these pods, pod HiLo_9 had the lowest unit efficiency ($\eta_{Unit} = 0.565$) and pod HiLo_5 had the highest unit efficiency ($\eta_{Unit} = 0.645$) at the design advance coefficient of $J=0.8$. Table A.3 presents the K_{TUnit} values for the pods in puller configuration.

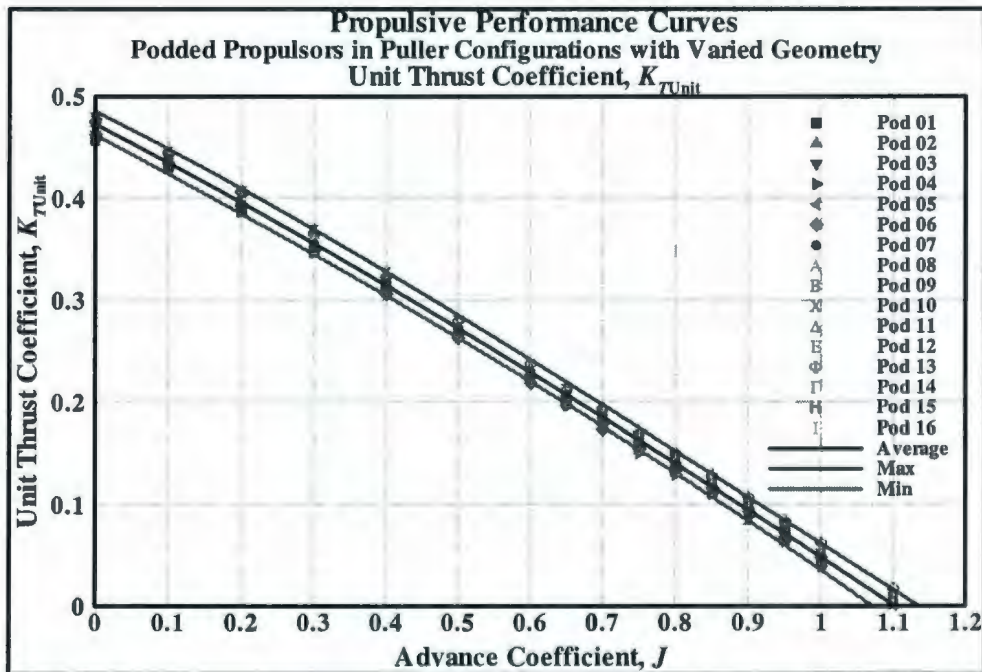


Figure 4.4: Experimental results: unit thrust or axial force coefficient of the pods in the series in puller configuration.

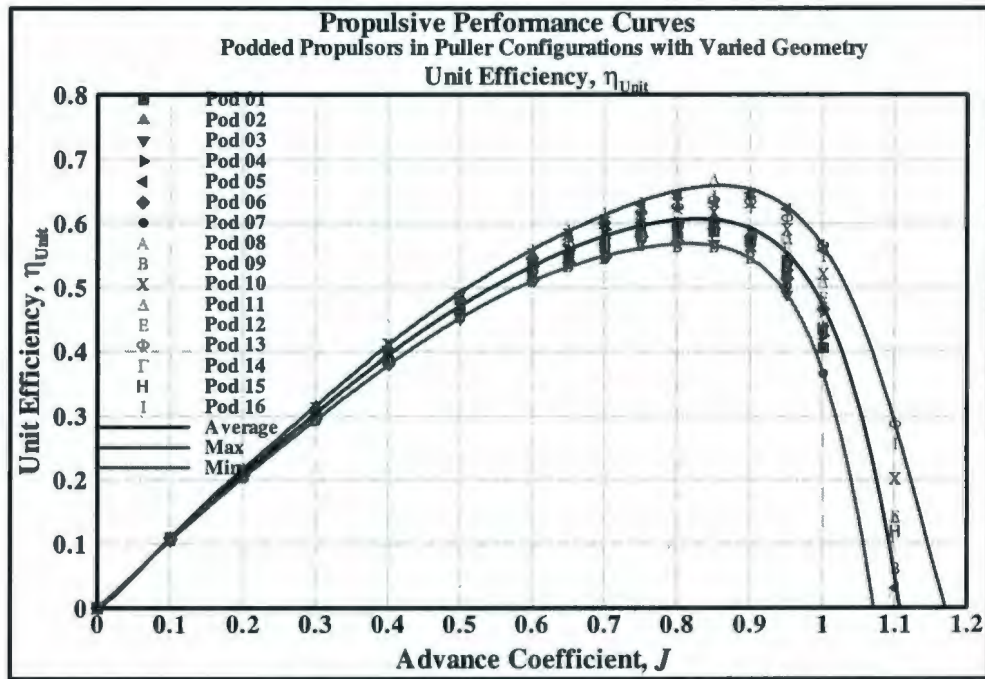


Figure 4.5: Experimental results: unit efficiency of the pods in the series in puller configuration.

4.2.2 Pod Series in Pusher Configurations

The propeller thrust coefficient, K_{TProp} , propeller torque coefficient, $10K_Q$ and propulsive efficiency, η_{Prop} values for each of the pods in the pusher pod series experiments (in the range of $J=0.0\sim 1.20$) are presented in Figures 4.6, 4.7 and 4.8, respectively.

For the pusher propulsors in the series, the K_{TProp} values at $J = 0$ of the pods ranged from 0.4564 to 0.4715, an approximately 4% spread based on the lowest K_{TProp} given by pod HiLo_7. At $J = 0.8$, the K_{TProp} values were in a range of 0.1469-0.1724 (approximately 17% spread based on the lowest K_{TProp}). At $J=0.8$, the highest K_{TProp} was given by pod HiLo_4 and the lowest K_{TProp} was given by pod HiLo_13. The torque coefficient ($10K_Q$)

Study of Pod with Varied Geometry

values of the different pods ranged from 0.6532 to 0.6852 (approximately 5% spread based on the lowest $10K_Q$ given by pod HiLo_12) at $J = 0$, and from 0.275 to 0.312 (approximately 14% spread based on the lowest $10K_Q$ given by pod HiLo_1) at $J = 0.8$. The η_{Prop} values of the different pods ranged from 0.666-0.712 at $J = 0.8$ and 0.580-0.702 at $J = 1.0$. The trends showed that for the pusher propulsors, there was significant variation in K_{TProp} , $10K_Q$ and η_{Prop} values with changes of the geometric parameters. At $J=0$, the thrust coefficients of the pods HiLo_2, HiLo_7, HiLo_8, HiLo_12, HiLo_13 and HiLo_14 were lower than those of pod HiLo_9 and the thrust coefficients of the remaining pods were higher than those of pod HiLo_9. At $J=0.8$, the propulsive efficiencies of the pods HiLo_5, HiLo_7, HiLo_9, HiLo_13, HiLo_14, HiLo_15, HiLo_16 were lower than those of pod HiLo_8 and the propulsive efficiencies of the remaining pods were higher than those of pod HiLo_8. This indicated that the efficiency of the propeller attached with pod HiLo_8 was approximately the average of all the other pods. Among the pods, pod HiLo_13 had the lowest efficiency ($\eta_{Prop} = 0.666$) and pod HiLo_12 had the highest efficiency ($\eta_{Prop} = 0.712$) at the design advance coefficient of $J=0.8$. Tables A.4 and A.5 present the K_{TProp} and $10K_Q$ values, respectively, for the pods in pusher configuration.

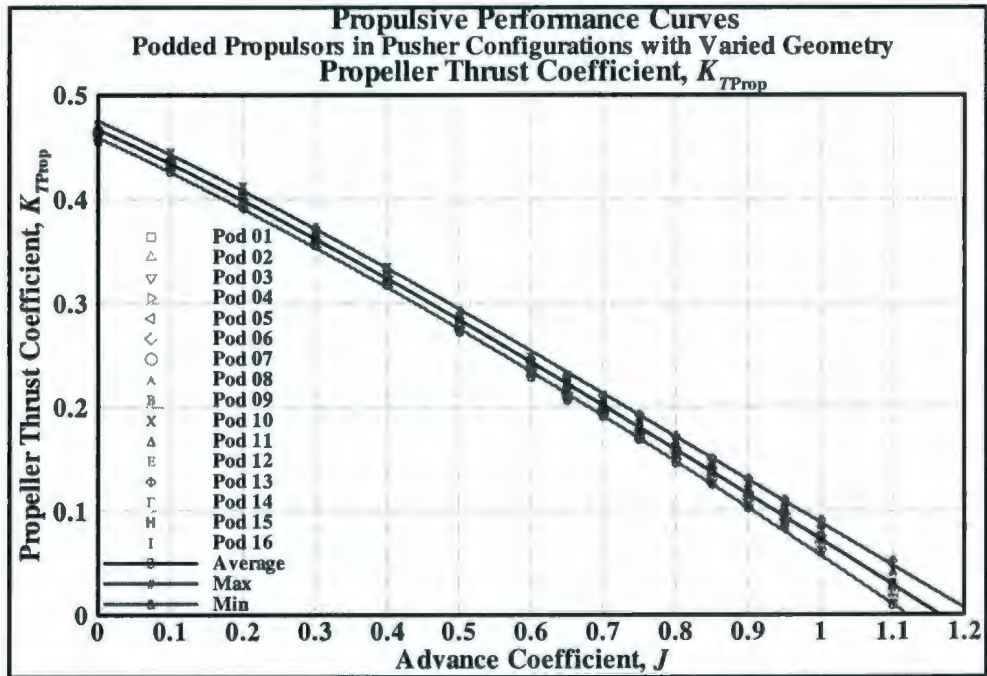


Figure 4.6: Experimental results: Propeller thrust coefficient of the pods in the series in pusher configuration.

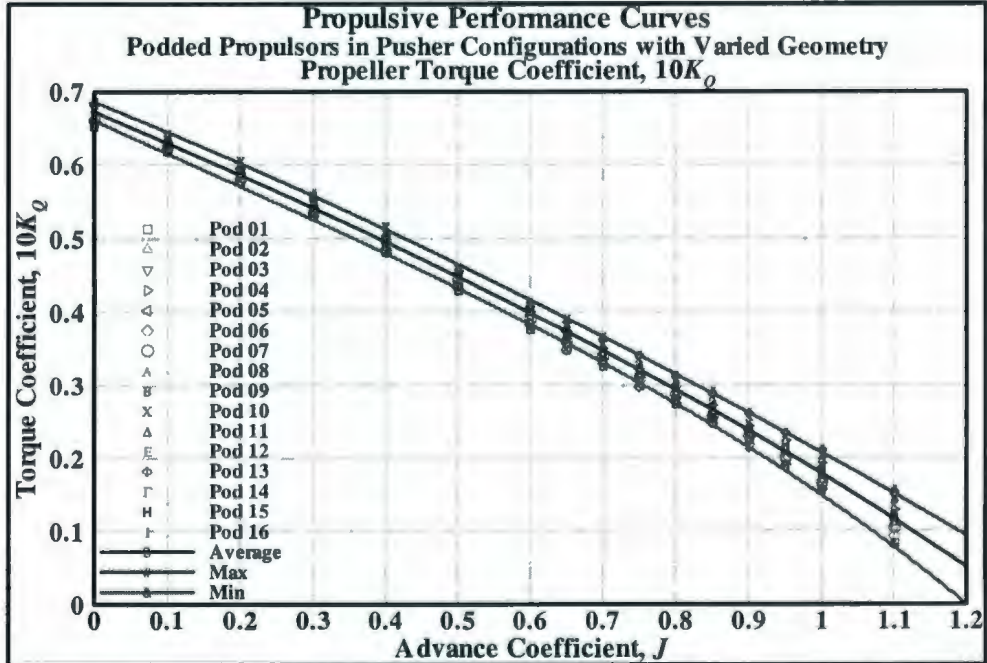


Figure 4.7: Experimental results: Propeller torque coefficient of the pods in the series in pusher configuration.

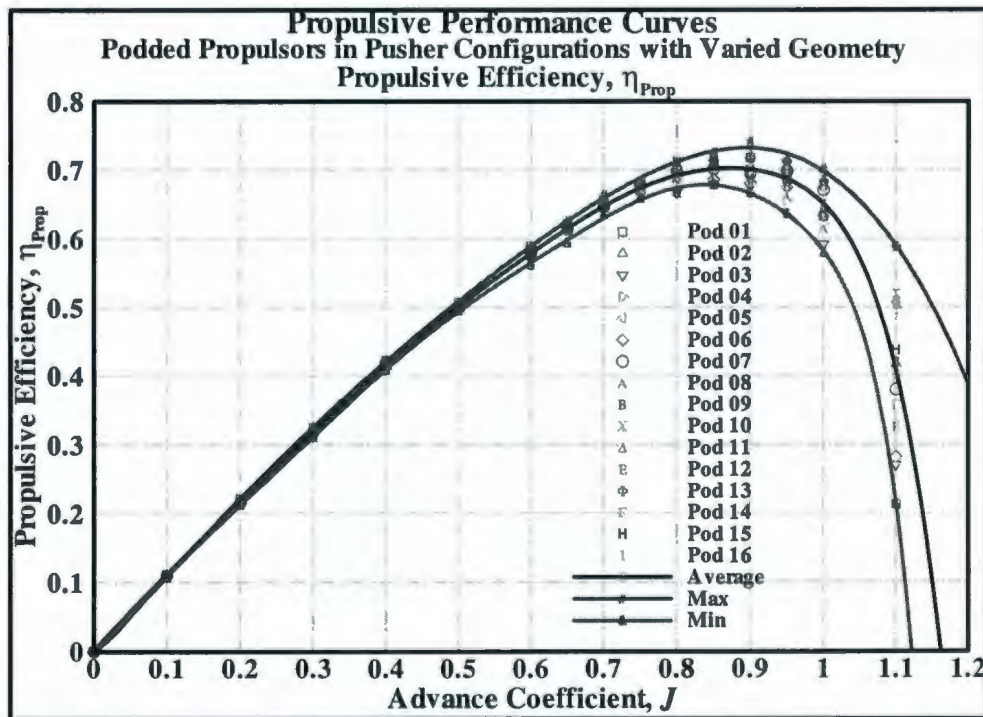


Figure 4.8: Experimental results: Propeller efficiency of the pods in the series in pusher configuration.

The K_{TUnit} and η_{Unit} values for each of the pods in the pusher pod series experiments (in the range of $J=0.0\sim 1.20$) are presented in Figures 4.9 and 4.10, respectively. The unit thrust coefficient (K_{TUnit}) values at $J = 0$ of the different pods ranged from 0.440-0.462, an approximately 5% spread based on the lowest K_{TUnit} given by pod HiLo_1. At $J = 0.8$, the K_{TUnit} values cover a ranged of 0.112-0.143 (approximately 18% spread based on the lowest K_{TUnit} given by pod HiLo_12). The η_{Unit} values of the different pods ranged from 0.514-0.634 at $J = 0.8$ and 0.232-0.415 at $J = 1.0$. The trends showed that there was significant variation in K_{TUnit} and η_{Unit} values with the change of the geometric parameters. At $J=0$, the unit thrust coefficients of the pods HiLo_1, HiLo_3, HiLo_4, HiLo_5, HiLo_6, HiLo_8, HiLo_16 were lower than those of pod HiLo_9 and the thrust

Study of Pod with Varied Geometry

coefficients of the remaining pods were higher than those of pod HiLo_9. Among the pods, pod HiLo_4 had the lowest unit efficiency ($\eta_{Unit} = 0.514$) and pod HiLo_11 had the highest unit efficiency ($\eta_{Unit} = 0.634$) at the advance coefficient of $J=0.8$. Table A.6 presents the K_{TUnit} values for the pods in pusher configuration.

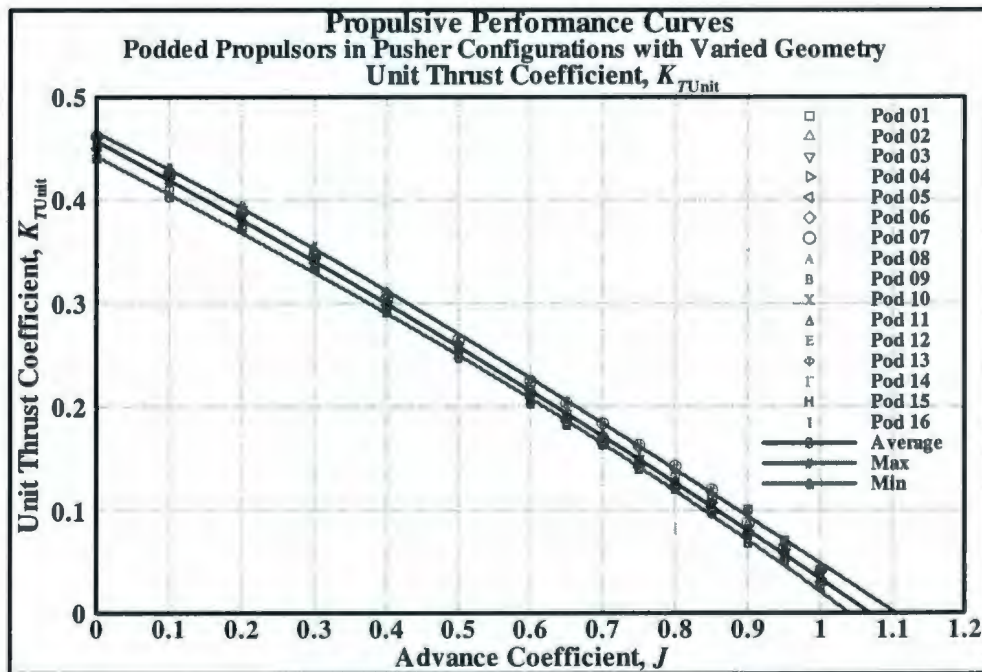


Figure 4.9: Experimental results: unit thrust or axial force coefficient of the pods in the series in pusher configuration.

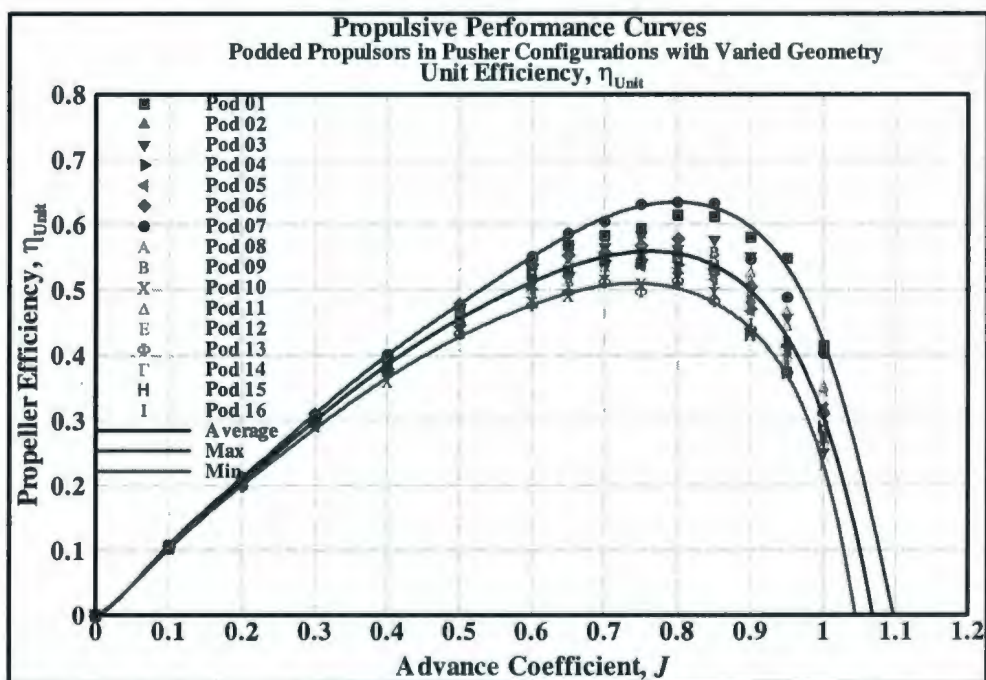


Figure 4.10: Experimental results: unit efficiency of the pods in the series in puller configuration.

4.3 DOE Analyses and Discussions

Design Expert[®] 7.03 (2005) from Statease, a stand-alone software for design of experiments was used to design the experiments and analyze the test series data. The analysis of the data resulted in the identification of the most significant factors and interactions of factors that affect the propulsive performance of the podded propulsors both in puller and pusher configurations. It is noted that the resulting model for the response is only valid within the ranges of the factors. The study was intended to be an extreme design based on the extreme dimensions used by the commercial pods. The method was used to determine how the interaction of the five parameters affected the

overall performance. Only the effects of the factors and interactions of factors were studied, not the quantitative values; although the quantitative values are important.

4.3.1 Discussion on Puller Configuration

Table 4.1 lists all the factors and interactions of factors that have significant influence on the performance coefficients: propeller thrust coefficient, K_{TProp} , propeller torque coefficient, K_Q , propeller efficiency, η_{Prop} , unit thrust coefficient, K_{TUnit} and unit efficiency, η_{Unit} for the puller propulsors in the pod series. The factors are designated as shown in Table 2.7 in Chapter 2. Table 4.1 shows that the significant factors that come up repeatedly over the range of advance coefficient values are A (the ratio of pod diameter to propeller diameter, D_{Pod}/D_{Prop}), D (the ratio of strut distance to propeller diameter, S_{Dist}/D_{Prop}), E (hub taper angle, H_{Angle}), AE (interaction of D_{Pod}/D_{Prop} and H_{Angle}) and BD (interaction of L_{Pod}/D_{Prop} and S_{Dist}/D_{Prop}). The factor C (the ratio of pod aft taper length to propeller diameter, TL/D_{Prop}) did not show any significant influence on the performance coefficients at any advance coefficient.

The factors H_{Angle} and D_{Pod}/D_{Prop} had significant impact on propeller thrust coefficient (K_{TProp}), unit thrust coefficient (K_{TUnit}) and torque coefficient (K_Q) for almost all values of advance coefficients, but as the value of advance coefficient increased from 0, interaction of D_{Pod}/D_{Prop} and H_{Angle} became as significant as the single factors D_{Pod}/D_{Prop} and H_{Angle} (in the range of advance coefficient, $J=0.3\sim 1.0$). The factor B (L_{Pod}/D_{Prop}) appeared to have significant effect in the form of interaction with D (S_{Dist}/D_{Prop}) on K_{TUnit} at high

Study of Pod with Varied Geometry

values of J (in the range of $J=0.75\sim 0.95$). The factor D (S_{Dist}/D_{Prop}) appeared to have significant effect on K_{TProp} and K_Q at moderate advance coefficients, as shown in Table 4.1. The propeller and unit efficiencies, η_{Prop} and η_{Unit} were mostly affected by H_{Angle} and D_{Pod}/D_{Prop} ; H_{Angle} being the most influential one at all advance coefficients. D_{Pod}/D_{Prop} played an important role when the advance coefficient was higher than 0.6.

Table 4.1: Fractional factorial design results: List of significant factors and interaction of factors for puller propulsors. Here, A is the ratio of pod diameter to propeller diameter, D_{Pod}/D_{Prop} , B is the ratio of pod length to propeller diameter, L_{Pod}/D_{Prop} , C is the ratio of pod taper length to propeller diameter, TL/D_{Prop} , D is the ratio of strut distance to propeller diameter, S_{Dist}/D_{Prop} , and E is the propeller hub taper angle, H_{Angle} .

Significant factor and interaction of factors in puller configurations										
J	K_{TProp}		K_{TUnit}		K_Q		η_{Prop}		η_{Unit}	
0.00	A, E		E		A, E		-	-	-	-
0.10	A, E		E		A, E		E		E	
0.20	A, E		E		A, E		E		E	
0.30	A, E	AE	A, E	AE	A, E	AE	E		E	
0.40	A, E	AE	A, E	AE	A, E	AE	E		E	
0.50	A, E	AE	A, E	AE	A, E	AE	E		E	
0.60	A, D, E	AE	A, E	AE	A, D, E	AE	A, E		E	
0.70	A, D, E	AE	A, E	AE	A, D, E	AE	A, E		E	
0.80	A, D, E	AE	A, E	AE, BD	A, D, E	AE	A, E		E	
0.90	A, D, E	AE	A	AE, BD	A, D, E	AE	A, E		A, E	
1.00	A, E		A	BD	A, E		A, E		A, E	
1.10	A, E		A	BD	A, E		A, E	AE	A, E	

As shown in Figures 4.11 and 4.12, the parameter D_{Pod}/D_{Prop} had a significant effect on K_{TProp} at $J=0.0$ and $J=0.8$, respectively. For a fixed propeller diameter, as the pod diameter increased the K_{TProp} increased. In the puller configuration, the larger pod diameter created larger blockage to the flow behind the propeller. The flow blockage reduced the local inflow velocity, thus the propeller operated at a lower effective advance

Study of Pod with Varied Geometry

coefficient, which resulted in increases in the K_{TProp} . As shown in Figure 4.12, the analysis also indicated that the factor A (D_{Pod}/D_{Prop}) was involved in an interaction at higher J values. This means that while the information in Figure 4.12 is valid, there might be indirect impact on K_{TProp} due to the interaction of D_{Pod}/D_{Prop} and H_{Angle} . The parameter A (D_{Pod}/D_{Prop}) had an effect on K_{TUnit} , K_Q , η_{Prop} and η_{Unit} similar to that of K_{TProp} for the advance coefficient values shown in Table 4.1. It is noted that the unusual scale of the ordinates of all figures in this section makes a direct comparison almost impossible. The plots were created using the Design Expert® software, which does not allow controlling the scale. However, the figures are not intended to compare to each other as each plot is different from the others by more than one factor and direct comparison would not make any physical sense.

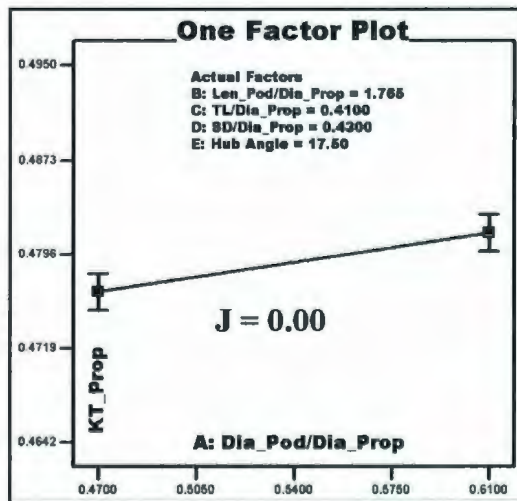


Figure 4.11: DOE Analysis: The effect of D_{Pod}/D_{Prop} (A) on propeller thrust at $J=0.0$ for puller propulsors.

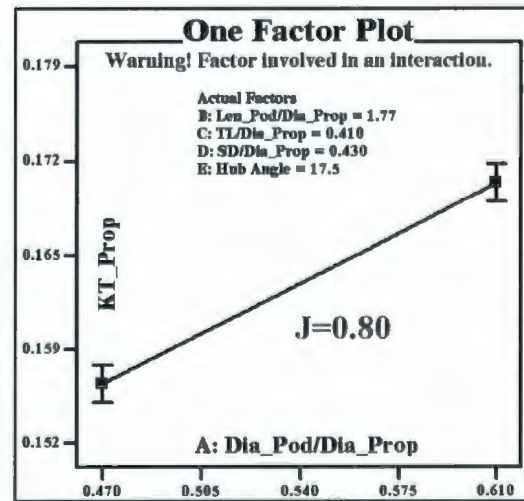


Figure 4.12: DOE Analysis: The effect of D_{Pod}/D_{Prop} (A) on propeller thrust at $J=0.8$ for puller propulsors.

Figures 4.13 and 4.14 show the effect of the strut distance, D (S_{Dist}/D_{Prop}) on K_{TProp} at advance coefficients of $J=0.6$ and 0.8 , respectively. The Figures show that as the strut distance increased the K_{TProp} tended to decrease slightly because of the decreasing blockage effect of the strut. A similar effect was found for K_Q . S_{Dist}/D_{Prop} did not show any effect on K_{TUnit} as an individual factor but had influence on K_{TUnit} as an interaction effect as described later (Figure 4.20).

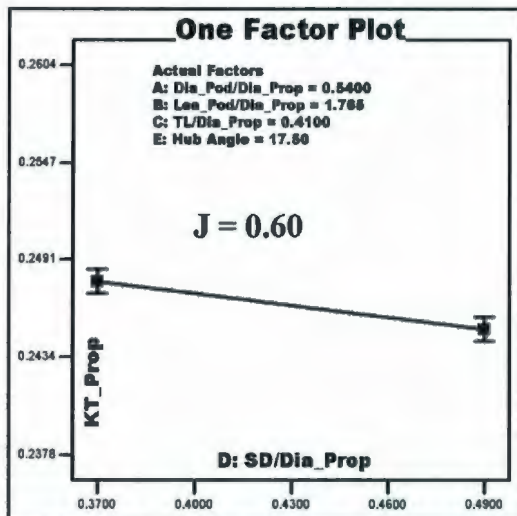


Figure 4.13: DOE Analysis: The effect of significant factors, S_{Dist}/D_{Prop} (D) on propeller thrust at $J=0.6$ for puller propulsors.

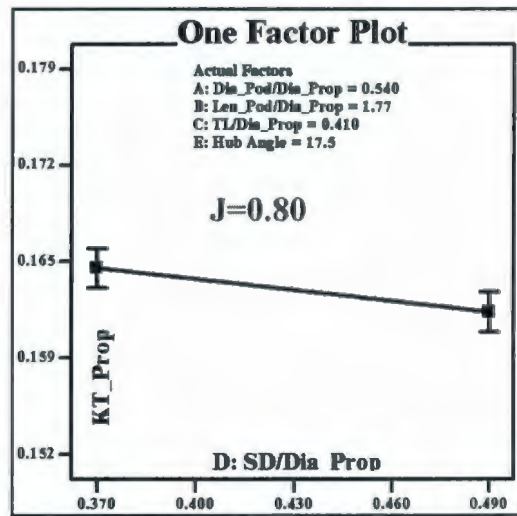


Figure 4.14: DOE Analysis: The effect of significant factors, S_{Dist}/D_{Prop} (D) on propeller thrust at $J=0.8$ for puller propulsors.

Figure 4.15 and 4.16 show the effect of hub angle, E (H_{Angle}) on K_{TProp} at advance coefficients of $J=0$ and $J=0.8$. As the hub angle increased, the K_{TProp} also increased. The increasing effect of the hub angle on K_{TProp} was also found in a previous study using the same instrumentation (Islam *et al.*, 2006c). It is also observed in the figures that as the advance coefficient increased, the effect of hub angle tended to reduce. This was also

observed in the previous study by the author (Islam *et al.* 2006a). Hub angle had a similar effect on K_{TUnit} , η_{Prop} and η_{Unit} .

It is likely that the higher hub angles lead to a lower overall inflow speed at the propeller due to the potential flow effect around the hub (and pod), whether in pusher or puller configuration. If this is the case, the influence would be greatest near the root sections and would diminish towards the tips. Another way to explain the higher thrust of the propellers with higher hub angle is to look at the blade geometry at the roots. For the pulling propeller with a high hub angle of 20° compared to that of 15° , the intersection between the blade root section and the hub surface makes the blade root section have a smaller angle of attack (this will reduce the thrust) and to have a substantially higher leading edge area (this will increase the thrust), the combined effect at this hub angle may have given an increase in thrust (for details see Islam *et al.* 2006a).

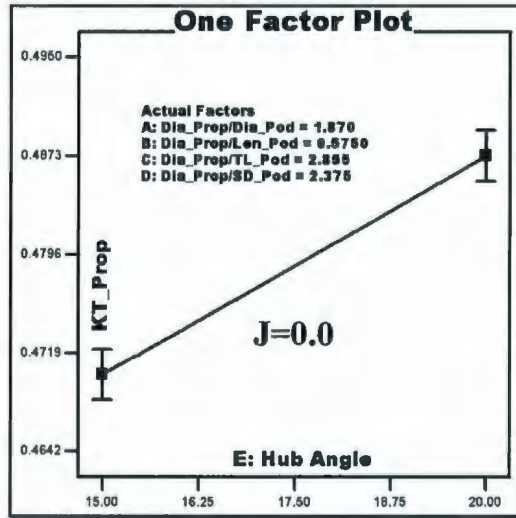


Figure 4.15: DOE Analysis: The effect of significant factor, H_{Angle} (E) on propeller thrust at $J=0.0$ for puller propulsors.

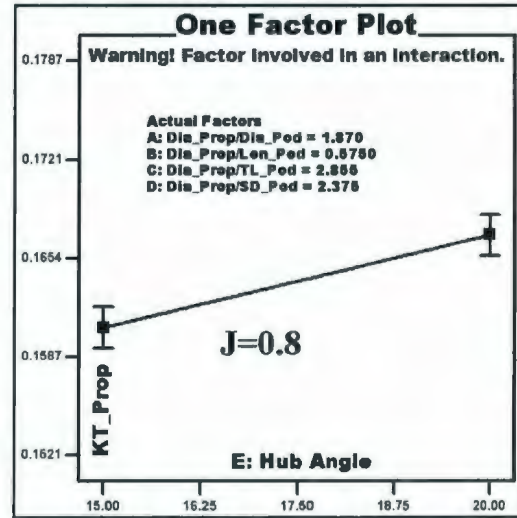


Figure 4.16: DOE Analysis: The effect of significant factor, H_{Angle} (E) on propeller thrust at $J=0.8$ for puller propulsors.

Figures 4.17 and 4.18 show that the parameter hub angle, H_{Angle} , had a significant but opposite effect on K_Q at $J=0$ and $J=0.8$, respectively. At the bollard pull condition, increasing the hub angle increased the propeller shaft torque, which can be attributed to the potential flow effect as mentioned in case of propeller thrust. However, at advance coefficient of $J=0.8$, increasing the hub angle decreased propeller torque unlike propeller thrust at that loading condition.

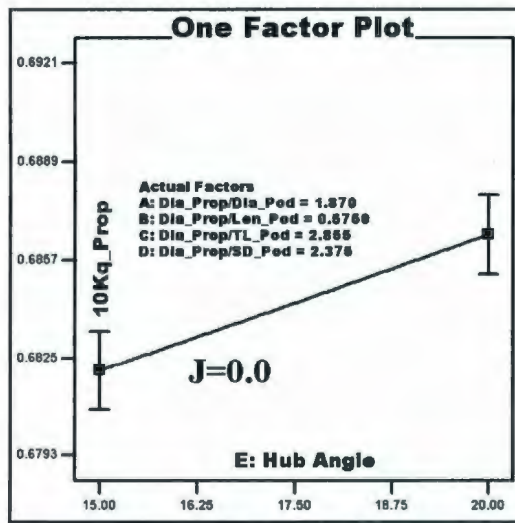


Figure 4.17: DOE Analysis: The effect of significant factor, H_{Angle} (E) on propeller torque at $J=0$ for puller propulsors.

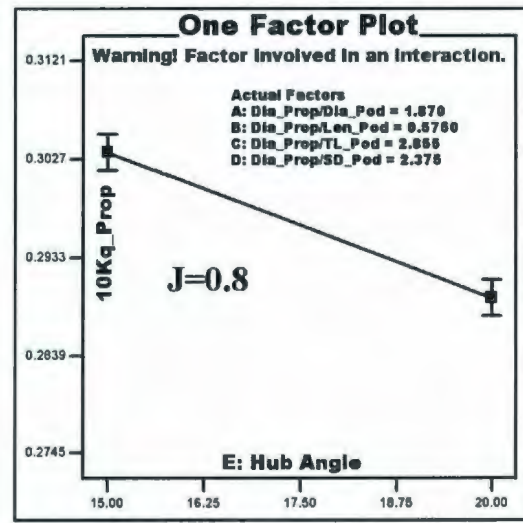


Figure 4.18: DOE Analysis: The effect of significant factor, H_{Angle} (E) on propeller torque at $J=0.8$ for puller propulsors.

Figure 4.19 shows the interaction effect AE (D_{Pod}/D_{Prop} and H_{Angle}) on K_{TProp} ; it shows that the influence of the factor D_{Pod}/D_{Prop} was more obvious at a high hub angle i.e. increasing the ratio increased K_{TProp} at a faster rate at high hub angle. When the factor D_{Pod}/D_{Prop} was low, there was little change in K_{TProp} (within 2% based on the lower K_{TProp}) due to change in hub angle. However, when the ratio was high, there was a highly significant effect of hub angle on K_{TProp} (approximately 8% based on the lower K_{TProp}). This indicated that for a fat pod with respect to the propeller (higher value of D_{Pod}/D_{Prop}), the hub angle had more effect on K_{TProp} (as the hub angle increases, the K_{TProp} increases) than a slender pod with a low value of the factor D_{Pod}/D_{Prop} . A similar interaction effect was also found on K_{TUnit} and K_Q .

Figure 4.20 shows the interaction effect BD (L_{Pod}/D_{Prop} and S_{Dist}/D_{Prop}) on K_{TUnit} at $J=0.8$; it shows that the effect of the factor L_{Pod}/D_{Prop} was opposite at the high and low values of S_{Dist}/D_{Prop} . At the low L_{Pod}/D_{Prop} value, the increase of S_{Dist}/D_{Prop} increased the K_{TUnit} , whereas at high L_{Pod}/D_{Prop} value, the increase of S_{Dist}/D_{Prop} decreased the K_{TUnit} . In other words, for the low S_{Dist}/D_{Prop} case, increasing L_{Pod}/D_{Prop} increased the K_{TUnit} , but for the high S_{Dist}/D_{Prop} case, increasing L_{Pod}/D_{Prop} decreased the K_{TUnit} .

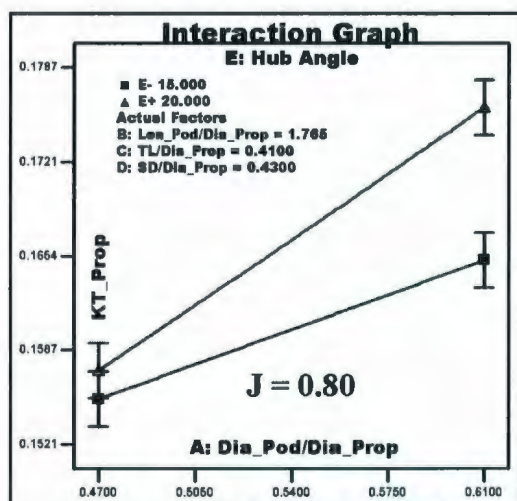


Figure 4.19: DOE Analysis: The interaction effect of significant factors, D_{Pod}/D_{Prop} (A) and H_{Angle} (E) on propeller thrust at $J=0.8$ for puller propulsors.

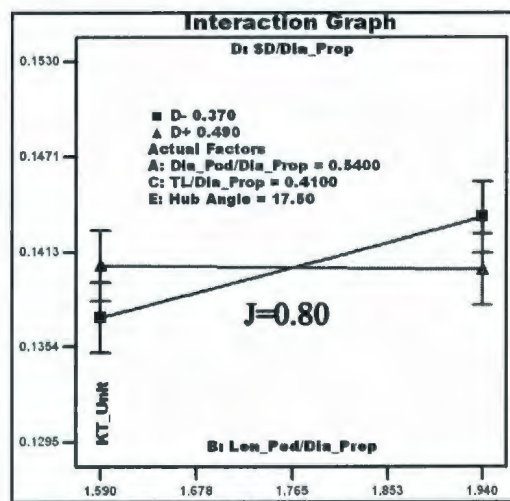


Figure 4.20: DOE Analysis: The interaction effect of significant factors, L_{Pod}/D_{Prop} (B) and S_{Dist}/D_{Prop} (D) on unit thrust at $J=0.8$ for puller propulsors.

4.4.2 Discussion on Pusher Configuration

Table 4.2 lists all the factors and interactions of factors that have significant influence on the performance coefficients K_{TProp} , K_Q , η_{Prop} , K_{TUnit} and η_{Unit} for the pusher propulsors in the pod series. Table 4.2 shows that the significant factors that came up repeatedly over the range of J values were A (D_{Pod}/D_{Prop}), B (L_{Pod}/D_{Prop}), C (TL), D (S_{Dist}/D_{Prop}), E

Study of Pod with Varied Geometry

(H_{Angle}), AB (interaction of $D_{\text{Pod}}/D_{\text{Prop}}$ and $L_{\text{Pod}}/D_{\text{Prop}}$) and BC (interaction of $L_{\text{Pod}}/D_{\text{Prop}}$ and TL).

The factor H_{Angle} had significant impact on $K_{T\text{Prop}}$, K_Q , η_{Prop} and η_{Unit} for all values of advance coefficient, whereas the factor A ($D_{\text{Pod}}/D_{\text{Prop}}$) had significant impact at moderate and high values of advance coefficient (in the range of $J=0.4\sim 1.1$). The factor B ($L_{\text{Pod}}/D_{\text{Prop}}$) had significant influence in the form of interaction with D ($S_{\text{Dist}}/D_{\text{Prop}}$) on $K_{T\text{Unit}}$ at moderate values of J (in the range of $J=0.4\sim 0.7$) and as an individual factor at high values of J (in the range of $J=0.9\sim 1.1$). The factor D ($S_{\text{Dist}}/D_{\text{Prop}}$) appeared to have significant effect on $K_{T\text{Prop}}$ and η_{Prop} at advance coefficients of 0.8 and higher. The factor C (TL/D_{Prop}) had a noticeable impact on $K_{T\text{Unit}}$ at low and moderate values of advance coefficient as shown in Table 4.2.

Study of Pod with Varied Geometry

Table 4.2: Fractional factorial design results: List of significant factors and interaction of factors for pusher propulsors. Here, A is the ratio of pod diameter to propeller diameter, D_{Pod}/D_{Prop} , B is the ratio of pod length to propeller diameter, L_{Pod}/D_{Prop} , C is the ratio of pod taper length to propeller diameter, TL/D_{Prop} , D is the ratio of strut distance to propeller diameter, S_{Dist}/D_{Prop} , and E is the propeller hub taper angle, H_{Angle} .

Significant factor and interaction of factors										
J	K_{TProp}		K_{TUnit}		K_Q		η_{Prop}		η_{Unit}	
0.00	E	BC	C	AB	E		-	-	-	-
0.10	E	BC	C	AB	E		E		E	AB
0.20	E	BC	C	AB	E		E		E	AB
0.30	E		C	AB	E		E		A, E	
0.40	A, E		A, C	BD	E		A, E		A, E	
0.50	A, E		A, C	BD	A, E		A, E		A, E	
0.60	A, E		A, C	BD	A, E		A, E		A, E	
0.70	A, E		A, C	BD	A, E		A, E		A, E	
0.80	A, D, E		A, C		A, E		A, D, E		A, E	
0.90	A, D, E		B, C		A, E		A, D, E		A, E	
1.00	A, D, E		B		A, E		A, D, E		A, D, E	
1.10	A, E		B		A, E		A, D, E		A, D, E	

Figure 4.21 shows the effect of the factor D_{Pod}/D_{Prop} on K_{TProp} at $J=0.8$. For a fixed propeller diameter, as the pod diameter increased the K_{TProp} increased. The larger pod diameter created larger blockage to the flow in front of the propeller. The blockage in the flow reduced the local flow velocity, thus the propeller operated at lower effective advance coefficient, which resulted in an increase in K_{TProp} . The parameter, D_{Pod}/D_{Prop} had similar effect on K_{TProp} , K_Q , η_{Prop} and η_{Unit} for the other advance coefficient values shown in Table 4.2. Figure 4.22 shows the effect of the factor D_{Pod}/D_{Prop} on K_{TUnit} at $J=0.8$. For a fixed propeller diameter, as the pod diameter increased the K_{TProp} decreased. A larger pod diameter means higher drag on the pod, along with a larger blockage effect, which resulted in lower unit thrust.

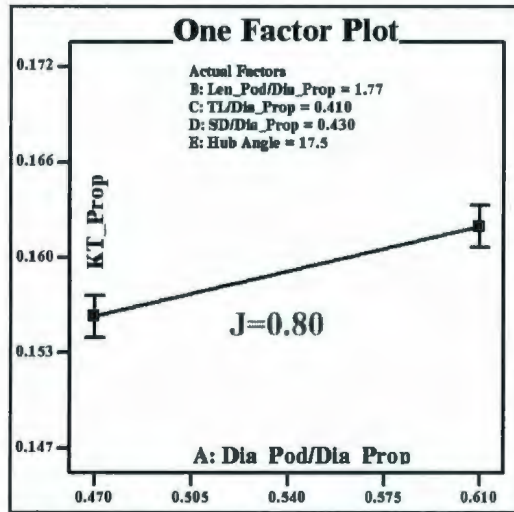


Figure 4.21: DOE Analysis: The effect of D_{Pod}/D_{Prop} (A) on propeller thrust at $J=0.8$ for pusher propulsors.

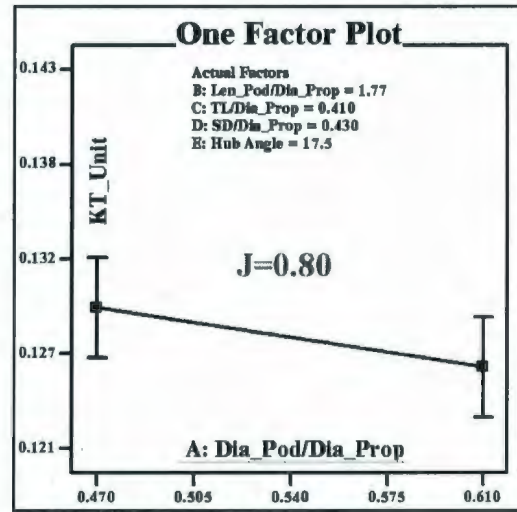


Figure 4.22: DOE Analysis: The effect of D_{Pod}/D_{Prop} (A) on unit thrust at $J=0.8$ for pusher propulsors.

Figure 4.23 and 4.24 show the effect of the factor taper length, C (TL/D_{Prop}) on $K_{T_{Unit}}$ at $J=0.0$ and $J=0.8$, respectively. For a fixed propeller diameter, as the pod taper length increased the $K_{T_{Unit}}$ increased. Taper length showed a similar effect on unit thrust at other advance coefficients but as the advance coefficient increased the effect decreased. The factor did not have significant effect on $K_{T_{Prop}}$, K_Q , η_{Prop} and η_{Unit} at any of the advance coefficients.

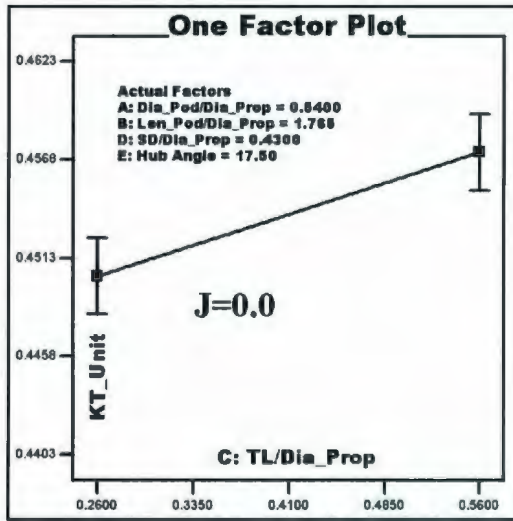


Figure 4.23: DOE Analysis: The effect of TL/D_{Prop} (C) on unit thrust at $J=0.0$ for pusher propulsors.

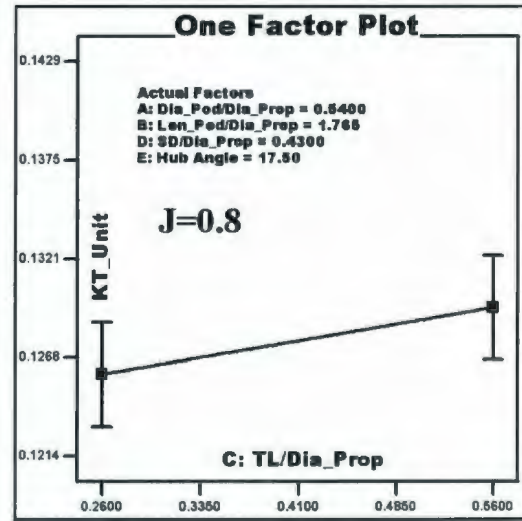


Figure 4.24: DOE Analysis: The effect of TL/D_{Prop} (C) on unit thrust at $J=0.8$ for pusher propulsors.

Figure 4.25 shows the effect of pod length, L_{Pod}/D_{Prop} on K_{TUnit} at $J=0.9$. As the pod length increased, the K_{TUnit} decreased meaning longer pods had lower unit thrust. This can be associated with the increased drag on the pod body with the increase of pod length. The parameter L_{Pod}/D_{Prop} showed a similar effect on only unit thrust at higher advance coefficients (J greater than 0.9). Figure 4.26 shows the effect of the strut distance, D (S_{Dist}/D_{Prop}) on propeller thrust; it shows that at $J=0.8$, as the strut distance increased, the K_{TProp} tended to decrease slightly because of decreasing blockage effect of the strut. The factor, S_{Dist}/D_{Prop} showed similar effect on η_{Prop} and η_{Unit} at high advance coefficients.

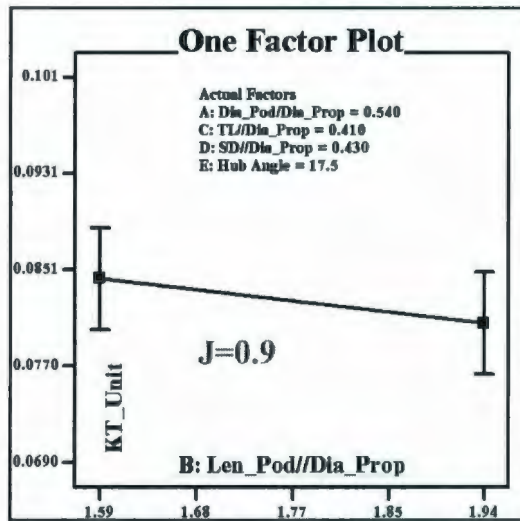


Figure 4.25: DOE Analysis: The effect of L_{Pod} / D_{Prop} (B) on unit thrust at $J=0.9$ for pusher propulsors.

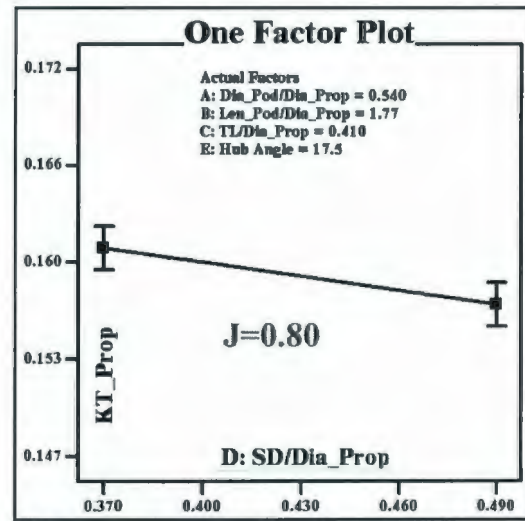


Figure 4.26: DOE Analysis: The effect of S_{Dist} / D_{Prop} (D) on propeller thrust at $J=0.8$ for pusher propulsors.

Figures 4.27 and 4.28 show the effect of hub angle, H_{Angle} on K_{TProp} at $J=0.0$ and $J=0.8$, respectively. As the hub angle increased, the K_{TProp} also increased. The effects are similar as in the puller configuration. The parameter, H_{Angle} had a similar effect on K_{TProp} , K_Q , η_{Prop} and η_{Unit} for the other advance coefficient values as shown in Table 4.2 but did not have any effect on K_{TUnit} at any advance coefficients. For the pusher propeller with a high hub angle of 20° , the angle of attack at the blade root section is increased substantially and the leading area is decreased; this combined effect at this hub angle range may have resulted in an increased thrust as well (Islam *et al.* 2006a).

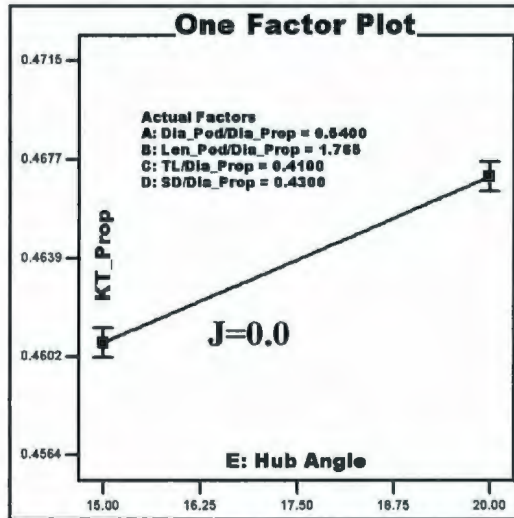


Figure 4.27: DOE Analysis: The effect of H_{Angle} (E) on propeller thrust at $J=0.0$ for pusher propulsors.

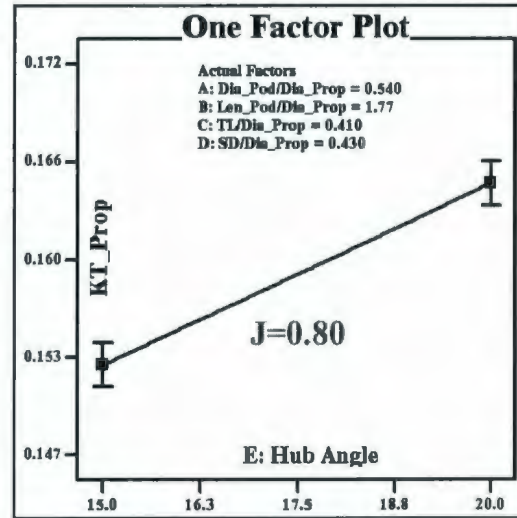


Figure 4.28: DOE Analysis: The effect of H_{Angle} (E) on propeller thrust at $J=0.8$ for pusher propulsors.

The interaction of factors B and C, i.e. BC, (L_{Pod}/D_{Prop} and TL/D_{Prop}) had noticeable effect on K_{TProp} when J was equal to 0.3 or less. Figure 4.29 shows that for constant propeller diameter, at $J=0$ and at lower taper length, increasing pod length resulted in lower propeller thrust, whereas at higher taper length, increasing pod length resulted in higher propeller thrust.

Figure 4.30 shows the interaction effect of AB (D_{Pod}/D_{Prop} and L_{Pod}/D_{Prop}) on unit thrust at $J=0$. It shows that for constant propeller diameter, at lower pod diameter, increasing pod length resulted in an increase in unit thrust, whereas at higher pod diameter, increasing pod length produced a lower unit thrust. A similar effect was found in the range of $J=0$ to 0.4.

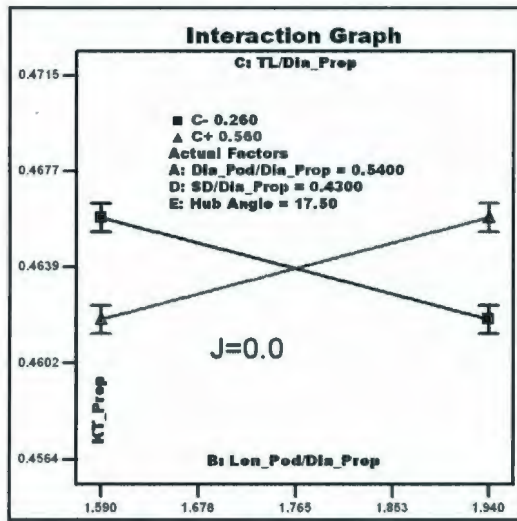


Figure 4.29: DOE Analysis: The interaction effect of L_{Pod}/D_{Prop} (B) and TL/D_{Prop} (C) on propeller thrust at $J=0$ for pusher propulsors.

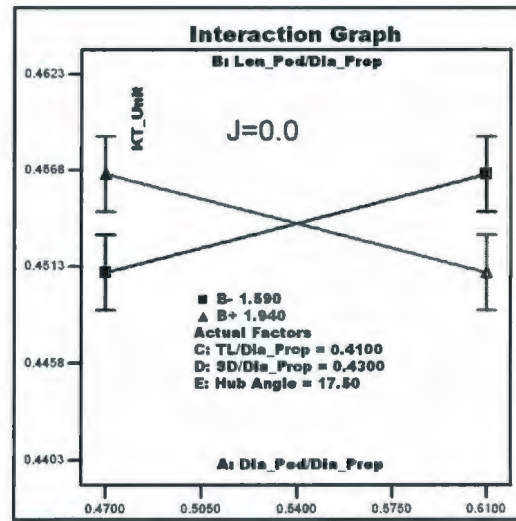


Figure 4.30: DOE Analysis: The interaction effect of D_{Pod}/D_{Prop} (A) and L_{Pod}/D_{Prop} (B) on unit thrust at $J=0$ for pusher propulsors.

4.5 Summary

This chapter presents the results and analysis of the experimental study of a series of 16 pods, which were designed using a fractional factorial design technique to study the effects of five geometric parameters (pod diameter, pod length, pod taper length, strut distance and propeller hub angle) of podded propulsors in pusher and puller configurations. The experimental data on the pod series were acquired using a custom-designed pod testing system at the OERC towing tank at Memorial University. The factors and interaction of factors that have significant influence on the performance coefficients K_{TProp} , K_Q , η_{Prop} , K_{TUnit} and η_{Unit} for both the puller and pusher propulsors in the pod series are presented. In puller configuration, the significant factors that come up repeatedly over the range of J values were A (the ratio of pod diameter to propeller diameter, D_{Pod}/D_{Prop}), D (the ratio of strut distance to propeller diameter, S_{Dist}/D_{Prop}), E

Study of Pod with Varied Geometry

(hub taper angle, H_{Angle}), AE (interaction of $D_{\text{Pod}}/D_{\text{Prop}}$ and H_{Angle}) and BD (interaction of $L_{\text{Pod}}/D_{\text{Prop}}$ and $S_{\text{Dist}}/D_{\text{Prop}}$). The factor C (the ratio of pod taper length to propeller diameter, TL/D_{Prop}) did not show any significant influence on the performance coefficients at any advance coefficient. It was found that in the pusher configuration, the significant factors that came up repeatedly over the range of J values were A ($D_{\text{Pod}}/D_{\text{Prop}}$), B ($L_{\text{Pod}}/D_{\text{Prop}}$), C (TL), D ($S_{\text{Dist}}/D_{\text{Prop}}$), E (H_{Angle}), AB (interaction of $D_{\text{Pod}}/D_{\text{Prop}}$ and $L_{\text{Pod}}/D_{\text{Prop}}$) and BC (interaction of $L_{\text{Pod}}/D_{\text{Prop}}$ and TL).

CHAPTER

5

**STUDY OF POD at
STATIC AZIMUTHING
CONDITIONS**

5 Study of Pod at Static Azimuthing Conditions

5.1 Chapter Objectives

This chapter presents the results, analysis and the subsequent interpretation of the experimental results of the propulsive characteristics of puller and pusher podded propulsors in static azimuthing open water conditions. It presents the variations in the performance coefficients of one of the two average pod units with change of azimuthing angle and advance coefficients in non-dimensional forms. A comparison of the performance coefficients at different azimuthing angles between the puller and the pusher configurations is also provided.

5.2 Test Results

The propeller thrust coefficient, K_{TProp} , propeller torque coefficient, $10K_Q$, unit thrust coefficient, K_{TUnit} , transverse force coefficient, K_{FY} , vertical force coefficient, K_{FZ} , axial moment coefficient, K_{MX} , transverse moment coefficient, K_{MY} , and steering moment coefficient, K_{MZ} , values versus advance coefficients at different static azimuthing angles for the pod unit in puller and pusher configurations are presented in this section. The static azimuthing angle was varied in the range of $+30^\circ$ to -30° with various increments (a total of 11 azimuthing angles) and the advance coefficient was varied from 0 to 1.2 as shown in section 3.2.2. The propeller thrust was defined in the direction of the propeller axis. The positive direction of azimuth angle for the pod unit is shown in Figure 2.11 in

Chapter 2. For example, in all Figures, the legend Port10 means the pod unit was placed at 10° away from the straight course position in an anticlockwise direction (looking toward the pod unit from the top).

5.2.1 Puller Configuration

The propeller thrust and torque coefficient curves of the model propulsor in puller configuration are shown in Figures 5.1 and 5.2, respectively. The propeller thrust coefficients remained approximately the same for 30° (Port) and -30° (Starboard) static azimuth angles. The same conclusion applies for other azimuthing conditions in the two opposite angular positions at all advance coefficient values. A few exceptions were observed, which might be attributed to experimental uncertainty or the variations in the local propeller blade induced axial velocity. At bollard pull condition, the propeller thrust remained approximately the same for all azimuthing conditions. In straight-ahead condition, the thrust curve crossed the zero thrust line when the advance coefficient exceeded 1.1. At azimuthing conditions, the positive thrust occurred beyond the advance coefficient values of zero thrust at the straight-ahead conditions. The propeller torque coefficients, as shown in Figure 5.2, showed a similar trend as the thrust coefficient in the corresponding operating conditions. Tables A.7 and A.8 present the propeller thrust and torque coefficients of the pod unit in all static azimuthing angles.

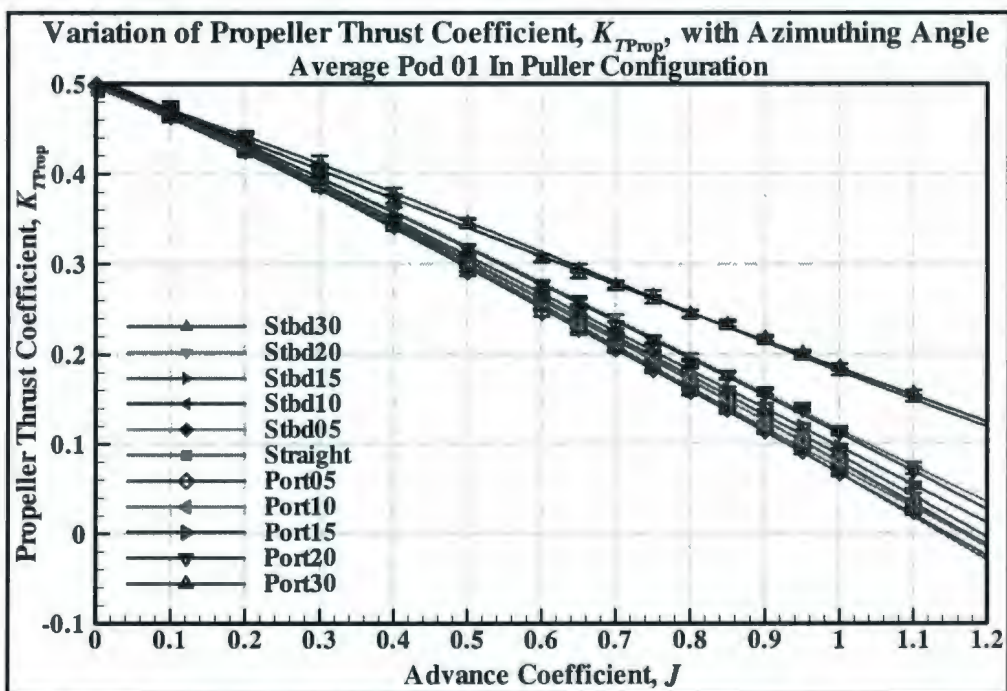


Figure 5.1: Propeller thrust coefficient vs. advance coefficient at constant values of azimuthing angles in the puller configuration.

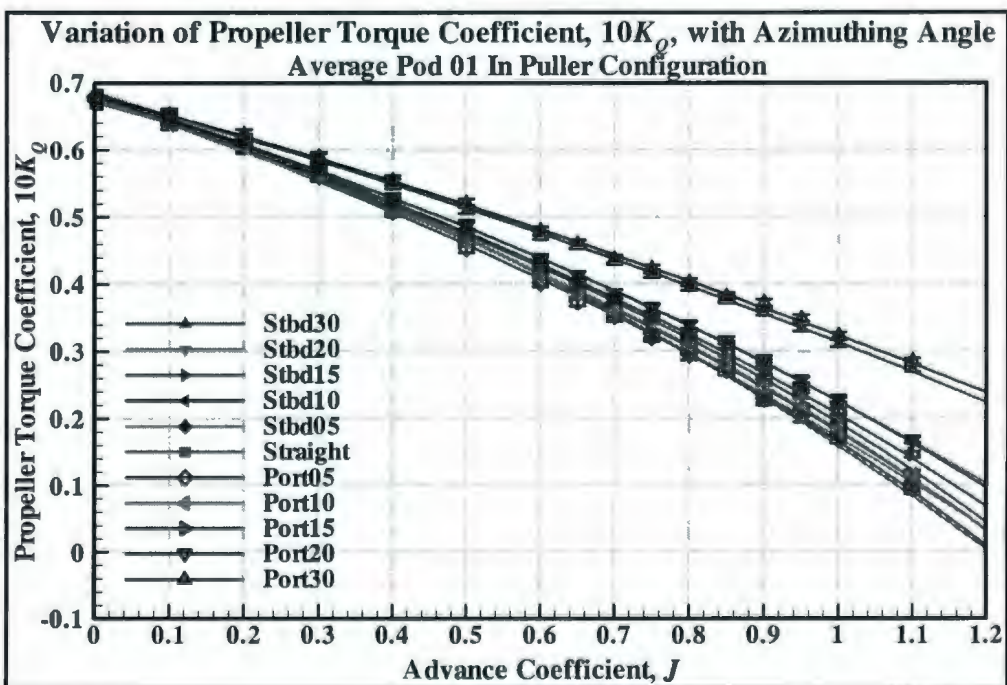


Figure 5.2: Propeller torque coefficient vs. advance coefficient at constant values of azimuthing angles in the puller configuration.

Study of pod at static azimuthing conditions

For puller configuration, the unit thrust, transverse force and vertical force coefficients of the pod for the range of advance coefficients and azimuth angles tested are presented in Figures 5.3, 5.4 and 5.5, respectively. The unit thrust decreased as the advance coefficient increased for all static azimuthing angles. At bollard pull condition, it did not remain the same as propeller thrust; as the azimuthing angle increased the unit thrust decreased in both azimuthing directions. The transverse force coefficient curves show an increase in magnitude with both positive and negative azimuthing angles but in opposite directions with the increase of advance coefficient, J . In bollard pull condition, as the azimuthing angle was increased, the magnitude of the transverse force on the pod unit also increased. The vertical force coefficients (downward positive) for a positive azimuthing angle, increased with the increase of advance coefficient from 0 to 0.8 (approximately), and then tended to decrease. However, for negative azimuthing conditions the vertical force acted upwards. In that condition, the nature of the curves of the vertical force coefficients was similar to that of the positive azimuthing conditions but of lower magnitude. The vertical force remained approximately constant (slightly negative, upward) at all azimuthing conditions at the bollard pull condition. Tables A.9, A.10 and A.11 present the unit thrust, transverse force and vertical force coefficients of the pod unit in all static azimuthing angles.

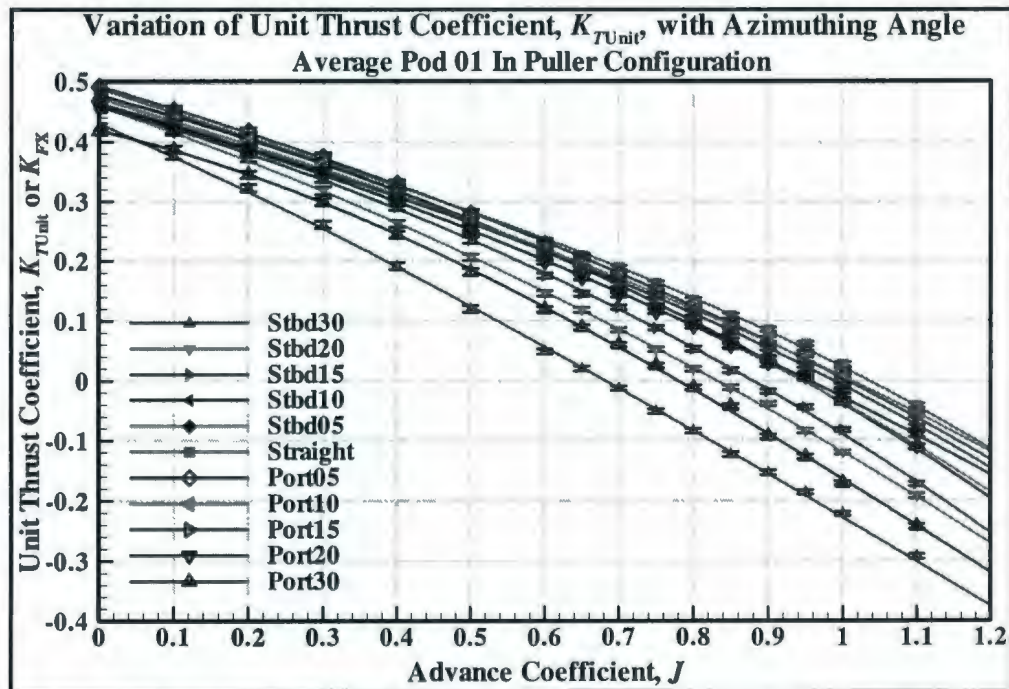


Figure 5.3: Unit thrust coefficient vs. advance coefficient at constant values of azimuthing angles in the puller configuration.

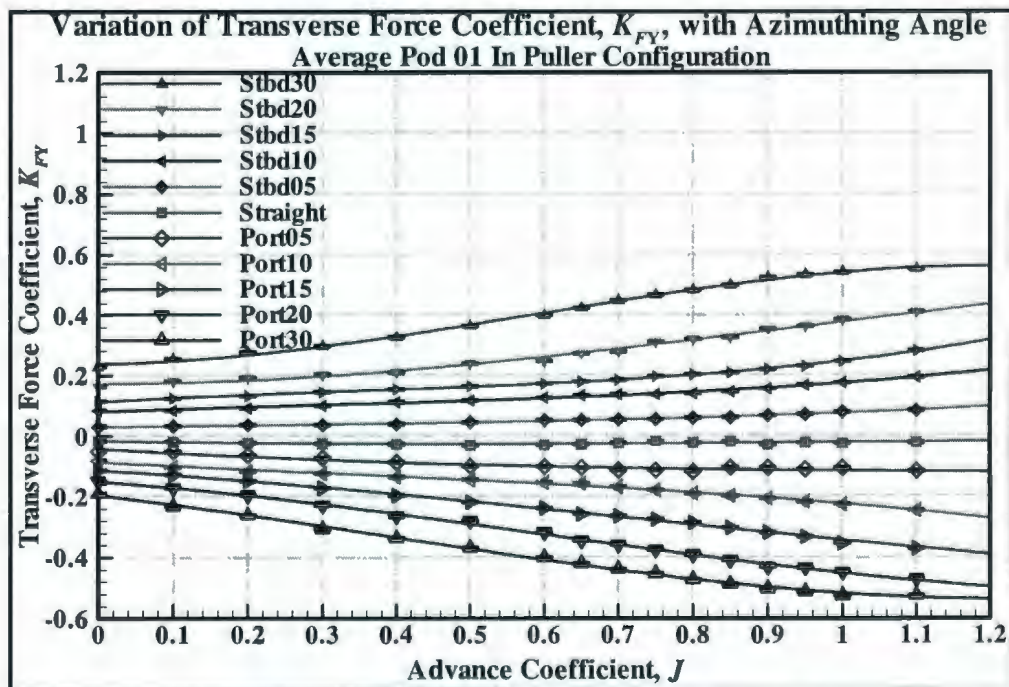


Figure 5.4: Transverse force coefficient vs. advance coefficient at constant values of azimuthing angles in the puller configuration.

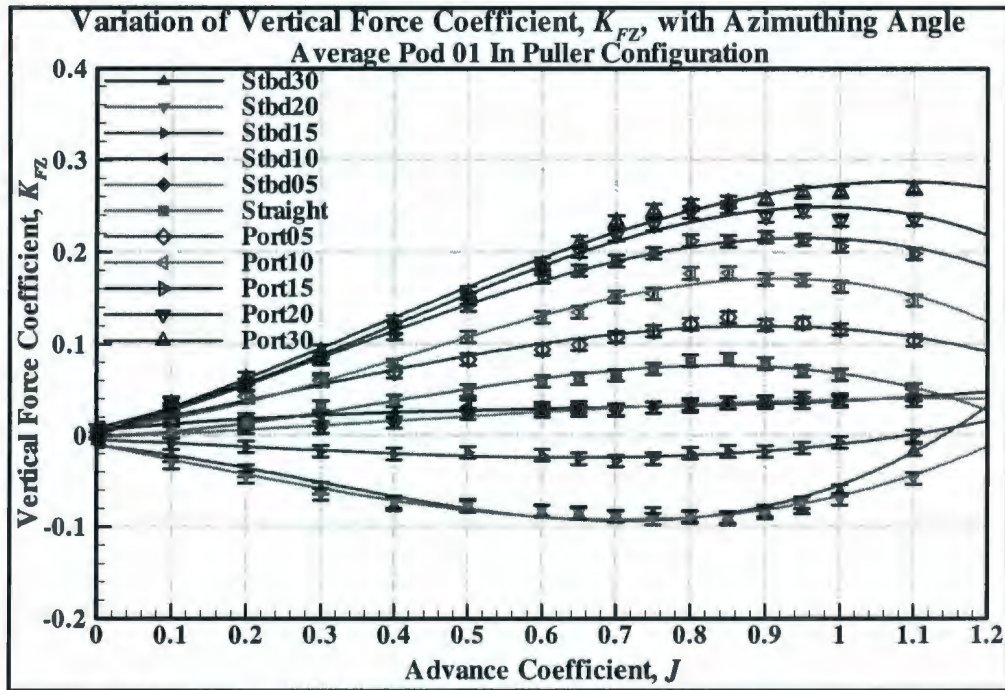


Figure 5.5: Vertical force coefficient vs. advance coefficient at constant values of azimuthing angles in the puller configuration.

The axial, transverse and steering moment curves are shown in Figures 5.6, 5.7 and 5.8, respectively. The trend of the axial moment coefficients, at all azimuthing angles is approximately similar to those of transverse force. Again, the trend of the transverse moment curves, at all azimuthing angles is approximately similar to those of unit thrust, which suggests that the primary contributor to the transverse moment is the unit thrust. Figure 5.8 shows the change of steering moment coefficients with advance coefficient and azimuth angles in puller configurations. The steering moment (vertical moment about z-axis) showed an increasing tendency in magnitude with the increase of advance coefficients for both positive and negative azimuthing angles but in opposite directions. At straight-ahead condition, the steering moment remained approximately the same with

Study of pod at static azimuthing conditions

the increase of advance coefficient. At bollard pull condition, the steering moment remained approximately constant (slightly less than zero) for all azimuthing angles. Tables A.12, A.13 and A.14 present the unit axial, transverse and steering moment coefficients of the pod unit in all static azimuthing angles.

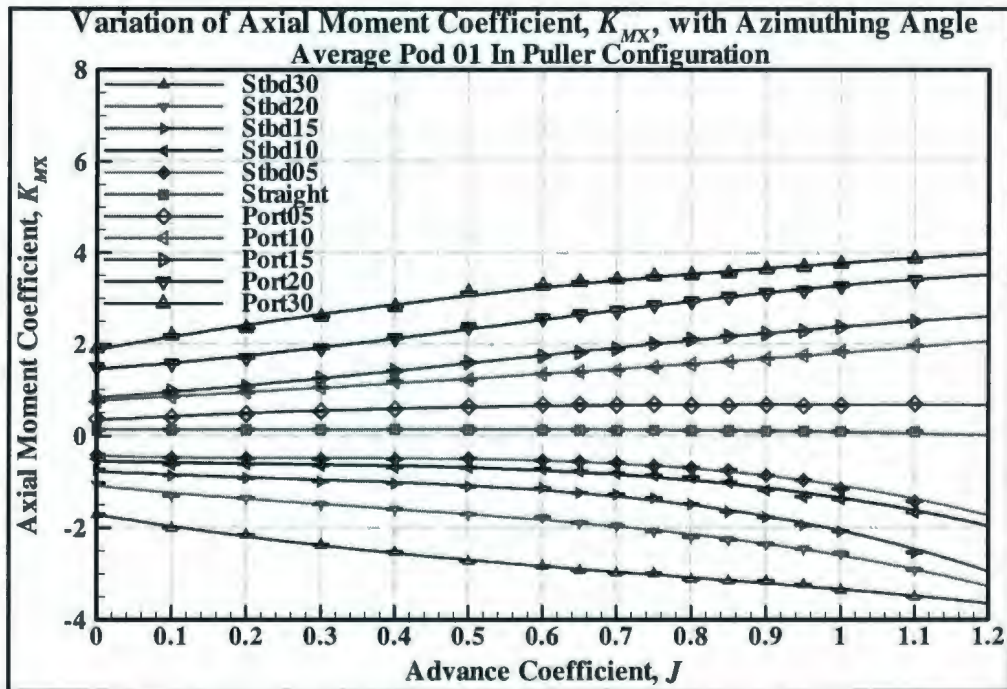


Figure 5.6: Axial moment coefficient vs. advance coefficient at constant values of azimuthing angles in the puller configuration.

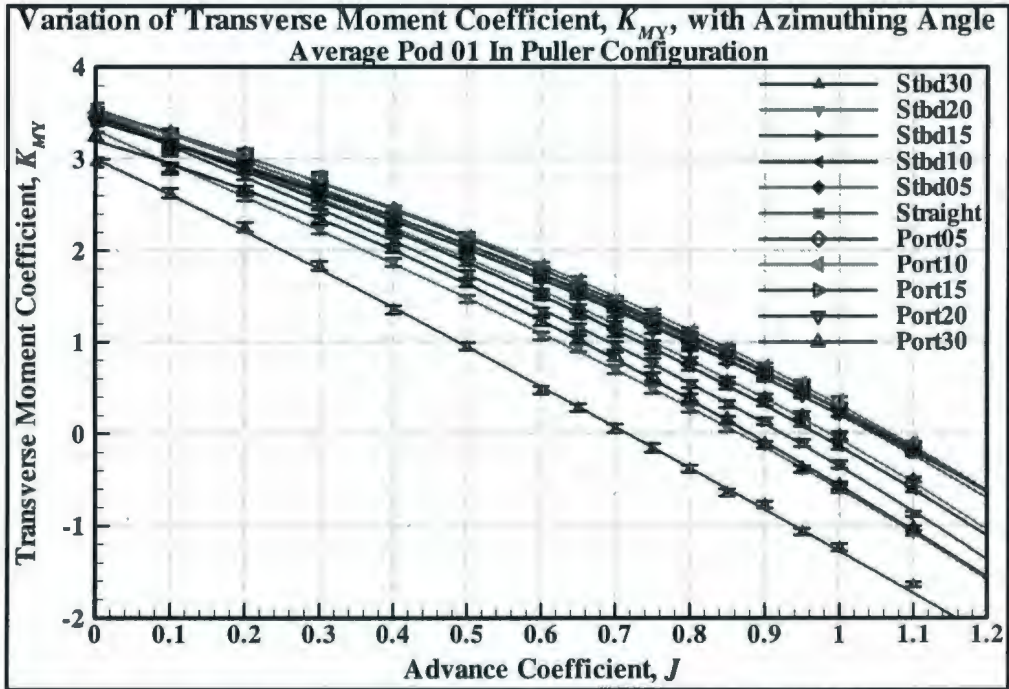


Figure 5.7: Transverse moment coefficient vs. advance coefficient at constant values of azimuthing angles in the puller configuration.

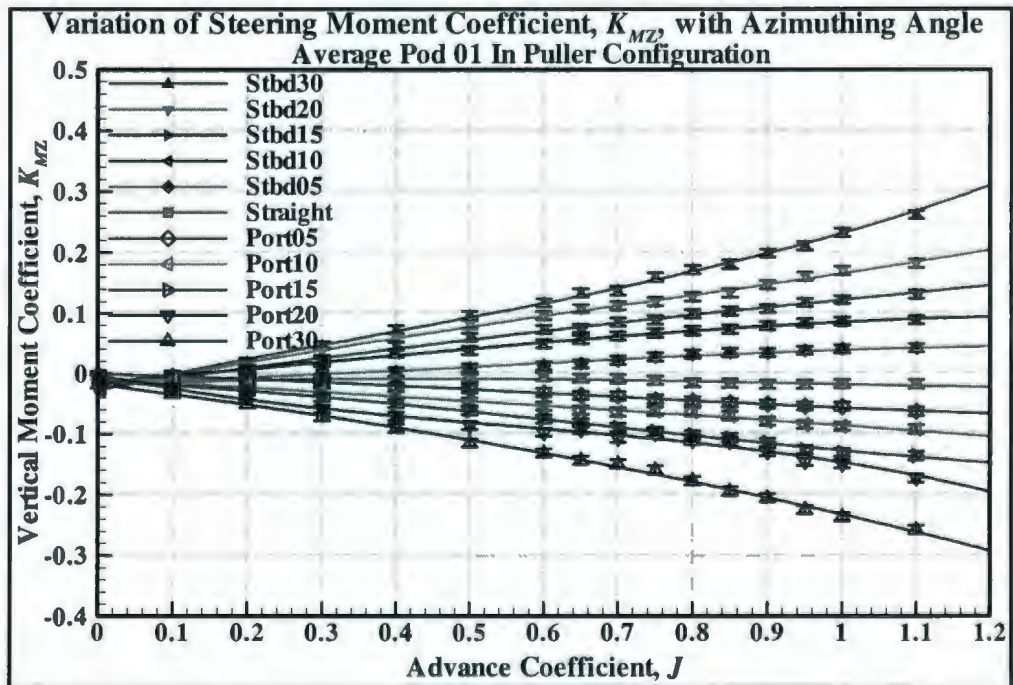


Figure 5.8: Steering moment coefficient vs. advance coefficient at constant values of azimuthing angles in the puller configuration.

5.2.2 Pusher Configuration

In the pusher configuration, the propeller thrust and torque coefficient curves, as shown in Figures 5.9 and 5.10, behaved differently for the opposite azimuthing conditions. For the range of advance coefficients considered, the propeller thrust coefficient was higher than those of the straight course conditions for positive (port) azimuth angles and were lower for negative (starboard) azimuth angles. An explanation for this trend is provided in section 5.3.1. At bollard pull condition, the thrust coefficient did not remain constant in contrast to puller configuration. The propeller torque coefficients showed a similar trend as the thrust coefficient in the corresponding operating conditions. Tables A.15 and A.16 present the propeller thrust and torque coefficients of the pod unit in all static azimuthing angles.

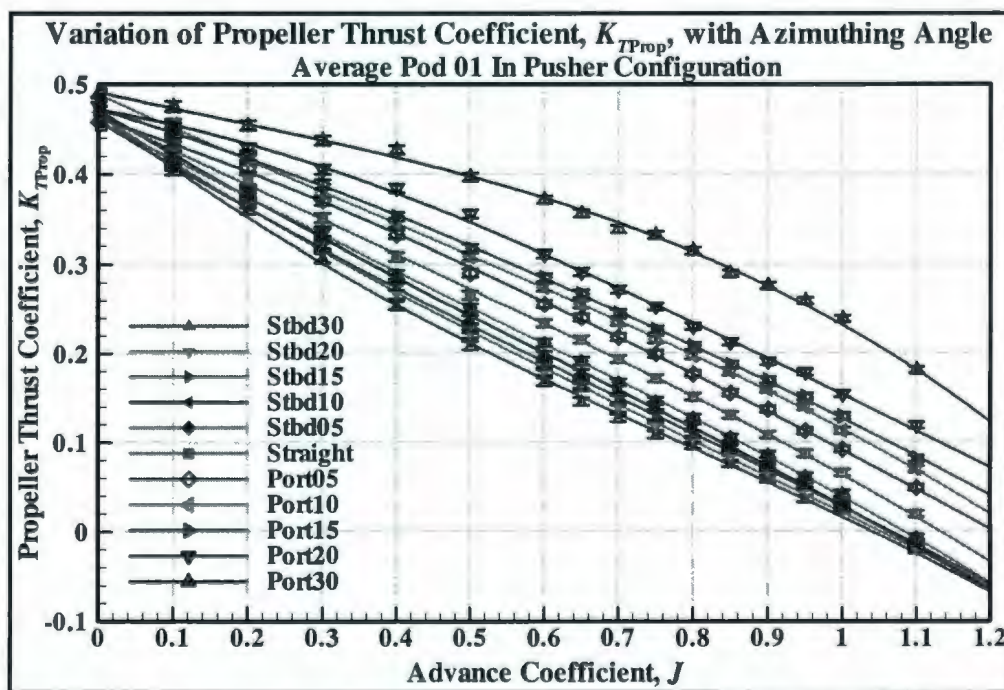


Figure 5.9: Propeller thrust coefficient vs. advance coefficient at constant values of azimuthing angles in the pusher configuration.

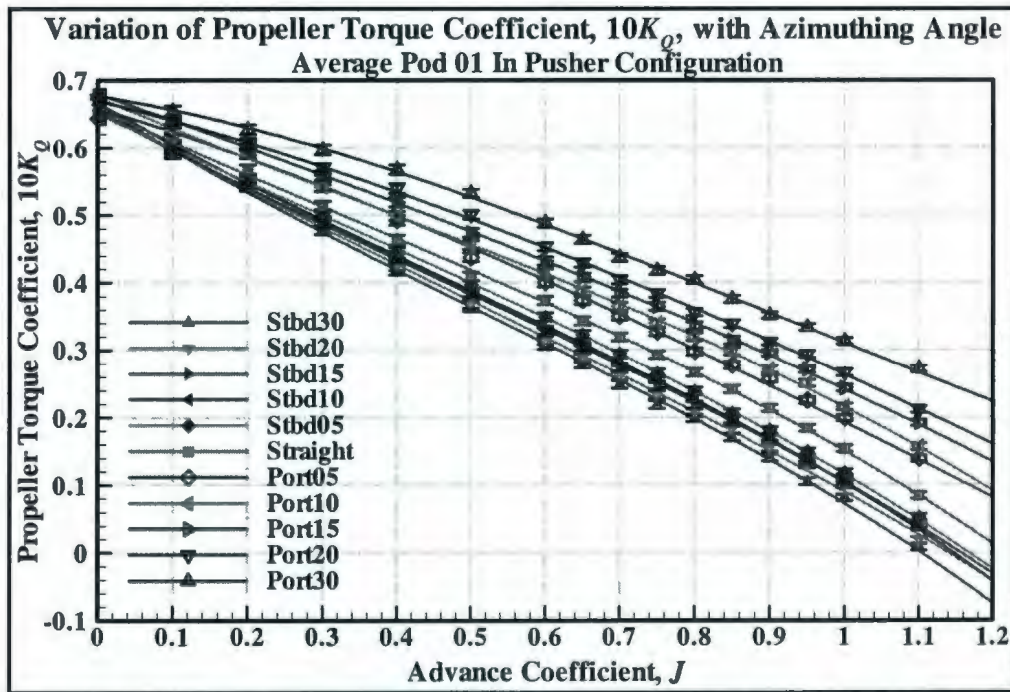


Figure 5.10: Propeller torque coefficient vs. advance coefficient at constant values of azimuthing angles in the pusher configuration.

The unit, transverse and the vertical force coefficients of the pod in pusher configuration for the range of advance coefficients are shown in Figures 5.11, 5.12 and 5.13, respectively. The nature and magnitude of the transverse force coefficient values with the change of advance coefficient and azimuthing conditions were different than those in puller configuration. The trend of the curves of the vertical force is different from the corresponding curves in the pull configuration. For straight-ahead condition, the vertical force acted upward and increased with increasing advance coefficients. At higher positive azimuthing angles, the vertical force acted downwards and tended to increase with increasing advance coefficient and azimuthing angles. For negative azimuthing conditions, the vertical force always acted upward and increased with increasing advance

Study of pod at static azimuthing conditions

coefficients and azimuthing angles. Tables A.17, A.18 and A.19 present the unit thrust, transverse force and vertical force coefficients of the pod unit in all static azimuthing angles.

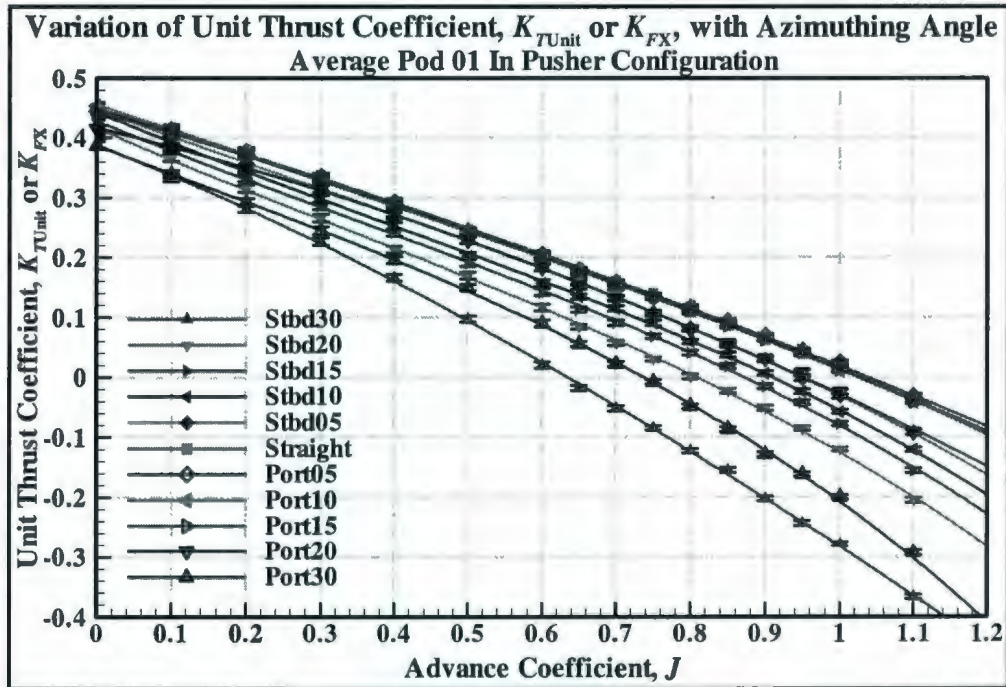


Figure 5.11: Unit thrust coefficient vs. advance coefficient at constant values of azimuthing angles in the pusher configuration.

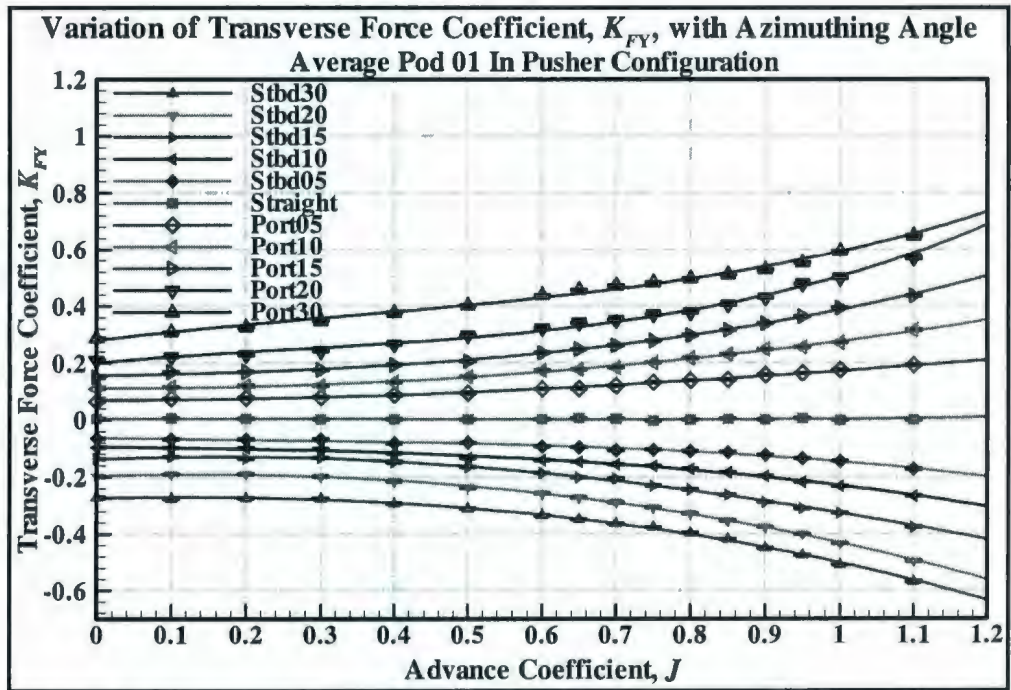


Figure 5.12: Transverse force coefficient vs. advance coefficient at constant values of azimuthing angles in the pusher configuration.

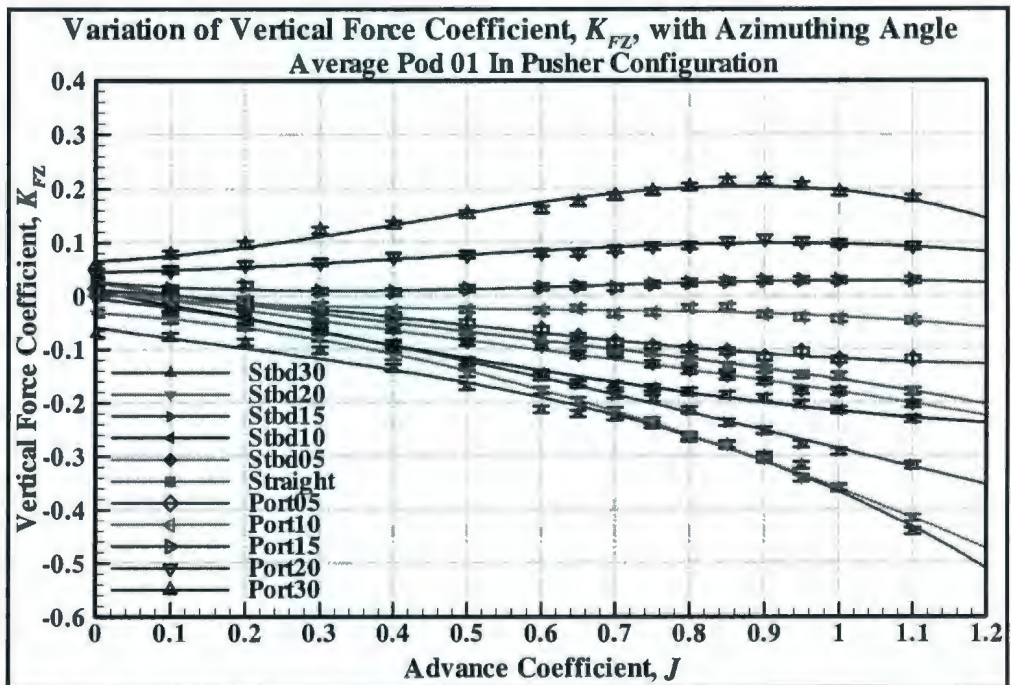


Figure 5.13: Vertical force coefficient vs. advance coefficient at constant values of azimuthing angles in the pusher configuration.

Study of pod at static azimuthing conditions

The axial, transverse and steering moment curves are shown in Figures 5.14, 5.15 and 5.16, respectively. The axial moment showed an increasing tendency with the increase of advance coefficients for positive azimuthing angles and a decreasing tendency with the increase of advance coefficients for negative azimuthing angles with a steady behaviour for straight course conditions. The transverse moment coefficient showed a different trend in the pusher configuration than the puller configuration with respect to advance coefficients and azimuthing conditions considered. A decreasing tendency with the increase of advance coefficients for all azimuthing conditions was observed. In this configuration, the transverse moment did not show any visible trend with the change of azimuthing conditions at fixed advance coefficients. The steering moment showed an increasing tendency with the increase of advance coefficients for positive azimuthing angles and a decreasing tendency with the increase of advance coefficients for negative azimuthing angles and a steady behaviour for straight course conditions. Tables A.20, A.21 and A.22 present the unit axial, transverse and steering moment coefficients of the pod unit in all static azimuthing angles.

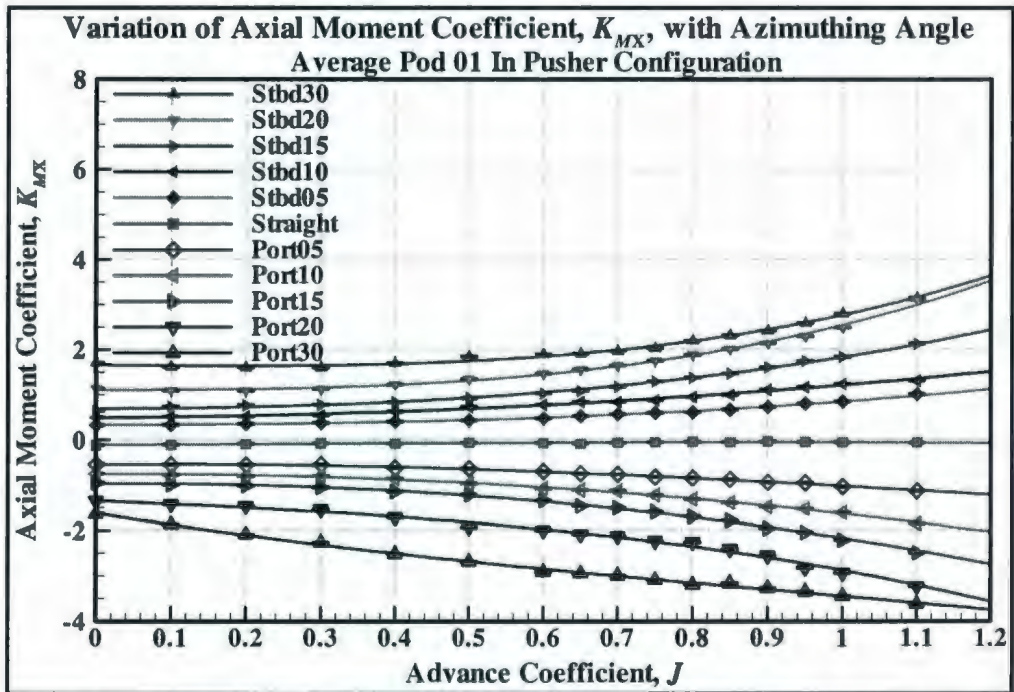


Figure 5.14: Axial moment coefficient vs. advance coefficient at constant values of azimuthing angles in the pusher configuration.

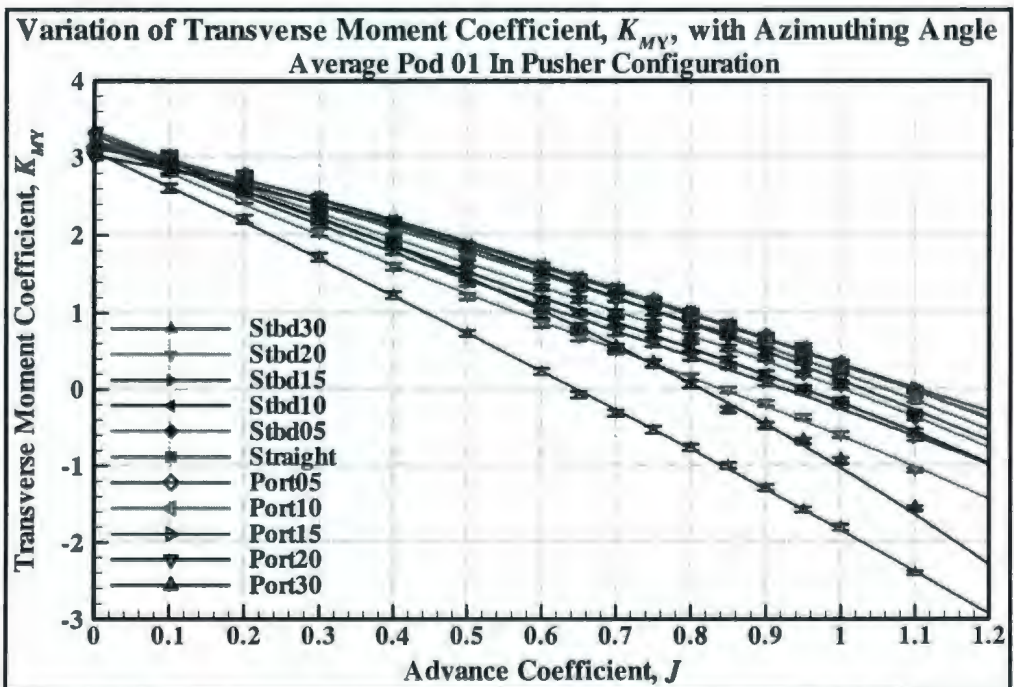


Figure 5.15: Transverse moment coefficient vs. advance coefficient at constant values of azimuthing angles in the pusher configuration.

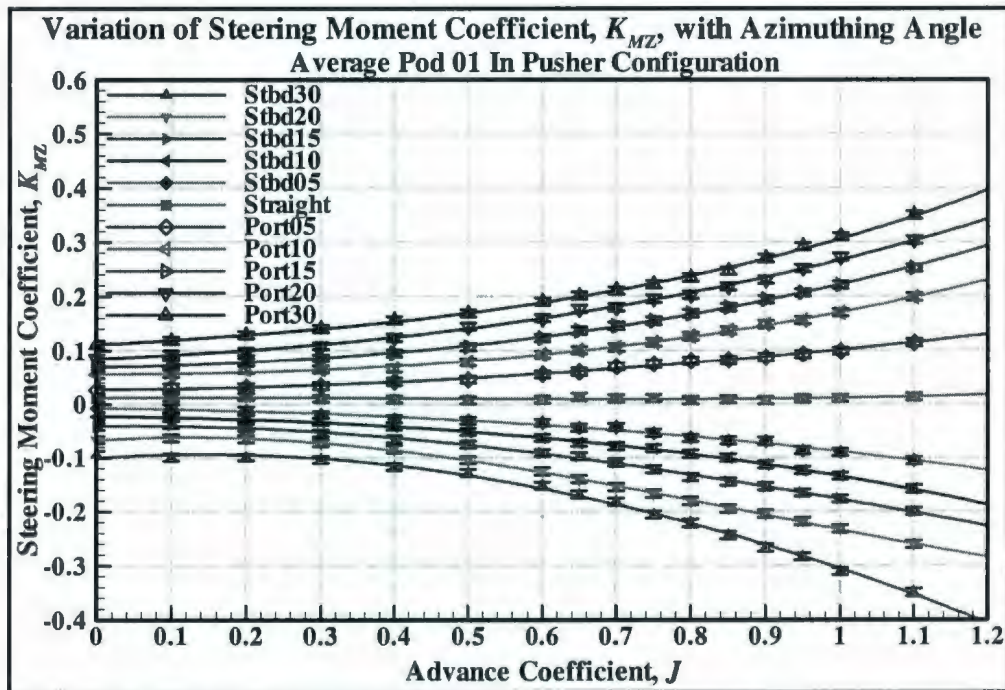


Figure 5.16: Steering moment coefficient vs. advance coefficient at constant values of azimuthing angles in the pusher configuration.

5.3 Discussion on Effects of Static Azimuthing Angles

In a podded propulsor, the forces and moments on the propeller and on the whole unit in azimuthing condition can be seen as produced through the following mechanism. In any azimuthing condition, the effective axial inflow velocity relative to the uniform inflow is reduced (i.e. with the cosine of the angle). This reduction essentially reduces the effective advance coefficient defined along the propeller axis and thus increases propeller shaft thrust and torque. At an azimuthing angle, as the propeller blades pass through the oblique inflow, the unequal angles of incidence results in a normal force (normal to the propeller shaft and acting on the propeller centre, Stettler 2004). Also, at higher azimuthing angles and at higher advance speeds, the transverse roll-up of the blade wake

Study of pod at static azimuthing conditions

along its top and bottom edges forms two dominant yet unequal vortex bundles. Regardless of the direction of rotation of the propeller, the net normal force is in the same direction, away from the inflow (Stettler 2004). Again, because of the shape of the pod-strut body, it induces hydrodynamic lift (normal force perpendicular to its axis inducing transverse force and steering moment) and drag (axial force along its axis acting as pod drag) forces, as well as a hydrodynamic moment (Stettler 2004). In puller configuration, depending on the geometry, it is possible for the strut to recover some of the rotational energy in the propeller slipstream, by acting as lifting bodies, which generates a force with a forward acting component (Halstensen and Leivdal 1990). In pusher configuration, as mentioned in (Stettler 2004), two kinds of hydrodynamic interaction occurs: firstly, the interaction effects due to the effects of the propeller inflow on the flow past the propulsor pod (i.e. an added resistance analogous to the drag augmentation or thrust deduction used for normal shafted propellers), and secondly, the converse (i.e. the effect of the pod wake on the propulsor inflow, analogous to the wake fraction and inflow wake field used for normal shafted propellers). These forces and moments together with the interaction between the pod and the propeller play an important role in determination of the propulsor maneuvering forces and moments, especially at moderate to large azimuthing angles.

Figure 5.17 illustrates the concept of propeller and pod wake inflow variations for a generic case for the puller and pusher podded propulsors in static azimuthing conditions. The figure shows the combination of pod and the propeller wake region due to the

Study of pod at static azimuthing conditions

uniform inflow and propeller blade rotation. In puller configuration there is a large region where the propeller wake interacts with the pod wake. In pusher configuration, a portion of the propeller blades works under the influence of pod wake. Thus, the inflow to the propeller disk can also possess circumferential variation due to the existence of the wake of the pod when the pod is azimuthed relative to the inflow. This conceptual wake interaction in pusher configuration was also observed in the flow visualization study by Stettler (2005). A brief discussion on the phenomena is followed next.

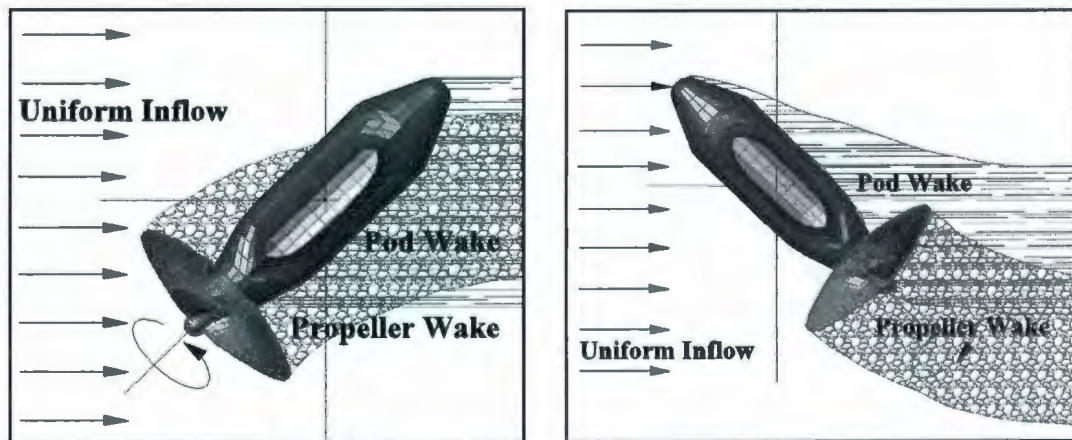


Figure 5.17: Conceptual propeller and pod wake at static azimuthing angles with: left for puller configuration and right for pusher configuration.

In the flow visualization and PIV studies, Stettler (2004) illustrated a wake distortion, which occurs when the propeller is subjected to oblique inflow. The upstream side of the wake is stretched, while the downstream side of the wake is compressed. The net effect is a slight difference in wake pitch as measured on the upstream and downstream sides of the wake. The magnitude of velocity (or induced velocity) is greater for the “upstream” or “outboard” side of the wake for the azimuthed case (for the horizontal wake cut). An

explanation for this wake velocity asymmetry can be understood by considering that the vortex wake undergoes distortion under the oblique inflow. Experiments for helicopters in forward flight have confirmed vortex wake distortion effects. Although the blade geometry and loading distribution of a helicopter blade is clearly different than a “typical” marine propeller, it can be expected that the same basic relationship between blade and tip helices would remain (Gray 1992, Done and Balmford 2001). For small azimuth angles, the effect is small, but noticeable. In the PIV study by Stettler (2004), it was found that the average total and average perturbation (induced) wake velocities for the conditions with azimuth are noticeably greater than the 0° condition. This increase in wake velocity is intuitively linked to an increase in thrust.

The unit thrust and the transverse force can be related to the propeller thrust and normal force components by equation 5.1.

$$\begin{bmatrix} T_{\text{Unit}} \\ F_Y \end{bmatrix} = \begin{bmatrix} \cos \theta & -\sin \theta \\ \sin \theta & \cos \theta \end{bmatrix} \begin{bmatrix} T_{\text{Prop}} \\ N \end{bmatrix} \quad 5.1$$

The propulsor also produces vertical forces at azimuthing conditions due to the pressure difference on the top and bottom of the unit, which results from the interaction effect between the pod-strut body and the propeller wake. The axial moment of the unit (moment about X axis) is primarily attributed to the transverse force and the shaft torque. The transverse moment on the unit is attributed mainly to the unit thrust and vertical force. The steering moment can primarily be attributed to the transverse force produced by the pod unit.

The unit thrust, transverse force, and steering moment, are important from a steering and manoeuvring point of view, whereas the unit vertical force, axial and transverse moments are important from a structural point of view. The unit force is generally related to the ship powering prediction and the combination of unit transverse force and steering moment is related to the steering and manoeuvrability of the ship. Adequate knowledge about the nature of global forces and moments with the change of loading and azimuthing conditions is essential for the improvement of the design of podded propulsors. This section presents a detailed discussion of the trend of the coefficients of the propeller and the pod unit with the change of the propeller loading (advance velocity) and azimuthing angle in static azimuthing conditions.

5.3.1 Propeller Shaft Local Thrust and Torque Coefficients

The propeller thrust coefficient curves at constant advance coefficients for the model pod unit in puller and pusher configurations are shown in Figures 5.18 and 5.19, respectively. In the puller propulsor the propeller thrust coefficient increased with increasing magnitude of azimuthing angle for a given advance coefficient and were approximately symmetric about the straight ahead condition (zero azimuth angle), i.e. approximately the same value for equal port and starboard static azimuth angles. At azimuthing angles in puller configurations, the inflow to the propeller blades becomes unsteady, and there is a spanwise non-uniform local velocity distribution over the blade. These resulted in an increased thrust at the azimuthing conditions at any advance coefficient value as compared to those at straight-ahead conditions at the corresponding operating conditions.

Study of pod at static azimuthing conditions

It should be noted that the advance coefficient is defined in the X direction of the inertia frame and not in the direction of the propeller axis. This means the effective advance coefficient in the direction of the propeller axis was reduced, which resulted in higher thrust in the corresponding operating conditions.

For a pusher propulsor, as shown in Figure 5.19, the propeller thrust coefficients were not symmetric at port and starboard azimuthing angles. For all advance coefficients, the propeller thrust coefficient was higher for positive (port) azimuthing angles than those in straight course conditions. On the other hand, the propeller thrust coefficients were lower for negative (starboard) azimuthing angles. In the tests, the maximum propeller thrust was found at a 30° azimuth angle on the port side and the lowest thrust was found at -30° azimuth angle on the starboard side. It was also observed that the propeller thrust was less sensitive to changes in the azimuthing angle (in the range from -30° to 30°) for starboard values than port values. This asymmetry in propeller thrust can be attributed to the presence of the pod-strut housing in front of the propeller (propeller works in the pod-strut wake) and the effect of the direction of propeller rotation (right-handed propeller). A possible explanation for these observations for pod in pusher configuration was reported in (Stettler 2004) as described below.

In pusher configuration, the strut in front of the propeller creates a blockage of the flow into the propeller across the top of the pod, and results in an induced swirl around the pod housing and into the propeller, in addition to the clockwise swirl induced by the normal

Study of pod at static azimuthing conditions

right-handed propeller rotation (Stettler 2004). This additional induced swirl causes an asymmetric swirl inflow into the propeller. For a positive propulsor rotation angle (port), the strut induced swirl decreases the normal clockwise inflow swirl to the right-handed propeller, and for a negative propulsor angle, it increases the normal clockwise inflow swirl to the propeller (Stettler 2004). The net result was increased angle of attack at the blades for positive propulsor rotation (increased lift i.e. shaft thrust and lift-induced drag i.e. shaft torque) and decreased angle of attack at the blades for negative propulsor rotation (decreased lift i.e. shaft thrust and lift-induced drag i.e. shaft torque). Also, as the azimuthing angle increase, the strut induced effect increases, thus increasing or decreasing of the propeller thrust and torque occurs in the corresponding azimuthing directions. This type of force asymmetry for “pusher” type pods and thrusters was also noted in (Norrby and Ridley 1980), and more recently in (Heinke 2004) and (Grygorowicz and Szantyr 2004).

Overall, the thrust from the puller propeller at any advance coefficient and at any azimuthing angle was found to be higher than the thrust for the pusher propeller in corresponding operating conditions. This is primarily attributed to the sign of the hub taper angle of the propellers in the two configurations (Islam *et al.* 2006a).

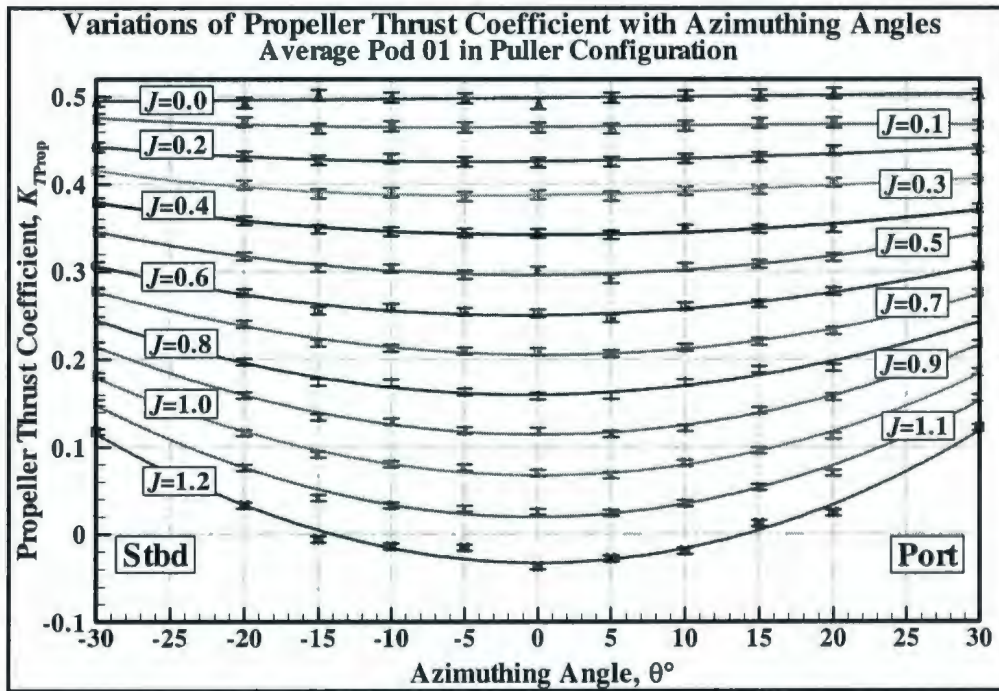


Figure 5.18: Propeller thrust coefficient vs. azimuthing angle at constant values of advance coefficient in the puller configuration (left handed propeller).

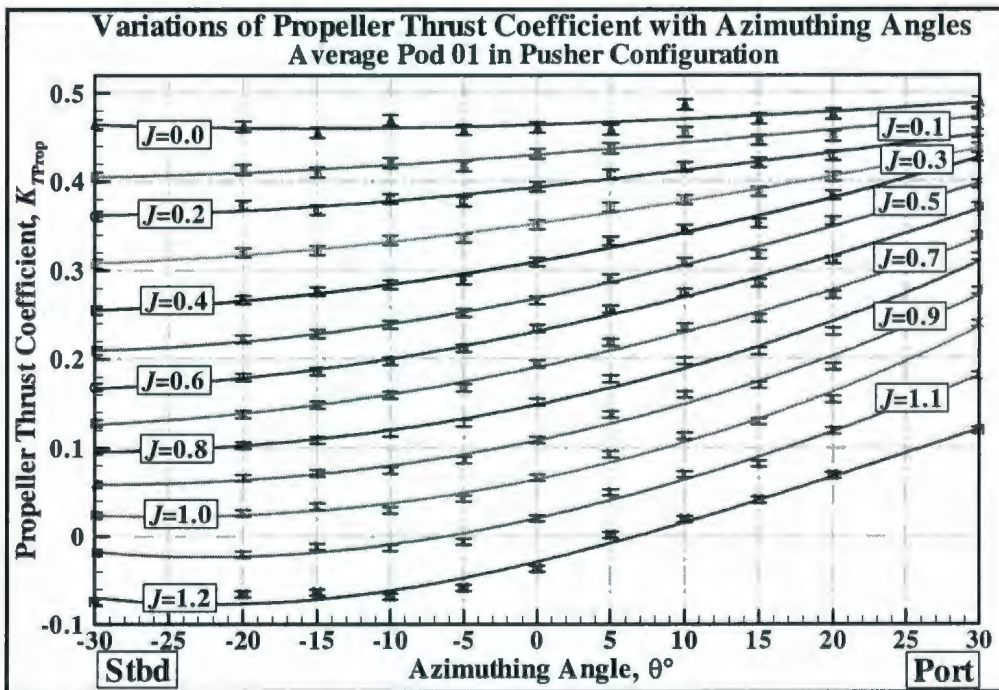


Figure 5.19: Propeller thrust coefficient vs. azimuthing angle at constant values of advance coefficient in the pusher configuration (right handed propeller).

Study of pod at static azimuthing conditions

The propeller torque coefficient curves in puller and pusher configurations are shown in Figures 5.20 and 5.21, respectively. The propeller torque was defined about the propeller axis. For a puller propulsor, shaft torque coefficient remained approximately the same for opposite static azimuth angles; this is similar to the propeller thrust coefficient values. As for the thrust coefficient, the torque along the propeller axis was increased compared with that at straight ahead courses. In pusher configuration, the shaft torque behaved similarly to that of the shaft thrust at the corresponding advance coefficient and azimuthing angles. Similarly to the thrust coefficient, the shaft torque coefficient in the puller configuration was higher than that in the pusher configuration at all corresponding operating conditions.

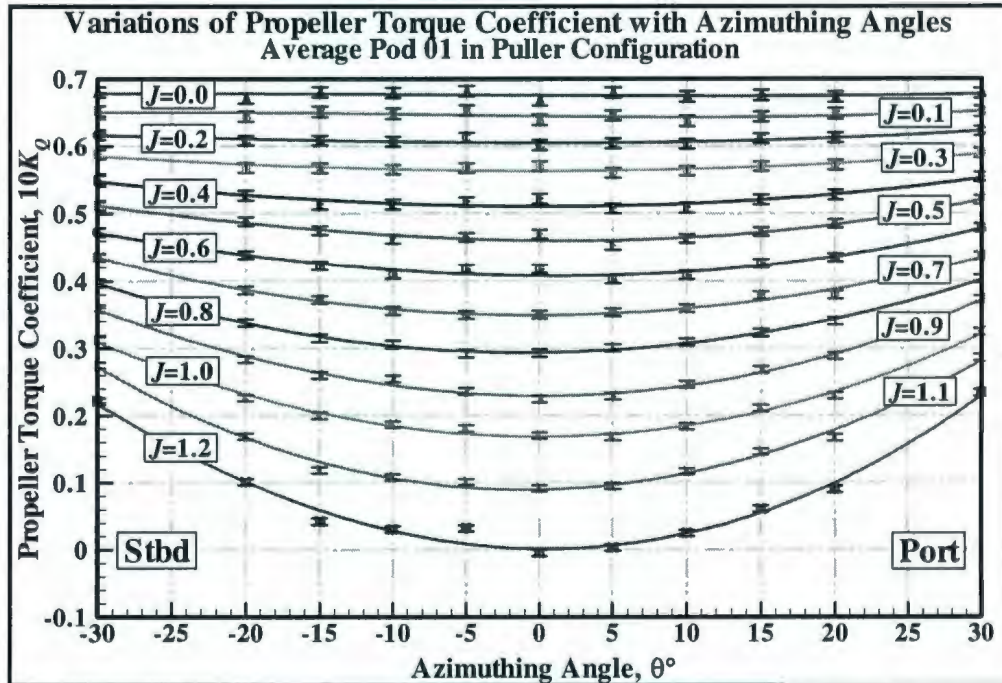


Figure 5.20: Propeller torque coefficient vs. azimuthing angle at constant values of advance coefficient in the puller configuration (left handed propeller).

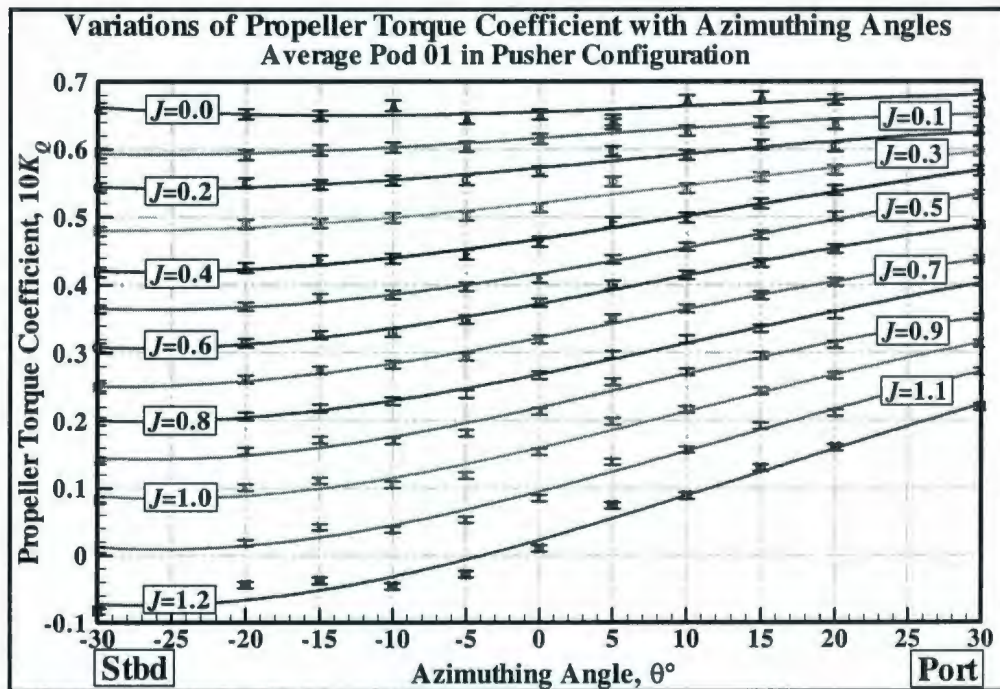


Figure 5.21: Propeller torque coefficient vs. azimuthing angle at constant values of advance coefficient in the pusher configuration (right handed propeller).

5.3.2 Unit Thrust Coefficients

For the pod in puller configuration, the unit thrust coefficients for the range of advance coefficients and azimuth angles tested are presented in Figure 5.22. The unit thrust coefficient, K_{TUnit} , sometimes also called the axial force coefficients, K_{FX} refers to the thrust of the whole pod unit whereas the propeller thrust is the thrust of the propeller only. It is the unit thrust which is of importance in assessing the thrust available for ship propulsion. The unit thrust coefficient decreased as the advance coefficient increased for a given azimuth condition. As the azimuthing angle was changed from 0° to 30° or from 0° to -30° , generally the K_{FX} decreased. However, there was an asymmetry such that the maximum thrust coefficient occurred at a positive (i.e. port) azimuthing angle of 10° for

Study of pod at static azimuthing conditions

most of the advance coefficients. The reduction of the axial force was stronger for the negative azimuth direction, i.e. for the left hand propeller and the clockwise azimuth direction (in the present case, 0° to -30° azimuth angles, see Figure 5.22). In other words, the force increase was greater with the azimuthing direction coinciding with the propeller rotation direction (the pod azimuths in a counter clockwise direction, looking down on the pod from above with a left hand screw propeller, looking from downstream). The asymmetry in unit thrust due to the propeller turning direction results from the interaction between the propeller wake and the strut. The strut acts as a lifting body and due to the propeller-strut interaction, it is likely that at small positive azimuthing conditions, thrust is added, or drag is reduced, on the unit. It is well known that a rudder downstream of a propeller adds thrust in certain steering (most) conditions (Carlton 1994, Halstensen and Leivdal 1990). It is well known that a left-handed propeller produces a "pull" to the port side implying that the rotation is stronger on the lower blade pass than the upper blade pass, which is nearer to the surface (Gerr 1989). The stronger swirl on the lower side with the strut rotated to port azimuthing angles leads to a lift force that has a component forward. This might have resulted in higher unit thrust at the small port azimuthing angles ($\leq 10^\circ$ port) as compared to that of the corresponding starboard azimuthing angles as well as straight-ahead conditions. Detailed experimental studies for local flow measurements using PIV or LDV are required to validate this speculation.

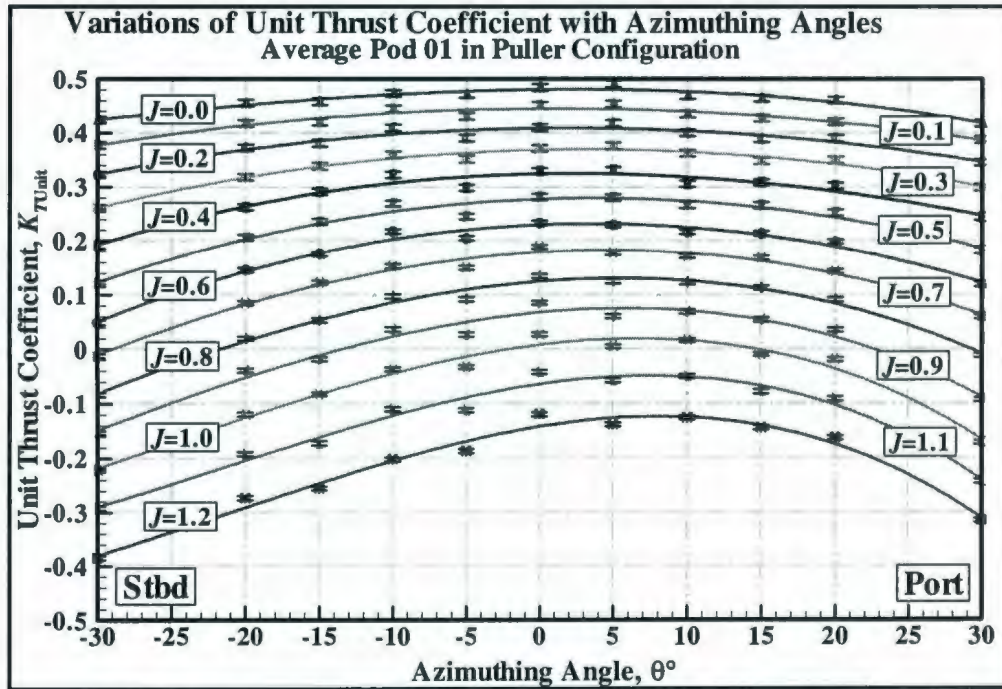


Figure 5.22: Unit thrust coefficient vs. azimuthing angle at constant values of advance coefficient in the puller configuration (left handed propeller).

For pusher configuration, Figure 5.23 shows the axial force or the unit thrust coefficient of the pod. As the azimuth angle was increased from 0° to 30° or from 0° to -30° , the K_{FX} decreased. There was an asymmetry such that the maximum thrust coefficient occurred at a positive (i.e. port) azimuthing angle of 10° . Similarly to the puller configuration, the reduction of the unit thrust was stronger for the negative azimuth direction, i.e. for the right hand propeller (looking from downstream), the counter clockwise azimuth direction (in the present case, $0^\circ - 30^\circ$ azimuth angles, looking down on the pod from above, see Figure 5.23). The asymmetry in unit thrust due to the propeller turning direction might have been due to the asymmetry of propeller thrust (see Figure 5.3). In pusher configuration, the total pod drag in opposite azimuthing angles

Study of pod at static azimuthing conditions

remains almost same, which means the differences in unit thrust in opposite azimuthing conditions was from the differences in the corresponding propeller thrust. Again, it could be because of the asymmetry due to the propeller rotation as for the puller propellers.

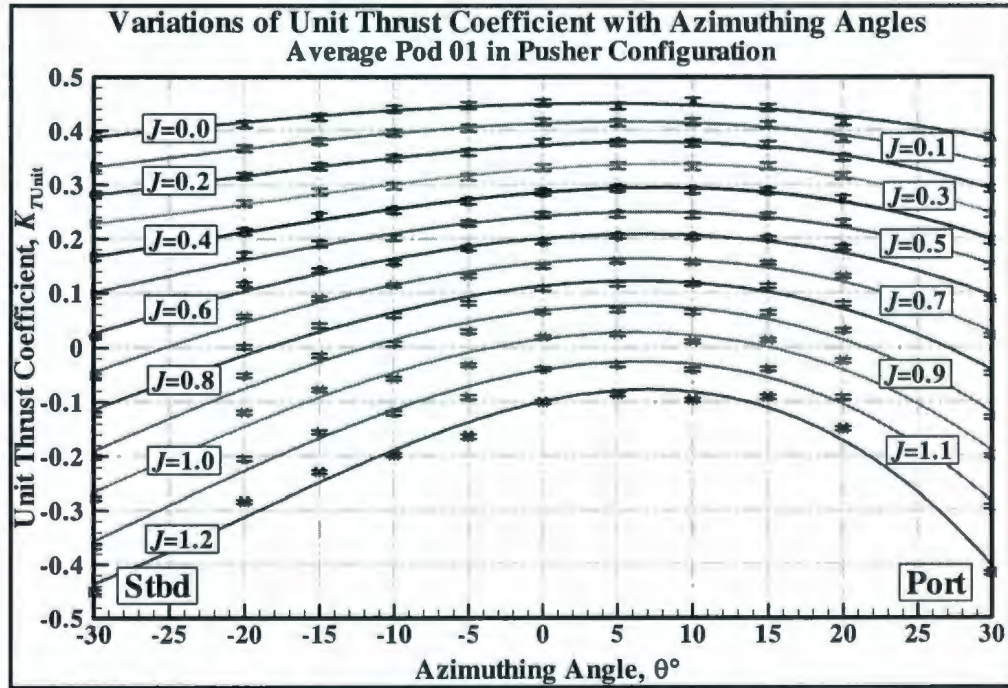


Figure 5.23: Unit thrust force coefficient vs. azimuthing angle at constant values of advance coefficient in the pusher configuration (right handed propeller).

Overall, the pod unit thrust in the pusher configuration at any advance coefficient and any azimuthing condition was lower than that for the puller configuration at the corresponding operating conditions.

5.3.3 Transverse Force Coefficients

For the puller configuration, Figure 5.24 shows the change of transverse force coefficients with advance coefficient and azimuth angles. The propulsor showed an increase of transverse force with increase of advance coefficient, J , in both positive and negative azimuth angles but as expected in opposite directions. Zero transverse force was found in the range of azimuth angles from 0 to -3° for different advance coefficients. In puller configurations, a left hand propeller in straight-ahead operating conditions produced a transverse force in the port direction (positive azimuthing angle) because of the propeller wake and strut interactions. Zero transverse force was obtained at a small negative (starboard) azimuthing angle.

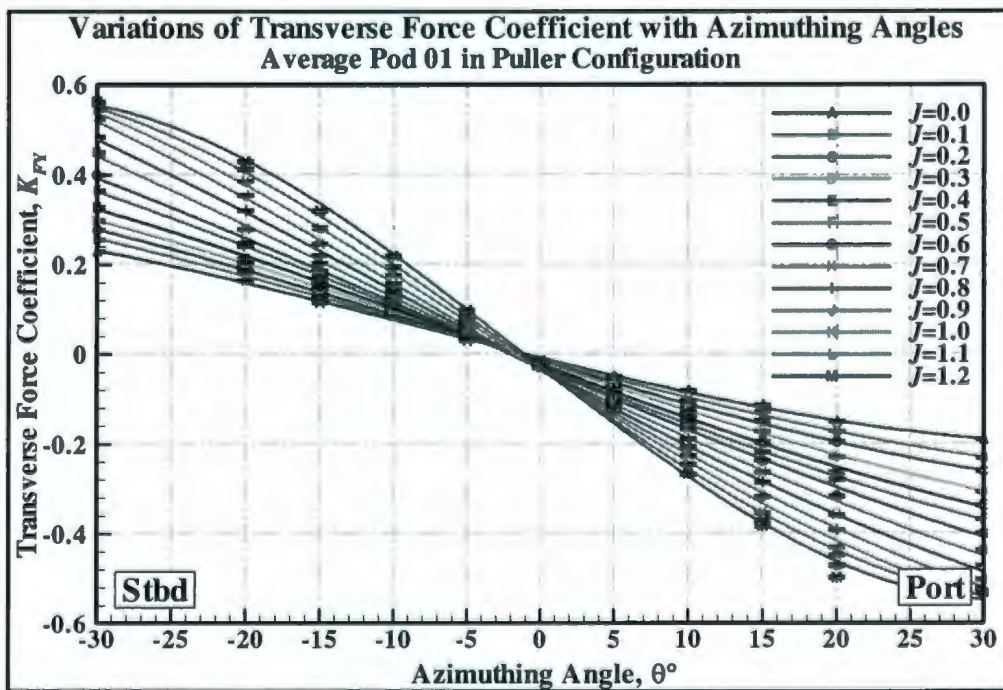


Figure 5.24: Unit transverse force coefficient vs. azimuthing angle at constant values of advance coefficient in the puller configuration (left handed propeller).

Study of pod at static azimuthing conditions

For pusher configuration pod, Figure 5.25 shows the change of transverse force coefficients with advance coefficient and azimuth angles. Zero transverse force was found in the range of azimuthing angles of 0° to -1° in starboard direction depending on the values of advance coefficients. The transverse force has two components: the pod drag component in the transverse direction and the propeller force component in the transverse direction. For pusher configurations in straight-ahead condition, the pod drag component in the transverse direction is near zero but the right-handed propeller still produces a small pull toward starboard direction. In this configuration, the difference in the transverse force coefficients in the two corresponding port and starboard azimuthing angles is more noticeable as compared to that in the puller configuration.

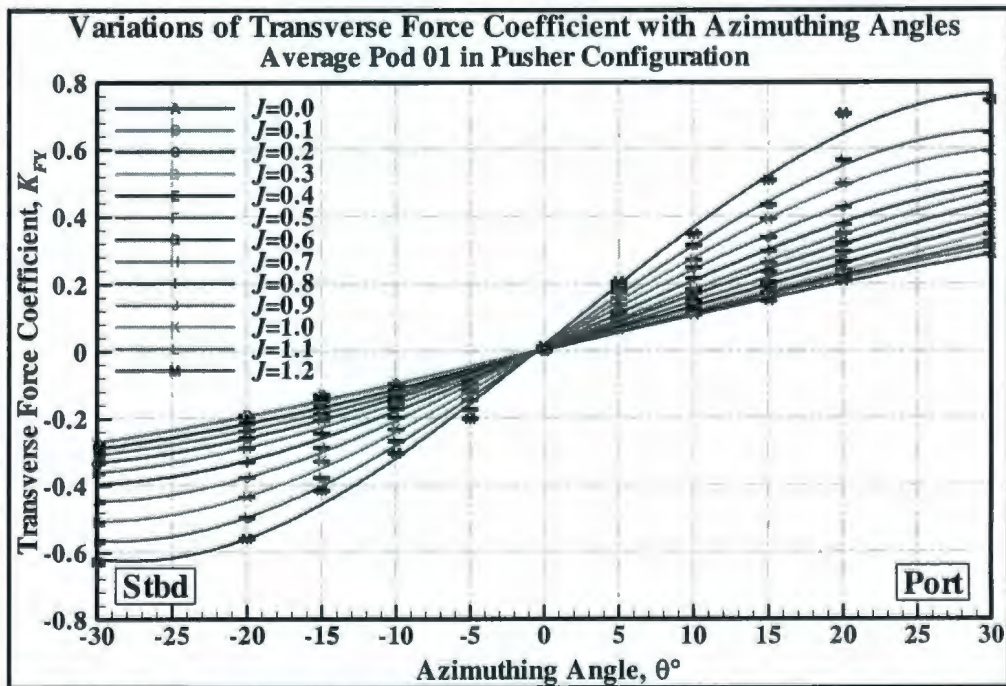


Figure 5.25: Unit transverse force coefficient vs. azimuthing angle at constant values of advance coefficient in the pusher configuration (right handed propeller).

5.3.4 Vertical Force Coefficients

The pod vertical force coefficients for puller and pusher configurations are shown in Figures 5.26 and 5.27, respectively. The vertical force was defined positive vertically downward. In puller configuration, the vertical force was mostly positive for positive azimuthing angles (port) and generally increased with the increase of azimuthing angle and advance coefficient. At negative azimuthing directions, there were a small amount of negative vertical force and the force increased with the increase of azimuthing angle and advance coefficients. In positive azimuthing angles, the inflow direction, propeller rotational direction (left handed) and the position of the strut behind the propeller might have caused high pressure on the top of the pod thus producing high downward vertical force at positive azimuthing angles. In negative azimuthing angles, however, the opposite effect took place because of the propeller worked against the inflow, thus producing negative vertical force. In pusher configuration, the negative vertical force was produced at negative azimuthing angles and the force increased with the increase of azimuthing angles and advance coefficients. At negative azimuthing angle (starboard), the interaction between the strut wake and the propeller wake (right-handed) produced low pressure on top of the pod body, thus producing high negative (upward) vertical force. Overall, the magnitude of the vertical force coefficients for the pusher configuration was higher than that of the puller configuration.

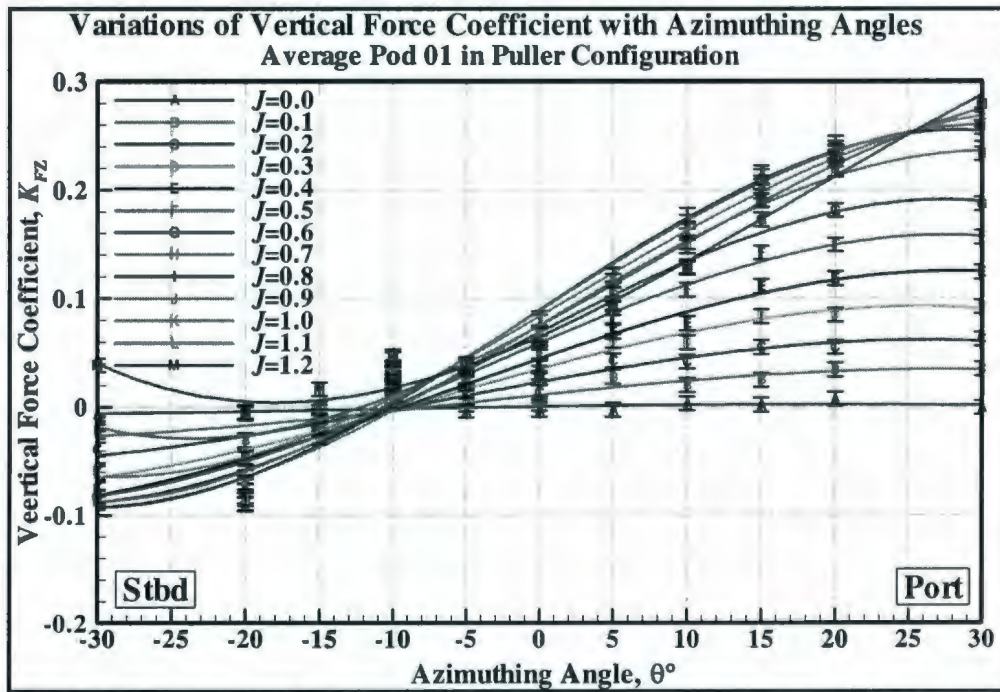


Figure 5.26: Unit vertical force coefficient vs. azimuthing angle at constant values of advance coefficient in the puller configuration (left handed propeller).

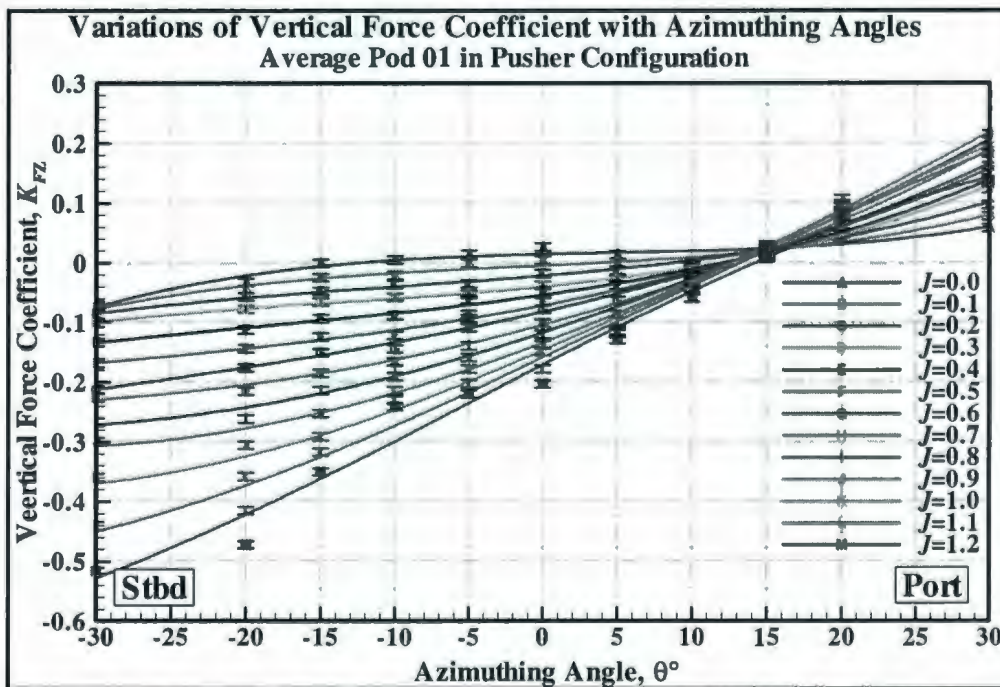


Figure 5.27: Unit vertical force coefficient vs. azimuthing angle at constant values of advance coefficient in the pusher configuration (right handed propeller).

5.3.5 Axial Moment Coefficients

The axial moment coefficients plotted against azimuthing angles at constant advance coefficient for the puller and pusher configurations are shown in Figure 5.28 and 5.29, respectively. The trends of the curves in both configurations are generally similar to those of transverse force coefficients in the corresponding configurations, but of different signs. The axial moment is primarily attributed to the transverse force and the shaft torque. Also, the sign of the propeller rotational direction (left handed propeller for the puller configuration and right handed propeller for the pusher configuration) might have contributed to the difference in the axial moment coefficients for the two configurations. The high magnitude of the axial moment coefficient is because the moment was calculated about the global unit centre, which is 1.68m vertically above the pod centre.

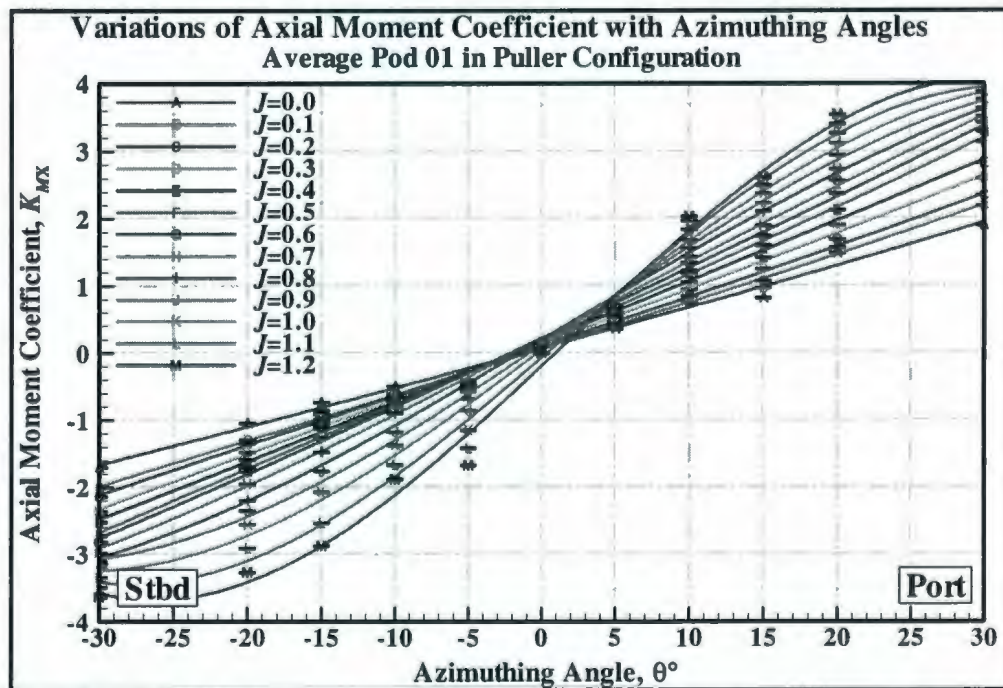


Figure 5.28: Unit axial moment coefficient vs. azimuthing angle at constant values of advance coefficient in the puller configuration (left handed propeller).

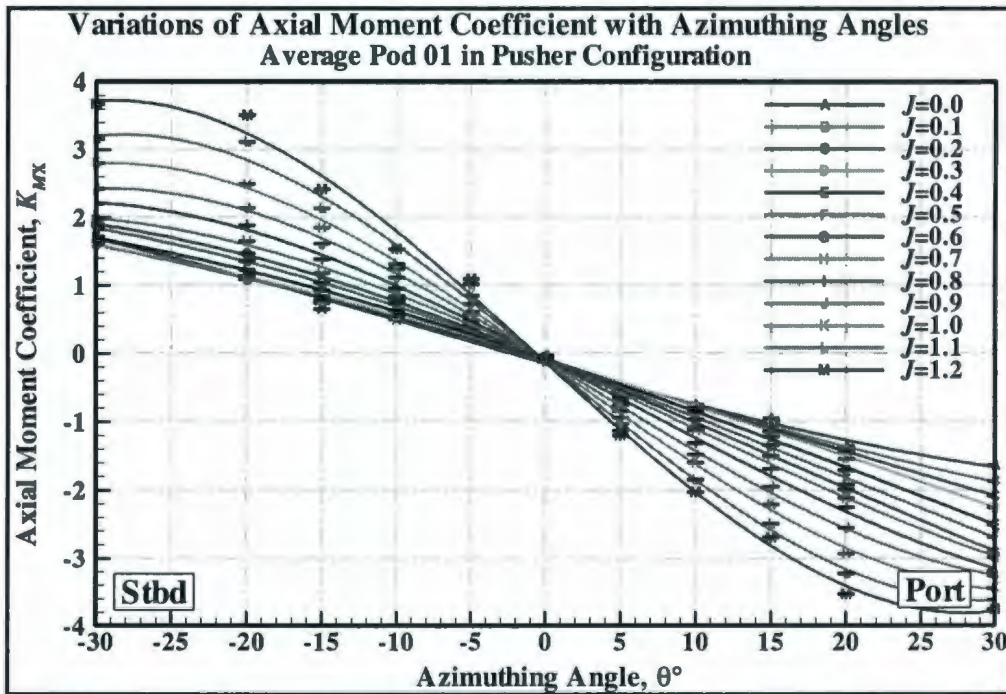


Figure 5.29: Unit axial moment coefficient vs. azimuthing angle at constant values of advance coefficient in the pusher configuration (right handed propeller).

5.3.6 Transverse Moment Coefficients

The transverse moment coefficient curves at constant advance coefficients are shown in Figure 5.30 and 5.31 for puller and pusher configurations, respectively. The trends of the curves in both configurations are generally similar to those of unit thrust coefficients in the corresponding configurations. The maximum transverse moment occurred at azimuthing angle of 10° Port in the both configurations and moment decreased from that angle in both directions of the azimuthing angles. This was observed at all advance coefficients except at bollard pull condition for puller configuration where the maximum moment occurred at straight-ahead condition. The transverse moment coefficient is primarily attributed to the unit thrust force. Similar to axial moment coefficient, the high

Study of pod at static azimuthing conditions

magnitude of the transverse moment coefficient is primarily due to the fact that the moment was calculated about the global unit centre, which is 1.68m vertically above the pod centre.

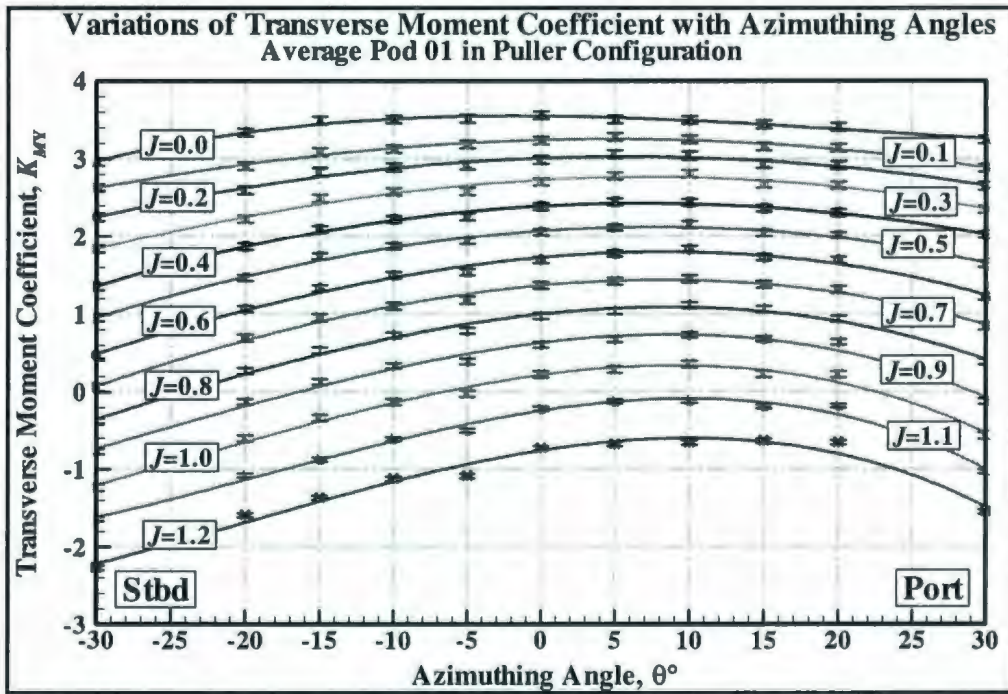


Figure 5.30: Unit transverse moment coefficient vs. azimuthing angle at constant values of advance coefficient in the puller configuration (left handed propeller).

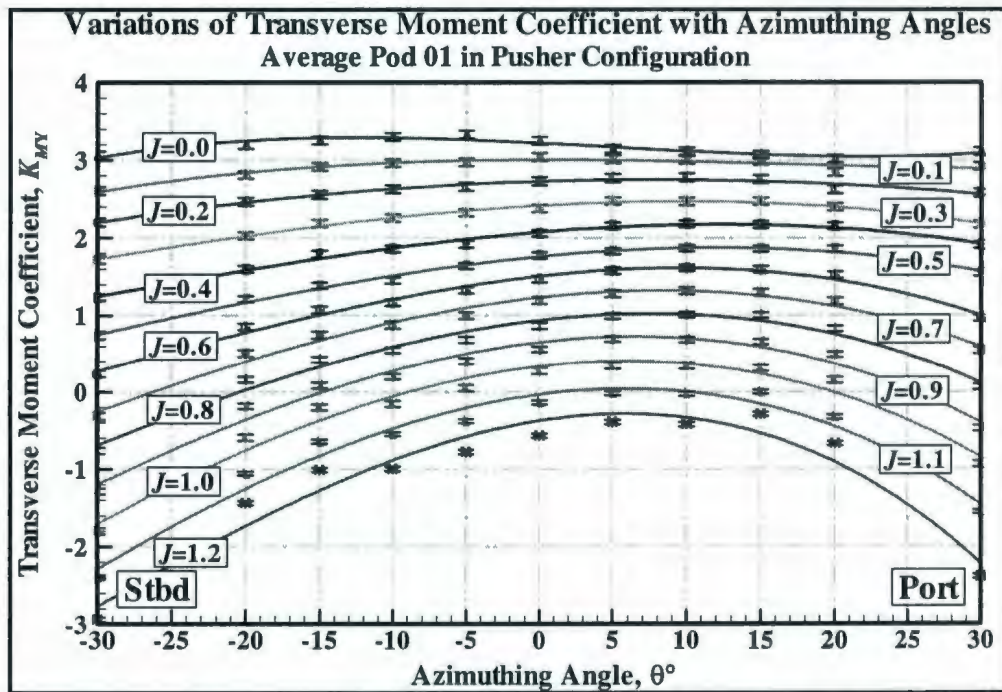


Figure 5.31: Unit transverse moment coefficient vs. azimuthing angle at constant values of advance coefficient in the pusher configuration (right handed propeller).

5.3.7 Steering Moment Coefficients

For puller configuration, the changes of steering moment coefficients with advance coefficients and azimuthing angles are shown in Figure 5.32. The steering moment (vertical moment about the z -axis) showed a decreasing tendency with increase of advance coefficient for positive azimuthing angles and an increasing tendency with the increase of advance coefficients for negative azimuthing angles. It was also observed that the steering moment was near zero for all advance coefficients in straight course conditions. For the puller propulsor, at straight-ahead condition, the transverse force generated small steering moments, which does not change with the increase of advance coefficients. The zero steering moments are generated in the range of azimuthing angles

Study of pod at static azimuthing conditions

between 0 and -2° at higher advance coefficients, which is essentially due to the non-zero transverse force at straight-ahead conditions.

In pusher configurations, Figure 5.33 shows the change of steering moment coefficients with advance coefficient and azimuth angles. The steering moment showed an increasing tendency with the increase of advance coefficients for positive azimuthing angles and a decreasing tendency with the increase of advance coefficients for negative azimuthing angles. The steering moment was near zero for all advance coefficients in straight course conditions, as in the puller configuration. The nature of the steering moment coefficient curves was different from those in puller configurations. At bollard pull conditions, the propeller thrust contributes significantly in providing the steering moments to the pod. In puller configuration and at the bollard pull condition, the propeller thrust remains almost the same for all of the azimuthing conditions, whereas in the pusher configurations it varies. This may have resulted in the variation of steering moment in the bollard pull condition for the pusher pod. The magnitude of the steering moments for the pusher pod was higher than for the puller propulsor at almost all corresponding azimuthing conditions and advance coefficients.

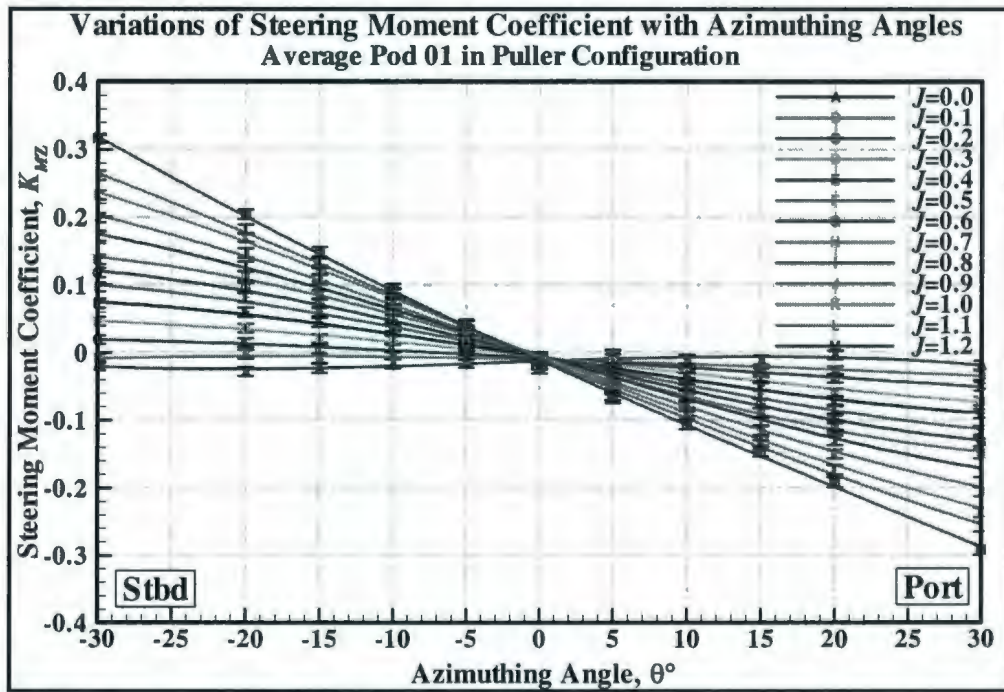


Figure 5.32: Unit steering moment coefficient vs. azimuthing angle at constant values of advance coefficient in the puller configuration (left handed propeller).

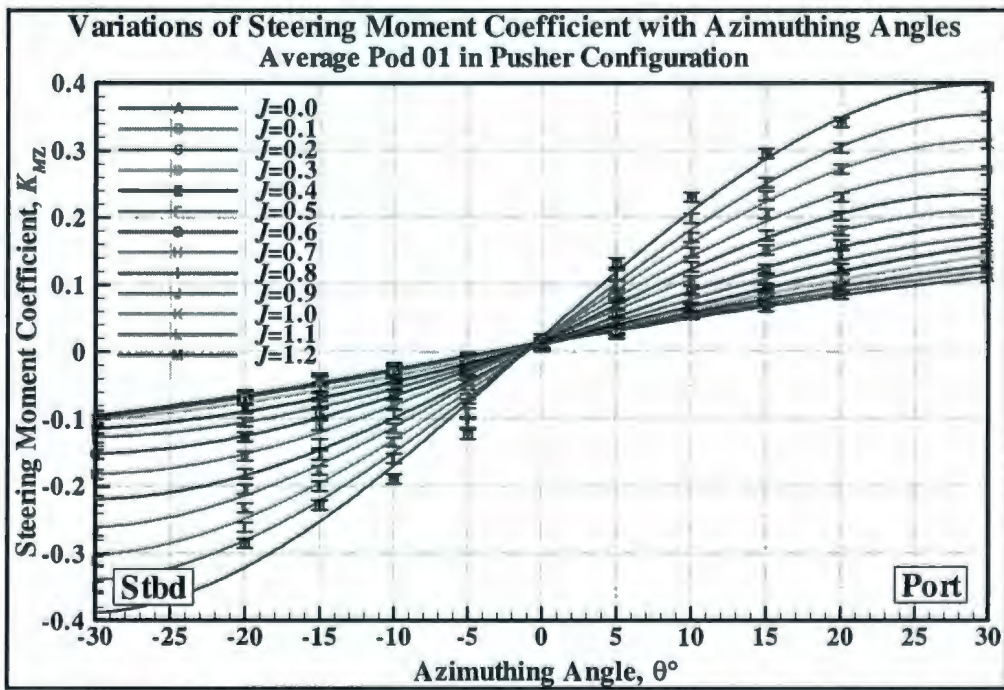


Figure 5.33: Unit steering moment coefficient vs. azimuthing angle at constant values of advance coefficient in the pusher configuration (right handed propeller).

5.4 Summary

The chapter presents the experimental study of shaft thrust and torque, unit forces and moments in the three orthogonal directions at different static azimuthing angles and advance coefficients for puller and pusher configurations. A model pod fitted with two propellers (for the two configurations) was tested using a custom designed pod testing system at various advance coefficients and at azimuthing angles ranging from -30° to 30° . The propeller shaft thrust and torque as well as the unit forces and moments were varied with the change of propeller loading and azimuthing angles and behaved differently for the two configurations, which justified separate study of the two configurations.

CHAPTER

6

**STUDY of POD at
DYNAMIC AZIMUTHING
CONDITIONS**

6 Study of pod at dynamic azimuthing conditions

6.1 Chapter Objectives

This chapter presents results and analyses of the experimental study into the effects of dynamic azimuthing conditions on the propulsive characteristics of a puller-podded unit in open water conditions. Results are presented for various sets of static azimuthing angles in the range of 0° to -360° and with varying advance coefficients. A comparative study of static and dynamic azimuthing conditions is presented and is then followed by studies into the effect of azimuthing rate and shaft rps in dynamic azimuthing conditions.

6.2 Static Azimuthing Conditions

The propeller thrust coefficient, K_{TProp} , propeller torque coefficient, $10K_Q$, unit thrust coefficient, K_{TUnit} , transverse force coefficient, K_{FY} , vertical force coefficient, K_{FZ} , axial moment coefficient, K_{MX} , transverse moment coefficient, K_{MY} , and steering moment coefficient, K_{MZ} values for the pod unit in puller configuration are presented in this section. The static azimuthing angle was varied in the range of 0° to 360° (presented as $+180^\circ$ to -180° , 0° being the straight-ahead condition) with various increments and the advance coefficients at the values discussed in section 2.3.3 in Chapter 2. The tests were conducted at 28 different azimuthing angles and 10 different advance coefficients. The positive azimuthing angle means the pod unit was azimuthed in the port position looking forward (anticlockwise rotation looking from top of the unit). For advance coefficients

higher than 0.8, the performance coefficients were not measured when the azimuthing angles were higher than $\pm 60^\circ$. This was mainly because of the limitations on the capacity of some of the load cells. Particularly, the thrust and the torque sensors of the pod unit were saturated at advance coefficients of 0.9 or higher and azimuthing angles larger than $\pm 60^\circ$.

6.2.1 Propeller Thrust and Torque

The plots for propeller thrust coefficient, $K_{T_{prop}}$, and propeller torque coefficient, $10K_Q$ within the entire range of azimuthing angles ($\pm 180^\circ$) at constant advance coefficients are presented in Figures 6.1, and 6.2, respectively.

The propeller thrust and torque coefficients of the puller propeller increased when the azimuthing angles were increased from the straight-ahead condition (0° angle) both in positive and negative azimuthing angles. In other words, the minimum thrust and torque were observed at straight-ahead condition at all of the advance coefficient values. The maximum propeller performance coefficients were observed at the azimuthing angles of $\pm 120^\circ$. The coefficients reduced when the azimuthing angles were greater than $\pm 120^\circ$, where flow separation on the propeller blades and the pod-strut body dominated. These were observed for all advance coefficients above 0.2. At bollard pull condition of $J=0.0$, the thrust and torque coefficients remained almost constant for all azimuthing angles as expected since there was no inflow to the propulsor. At an advance coefficient of 0.2, the thrust and torque coefficients in the positive azimuthing angles behaved similar to the

Study of pod at dynamic azimuthing conditions

other higher advance coefficients but in the negative azimuthing angles, no clear pattern was observed. For a left-handed propeller and for low advance coefficients (i.e. $J=0.2$), at negative azimuthing angles higher than 90° , the propeller works against the inflow and the propeller wash dominates over the inflow. At that low advance coefficient, the resultant inflow velocity into the propeller blade was smaller than that at the positive azimuthing conditions, where the propeller works along the inflow. At higher advance coefficients, the inflow was high enough to minimize the wash-inflow interaction and the inflow dominated in producing the thrust and the torque. There was some scatter at the large azimuthing angles, which can be attributed to the unsteady nature of the reverse wash and separation (at azimuthing angles greater than $\pm 90^\circ$). The curves at different advance coefficients clearly show a non-linear trend, which can be associated with the changing inflow characteristics as the azimuthing angle changes. Small asymmetries in location and magnitude of the maxima might be due to the influences of propeller rotation direction and the interaction between the propeller wash and the pod-strut body. Propeller thrust and torque coefficient showed similar trends at corresponding azimuthing angles and advance coefficients, which confirms the proportional nature of lift and drag produced by the propeller blade elements. Tables A.23 and A.24 present the propeller thrust and torque coefficients data for the pod unit at all azimuthing angles, respectively.

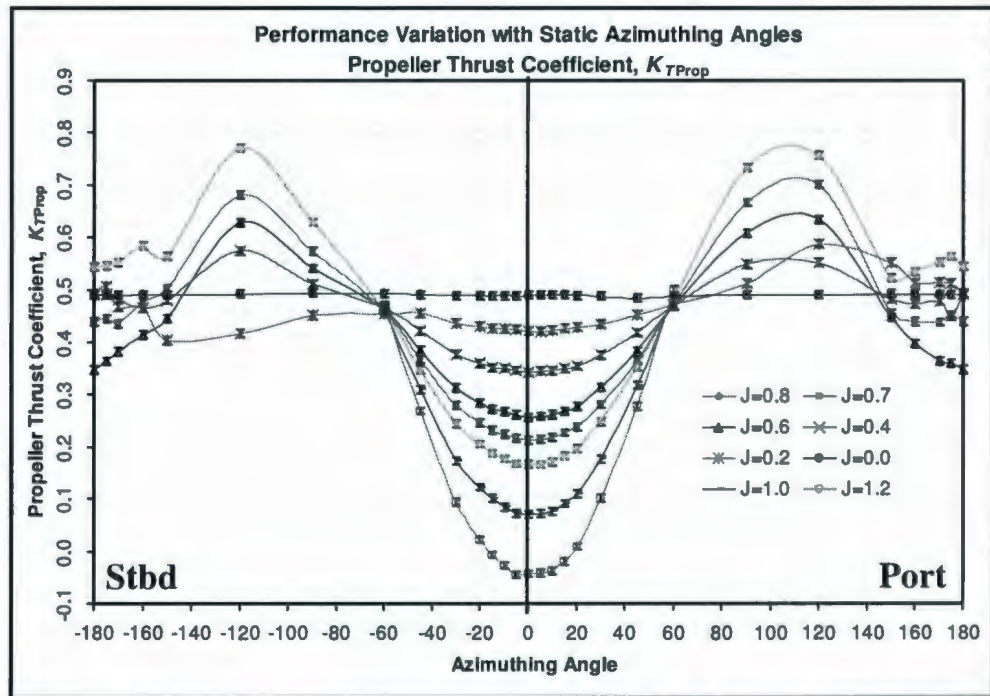


Figure 6.1: Experimental results: propeller thrust coefficient of the model pod unit in puller configuration (left-handed propeller in static azimuthing conditions).

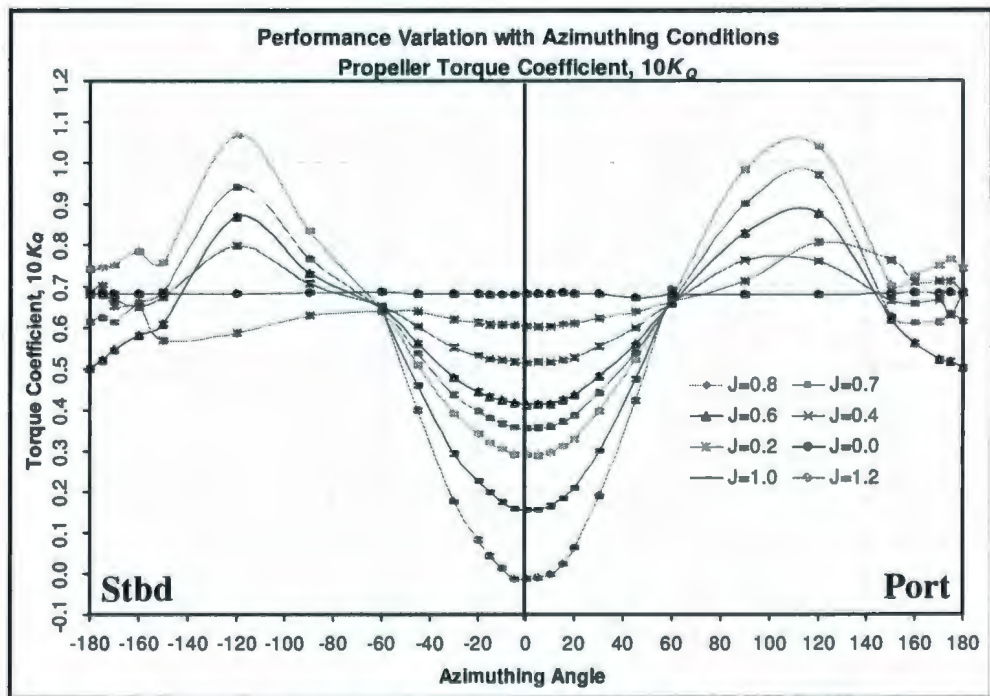


Figure 6.2: Experimental results: propeller torque coefficient of the model pod unit in puller configuration (left-handed propeller in static azimuthing conditions).

6.2.2 Unit Forces and Moments

The unit thrust, transverse and vertical force coefficients, axial, transverse, and steering moment coefficients were calculated from the load cell outputs, applying a transformation from the load cell (global unit) coordinate system to the global unit centre (vertically above the pod centre), as discussed in section 2.5 in Chapter 2.

The unit thrust coefficients K_{FX} or K_{TUnit} for the pod unit at each of the azimuthing angles within the entire range of azimuthing angles ($\pm 180^\circ$) at constant advance coefficients is presented in Figure 6.3. The unit thrust coefficients decreased for both azimuthing directions but the reduction was visibly stronger for negative azimuthing angles particularly for higher J values and within the $\pm 90^\circ$ range of azimuthing angles. The unit thrust coefficients increased in magnitude for high advance coefficients (greater than 0.4) tested as the azimuthing angle was increased further beyond $\pm 120^\circ$. There was some scatter at these larger azimuthing angles than $\pm 90^\circ$, which can be attributed to the unsteady nature of the reverse wash and separation on the propeller and the pod-strut body.

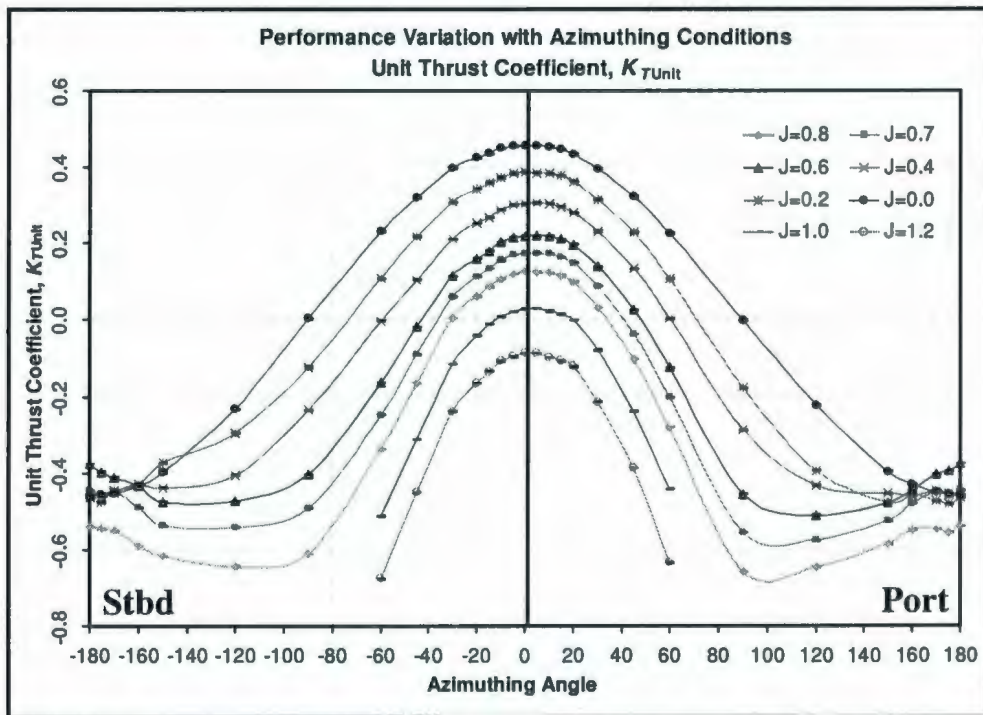


Figure 6.3: Experimental results: unit thrust coefficient of the model pod unit in puller configuration (left-handed propeller in static azimuthing conditions).

The transverse force coefficient, as shown in Figure 6.4, showed strong dependency on propeller loading and azimuthing angle. The nature is similar to that of a classical rudder. For all advance coefficients, the transverse force coefficients increased with both positive and negative azimuthing angles from the straight-ahead position. The maximum transverse force coefficient was found in the range of $\pm 60^\circ$ to $\pm 90^\circ$ for different advance coefficients. For larger azimuthing angles, the transverse force decreased and approached zero at an azimuthing angle of 180° . For the pod unit with the puller propeller, the zero transverse force was observed to be in the range of 0° to -2° azimuthing angle depending upon the advance coefficient.

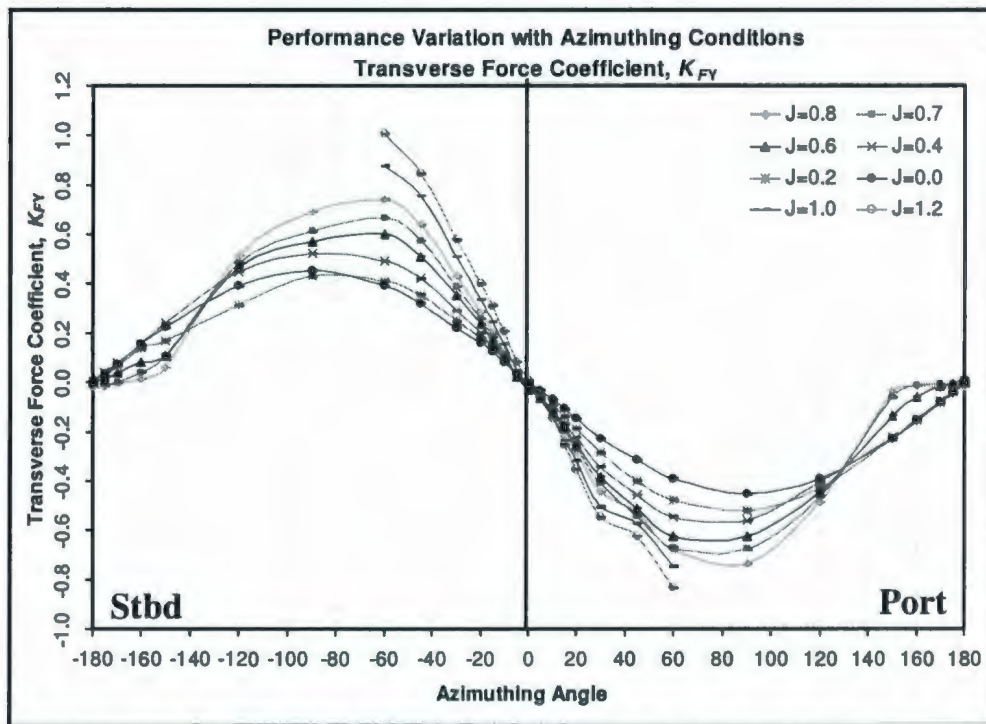


Figure 6.4: Experimental results: transverse force coefficient of the model pod unit in puller configuration (left-handed propeller in static azimuthing conditions).

The resultant horizontal force coefficient i.e. $K_{FR} = \sqrt{(K_{FX}^2 + K_{FY}^2)}$, as shown in Figure 6.5, showed strong dependency on propeller loading and azimuthing angle. The resultant force was the least in straight-ahead conditions for all advance coefficients. The maximum resultant force was observed at $\pm 90^\circ$. At positive azimuthing conditions, the resultant horizontal force was higher than that at the negative azimuthing conditions for all advance coefficients higher than 0.2.

It was observed that the trends of the transverse and the resultant force coefficients in the moderate range of azimuthing angles of $\pm 60^\circ$, were approximately linear.

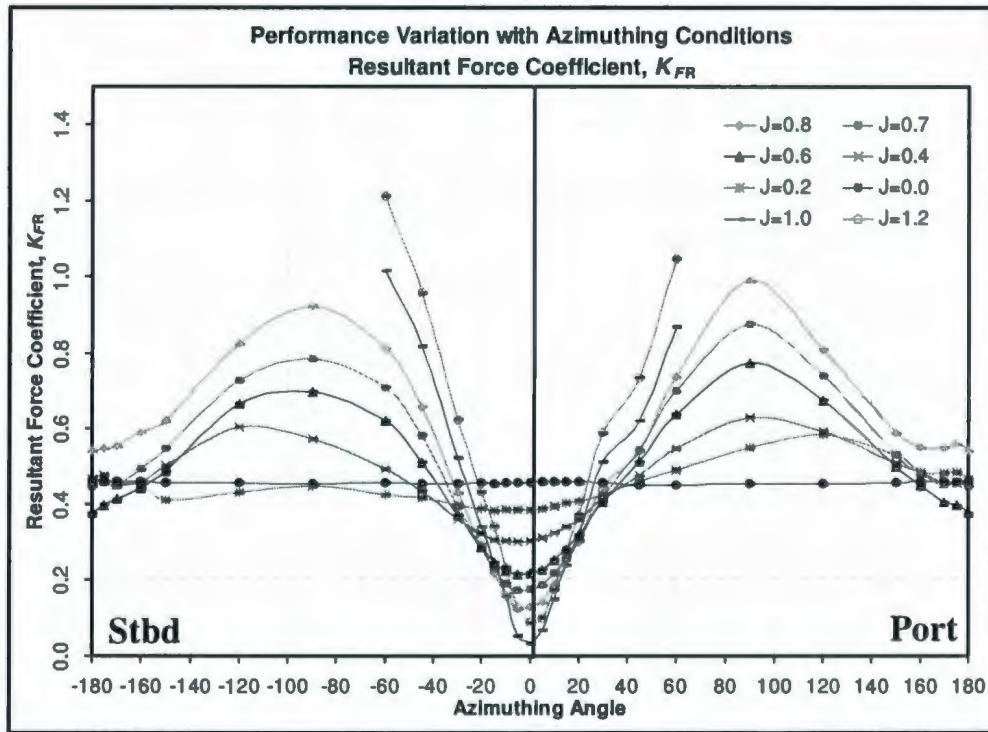


Figure 6.5: Experimental results: unit horizontal resultant force coefficient of the model pod unit in puller configuration (left-handed propeller in static azimuthing conditions).

The vertical force coefficient curves at different static azimuthing angles and at constant advance coefficients are shown in Figure 6.6. The vertical force coefficients were positive (vertically downward) for azimuthing angles of 0° to -120° for all advance coefficients. The maximum vertical force was observed at azimuthing angle of -60° . In the azimuthing angle range of 0° to 180° , the vertical force coefficients were negative (upward) or near zero at low advance coefficients ($J \leq 0.4$) and positive for higher advance coefficients. At the bollard pull condition, the vertical force on the unit was near zero for all azimuthing angles. With the increase of advance coefficients the vertical force increased at all azimuthing angles. The magnitude of the vertical force in the negative

Study of pod at dynamic azimuthing conditions

azimuthing angles were much higher than at the positive azimuthing angles. The vertical force (lift on the propulsor) is the resultant of the interaction between the inflow velocity, the propeller wash and the wake of the pod-strut body, which resulted in a pressure difference between the top and bottom of the unit. The asymmetric nature of the vertical force coefficient between the positive and the negative azimuthing angles in the figure implies that the direction of rotation of the propeller plays an important role. Since the geometry is symmetric, the only variation between the cases of positive and negative of an azimuthing angle is the orientation of the propeller wash with respect to the inflow. For the negative azimuthing angles the propeller wash and the inflow are somewhat aligned whereas for positive azimuthing angles they oppose to each other. Tables A.25, A.26 and A.27 present the unit thrust, transverse and vertical force coefficients data for the pod unit at all azimuthing angles, respectively.

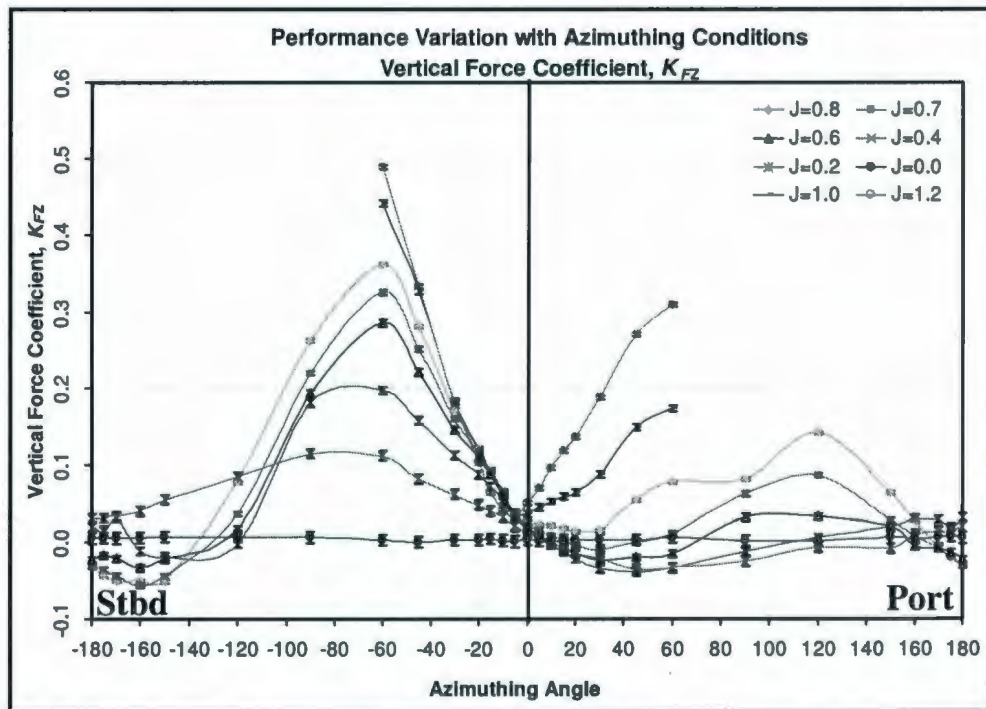


Figure 6.6: Experimental results: vertical force coefficient of the model pod unit in puller configuration (left-handed propeller in static azimuthing conditions).

The plots for axial moment at constant advance coefficients are shown in Figure 6.7. The axial moment was calculated on the global centre, which is 0.5m above the pod centre and is primarily attributed to the transverse force. Thus the main contribution of the axial moment was from the transverse force. The nature of the axial moment coefficient curves is similar to those of transverse force coefficient curves only in the reverse order primarily because of the sign convention used. The maximum positive and negative axial moment occurred in the azimuthing angle range of $\pm 60^\circ$ to $\pm 120^\circ$.

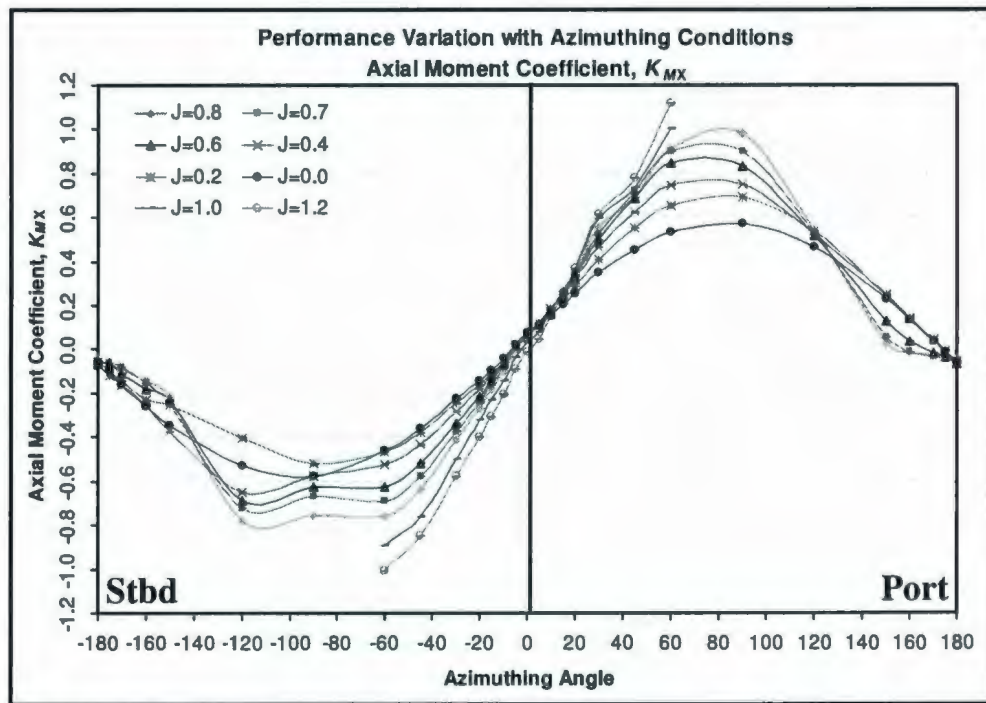


Figure 6.7: Experimental results: axial moment coefficient of the model pod unit in puller configuration (left-handed propeller in static azimuthing conditions).

Figure 6.8 shows the transverse moment coefficient curves at different azimuthing angles and advance coefficients. The transverse moment depends on the propeller thrust, axial unit force and pod drag. The maximum transverse moment coefficient was observed around straight-ahead condition for all advance coefficients. The nature of the curves is similar to those of unit thrust component for all azimuthing angles.

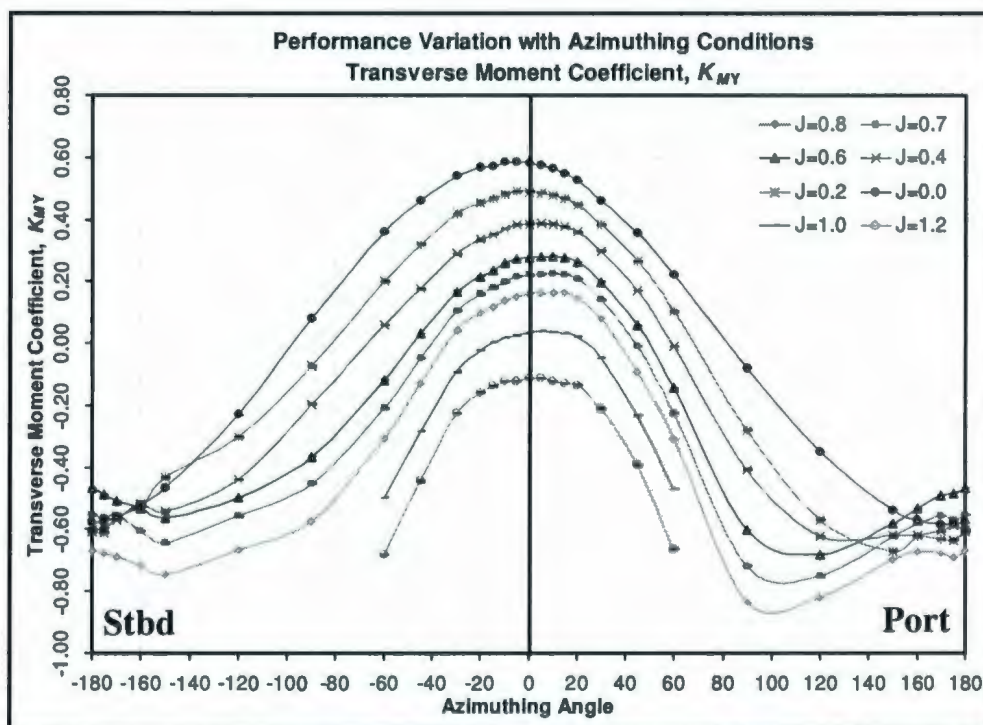


Figure 6.8: Experimental results: transverse moment coefficient of the model pod unit in puller configuration (left-handed propeller in static azimuthing conditions).

The steering moment coefficient, as shown in Figure 6.9, shows nonlinear nature with the change of advance coefficients and azimuthing angle. The steering moment coefficient increased with the larger azimuthing angles up to $\pm 90^\circ$. For further increase in azimuthing angle up to $\pm 180^\circ$, a decrease in steering moment was observed. These were observed for all advance coefficients but at the bollard pull condition. The steering moment on the propulsor was almost zero for the bollard pull conditions for all azimuthing angles. Tables A.28, A.29 and A.30 present the unit axial, transverse and steering moment coefficients data for the pod unit at all azimuthing angles, respectively.

Study of pod at dynamic azimuthing conditions

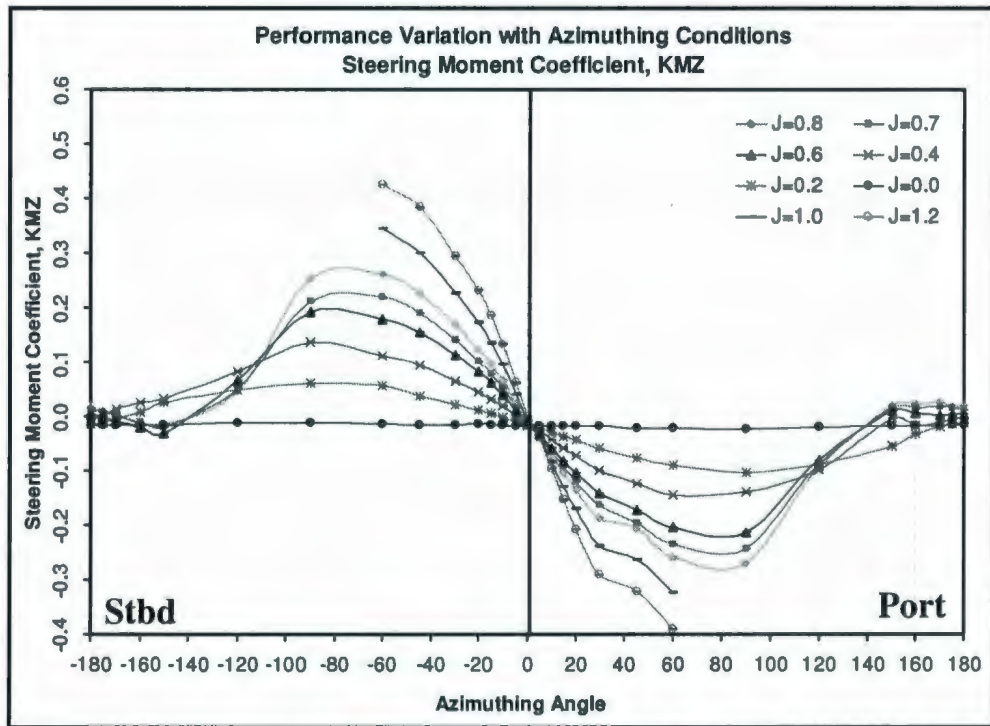


Figure 6.9: Experimental results: steering moment coefficient of the model pod unit in puller configuration (left-handed propeller in static azimuthing conditions).

6.3 Dynamic Azimuthing Conditions

In the present dynamic azimuthing tests, the pod unit with the propeller was rotated about the vertical axis, Z, (azimuthing) in a continuous motion at a certain azimuthing rate, while the whole test unit was moved forward at a specific advance velocity and propeller shaft rps. The conceptual pod and propeller wash at different operating conditions under dynamic azimuthing is shown in Figure 6.10. The figure shows the pod wake and the propeller wash due to the uniform inflow, the blade wake due to rotation and the interaction wake from the propeller and the pod. The figure shows that, roughly, the wake varies a lot with the change of azimuthing direction as well as the angular location of the unit. At any instance during dynamic azimuthing conditions, the local inflow into the propeller blade depends on three components, namely: contribution from the uniform inflow, contribution from the propeller rotation and contribution from the dynamic azimuthing. For example, in the top left sketch of Figure 6.10, the total inflow velocity is the addition of the contribution from the uniform inflow and the contribution from the propeller rotation with a deduction of the contribution from the dynamic azimuthing. Again, in the bottom left sketch of Figure 6.10, the total inflow velocity is the addition of the contribution from the azimuthing and the contribution from the propeller rotation with a deduction of the contribution from the uniform inflow. Thus, depending on the angular position of the pod, propeller rotation and azimuthing direction of the propulsor, the performance coefficients change even if the uniform inflow remains same. Certainly, the propeller rotation has opposite effect on top and bottom blade pass in the opposite azimuthing position.

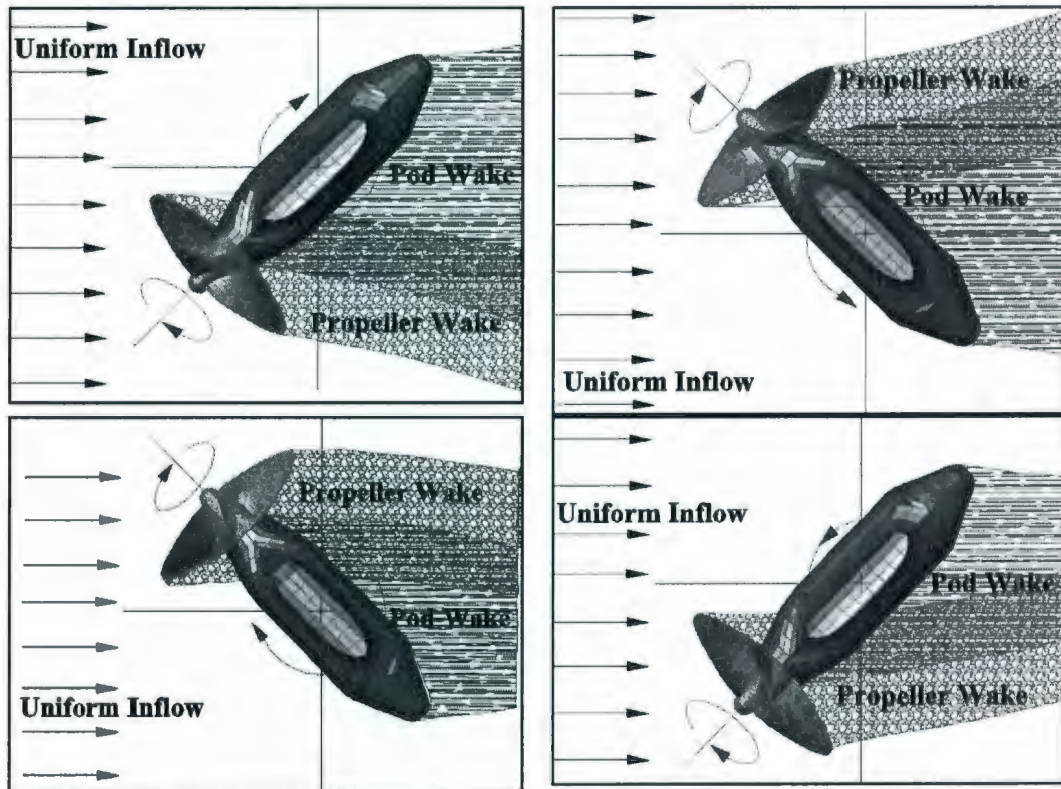


Figure 6.10: Conceptual propeller wash and pod wake at dynamic azimuthing conditions for a left-handed propeller: from top left clockwise, clockwise azimuthing at the 1st quadrant (Port), counter-clockwise azimuthing in the 4th quadrant (Starboard), counter-clockwise azimuthing in the 1st quadrant (Port) and clockwise azimuthing in the 4th quadrant (Starboard).

In the current study, measurements were taken of the forces and moments acting on the propeller and the whole pod unit at different advance coefficients, and at different dynamic azimuthing rates. Typically, a full scale podded propulsor azimuths at a rate of 2.5°/s at the vessel's service speed (requirement from the SOLAS, Sorsimo 2006). During manoeuvring at slow speeds where less torque is required than in the full speed mode, the azimuthing rate is approximately 5°/s. Depending on the ratio of the maximum vessel speed to the maximum steering torque at the lower speeds, manoeuvring at 12°/s azimuthing rate can be considered as a special case (Sorsimo 2006). For the present

dynamic azimuthing study, the tests were conducted at the model scale rates of 2°, 5°, 10°, 15° and 20°/s with azimuthing angles between 0° and ±60°. Measurements were made at different advance coefficients ranging from $J=0.0$ to $J=1.2$ and at two different propeller shaft rps of 15 and 8.

6.3.1 Effects of Dynamic Azimuthing

In the dynamic azimuthing tests, the sweep angle from 0° to 360° could not be covered within a test run in the towing tank due to the restriction on the length of the tank. In order to complete the required range, the sweep range was divided into sections with overlaps and completed over a number of test runs. In the figures given for the comparison of performance parameters in static and dynamic azimuthing conditions, the merged raw data for the dynamic azimuthing was used unlike the static case in which the segment means are shown. In each range of sweep angle, an additional 5° was added to make sure that the acceleration and deceleration part to achieve the required azimuthing rate was not included in the considered sweep range. The data acquisition rate for both static and dynamic case was 5000 Hz for forces and moments and 500 Hz for azimuthing angle. An azimuthing rate of 10°/sec was used in this part of the study. A 10th order polynomial fit was used to represent the mean level of the dynamic test data to facilitate the comparison of the static and dynamic test results at corresponding operating conditions. The comparison for the two conditions was made at two advance coefficient values of 0.2 (low advance coefficient) and 0.5 (moderate advance coefficient).

Study of pod at dynamic azimuthing conditions

Figures 6.11 and 6.12 compare the propeller thrust and torque coefficients between the static and dynamic azimuthing conditions in the azimuthing range from 0° to 360° . The figures show the original unfiltered experimental results in dynamic azimuthing conditions and the averaged results in the static azimuthing conditions. In both figures, the left hand side figure is for low advance coefficient of $J = 0.2$ while the right hand side figure is given for $J = 0.5$. Both the thrust and torque coefficients at static azimuthing conditions (represented by the solid round black dots) fell close to the polynomial curve fit for the dynamic azimuthing data (black solid line). Thus, the mean values of the static case coincided well with the mean values the dynamic azimuthing results for both $J = 0.2$ and $J = 0.5$ cases for 0° to 360° . The discrepancy observed for $J = 0.2$ in the range of azimuthing angle from 120° to 270° can be attributed to the unsteady nature of the operating condition at these angles. Also the polynomial fit under estimates the second peak for the $J = 0.5$ case around 250° . The fluctuations in the magnitude of both the thrust and the torque coefficients (the shaded area in the figures) for both advance coefficients show that in dynamic azimuthing conditions, the propeller thrust and torque fluctuate over a considerable range and care should be taken in designing the propeller bearings which would be subjected to this kind of fluctuation force. A further discussion on the nature and accuracy of the fluctuation of the pod performance coefficients is provided later in this section.

Study of pod at dynamic azimuthing conditions

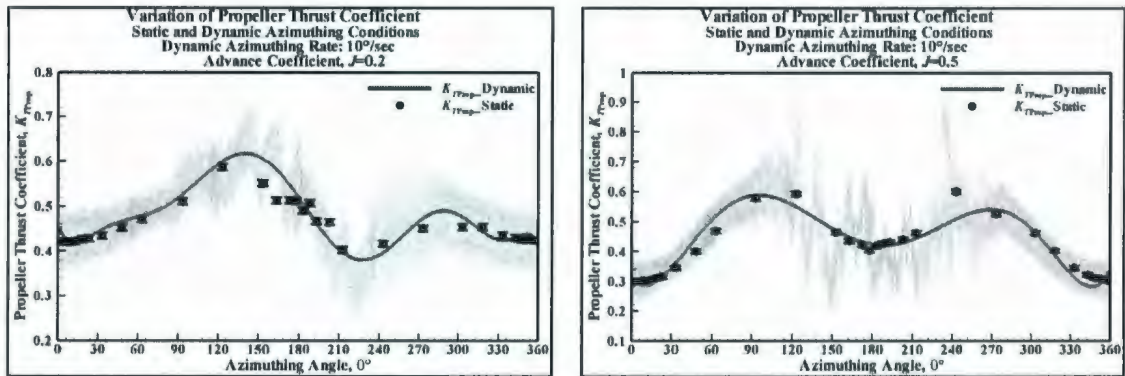


Figure 6.11: Experimental results: comparison of propeller thrust coefficient of the model pod unit at static (black solid circle) and dynamic azimuthing conditions (black dots for raw unfiltered data and black line for 10th order polynomial fit to the raw data).

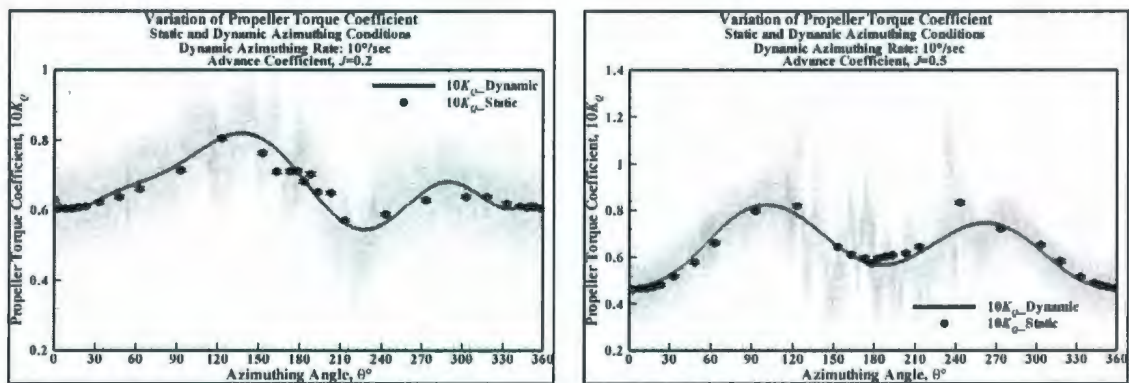


Figure 6.12: Experimental results: comparison of propeller torque coefficient of the model pod unit at static (black solid circle) and dynamic azimuthing conditions (black dots for raw unfiltered data and black line for 10th order polynomial fit to the raw data).

The comparison between the static and dynamic azimuthing conditions in the azimuthing angle range from 0° to 360° and at the advance coefficients of $J = 0.2$ and $J = 0.5$ for unit thrust, transverse force and horizontal resultant force coefficients are shown in Figures 6.13, 6.14 and 6.15, respectively. High fluctuations in the magnitude of these global force coefficients were observed, specifically in the range of azimuthing angles between 90° to 270° (reverse wash condition). At the higher advance coefficient of $J = 0.5$, the

Study of pod at dynamic azimuthing conditions

fluctuations were larger than those at lower advance coefficient of $J = 0.2$. The mean force coefficients at static azimuthing conditions compare well with the 10th order polynomial fit to the dynamic azimuthing data for most of the azimuthing angles. The fluctuation of the transverse force coefficient at dynamic azimuthing condition was less than the propeller or the unit thrust coefficient at all azimuthing angles.

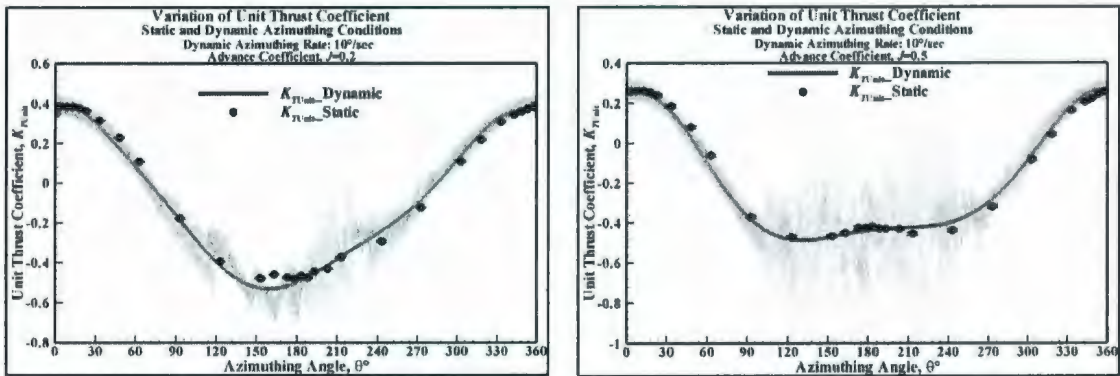


Figure 6.13: Experimental results: comparison of unit thrust coefficient of the model pod unit at static (black solid circle) and dynamic azimuthing conditions (black dots for raw unfiltered data and black line for 10th order polynomial fit to the raw data).

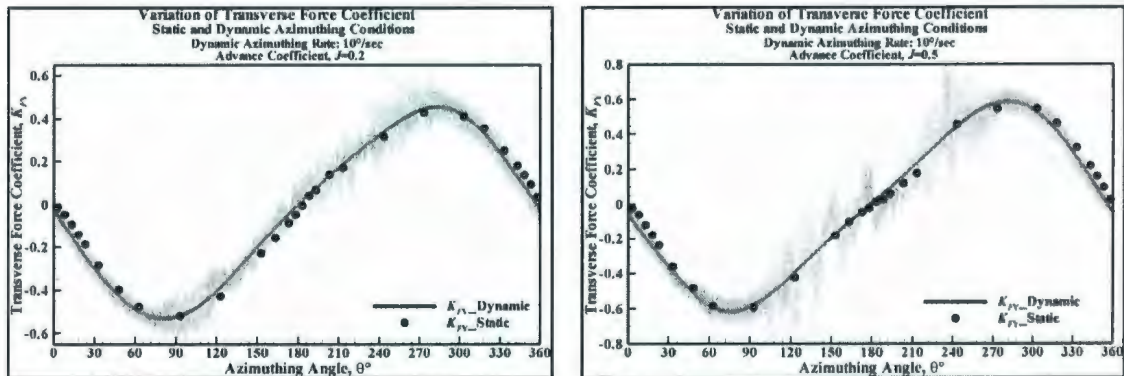


Figure 6.14: Experimental results: comparison of transverse force coefficient of the model pod unit at static (black solid circle) and dynamic azimuthing conditions (black dots for raw unfiltered data and black line for 10th order polynomial fit to the raw data).

Study of pod at dynamic azimuthing conditions

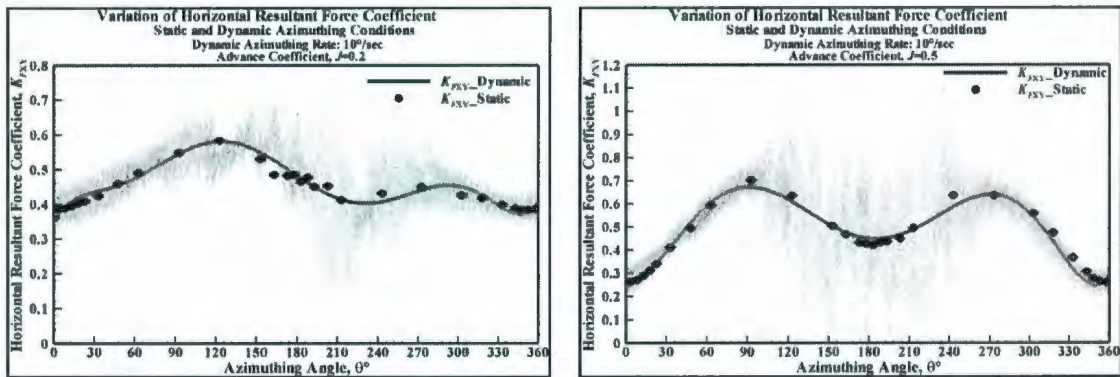


Figure 6.15: Experimental results: comparison of resultant horizontal force coefficient of the model pod unit at static (black solid circle) and dynamic azimuthing conditions (black dots for raw unfiltered data and black line for 10th order polynomial fit to the raw data).

Figure 6.16 compares the steering moment coefficient between the static and dynamic azimuthing conditions at advance coefficients of $J=0.2$ and $J = 0.5$. The steering moment coefficient at static azimuthing conditions (represented by the solid round black dots) fell close to the polynomial curve fit to the dynamic azimuthing data. Thus, the mean values of the static case coincide well with those of the dynamic azimuthing for both $J = 0.2$ and $J = 0.5$ cases for 0° to 360° . Similarly to the other force coefficients mentioned above, the discrepancy observed both at $J = 0.2$ and $J = 0.5$ in the range of azimuthing angle from 90° to 270° can be attributed to the unsteady nature of the operating condition and to the polynomial fit used. The fluctuation of the magnitude of the steering moment coefficient for both advance coefficients shows that at dynamic azimuthing conditions, the steering moment fluctuates within a considerable range and this should be taken into account when designing the radial and/or slewing bearing which would have to resist these large fluctuating moments.

Study of pod at dynamic azimuthing conditions

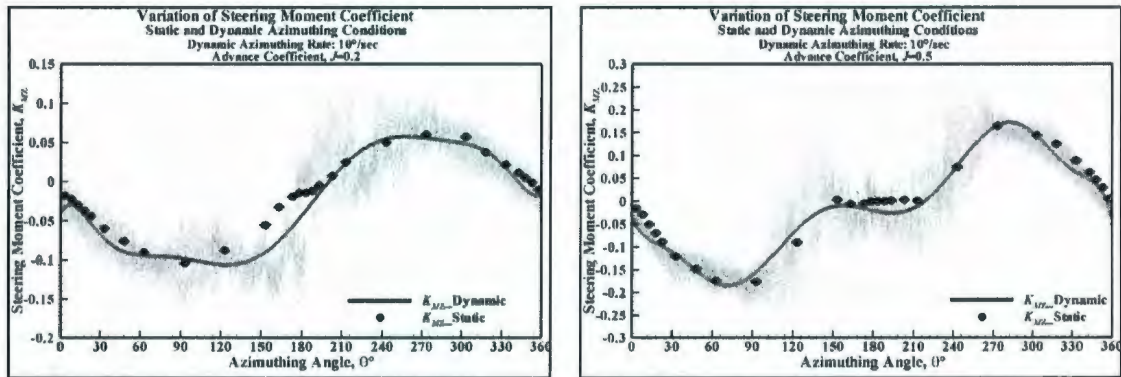


Figure 6.16: Experimental results: comparison of steering moment coefficient of the model pod unit at static (black solid circle) and dynamic azimuthing conditions (black dots for raw unfiltered data and black line for 10^{th} order polynomial fit to the raw data).

Overall, for all forces and moments and especially in the reverse wash conditions, large fluctuations of forces and moments in the form of spikes were observed. For example, Figure 6.17 compares the fluctuations in the magnitude of the propeller thrust coefficient for static and dynamic azimuthing conditions at some high azimuthing angles (90° to 270° , reverse wash condition) and at an advance coefficient of $J=0.5$. In the figure, the oval markers indicate 5 azimuthing angles in dynamic condition and those are related to the unfiltered data for the corresponding static azimuthing angles. This illustrates the level of fluctuations observed in the static and dynamic cases. It shows that both cases, the propeller thrust fluctuated over a considerable range. It is also found that the range of fluctuation of the forces and moments in the static azimuthing tests (for a fixed azimuthing angle) was slightly lower than that in the dynamic azimuthing tests in the corresponding operating conditions. This difference can either be a reality or an uncertainty inherent to the measurements. A further study in evaluating the uncertainty of the measurements in the dynamic azimuthing cases is required to justify this difference.

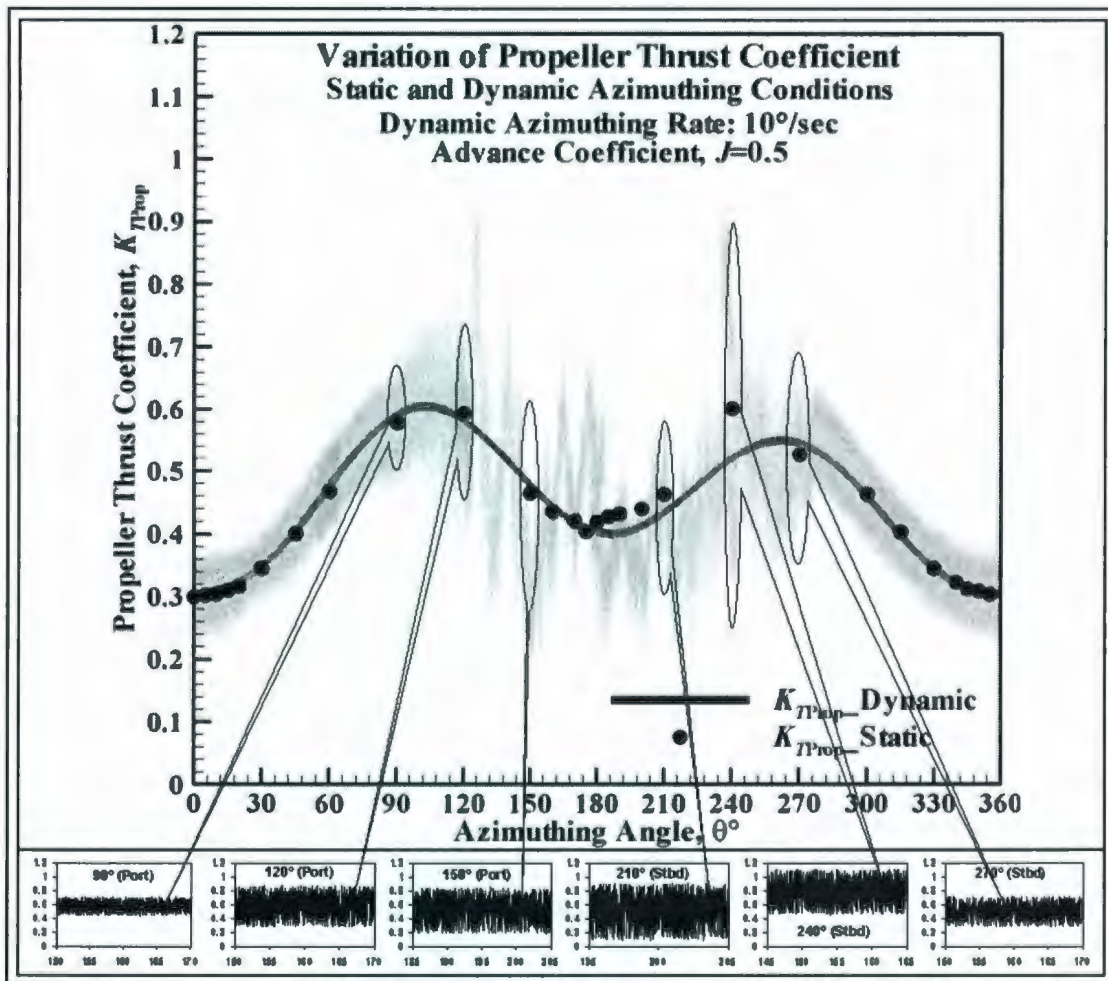


Figure 6.17: Experimental results: comparison of propeller thrust coefficient of the model pod unit at static (black solid circle) and dynamic azimuthing conditions (black dots for raw unfiltered data and black solid line for 10th order polynomial fit to the raw data).

This form of fluctuating loads was also reported in the study by Woodward (2006). Woodward found that these spike loads do not influence the manoeuvring response assessment and have only a minor impact on the manoeuvring response itself. Model test observations also indicate that the spike loads influence the roll behaviour of the ship and, in extreme cases, may even compromise the stability (Woodward 2006).

Nevertheless, the spike loads have a significant impact on the structural design, shaft and stock bearings and other related systems. Thus, careful attention should be paid to the manoeuvring related design and operational implications, to better understand and control the influence of the spike loads experienced by pod drives (Woodward 2006).

6.3.2 Effects of Azimuthing Rate

The experimental study into the effect of azimuthing rate on the propeller and unit forces and moments at dynamic azimuthing conditions within the range of $+60^\circ$ to -60° was carried out for two advance coefficients of $J = 0.2$ (low) and $J = 0.8$ (high). The propeller thrust and torque coefficients and the unit forces and moment coefficients were measured at azimuthing rates of $2^\circ/\text{sec}$, $5^\circ/\text{sec}$, $10^\circ/\text{sec}$, $15^\circ/\text{sec}$, and $20^\circ/\text{sec}$ for the above operating conditions. The data at the dynamic azimuthing conditions are presented in terms of a 3rd order polynomial fit. The original unfiltered data at different azimuthing rates was too hard to distinguish as shown in Figure 6.18 for the case of propeller thrust coefficient. Each of the performance coefficients is presented in terms of a 3rd order polynomial for all of the azimuthing rates for each advance coefficient separately.

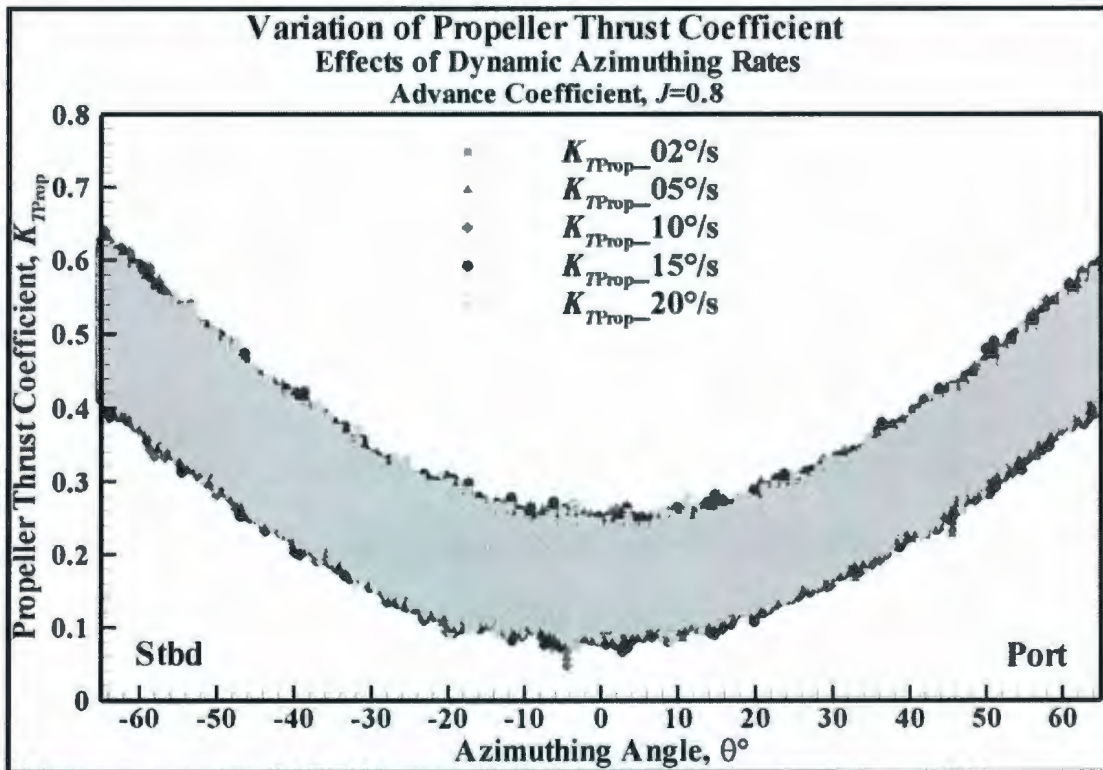


Figure 6.18: Experimental results: Original unfiltered data showing the variation of propeller thrust coefficient of the model pod unit with azimuthing rate in dynamic conditions.

For propeller thrust and torque coefficients, as shown in Figures 6.19 and 6.20, respectively, the azimuthing rate did not have any noticeable effect when the azimuthing rate was equal to or higher than $5^\circ/\text{sec}$ for positive azimuthing angles. This was observed for both advance coefficients. The slight difference in the performance coefficients with the change of azimuthing rate that was observed, especially in the azimuthing range of 0° to -60° was not consistent in terms of the change in azimuthing rate. The difference was not significant as it stayed within the uncertainty limit of the measurement (see chapter 3 for details). Also, the uncertainty analysis was carried out only for the static cases and the applicability of the error bars in the test results in dynamic cases requires further study.

Study of pod at dynamic azimuthing conditions

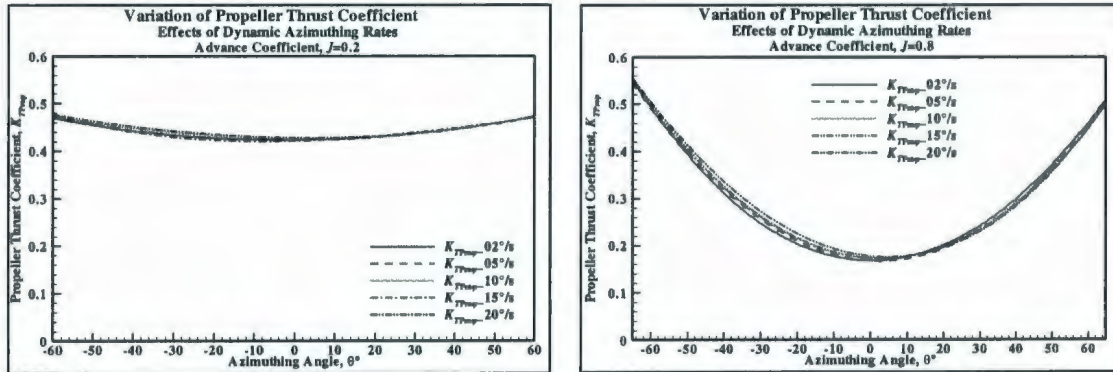


Figure 6.19: Experimental results: Variation of propeller thrust coefficient of the model pod unit with azimuthing rate in dynamic conditions.

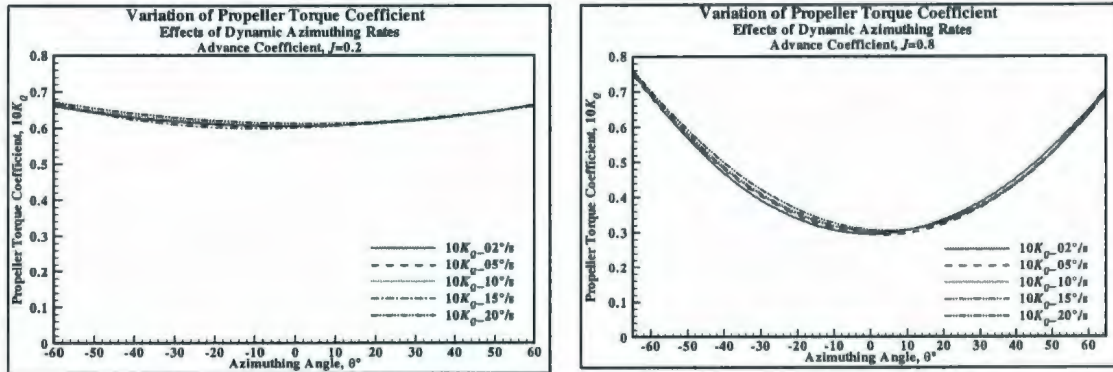


Figure 6.20: Experimental results: Variation of propeller torque coefficient of the model pod unit with azimuthing rate in dynamic conditions.

Figures 6.21, 6.22, and 6.23 show the effect of azimuthing rate on the unit thrust, transverse force and steering moment coefficients at two different advance coefficients. Overall, at advance coefficients of $J = 0.2$ and $J = 0.8$, the azimuthing rate did not show any appreciable effect on the performance coefficients. Similarly to propeller thrust and torque coefficients, the minor difference in the performance coefficients might be attributed to measurement error.

Study of pod at dynamic azimuthing conditions

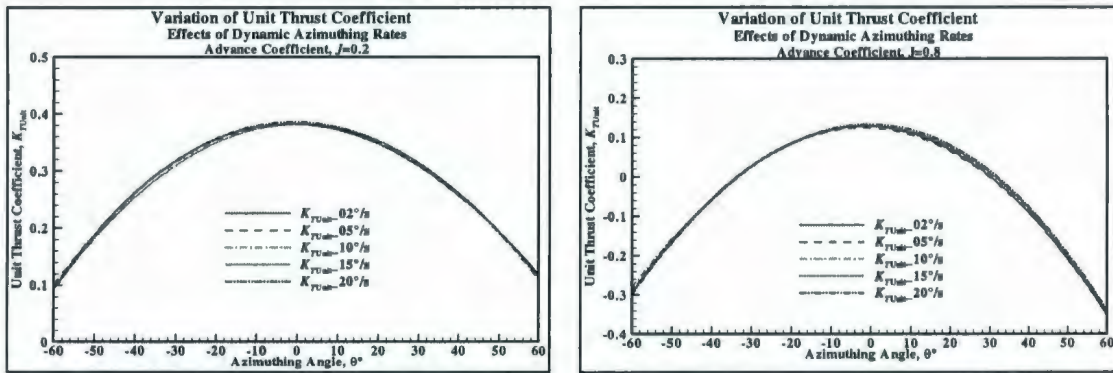


Figure 6.21: Experimental results: Variation of unit thrust coefficient of the model pod unit with azimuthing rate in dynamic conditions.

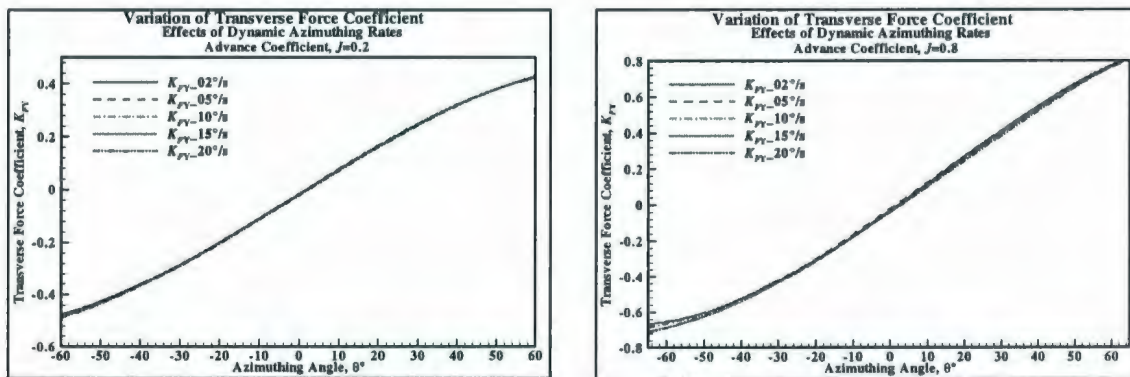


Figure 6.22: Experimental results: Variation of transverse force coefficient of the model pod unit with azimuthing rate in dynamic conditions.

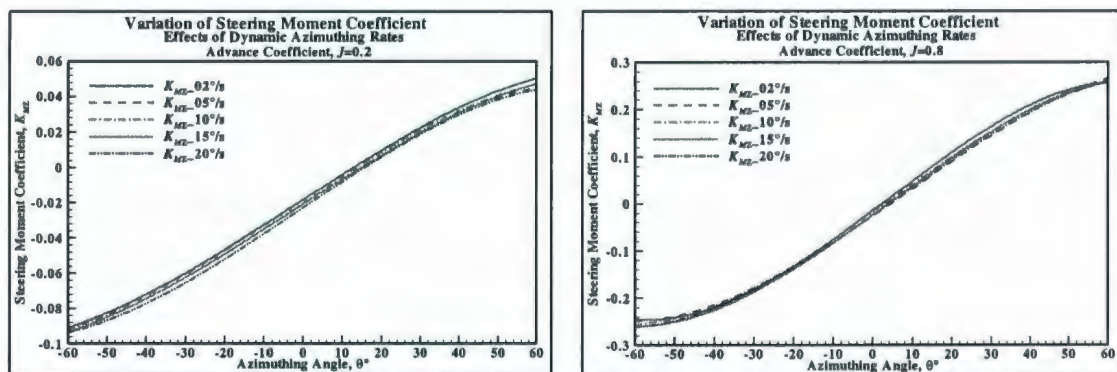


Figure 6.23: Experimental results: Variation of steering moment coefficient of the model pod unit with azimuthing rate in dynamic conditions.

6.3.3 Effects of Propeller Shaft rps

The study of the effect of propeller shaft rps on the performance coefficients at different azimuthing rates and advance coefficients at dynamic azimuthing conditions is presented in this section. The study was carried out at two propeller shaft rps of 8 and 15 and at the advance coefficients of $J = 0.2$ and $J = 0.8$ and at azimuthing rates of $2^\circ/\text{sec}$, $5^\circ/\text{sec}$, $10^\circ/\text{sec}$, $20^\circ/\text{sec}$. The carriage speed was varied to maintain the same advance coefficients for the shaft rps of the two propellers.

The propeller and the unit performance coefficients at the two shaft rps with various azimuthing rates and advance coefficients are shown in Figures 6.24 to 6.28. It was observed that at both advance coefficients of 0.2 and 0.8 as the shaft rps was increased from 8 to 15, the performance coefficients slightly increased and the increase was more obvious as the azimuthing angle increased. The increase in the performance coefficients due to the increase of propeller shaft rps was not noticeably affected by the change of azimuthing rate.

The increase of the performance coefficient values with the increase of propeller shaft rps can be attributed to two factors, namely: *Reynolds Number* and the added mass effects. The *Reynolds Number* based on the propeller blade chord length at 70% of the radius at the propeller rps of 15 and 8 varied between 4.5×10^5 to 5.5×10^5 and 2.5×10^5 to 3.5×10^5 , respectively, depending upon the advance velocity range used. Thus, the increase in the performance coefficients might be attributed to the *Reynolds Number* effects. A detailed discussion of this effect is provided in section 2.8. The *Reynolds Number* in the tests at

Study of pod at dynamic azimuthing conditions

shaft rps of 8 might be too low to produce any meaningful results. However, the results show the *Scale Effect* in the study. A simplified theoretical account for the added mass effect with constant propeller shaft rps with azimuthing range of 0° to 180° was presented by Woodward (2006). Woodward (2006) found that the total effect of added mass was very small. Thus the difference in the performance coefficients due to the change of shaft rps can primarily be attributed to the change in flow condition (laminar, turbulent or transient) over the pod-strut-propeller bodies. It is noted that the difference fell inside the uncertainty band of the measurement. The increase in performance coefficients with the increase of shaft rps was consistent within the range of azimuthing angles. However, it might be attributed to the uncertainty in the measurements.

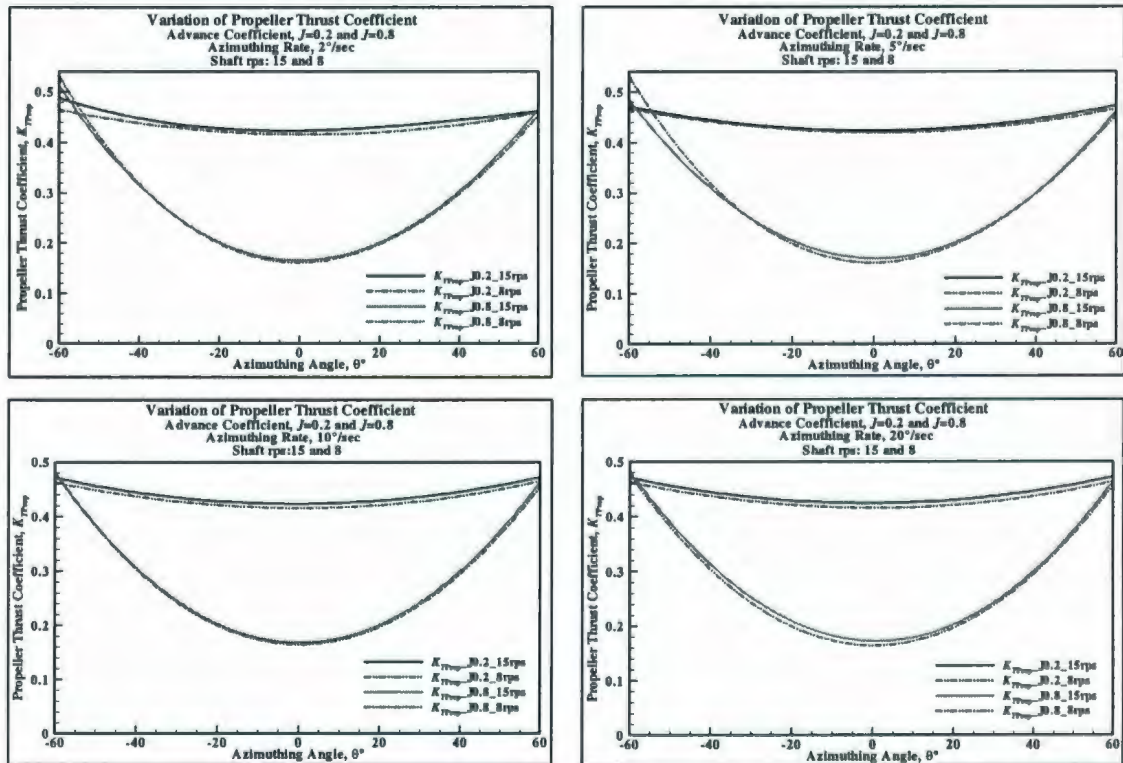


Figure 6.24: Experimental results: Variation of propeller thrust coefficient of the model pod unit with shaft rps and azimuthing rate in dynamic conditions.

Study of pod at dynamic azimuthing conditions

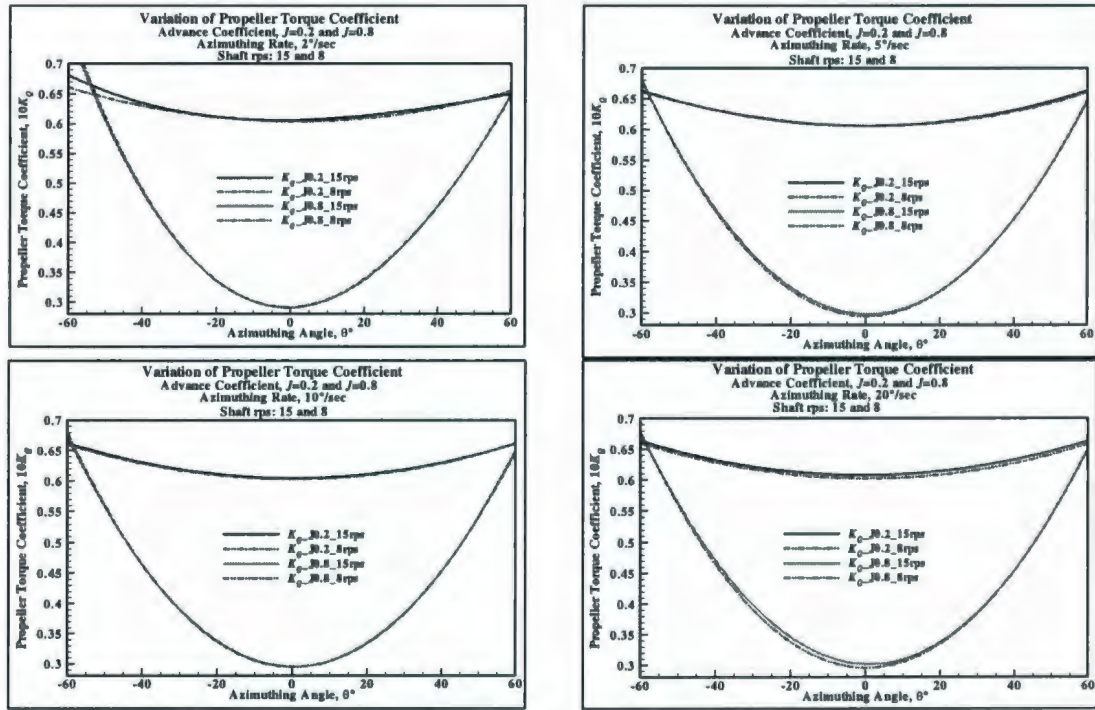


Figure 6.25 Experimental results: Variation of propeller torque coefficient of the model pod unit with shaft rpm and azimuthing rate in dynamic conditions.

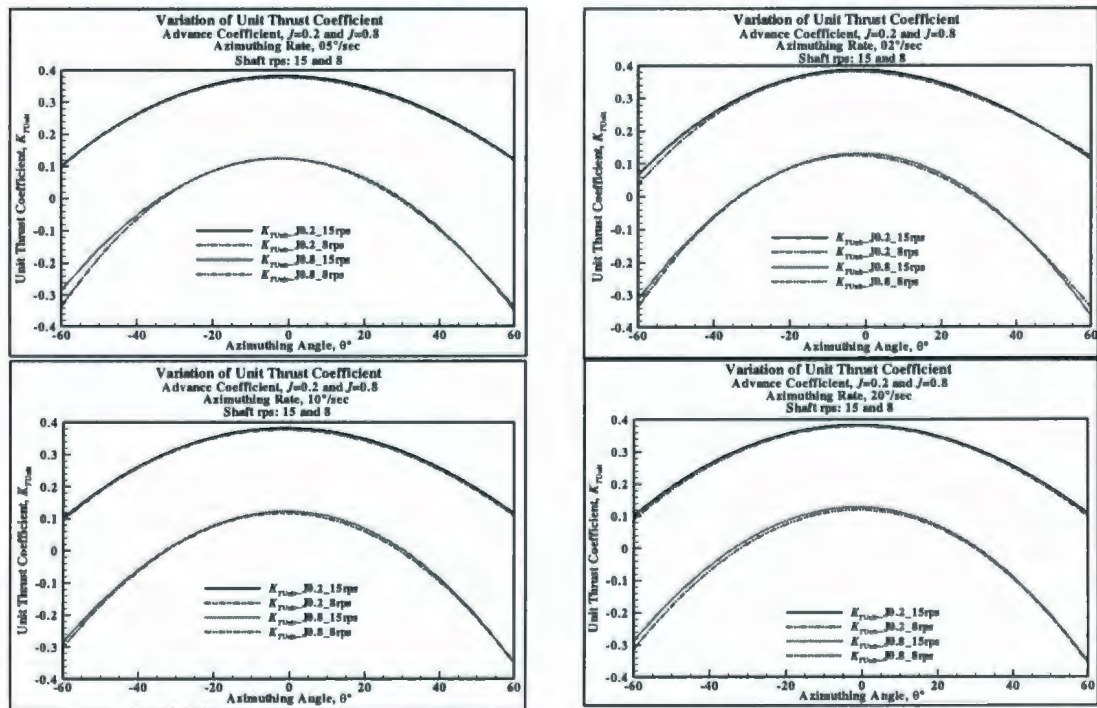


Figure 6.26: Experimental results: Variation of unit thrust coefficient of the model pod unit with shaft rpm and azimuthing rate in dynamic conditions.

Study of pod at dynamic azimuthing conditions

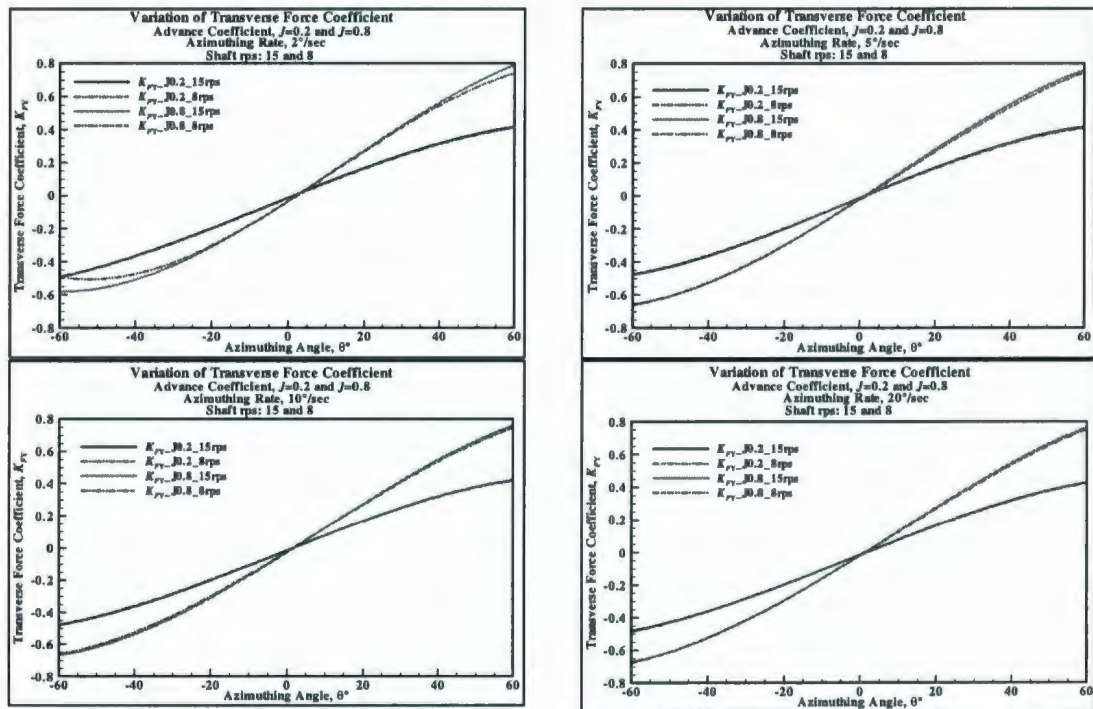


Figure 6.27: Experimental results: Variation of transverse force coefficient of the model pod unit with shaft rpm and azimuthing rate in dynamic conditions.

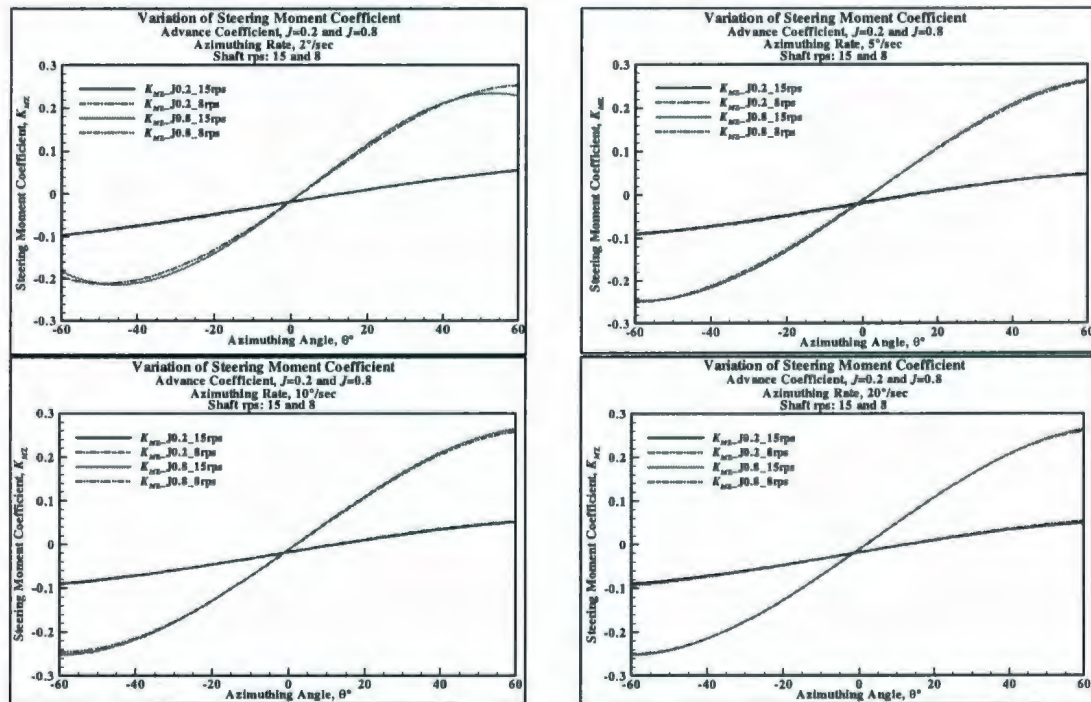


Figure 6.28: Experimental results: Variation of steering moment coefficient of the model pod unit with shaft rpm and azimuthing rate in dynamic conditions.

6.4 Summary

The experimental study into the effects of azimuthing angles, azimuthing rate and shaft rps on the propulsive characteristics of a puller podded unit in open water conditions at dynamic azimuthing conditions is presented in this chapter. The coefficients of the propeller and the pod unit showed a strong dependence on the propeller loading (advance velocity) and azimuthing angle. The open water characteristics were mostly irregular for the astern thrust conditions in the azimuthing angle beyond the range of 90° to 270° , where flow separation at the propeller blades and the pod-strut body might have occurred. The performance coefficients in static azimuthing conditions fit well with the 10th order polynomial fit of the data obtained in the dynamic azimuthing condition in the corresponding azimuthing angles. The azimuthing rate did not show any noticeable effect on the performance coefficients in the range of azimuthing angles from $+60^\circ$ to -60° . At the advance coefficients of 0.2 and 0.8, as the shaft rps was increased from 8 rps to 15 rps, the performance coefficients slightly increased and the increase was more obvious as the azimuthing angle increased. The increase in the performance coefficients due to the increase of propeller shaft rps was not noticeably affected by the change of azimuthing rate.

CHAPTER

7

CONCLUSIONS

7 Conclusions

7.1 Chapter Objectives

In this experimental research work, the performance of puller and pusher types of podded propulsors with varied geometry at various static and dynamic azimuthing conditions in open water conditions was investigated. A summary of the objectives of this thesis work is provided first. Next, a summary of the results and analyses of the study is presented. The conclusions derived from the results and analyses are given. Finally, the chapter states a few recommendations for related future research work.

7.2 Summary of the Objectives

The thesis research consisted of two major parts. The first part focused on the propulsive performance of podded propulsors with varied geometry both in pusher and puller configurations in open water. An experimental study was made on the effects of five pod geometric parameters on propeller thrust, torque and efficiency, unit thrust and efficiency of the propulsors. The geometric parameters of the propulsors included three geometric parameters of the pod (length, diameter and taper length) as well as propeller hub taper angle and lateral strut distance from the propeller plane. The work used a fractional factorial design and analysis approach to study the parameters. A systematic series that varied the parameters within a range was used to determine the effect of the parameters on the performance coefficients. This provided a comprehensive set of data that was used

Conclusions

in the design and study of these propulsors. The outcome of this study was a quantification of the most significant geometric parameters of podded propulsors in affecting thrust, torque and efficiency. The results also provided guidelines to designers to design podded propulsors with a geometric shape suitable for a specific configuration. The second part of the research work focused on hydrodynamic properties of the podded propulsors in static and dynamic azimuthing conditions. To address the research question on the hydrodynamic behaviour of the podded propulsors at static and dynamic azimuthing conditions, two separate experimental studies were carried out. In the first study, two podded propulsors were tested to measure the forces and moments on the propeller and the unit at different static azimuthing angles within the range from -30° to 30° . The tests were performed both with puller and pusher configurations. The results were used to evaluate the variations of the performance coefficients at different loading conditions and configurations at static azimuthing positions. In the second study, a second dynamometer system was used to measure forces and moments of a pod unit of smaller size at different dynamic azimuthing conditions in the range of 0° to 360° azimuthing positions. The results helped to evaluate the nature of the forces and moments on the pod unit as the propulsor azimuths dynamically, supplying some fundamental information with respect to manoeuvring loads from the pod and also a base for the validation of numerical modeling. Additional study was carried out to evaluate the effects of azimuthing rate and propeller shaft rps on the performance coefficients at dynamic azimuthing conditions.

7.3 Summary of the Results

7.3.1 Pods with Varied Geometry

A series of 16 pods was designed using a fractional factorial design technique to study the effects of five geometric parameters (pod diameter, pod length, pod taper length, strut distance and propeller hub angle) of podded propulsors in pusher and puller configurations. The curves for each of the performance coefficients of the pods showed variations suggesting significant effects of the geometric parameters. The findings of the design of experiment analysis of the data are summarized at follows:

For a fixed propeller diameter, as the pod diameter increased, the propeller thrust, torque and efficiency increased for both puller and pusher propulsors; this might be attributed to the blockage effect of the pod. However, the increase in pod diameter resulted in a decrease in unit thrust for the pusher propulsors.

Pod length did not show an obvious effect on the performance coefficients of the puller propulsors, but it showed some effect on unit thrust coefficient of the pusher propulsors at higher advance coefficients. At advance coefficients of 0.9 or higher, for a fixed propeller diameter, as the pod length increased the propulsor unit thrust coefficient decreased, meaning that longer pods had lower unit thrust in the pusher configuration.

Conclusions

For the puller propulsors, as the hub taper angle increased, both propeller and propulsor unit thrust coefficients and efficiencies increased for all ranges of advance coefficients; this was more pronounced at low advance coefficients. However, hub angle had opposite effects on torque coefficients at low and high advance coefficients. The torque increased with increasing taper angle at advance coefficients of 0.7 or lower but decreased at higher advance coefficients. For the pusher propulsors, as the hub taper angle increased, propeller and unit thrusts and propeller torque coefficients and efficiencies increased for all ranges of advance coefficients.

The ratio of strut distance to propeller diameter had moderate effects on propeller thrust and torque coefficients for puller propulsors at moderate advance coefficients but only on propeller thrust for pusher propulsors. As the distance of the strut leading edge from the propeller plane increased, the propeller thrust and torque coefficient decreased.

Taper length of the pod aft end, the end away from the propeller, did not have any significant influence on performance of the puller propulsors within the range tested. However, it had significant effect on unit thrust of the pusher propulsors at all advance coefficients. For a fixed propeller diameter, as the pod taper length increased, the unit thrust also increased due to less pod drag on pods with high taper length.

The interaction of the factors pod diameter and hub angle had significant effect on both propeller and unit thrust and torque coefficients at moderate advance coefficient for the

Conclusions

puller propulsors. For a fat pod, the influence of increased hub taper angle, which caused an increase in propeller and unit thrust coefficients, was more pronounced than the slender pod. The interaction of the factors showed little or no effect for the pusher propulsors.

For the pusher propulsors, the interaction of the factors pod length and pod taper length had noticeable effect on propeller thrust for low advance coefficients. When the ratio of the pod taper length to propeller diameter was low, increasing pod length resulted in lower propeller thrust, whereas at higher taper length increasing pod length resulted in higher propeller thrust.

For the pusher propulsors, the interaction effect of pod diameter and pod length was significant on unit thrust coefficient at low advance coefficients. The analysis showed that for a slender pod (low value of pod diameter to propeller diameter), increasing pod length resulted in an increase in unit thrust, whereas the opposite is true for the pod with a high value of the ratio of pod diameter to propeller diameter.

For the puller propulsors, the interaction effect of pod length and strut distance was significant on unit thrust coefficient at moderate advance coefficients. The analysis showed that the impact of pod length was opposite at high and low values of strut distance. At the low pod length value, the increase of strut distance increased the unit

Conclusions

thrust, whereas at high pod length value, the increase of strut distance decreased the unit thrust.

The measurements showed that there were significant variations in the propeller thrust, torque, unit thrust and propeller and unit efficiencies values due to the variations of the geometric parameters of the pods. The uncertainty analysis of the measurements showed that the level of uncertainty was within acceptable limits. The variations of the performance coefficients due to the geometry variations were outside the value of the errors, which implied that the results were significant.

7.3.2 Pods at Static Azimuthing Conditions

An experimental study of the performance coefficients of a model pod unit at different static azimuthing angles and advance coefficients was presented for puller and pusher configurations. A model pod fitted with two different propellers (for the two configurations) was tested using a custom designed pod testing system at various advance coefficients and at azimuthing angles ranging from -30° to 30° . Propeller thrust and torque and unit forces and moments in the three coordinate directions were measured at each of the operating conditions.

For the puller propulsor with a left handed propeller (viewing upstream), the propeller thrust coefficient remained approximately the same for equal positive (port, counter-clockwise rotation viewing from top) and negative (starboard, clockwise rotation viewing

Conclusions

from top) static azimuth angles. The thrust along the propeller axis was increased at azimuthing angles in comparison to the straight-ahead condition. For a pusher propulsor with a right-handed propeller (viewing upstream), the propeller thrust coefficient was not symmetrical at port and starboard azimuthing angles. For all advance coefficients, the propeller thrust coefficient was higher for port azimuthing angles and lower for negative starboard azimuthing angles than those in straight course conditions. In the pusher configuration, the propeller thrust was less sensitive to changes in the azimuthing angle (in the range from -30° to 30°) for starboard values than port values. Overall, the thrust from the puller propeller at any advance coefficient and at any azimuthing angle was found to be higher than the thrust for the pusher propeller in corresponding operating conditions. The trend of the propeller torque coefficient curves was similar to those of the thrust coefficients in corresponding operating conditions.

For puller and pusher configurations, the unit thrust coefficient decreased as the advance coefficient increased as expected. As the azimuthing angle was changed from 0° to 30° or from 0° to -30° , generally the unit thrust coefficient decreased. However there was an asymmetry such that the maximum unit thrust coefficient occurred at a positive (i.e. port) azimuthing angle of 10° for most of the advance coefficients. In both configurations, the reduction of the unit thrust was stronger for the negative azimuth direction. Overall, the pod unit thrust in the pusher configuration at any advance coefficient and at any azimuthing angle was lower than that for the puller configuration in the corresponding operating conditions.

Conclusions

Both in puller and pusher configurations, the propulsor showed an increase of transverse force with both positive and negative azimuth angles but in opposite directions with the increase of advance coefficient. The trend and magnitude of the transverse force in the pusher configuration, with the change of advance coefficient and azimuthing conditions, were different to those in the puller configuration. In the puller configuration, zero transverse force was found in the range of azimuth angles from 0 to -3° for different advance coefficients, but in pusher configuration, zero transverse force was found in the range of azimuth angles from 0 to -1° for different advance coefficients. It should be noted that the propeller in the puller configuration was a left-handed and the propeller in the pusher configuration was a right-handed, viewing from downstream.

In puller configuration, the vertical force was mostly positive (vertically downward) for positive azimuthing angles (port) and generally increased with the increase of azimuthing angle and advance coefficient. At negative azimuthing directions, there was a small amount of negative vertical force and the force increased with the increase of azimuthing angle and advance coefficients. At positive azimuthing angles, the inflow direction, propeller rotational direction (left handed) and the position of the strut behind the propeller might have caused high pressure on the top of the pod thus producing high downward vertical force at positive azimuthing angles. At negative azimuthing angles, however, the opposite effect took place because of the propeller worked against the inflow, thus producing negative (vertically upward) vertical force. In pusher configuration with a right-handed propeller, the negative vertical force was produced at

Conclusions

negative azimuthing angles and the force increased with the increase of azimuthing angles and advance coefficients. At negative azimuthing angle (starboard), the interaction between the strut wake and the propeller wash might have produced low pressure on top of the pod body, thus producing high negative (upward) vertical force. Overall, the magnitude of the vertical force coefficients for the pusher configuration was higher than those of the puller configuration.

The axial moment was defined as the moment about the X-axis (longitudinal) and was considered clockwise as positive. The trends of the axial moment curves in both configurations were generally similar to those of transverse force coefficients in the corresponding configurations, but of different signs. The axial moment coefficient was attributed to the transverse force and the shaft torque, with the transverse force being the main contributor. The high magnitude of the axial moment coefficient was primarily due to the fact that the moment was calculated about the global unit center, which was 1.68m vertically above the pod center.

The transverse moment was defined as the moment about the Y-axis (transverse) and was considered clockwise as positive. The transverse moment coefficient curves in both configurations are generally similar to those of unit thrust coefficients in the corresponding configurations. The maximum transverse moment occurred at azimuthing angle of $+10^\circ$ (Port) in the both configurations and the moment decreased from that angle in both directions of the azimuthing angles. This was observed at all advance coefficients

Conclusions

except at bollard pull condition where the maximum moment occurred at straight-ahead condition. The transverse moment coefficient is primarily attributed to the unit thrust force. Similarly to axial moment coefficient, the high magnitude of the transverse moment coefficient is primarily due to the fact that the moment was calculated about the global unit center, which is 1.68m vertically above the pod center.

The steering moment was defined as the moment about the Z-axis (vertical) and was considered clockwise as positive. The steering moment showed an increasing tendency with the increase of advance coefficients for both positive and negative azimuthing angles but in opposite direction. This was observed for both puller and pusher configurations. At the bollard pull condition, the steering moment remained almost constant with the change of azimuthing conditions in the puller configuration, but changed in the pusher configuration. Again, the magnitude of steering moments for the pusher pod was higher than the puller one at almost all corresponding azimuthing conditions and advance coefficients. Also, coupled with the higher transverse force generated by a pusher propulsor in corresponding conditions, means that higher steering forces would be generated by this pusher propulsor as compared with the puller propulsor.

7.3.3 Pods at Dynamic Azimuthing Conditions

The propeller thrust and torque coefficients of the puller propeller were increasing when the azimuthing angles were increased from straight-ahead condition (0° angle) both in

Conclusions

positive and negative azimuthing angles. The maximum propeller coefficients were observed at the azimuthing angles of $\pm 120^\circ$. At the bollard pull condition, the thrust and torque coefficients remained almost constant for all azimuthing angles. There was some scatter at the large azimuthing angles, which can be attributed to the unsteady nature of the reverse wash and separation (at azimuthing angles greater than $\pm 120^\circ$). The curves at different advance coefficients clearly show regular non-linear trends, which can be associated with the changing wake characteristics as the azimuthing angle changes. Small asymmetries in location and magnitude of the maxima might be due to the influences of propeller rotation direction and the interaction between the propeller wash and the pod-strut body. Propeller thrust and torque coefficient showed similar trends at corresponding azimuthing angles and advance coefficients.

The unit thrust coefficients decreased for both azimuthing directions but the reduction was visibly stronger for negative azimuthing angles. A similar trend was found for all advance coefficients and within the range of azimuthing angles of $\pm 90^\circ$. The unit thrust coefficients increased as the azimuthing angle was increased further beyond $\pm 90^\circ$.

The transverse force coefficient of the propulsor with left-handed propeller showed strong dependency on propeller loading and azimuthing angle. The nature is similar to that of a classical rudder. For all advance coefficients, the transverse force coefficients increased with both positive and negative azimuthing angles from straight-ahead condition. The maximum transverse force coefficient was found in the range of $\pm 60^\circ$ to

Conclusions

$\pm 90^\circ$. For the pod unit with the puller propeller, the zero transverse force was found for the azimuthing angle in the range of 0° to -2° depending upon the advance coefficient.

The vertical force coefficients were positive (vertically downward) for azimuthing angles of 0° to -120° for all advance coefficients. The maximum vertical force was observed at azimuthing angle of -60° . In the azimuthing angle range of 0° to 180° , the vertical force coefficients were negative (upward) or near zero at low advance coefficients ($J \leq 0.4$) and positive for higher advance coefficients and increased with the increase of advance coefficients. At the bollard pull conditions, the vertical force on the unit was near zero. The vertical force (lift on the propulsor) is the resultant on the interaction between the inflow velocity and the propeller wash, which resulted in a pressure difference between the top and bottom of the pod.

The nature of the axial moment coefficient curves was similar to those of transverse force coefficient curves but of opposite sign primarily because of the sign convention used. The maximum positive and negative axial moment occurred in the azimuthing angle range of $\pm 60^\circ$ to $\pm 120^\circ$.

The maximum transverse moment coefficient was observed approximately at the straight-ahead condition for all advance coefficients. The nature of the curves was similar to those of unit thrust component for all azimuthing angles.

Conclusions

The steering moment coefficient varied in a nonlinear fashion with the change of advance coefficients and azimuthing angles. The steering moment coefficient was increasing with the larger azimuthing angles up to $\pm 90^\circ$. For further increase in azimuthing angle up to $\pm 180^\circ$, a decrease in steering moment was observed. These were observed for all advance coefficients but at the bollard pull condition. The steering moment on the propulsor was almost zero for bollard pull conditions for all azimuthing angles.

The comparative study of the propeller thrust and torque coefficients and unit forces and moments between the static and dynamic azimuthing conditions in the azimuthing range from 0° to 360° and at advance coefficients of 0.2 and 0.5 shows that the performance coefficients at static azimuthing conditions coincided well onto the 10th order polynomial curve fit for the dynamic azimuthing data. The discrepancy observed in the range of azimuthing angles from 120° to 270° might be attributed to the unsteady nature of the operating condition. In dynamic azimuthing conditions, the fluctuation of the magnitude of the performance coefficients for both advance coefficients shows a considerable range and care should be taken while designing the propeller and pod bearings, which would be subjected to the fluctuating forces.

Propeller thrust and torque coefficients, unit thrust and transverse force coefficients and the steering moment coefficients were not noticeably affected by the azimuthing rate for both high and low advance coefficients. The slight difference in the performance coefficients with the change of azimuthing rate that was observed, especially in the

Conclusions

azimuthing range of 0° to -60° was within the limit of uncertainty bar, hence was not significant.

The propeller and the unit performance coefficients changed noticeably with the change of propeller shaft rps. It was observed that at both advance coefficients of 0.2 and 0.8, as the shaft rps was increased from 8 to 15, the performance coefficients slightly increased and the increase was more obvious as the azimuthing angle increased. The increase in the performance coefficients due to the increase of propeller shaft rps was not noticeably changed by the change of azimuthing rate.

7.3.4 Uncertainty Analysis

The calculated uncertainty levels in the podded propulsor experiments in both pod test equipment were found to be comparable with commercial standard equipment and similar analyses. The custom-made podded propulsor dynamometer systems demonstrated the capability of achieving uncertainty limits close to those of commercial standard equipment.

The primary element of the uncertainty of the propeller performance coefficients was the bias error (60% or more of the total uncertainty for the NSERC pod system and 80% or more on the total uncertainty for the IOT pod system). To reduce the overall uncertainty in the final results, the primary focus should be to reduce the bias error in the equipment. However, for the global performance coefficients, generally, the primary element of the

Conclusions

uncertainty was precision error (about 60% or more of the total uncertainty). The IOT dynamometer system produced lower uncertainty limit for the global performance coefficients of the two systems.

One possible approach to improve accuracy of the uncertainties in propeller thrust and torque of the podded propulsor tests is to run experiments at higher shaft rps. At higher shaft rps, higher advance speeds will be required to achieve the desired advance coefficients. Under these conditions the magnitudes of the thrust and torque will be larger relative to the uncertainty levels. Correspondingly, the percent error for each of these measured variables would be reduced, which results in less overall uncertainty in the thrust and torque coefficients.

The uncertainty analysis results provided strong evidence that the experimental data obtained using both the NSERC and IOT pod dynamometer system presented the true performance characteristics of the model scale podded propulsors under consideration.

7.4 Main Findings

The Fractional Factorial Design of Experiment (FFD) technique was found to be very useful in designing a series of 16 pods and in the analysis of the test results to study the effects of five geometric parameters on the propulsive performance of model podded propulsor in straight-ahead conditions.

Conclusions

The analysis of the pod series test results provided information on the geometric parameters, which have noticeable effect on propulsive characteristics of the propulsor. The analysis provides valuable information to podded propulsor designers.

Separate studies were carried out for puller and pusher configurations. Factors that were found significant in the puller configuration did not necessarily show to be significant in the pusher configuration.

In static azimuthing conditions in the range of $+30^\circ$ to -30° , the propeller and unit performance coefficients changed in a non-linear fashion with the change of propeller loading and azimuthing angles.

The static azimuthing test results also showed that the performance coefficient curves were different for the puller and pusher configurations, which justified separate study of the two configurations.

In the dynamic azimuthing study, the coefficients of the propeller and the pod unit showed a strong dependence on the propeller loading (advance velocity) and azimuthing angle. The open water characteristics were mostly irregular for the astern thrust conditions in the azimuthing angle beyond the range 90° to 270° , where the flow separation at the propeller blades and the pod-strut body occurred.

Conclusions

The dynamic azimuthing rate did not show any noticeable effect on the performance coefficients in the range of azimuthing angles from $+60^\circ$ to -60° for the advance coefficients of 0.2 and 0.8.

All of the performance coefficients, and at both advance coefficients of 0.2 and 0.8, as the shaft rps was increased from 8 rps to 15 rps, the performance coefficients slightly increased and the increase was more obvious as the azimuthing angle increased. The increase in the performance coefficients due to the increase of propeller shaft rps was not noticeably affected by the change of azimuthing rate.

7.5 Recommendations for Further Study

There are a few areas that are recommended for further study. Concerning the geometry of the podded propulsor, the next step should be the optimization of the pod body using possibly the response surface methods such as the central composite design (CCD) method based on the significant geometric parameters observed after the factorial design. In the current study, the propellers were not designed for each geometric variation. In future, it will be worthwhile to carry out a propeller study that could be run factorially with one pod design so that interaction between the propeller parameters for a podded propulsor could be found. This would be useful for the propeller designers.

In the current study, a symmetric strut design was used so that the same pod pieces in push and pull mode could be used and reduce the number of factors used in the factorial

Conclusions

design. A few commercial struts are asymmetric (wake adapted strut) and usually an extension is used in the aft side and around the base for strength purposes. The struts were made as a symmetric form, so as not to introduce any effects of the strut being used as a pusher in one set of tests, and a puller in the next set. This also had the benefit of reducing the machining time and kept the number of pieces to a minimum. However, the instrumentation design makes it possible to allow one to change geometric aspects of the strut as well. It would be interesting to design a series of experiments that alters the strut geometry. Some of the strut geometric parameters that could be altered are: strut foil shape, strut length, strut thickness, and strut asymmetry or twist angles.

As a continuation of the podded propulsor's study at azimuthing conditions, two pods could be studied simultaneously to examine the interaction effects between the pods at various configurations. The study could include the distance between the two pods, the position of the pods (transverse or tandem). The studies in the current research work are in open water condition. It is important to continue the studies in azimuthing conditions (single and dual pods) with the pod fitted behind a ship model, which would be very useful for the industrial users. .

A study could be carried out to examine the local flow velocities etc. of the podded propulsor at different configurations and azimuthing conditions. The study might include the LDV or PIV study to validate some of the speculations offered in the current thesis about the trends of the performance coefficients at different configurations. A dedicated

Conclusions

study on the local flow conditions of various pod shapes would reveal the reason for the increased propeller thrust and torque with the increase of pod diameter as observed in the current study.

Another interesting yet important study would be to examine the performance coefficients of the puller and pusher pods at different configurations and azimuthing conditions under cavitating conditions. Cavitation was one of the main reasons for pod failure and it is an important aspect of podded propulsor design. The cavitation behaviour is expected to be variable with the change of pod configurations and azimuthing angles and it is important to evaluate the cavitation characteristics at those conditions.

References

- Anderson, M. J., Whitcomb, P., 1996, Optimize your process optimization efforts, Minnesota, www.statease.com.
- Anon., 2000, Editorial Comment: Optimizing pods for sustained market thrust, Royal Institution of Naval Architects, *Naval Architect*, London, November, pg. 3.
- Anon., 2001, Editorial Comment: Pressing ahead with pods, Royal Institution of Naval Architects, *Naval Architect*, London, September, pg. 3.
- Atlar, M., Liu, P., Allema, Ir. J. H., Ishikawa, S., Kim, S., Poustoshniy, A. V., Sanchez-Caja, A., Sasaki, N., and Traverso, A., 2005, The Specialist Committee on Azimuthing Podded Propulsion: Final Report and Recommendations to the 24th ITTC, *In proceedings of the 24th ITTC*, Volume II, pp. 543-587.
- Backlund, A. and Kuuskoski, J., 2000, The contrarotating propeller concept with a podded drive, *In the Motor Ship Marine Propulsion Conference*, Amsterdam, The Netherlands, 12 p.
- Bose, N. and Luznik, L., 1996, Uncertainty analysis in propeller open water tests, *International Shipbuilding Progress*, Vol. 43, no. 435, pp. 237-246.
- Bose, N., Billet, M., Anderson, P., Atlar, M., Dugue, C., Ferrando, M., Qian, W., and Shen, Y., 1999, Specialist committee on unconventional propulsors: Final report and recommendation to the 22nd international towing tank conference, Technical Report, *Proceeding of the 22nd ITTC*, USA.

References

- Bushkovsky, V. A., Pustoshny, A. V., Vasiliev, A., and Veikonheimo, T., 2003, A crash-stop study for an Azipod®-propelled vessel, *FAST 2003*, Naples, Italy, Vol. 2, pp. 1-6.
- Carlton, J. S., 1994, *Marine propellers and propulsion*, Butterworth Heinemann.
- Carlton, J. S., 2002, Podded propulsors: some design and service experience, *The Motor Ship Marine Propulsion Conference*, Copenhagen, Denmark, April 9-10, 7p.
- Chen, B. Y.-H. and Tseng, C. L., 1995, A contrarotating propeller design for a high speed patrol boat with pod propulsion, *In proceedings in the 3rd International Conference on Fast Sea Transportation (FAST 1995)*, Germany, pp. 1003-1013.
- Coleman, H. W. and Steele, W. G., 1999, *Experimentation and uncertainty analysis for engineers*, Wiley Interscience.
- Design Expert, 2005, Design of experiment software, www.statease.com.
- Done, G. and Balmford, D., *Bramwell's Helicopter Dynamics*, 2nd Edition, American Institute of Aeronautics and Astronautics, Reston, VA, 2001.
- Galway, R. D., 1980, A comparison of methods for calibration and use of multi-component strain gauge wind tunnel balances, Aeronautical Report LR-600, NRC No. 18227, National Aeronautical Establishment, National Research Council, Canada, 40p.
- Gerr, D., 1989, *Propeller handbook*, International marine publishing, Camden, Maine.
- Goubault, P. and Pérrée, J., 2004, Parametric investigations designed to help focused pod technology development, *In Proceedings of the 1st International Conference on*

References

- Technological Advances in Podded Propulsion*, Newcastle University, UK, April, pp. 27-28.
- Gray, R. B., 1992, Vortex modeling for rotor aerodynamics – The 1991 Alexander A. Nikolsky lecture, *Journal of the American Helicopter Society*, Vol. 37, No. 1.
- Grygorowicz, M. and Szantyr, J. A., 2004, Open water experiments with two pods propulsor models, *In Proceedings of the 1st International Conference on Technological Advances in Podded Propulsion*, Newcastle University, UK, April, pp. 357-370.
- Halstensen, S. O. and Leivdal, P. A., 1990, The development of the *SpeedZ* propulsion system, *In proceedings in the 7th International High Speed Surface Craft Conference*, 8p.
- Hawkins, D. and Lye, L. M., 2006, Use of DOE methodology for investigating conditions that influence the tension in marine risers for FPSO ships, *In Proceedings of the 1st International Structural Specialty Conference*, Calgary, Alberta.
- He, M., 2006, Propeller wake impingement on a strut. PhD thesis, Faculty of Engineering and applied Science, Memorial University of Newfoundland, 250p.
- He, M., Veitch, B., Bose, N. and Liu, P., 2005b, An investigation on wake/strut interaction of a tractor-Type podded propulsor, *In proceedings of the 7th CMHSC*, Halifax, NS Canada, September 21-22, 8p.
- He, M., Veitch, B., Bose, N., Bruce, C., and Liu, P., 2005a, Numerical simulations of propeller wake impacting on a strut, *In proceedings of the CFD2005*, St John's, NL Canada, August, 8p.

References

- Heinke, H. J., 2004, Investigation about the forces and moments at podded drives, *In Proceedings of the 1st International Conference on Technological Advances in Podded Propulsion*, Newcastle University, UK, April, pp. 305-320.
- Hess, D.E., Nigon, R.T. and Bedel, J. W., 2000, Dynamometer calibration and usage, Research and Development Report No. NSWCCD-50-TR-2000/040, Hydromechanics Directorate, Carderrock Division, Naval Surface Warfare Center, West Bethesda, Maryland, 31p.
- Islam, M. F., 2004, Numerical investigation on effects of hub taper angle and pod-strut geometry on propulsive performance of pusher propeller configurations, Master of Engineering thesis, Memorial University of Newfoundland, Canada, 136 p.
- Islam, M. F., 2006, Uncertainty analysis of NSERC-NRC pod dynamometer system, Ocean Engineering Research Center (OERC) Report No. OERC-2006-05, St. John's, NL, Canada, 96p.
- Islam, M. F., 2006a, Calibration and usages of NSERC-NRC pod dynamometer system, Ocean Engineering Research Centre (OERC) Report No. OERC-2006-04, St. John's, NL, Canada, 2006, 80p.
- Islam, M. F., 2006b, Cavitation performance testing of podded propellers with different hub taper angles, Ocean Engineering Research Centre (OERC) Report No. OERC-2006-03, St. John's, NL, Canada, 2006, 62p.
- Islam, M. F., Akinturk A., Veitch B., and Liu P., 2007b, Performance characteristics of a podded propulsor during dynamic azimuthing, *In proceedings of the 8th CMHSC 2007*, St. John's, Canada, 8p.

References

- Islam, M. F., Liu, P., and Veitch, B., 2008d, *PROPELLA: A numerical tool to investigate various aspects of podded propulsors, To be published in the Journal of Naval Architecture and Marine Engineering, JNAME*, 10 p.
- Islam, M. F., MacNeill A., Veitch B., Akinturk A., and Liu P., 2007a, Gap effect on performance of podded propulsors in straight and static azimuthing conditions, *In proceedings of the 8th CMHSC 2007*, St. John's, Canada, 9p.
- Islam, M. F., Molloy, S., He, M., Veitch, B., Bose, N., and Liu, P., 2006b, Hydrodynamic study of podded propulsors with systematically varied geometry, *In proceedings of the 2nd International Conference on Technological Advances in Podded Propulsion*, Brest, France, 14p.
- Islam, M. F., Taylor, R., Quinton, J., Veitch, B., Bose, N., Colbourne, B., and Liu, P., 2004, Numerical investigation of propulsive characteristics of podded propeller", *In proceedings of the 1st International Conference on Technological Advances in Podded Propulsion*, Newcastle University, UK, April, pp. 513-525.
- Islam, M. F., Veitch B, Molloy S, Bose N, and Liu P., 2008a, Effects of geometry variations on the performance of podded propulsors, *To be appeared in SNAME Transaction*, Florida, USA, 17p.
- Islam, M. F., Veitch B., Akinturk A., Bose N., and Liu P., 2008b, Performance study of podded propulsor in static azimuthing conditions, *being reviewed in the Journal of International Shipbuilding Progress*, 15p.

References

- Islam, M. F., Veitch, B., and Liu, P., 2008c, Experimental research on marine podded propulsors, *To be Published in the Journal of Naval Architecture and Marine Engineering, JNAME*, 11 p.
- Islam, M. F., Veitch, B., Bose, N., and Liu, P., 2005, Cavitation characteristics of pushing and pulling podded propellers with different hub taper angles, *In proceedings of the 7th CMHSC*, Halifax, NS Canada, September 21-22, 7p.
- Islam, M. F., Veitch, B., Bose, N., and Liu, P., 2006a, Numerical study of hub taper angle on podded propeller performance, *Journal of Marine Technology*, Vo. 43, No. 1, pp. 1-10.
- Islam, M. F., Veitch, B., Bose, N., and Liu, P., 2006c, Hydrodynamic characteristics of pod propeller units of highly tapered hub, *In proceedings, Propellers/Shafting, Society of Naval Architects and Marine Engineers*, Virginia Beach, USA, 12p.
- ITTC – Recommended Procedures, 2002, Propulsion, Performance - Podded Propeller Tests and Extrapolation, 7.5- 02-03-01.3, Revision 00.
- Jessup, S., Bose, N., Dugué, C., Esposito, P.G., Holtrop, J., Lee, J.T., Mewis, F., Pustoshny, A., Salvatore, F., Shirose, Y., (2002). The Propulsion Committee: Final Report and Recommendations to the 23rd ITTC, Proceedings of the 23rd ITTC - Volume I, pp. 89-151.
- Kanerva, M., 1999, Ferries of the future, *In proceedings of the Conference Cruise and Ferry 99*, Paper No. 3, London, UK, 22 p.
- Karafiath, G. and Lyons, D., 1998, Hydrodynamic performance with pod propulsion - U.S. Navy experience, *American Towing Tank Conference*, Iowa City.

References

- Karafiath, G. and Lyons, D., 1999, Pod propulsion hydrodynamics - U.S. Navy experience, *In proceedings in The 5th International Conference on Fast Sea Transportation (FAST '99)*, Seattle, USA, pp. 119-135.
- Kim, S.-E. and Choi, S.-H., 2002, Model tests on propulsion systems for ultra large container vessel, *In proceedings of the Twelfth International Offshore and Polar Engineering Conference*, Kitakyushu, Japan, pp. 520-524.
- Kurimo, R., 1998, Sea trial experience of the first passenger cruiser with podded propulsors, *In proceedings of the 7th International. Symposium on Practical Design of Ships and Mobile units (PRADS)*, pp. 743-748.
- Laukia, K., 1996, The Azipod[®] system-operational experience and designs for the future, in Redundancy vs. Reliability, *The Motor Ship 18th Annual Marine Propulsion Conference*, Hamburg, Germany, pp. 77-94.
- Lepeix, R., 2001, Hydrodynamic trends in hull lines of podded driven large cruise vessels, *In proceedings in Conference on Practical Designs of Ships and Other Floating Structures (PRADS)*, Shanghai, China, pp. 767-776.
- Lewis, E. V. (Editor) 1990, *Principles of Naval Architecture: Resistance, Propulsion and Vibration*, Society of Naval Architects & 2nd Rev edition, 1990.
- Liu, P., 2006, The design of a podded propeller base model geometry and prediction of its hydrodynamics, Technical Report no. TR-2006-16, Institute for Ocean Technology, National Research Council, Canada, 16p.

References

- Lye, L., 2002, Course Notes, Similitude and Dimensional Analysis, Graduate Studies, Faculty of Engineering, Memorial University, Newfoundland and Labrador, September -December.
- MacNeill, A., Taylor, R., Molloy, S., Bose, N., Veitch, B., Randell, T., and Liu, P., 2004, Design of Model Pod Test Unit, *In proceedings of the 1st International Conference on Technological Advances in Podded Propulsion*, Newcastle University, UK, April, pp. 447-458.
- Mewis, F., 2001, The efficiency of pod propulsion, *HADMAR 2001*, Bulgaria, October, 7p.
- Molloy, S., 2003, A proposal for Doctoral research in the Faculty of Engineering and Applied Science, Engineering and Applied Science, Memorial University of Newfoundland.
- Molloy, S., Islam, M. F., He. M., Veitch, B., Bose, N., Wang, J., Akinturk, A., and Liu, P., 2005, Use of factorial design in podded propulsors geometric series, *In proceedings of the 7th CMHSC*, Halifax, NS Canada, September 21-22, 8p.
- Montgomery, D.C., 2005, Design and analysis of experiments, sixth Edition, Wiley & Sons, USA, 189p.
- Myers, R. H. and Montgomery, D. C., 2002, Response Surface Methodology: Process and Product Optimization Using Designed Experiments, 2nd Edition, John Wiley and Sons.
- Niini, M., 1997, Azipod[®] propulsion breakthrough for large cruise ships, *In proceedings of the Conference Cruise and Ferry 97*, London, UK, 14p.

References

- Norrby, R. A., and Ridley, D. E., 1980, Notes on thrusters for ship maneuvering and dynamic positioning, *SNAME Transactions*, Vol. 88, pp. 377-402.
- Pakaste, R., Laukia, K., Wilhelmson, M., Kuuskoski, 1999, Experience with Azipod[®] propulsion systems on board marine vessels, *ABB Review*, Issue 2, 12p.
- Rains, D. A. and Vanlandingham, D. J., 1981, Hydrodynamics of podded ship propulsion, *Journal of Hydronautics*, Vol. 14, No. 14, pp. 18-24.
- Raynor, S. J., 1998, The benefits of podded propulsion in the offshore market, *Dynamic Positioning Conference: Thrusters and Drive Systems*, Houston, TX, USA, pp. 1-11.
- Reichel, M., 2007, Manoeuvring forces on azimuthing podded propulsor model, *Polish Maritime Research*, Versita, ISSN: 1233-2585, Vol. 14, No. 2, pp 3-8.
- Ryan, T. P., 2007, *Modern Experimental Design*, John Wiley and Sons.
- Sasaki, N., Laapio, J., Fagerstrom, B., Juurmaa, K., and Wilkman, G., 2004, Full scale performance of double acting tankers, *In proceedings of the 1st International Conference on Technological Advances in Podded Propulsion*, School of Marine Science and Technology, University of Newcastle, Newcastle, UK, 14p.
- Sorsimo, S., 2006, Personal communication, Manager, Sales, ABB.
- Stettler, J. W., 2004, Steady and unsteady dynamics of an azimuthing podded propulsor related to vehicle maneuvering, PhD thesis, Massachusetts Institute of Technology, 187p.
- Stettler, J. W., Hover, F. S., and Triantafyllou, M. S., 2004, Preliminary results of testing on the dynamics of an azimuth podded propulsor relating to vehicle

References

- manoeuvring, In Proc. of the 1st International Conference on Technological Advances in Podded Propulsion, University of Newcastle, UK, April, pp. 321-338.
- Szantyr, J. A., 2001a, Hydrodynamic model experiments with pod propulsor, *International symposium of ship propulsion (Lavrentiev Lectures)*, State Marine Technical University, St. Petersburg, Russia, pp. 95-104.
- Szantyr, J. A., 2001b, Hydrodynamic model experiments with pod propulsor, *Oceanic Engineering International*, Vol. 5, No.2, pp. 95-103.
- Taylor, R. Veitch, B., and Bose, N., 2005, The influence of hub taper angle on podded propeller performance: 'propeller only' tests vs. 'podded propeller unit' tests, *In proceedings of the 7th CMHSC*, Halifax, NS Canada, September 21-22, 8p.
- Taylor, R., 2006, Experimental investigation of the influence of hub taper angle on the performance of push and pull configuration podded propellers, Master's of Engineering Thesis, Memorial University of Newfoundland, Canada, 120p.
- Terwisga, T. V., Quadvlieg, F., and Valkhof, H., 2001, Steerable propulsion units: Hydrodynamic issues and design consequences, Paper written on the occasion of the 80th anniversary of Schottel GmbH & Co.
- Toxopeus, S. and Loeff, G., 2002, Manoeuvring aspects of fast ships with pods, *In proceedings in Euro Conference on High-Performance Marine Vehicles HIPER'02*, Bergen, pp. 392-406.

References

- Tozer, D. and Penfold, A., 2002, Ultra-large container ships: Designing to the limit of current and projected terminal infrastructure capabilities, Lloyd's Register Technical Association.
- Trägårdh, P., Lindell, P., and Sasaki, N., 2004, Double acting tanker - experience from model tests and sea trials, *In proceedings of the 1st International Conference on Technological Advances in Podded Propulsion*, Newcastle University, UK, April, 11p.
- Van Terwisga, T., Quadvlieg, F., and Valkhof, H., 2001, Steerable propulsion units: hydrodynamic issues and design consequences, Paper written on the occasion of the 80th anniversary of Schottel GmbH & Co., presented on 11 August 2001.
- Wang, J., 2007, Prediction of propeller performance on a model podded propulsor in ice (Propeller-Ice Interaction), PhD thesis, Faculty of Engineering and technology, Memorial University of Newfoundland, 251p.
- Woodward, M. D., 2006, Steady control and response of pod driven ships, PhD thesis, School of Marine Science and Technology, University of Newcastle-upon-Tyne, 255p.
- Woodward, M.D., Atlar, M., and Clarke, D., 2004, A comparison of the stopping modes for pod-driven ships, *In Proceedings of the 1st International Conference on Technological Advances in Podded Propulsion*, Newcastle University, UK, April, pp. 339-356.

APPENDIX

A

DATA TABLES

Data Tables

Table A.1: Pod series data in straight-ahead puller configuration: propeller thrust coefficient, K_{TProp} .

J	Pod 01	Pod 02	Pod 03	Pod 04	Pod 05	Pod 06	Pod 07	Pod 08	Pod 09	Pod 10	Pod 11	Pod 12	Pod 13	Pod 14	Pod 15	Pod 16
0.00	0.4688	0.4865	0.4693	0.4850	0.4833	0.4691	0.4689	0.4826	0.4763	0.4900	0.4924	0.4721	0.4903	0.4719	0.4642	0.4950
0.10	0.4425	0.4542	0.4410	0.4549	0.4556	0.4430	0.4430	0.4544	0.4490	0.4615	0.4638	0.4436	0.4617	0.4448	0.4424	0.4640
0.20	0.4048	0.4179	0.4038	0.4174	0.4179	0.4044	0.4041	0.4157	0.4092	0.4200	0.4260	0.4052	0.4260	0.4054	0.4055	0.4267
0.30	0.3663	0.3782	0.3636	0.3731	0.3777	0.3640	0.3666	0.3741	0.3723	0.3857	0.3860	0.3688	0.3885	0.3689	0.3675	0.3867
0.40	0.3308	0.3327	0.3230	0.3290	0.3363	0.3246	0.3281	0.3330	0.3311	0.3440	0.3481	0.3269	0.3507	0.3274	0.3321	0.3410
0.50	0.2825	0.2858	0.2807	0.2874	0.2906	0.2788	0.2822	0.2902	0.2881	0.3013	0.3059	0.2839	0.3083	0.2828	0.2829	0.2999
0.60	0.2403	0.2432	0.2386	0.2439	0.2448	0.2378	0.2400	0.2422	0.2483	0.2565	0.2601	0.2420	0.2601	0.2435	0.2466	0.2604
0.65	0.2179	0.2200	0.2162	0.2189	0.2266	0.2146	0.2192	0.2194	0.2268	0.2341	0.2374	0.2230	0.2408	0.2265	0.2227	0.2403
0.70	0.2022	0.2004	0.1945	0.2023	0.2045	0.1941	0.1994	0.2000	0.2067	0.2153	0.2149	0.2007	0.2201	0.2071	0.2041	0.2193
0.75	0.1773	0.1776	0.1765	0.1792	0.1795	0.1733	0.1796	0.1787	0.1899	0.1907	0.1966	0.1817	0.1954	0.1831	0.1834	0.1966
0.80	0.1587	0.1579	0.1521	0.1553	0.1616	0.1549	0.1581	0.1551	0.1683	0.1729	0.1760	0.1631	0.1786	0.1657	0.1649	0.1787
0.85	0.1376	0.1365	0.1334	0.1395	0.1379	0.1339	0.1379	0.1348	0.1472	0.1481	0.1529	0.1411	0.1548	0.1422	0.1429	0.1549
0.90	0.1130	0.1166	0.1129	0.1136	0.1139	0.1102	0.1139	0.1134	0.1230	0.1271	0.1341	0.1187	0.1368	0.1231	0.1243	0.1344
0.95	0.0946	0.0922	0.0883	0.0916	0.0933	0.0909	0.0942	0.0916	0.1057	0.1090	0.1097	0.0999	0.1115	0.1025	0.1046	0.1138
1.00	0.0720	0.0662	0.0652	0.0671	0.0644	0.0684	0.0697	0.0666	0.0833	0.0871	0.0845	0.0762	0.0906	0.0816	0.0801	0.0890
1.10	0.0262	0.0168	0.0205	0.0170	0.0186	0.0207	0.0242	0.0197	0.0332	0.0379	0.0409	0.0310	0.0468	0.0384	0.0356	0.0447
1.20	-0.0299	-0.0233	-0.0371	-0.0228	-0.0201	-0.0291	-0.0294	-0.0209	-0.0120	-0.0070	-0.0049	-0.0163	-0.0015	-0.0101	-0.0145	-0.0084

Table A.2 : Pod series data in straight-ahead puller configuration: propeller torque coefficient, $10K_Q$.

J	Pod 01	Pod 02	Pod 03	Pod 04	Pod 05	Pod 06	Pod 07	Pod 08	Pod 09	Pod 10	Pod 11	Pod 12	Pod 13	Pod 14	Pod 15	Pod 16
0.00	0.6698	0.6828	0.6798	0.6806	0.6848	0.6856	0.6829	0.6815	0.6808	0.6891	0.6921	0.6830	0.6916	0.6825	0.6795	0.6854
0.10	0.6367	0.6444	0.6462	0.6480	0.6443	0.6471	0.6446	0.6440	0.6492	0.6497	0.6511	0.6433	0.6511	0.6454	0.6453	0.6515
0.20	0.5972	0.5991	0.6037	0.6049	0.6008	0.6054	0.6025	0.6002	0.6082	0.6019	0.6078	0.6038	0.6092	0.6057	0.6067	0.6077
0.30	0.5564	0.5519	0.5601	0.5571	0.5559	0.5625	0.5621	0.5520	0.5669	0.5638	0.5625	0.5635	0.5667	0.5648	0.5656	0.5653
0.40	0.5066	0.4986	0.5099	0.4991	0.4982	0.5123	0.5126	0.4986	0.5120	0.5062	0.5122	0.5136	0.5124	0.5102	0.5192	0.5155
0.50	0.4587	0.4460	0.4633	0.4510	0.4445	0.4568	0.4591	0.4491	0.4662	0.4602	0.4655	0.4656	0.4643	0.4623	0.4659	0.4677
0.60	0.4018	0.3954	0.4112	0.3949	0.3988	0.4076	0.4088	0.3955	0.4184	0.4103	0.4110	0.4079	0.4152	0.4123	0.4177	0.4109
0.65	0.3772	0.3645	0.3789	0.3656	0.3679	0.3787	0.3796	0.3629	0.3898	0.3772	0.3835	0.3844	0.3873	0.3909	0.3897	0.3832
0.70	0.3534	0.3374	0.3506	0.3368	0.3391	0.3533	0.3548	0.3387	0.3630	0.3525	0.3561	0.3538	0.3605	0.3643	0.3645	0.3572
0.75	0.3221	0.3089	0.3272	0.3107	0.3095	0.3186	0.3249	0.3091	0.3336	0.3261	0.3325	0.3288	0.3288	0.3341	0.3346	0.3268
0.80	0.2955	0.2767	0.2993	0.2745	0.2802	0.2960	0.3000	0.2760	0.3101	0.2974	0.3024	0.3038	0.3063	0.3093	0.3121	0.3021
0.85	0.2656	0.2495	0.2689	0.2484	0.2515	0.2661	0.2705	0.2462	0.2816	0.2655	0.2653	0.2766	0.2741	0.2774	0.2798	0.2698
0.90	0.2330	0.2142	0.2342	0.2146	0.2145	0.2306	0.2344	0.2129	0.2464	0.2299	0.2363	0.2417	0.2442	0.2494	0.2508	0.2396
0.95	0.2032	0.1802	0.2002	0.1835	0.1852	0.2013	0.2059	0.1804	0.2221	0.1997	0.2074	0.2123	0.2104	0.2190	0.2213	0.2089
1.00	0.1678	0.1461	0.1660	0.1481	0.1468	0.1672	0.1708	0.1438	0.1895	0.1727	0.1701	0.1783	0.1772	0.1885	0.1845	0.1719
1.10	0.0947	0.0699	0.0923	0.0708	0.0761	0.0881	0.0916	0.0715	0.1078	0.0994	0.1036	0.1060	0.1118	0.1142	0.1119	0.1046
1.20	-0.0053	-0.0208	-0.0100	-0.0159	-0.0171	0.0042	0.0057	-0.0155	0.0317	0.0213	0.0244	0.0230	0.0322	0.0310	0.0258	0.0183

Data Tables

Table A.3: Pod series data in straight-ahead puller configuration: propulsor (unit) thrust coefficient, K_{TUnit} .

J	Pod 01	Pod 02	Pod 03	Pod 04	Pod 05	Pod 06	Pod 07	Pod 08	Pod 09	Pod 10	Pod 11	Pod 12	Pod 13	Pod 14	Pod 15	Pod 16
0.00	0.4620	0.4836	0.4632	0.4780	0.4707	0.4622	0.4576	0.4685	0.4659	0.4792	0.4788	0.4607	0.4760	0.4611	0.4577	0.4840
0.10	0.4307	0.4450	0.4289	0.4439	0.4431	0.4353	0.4322	0.4319	0.4351	0.4450	0.4479	0.4342	0.4453	0.4300	0.4305	0.4499
0.20	0.3841	0.4085	0.3926	0.4040	0.4060	0.3934	0.3932	0.3945	0.3892	0.4067	0.4102	0.3895	0.4075	0.3880	0.3924	0.4095
0.30	0.3407	0.3647	0.3497	0.3525	0.3646	0.3495	0.3560	0.3537	0.3487	0.3693	0.3709	0.3516	0.3666	0.3467	0.3528	0.3670
0.40	0.3032	0.3208	0.3092	0.3135	0.3188	0.3063	0.3151	0.3158	0.3094	0.3273	0.3301	0.3099	0.3236	0.3058	0.3163	0.3281
0.50	0.2645	0.2674	0.2624	0.2699	0.2742	0.2634	0.2696	0.2715	0.2660	0.2798	0.2833	0.2685	0.2801	0.2637	0.2677	0.2849
0.60	0.2212	0.2248	0.2233	0.2201	0.2274	0.2183	0.2295	0.2261	0.2234	0.2373	0.2365	0.2229	0.2376	0.2204	0.2262	0.2406
0.65	0.1866	0.1969	0.2003	0.1972	0.2067	0.1972	0.2035	0.2050	0.2010	0.2125	0.2171	0.2040	0.2122	0.2019	0.2028	0.2182
0.70	0.1735	0.1761	0.1767	0.1786	0.1822	0.1735	0.1833	0.1825	0.1779	0.1904	0.1956	0.1833	0.1943	0.1832	0.1867	0.1974
0.75	0.1522	0.1530	0.1585	0.1506	0.1630	0.1548	0.1629	0.1595	0.1581	0.1668	0.1711	0.1596	0.1701	0.1618	0.1658	0.1732
0.80	0.1351	0.1307	0.1385	0.1295	0.1419	0.1330	0.1386	0.1350	0.1375	0.1475	0.1530	0.1415	0.1507	0.1410	0.1460	0.1511
0.85	0.1126	0.1115	0.1130	0.1107	0.1176	0.1164	0.1178	0.1120	0.1173	0.1212	0.1311	0.1188	0.1291	0.1216	0.1236	0.1282
0.90	0.0884	0.0839	0.0931	0.0884	0.0969	0.0934	0.0931	0.0870	0.0941	0.1017	0.1072	0.0980	0.1081	0.0997	0.1001	0.1046
0.95	0.0762	0.0633	0.0647	0.0639	0.0763	0.0684	0.0685	0.0696	0.0726	0.0780	0.0791	0.0790	0.0847	0.0814	0.0769	0.0857
1.00	0.0466	0.0401	0.0454	0.0395	0.0514	0.0489	0.0393	0.0433	0.0509	0.0566	0.0544	0.0542	0.0630	0.0547	0.0505	0.0594
1.10	-0.0013	-0.0104	-0.0077	-0.0018	0.0014	-0.0051	-0.0023	0.0012	0.0038	0.0115	0.0084	0.0086	0.0183	0.0072	0.0076	0.0153
1.20	-0.0612	-0.0500	-0.0719	-0.0457	-0.0413	-0.0572	-0.0619	-0.0503	-0.0525	-0.0435	-0.0501	-0.0400	-0.0309	-0.0466	-0.0458	-0.0409

Table A.4: Pod series data in straight-ahead pusher configuration: propeller thrust coefficient, K_{TProp} .

J	Pod 01	Pod 02	Pod 03	Pod 04	Pod 05	Pod 06	Pod 07	Pod 08	Pod 09	Pod 10	Pod 11	Pod 12	Pod 13	Pod 14	Pod 15	Pod 16
0.00	0.4655	0.4681	0.4598	0.4638	0.4643	0.4564	0.4641	0.4715	0.4605	0.4712	0.4667	0.4576	0.4672	0.4601	0.4595	0.4660
0.10	0.4354	0.4408	0.4302	0.4356	0.4392	0.4267	0.4328	0.4429	0.4327	0.4445	0.4393	0.4322	0.4371	0.4335	0.4317	0.4390
0.20	0.4038	0.4019	0.3978	0.3975	0.4059	0.3924	0.3936	0.4116	0.3968	0.4119	0.4095	0.3960	0.4054	0.3949	0.3962	0.4029
0.30	0.3618	0.3667	0.3566	0.3616	0.3654	0.3571	0.3574	0.3733	0.3665	0.3692	0.3685	0.3609	0.3731	0.3586	0.3579	0.3632
0.40	0.3210	0.3283	0.3213	0.3264	0.3288	0.3213	0.3186	0.3271	0.3203	0.3347	0.3343	0.3200	0.3320	0.3239	0.3208	0.3334
0.50	0.2745	0.2838	0.2740	0.2855	0.2867	0.2728	0.2778	0.2871	0.2767	0.2914	0.2934	0.2741	0.2855	0.2842	0.2770	0.2877
0.60	0.2329	0.2415	0.2358	0.2416	0.2435	0.2297	0.2371	0.2438	0.2378	0.2481	0.2500	0.2357	0.2465	0.2393	0.2332	0.2478
0.65	0.2101	0.2223	0.2108	0.2216	0.2261	0.2073	0.2136	0.2198	0.2162	0.2302	0.2291	0.2135	0.2295	0.2168	0.2159	0.2276
0.70	0.1921	0.2012	0.1921	0.2006	0.2042	0.1923	0.1971	0.2018	0.1974	0.2103	0.2060	0.1960	0.2112	0.1956	0.1974	0.2102
0.75	0.1710	0.1801	0.1708	0.1786	0.1830	0.1695	0.1755	0.1833	0.1782	0.1909	0.1860	0.1740	0.1926	0.1741	0.1766	0.1892
0.80	0.1511	0.1587	0.1469	0.1600	0.1634	0.1497	0.1571	0.1600	0.1561	0.1695	0.1670	0.1549	0.1724	0.1523	0.1571	0.1660
0.85	0.1317	0.1405	0.1269	0.1413	0.1433	0.1261	0.1334	0.1431	0.1359	0.1487	0.1464	0.1330	0.1508	0.1339	0.1369	0.1481
0.90	0.1133	0.1211	0.1033	0.1171	0.1191	0.1039	0.1123	0.1191	0.1122	0.1275	0.1274	0.1088	0.1312	0.1108	0.1120	0.1244
0.95	0.0892	0.0979	0.0881	0.0973	0.1009	0.0845	0.0932	0.1003	0.0943	0.1083	0.1054	0.0887	0.1108	0.0924	0.0958	0.1089
1.00	0.0644	0.0773	0.0602	0.0754	0.0776	0.0626	0.0700	0.0773	0.0730	0.0887	0.0870	0.0682	0.0911	0.0701	0.0730	0.0883
1.10	0.0102	0.0284	0.0160	0.0299	0.0352	0.0151	0.0229	0.0304	0.0275	0.0429	0.0428	0.0228	0.0518	0.0226	0.0285	0.0440
1.20	-0.0412	-0.0225	-0.0351	-0.0192	-0.0163	-0.0296	-0.0246	-0.0205	-0.0186	-0.0019	-0.0086	-0.0106	0.0017	-0.0199	-0.0176	-0.0020

Data Tables

Table A.5: Pod series data in straight-ahead pusher configuration: propeller torque coefficient, $10K_Q$.

J	Pod 01	Pod 02	Pod 03	Pod 04	Pod 05	Pod 06	Pod 07	Pod 08	Pod 09	Pod 10	Pod 11	Pod 12	Pod 13	Pod 14	Pod 15	Pod 16
0.00	0.6571	0.6552	0.6579	0.6818	0.6852	0.6588	0.6609	0.6832	0.6585	0.6790	0.6834	0.6578	0.6828	0.6656	0.6532	0.6740
0.10	0.6188	0.6349	0.6268	0.6311	0.6314	0.6220	0.6240	0.6421	0.6324	0.6421	0.6343	0.6243	0.6322	0.6373	0.6269	0.6316
0.20	0.5789	0.5925	0.5871	0.5853	0.5956	0.5812	0.5808	0.6048	0.5891	0.6054	0.5956	0.5834	0.5964	0.5903	0.5872	0.5981
0.30	0.5311	0.5380	0.5424	0.5420	0.5445	0.5361	0.5344	0.5619	0.5509	0.5568	0.5470	0.5383	0.5550	0.5494	0.5407	0.5528
0.40	0.4828	0.4978	0.4920	0.5071	0.4996	0.4981	0.4836	0.5072	0.4927	0.5168	0.5064	0.4941	0.5044	0.4931	0.4890	0.5077
0.50	0.4304	0.4487	0.4360	0.4570	0.4507	0.4342	0.4441	0.4612	0.4386	0.4581	0.4619	0.4319	0.4543	0.4494	0.4377	0.4611
0.60	0.3775	0.4014	0.3847	0.4013	0.3965	0.3832	0.3906	0.4139	0.3967	0.4089	0.4098	0.3837	0.4078	0.3903	0.3838	0.4071
0.65	0.3501	0.3734	0.3559	0.3740	0.3738	0.3490	0.3600	0.3823	0.3658	0.3911	0.3844	0.3573	0.3879	0.3649	0.3603	0.3882
0.70	0.3267	0.3468	0.3324	0.3512	0.3428	0.3292	0.3397	0.3537	0.3403	0.3656	0.3556	0.3329	0.3636	0.3356	0.3363	0.3650
0.75	0.2989	0.3188	0.3075	0.3232	0.3227	0.2988	0.3093	0.3319	0.3161	0.3380	0.3274	0.3073	0.3406	0.3067	0.3109	0.3355
0.80	0.2750	0.2949	0.2806	0.2984	0.3000	0.2765	0.2869	0.3027	0.2860	0.3094	0.2990	0.2856	0.3122	0.2806	0.2808	0.3099
0.85	0.2509	0.2647	0.2524	0.2731	0.2722	0.2487	0.2572	0.2851	0.2593	0.2850	0.2730	0.2627	0.2887	0.2566	0.2580	0.2908
0.90	0.2261	0.2408	0.2154	0.2451	0.2384	0.2189	0.2307	0.2504	0.2318	0.2577	0.2463	0.2338	0.2620	0.2285	0.2293	0.2626
0.95	0.1968	0.2106	0.1926	0.2247	0.2138	0.1896	0.2017	0.2292	0.2108	0.2300	0.2252	0.2106	0.2353	0.2042	0.2073	0.2349
1.00	0.1621	0.1752	0.1619	0.1933	0.1872	0.1574	0.1661	0.2002	0.1823	0.2055	0.2008	0.1869	0.2120	0.1736	0.1716	0.2084
1.10	0.0833	0.1189	0.1034	0.1295	0.1215	0.0935	0.1054	0.1352	0.1142	0.1441	0.1462	0.1224	0.1539	0.1108	0.1139	0.1566
1.20	-0.0097	0.0400	0.0149	0.0406	0.0478	0.0145	0.0213	0.0344	0.0379	0.0819	0.0731	0.0505	0.0887	0.0404	0.0391	0.0786

Table A.6: Pod series data in straight-ahead pusher configuration: propulsor (unit) thrust coefficient, K_{TUnit} .

J	Pod 01	Pod 02	Pod 03	Pod 04	Pod 05	Pod 06	Pod 07	Pod 08	Pod 09	Pod 10	Pod 11	Pod 12	Pod 13	Pod 14	Pod 15	Pod 16
0.00	0.4403	0.4505	0.4583	0.4524	0.4502	0.4607	0.4617	0.4623	0.4582	0.4448	0.4537	0.4610	0.4497	0.4475	0.4560	0.4517
0.10	0.4031	0.4186	0.4238	0.4211	0.4213	0.4236	0.4260	0.4319	0.4262	0.4184	0.4176	0.4282	0.4114	0.4189	0.4203	0.4190
0.20	0.3725	0.3823	0.3912	0.3783	0.3859	0.3874	0.3883	0.3951	0.3856	0.3842	0.3801	0.3852	0.3737	0.3855	0.3829	0.3754
0.30	0.3347	0.3424	0.3494	0.3437	0.3396	0.3484	0.3463	0.3562	0.3444	0.3398	0.3381	0.3486	0.3422	0.3437	0.3424	0.3432
0.40	0.2953	0.3009	0.3058	0.3020	0.2987	0.3107	0.3050	0.3066	0.3004	0.2922	0.2989	0.3019	0.2964	0.3045	0.2999	0.3011
0.50	0.2553	0.2570	0.2592	0.2564	0.2521	0.2610	0.2651	0.2660	0.2605	0.2505	0.2541	0.2567	0.2478	0.2555	0.2520	0.2544
0.60	0.2134	0.2121	0.2181	0.2169	0.2090	0.2163	0.2255	0.2188	0.2140	0.2060	0.2127	0.2108	0.2036	0.2101	0.2101	0.2097
0.65	0.1924	0.1902	0.1940	0.1901	0.1887	0.1866	0.2041	0.2014	0.1875	0.1859	0.1915	0.1897	0.1864	0.1831	0.1836	0.1893
0.70	0.1712	0.1696	0.1687	0.1715	0.1702	0.1648	0.1844	0.1783	0.1682	0.1687	0.1714	0.1692	0.1672	0.1660	0.1644	0.1739
0.75	0.1489	0.1456	0.1505	0.1479	0.1449	0.1420	0.1635	0.1568	0.1469	0.1441	0.1493	0.1452	0.1420	0.1470	0.1407	0.1533
0.80	0.1328	0.1228	0.1241	0.1262	0.1257	0.1256	0.1429	0.1337	0.1250	0.1255	0.1297	0.1277	0.1261	0.1221	0.1214	0.1290
0.85	0.1136	0.1034	0.1077	0.1077	0.1039	0.0979	0.1203	0.1182	0.1069	0.1044	0.1102	0.1029	0.1031	0.1009	0.1022	0.1076
0.90	0.1011	0.0814	0.0830	0.0806	0.0778	0.0772	0.0881	0.0904	0.0808	0.0779	0.0909	0.0783	0.0804	0.0792	0.0690	0.0821
0.95	0.0714	0.0524	0.0584	0.0617	0.0583	0.0520	0.0652	0.0711	0.0588	0.0623	0.0666	0.0556	0.0582	0.0526	0.0511	0.0614
1.00	0.0423	0.0297	0.0255	0.0336	0.0377	0.0307	0.0421	0.0434	0.0327	0.0409	0.0446	0.0316	0.0416	0.0253	0.0312	0.0344
1.10	-0.0085	-0.0240	-0.0264	-0.0186	-0.0206	-0.0333	-0.0082	-0.0045	-0.0098	-0.0073	-0.0091	-0.0051	-0.0014	-0.0177	-0.0228	-0.0088
1.20	-0.0827	-0.0760	-0.0875	-0.0726	-0.0803	-0.0916	-0.0753	-0.0514	-0.0506	-0.0583	-0.0662	-0.0439	-0.0430	-0.0763	-0.0742	-0.0746

Data Tables

Table A.7: Performance coefficient of average pod 01 at azimuthing conditions and in puller configuration: propeller thrust coefficient, K_{TProp} .

J	-30°	-20°	-15°	-10°	-5°	0°	5°	10°	15°	20°	30°
0.00	0.4947	0.4933	0.5021	0.4991	0.4982	0.4921	0.4987	0.5015	0.5020	0.5042	0.5024
0.10	0.4749	0.4713	0.4636	0.4666	0.4653	0.4649	0.4638	0.4667	0.4699	0.4704	0.4674
0.20	0.4421	0.4323	0.4273	0.4296	0.4255	0.4247	0.4255	0.4291	0.4311	0.4386	0.4395
0.30	0.4148	0.3991	0.3891	0.3905	0.3860	0.3879	0.3862	0.3925	0.3937	0.4020	0.4053
0.40	0.3794	0.3582	0.3484	0.3459	0.3443	0.3438	0.3421	0.3488	0.3488	0.3499	0.3722
0.50	0.3462	0.3176	0.3043	0.3036	0.2966	0.3011	0.2916	0.3052	0.3089	0.3165	0.3449
0.60	0.3068	0.2760	0.2556	0.2591	0.2543	0.2525	0.2467	0.2603	0.2637	0.2776	0.3065
0.65	0.2953	0.2576	0.2397	0.2357	0.2265	0.2284	0.2280	0.2337	0.2450	0.2598	0.2886
0.70	0.2774	0.2403	0.2191	0.2130	0.2098	0.2090	0.2065	0.2136	0.2203	0.2326	0.2754
0.75	0.2669	0.2168	0.2000	0.1939	0.1859	0.1847	0.1838	0.1984	0.2087	0.2154	0.2608
0.80	0.2451	0.1973	0.1743	0.1737	0.1632	0.1584	0.1590	0.1739	0.1887	0.1911	0.2445
0.85	0.2347	0.1778	0.1553	0.1489	0.1400	0.1381	0.1390	0.1511	0.1601	0.1763	0.2325
0.90	0.2157	0.1594	0.1343	0.1296	0.1191	0.1183	0.1151	0.1220	0.1421	0.1575	0.2181
0.95	0.1988	0.1421	0.1121	0.1054	0.0983	0.0976	0.0924	0.1046	0.1195	0.1394	0.2013
1.00	0.1809	0.1162	0.0915	0.0806	0.0766	0.0702	0.0678	0.0817	0.0962	0.1132	0.1861
1.10	0.1508	0.0762	0.0419	0.0334	0.0291	0.0258	0.0246	0.0354	0.0539	0.0702	0.1569
1.20	0.1175	0.0330	-0.0058	-0.0138	-0.0153	-0.0364	-0.0276	-0.0190	0.0121	0.0244	0.1221

Table A.8: Performance coefficient of average pod 01 at azimuthing conditions and in puller configuration: propeller torque coefficient, $10K_Q$.

J	-30°	-20°	-15°	-10°	-5°	0°	5°	10°	15°	20°	30°
0.00	0.6800	0.6711	0.6798	0.6789	0.6817	0.6680	0.6797	0.6737	0.6752	0.6729	0.6784
0.10	0.6516	0.6444	0.6513	0.6485	0.6537	0.6393	0.6456	0.6377	0.6439	0.6488	0.6517
0.20	0.6166	0.6086	0.6087	0.6065	0.6129	0.6019	0.6046	0.6036	0.6118	0.6129	0.6228
0.30	0.5877	0.5682	0.5679	0.5657	0.5679	0.5707	0.5607	0.5636	0.5703	0.5724	0.5901
0.40	0.5493	0.5271	0.5138	0.5138	0.5178	0.5223	0.5079	0.5094	0.5212	0.5281	0.5544
0.50	0.5116	0.4890	0.4757	0.4631	0.4657	0.4701	0.4534	0.4637	0.4738	0.4858	0.5207
0.60	0.4729	0.4389	0.4232	0.4104	0.4186	0.4184	0.4026	0.4092	0.4264	0.4350	0.4795
0.65	0.4593	0.4131	0.3958	0.3883	0.3844	0.3839	0.3746	0.3869	0.3995	0.4126	0.4601
0.70	0.4357	0.3865	0.3726	0.3562	0.3502	0.3504	0.3539	0.3594	0.3787	0.3795	0.4375
0.75	0.4162	0.3664	0.3484	0.3362	0.3228	0.3209	0.3210	0.3469	0.3534	0.3643	0.4231
0.80	0.3971	0.3382	0.3154	0.3061	0.2926	0.2934	0.3005	0.3091	0.3232	0.3407	0.4033
0.85	0.3784	0.3102	0.2890	0.2800	0.2746	0.2700	0.2720	0.2811	0.2987	0.3165	0.3820
0.90	0.3592	0.2838	0.2601	0.2546	0.2363	0.2249	0.2291	0.2462	0.2681	0.2888	0.3733
0.95	0.3351	0.2563	0.2367	0.2171	0.2093	0.1997	0.2081	0.2251	0.2429	0.2580	0.3499
1.00	0.3120	0.2265	0.2000	0.1865	0.1807	0.1702	0.1682	0.1838	0.2110	0.2297	0.3242
1.10	0.2746	0.1691	0.1183	0.1079	0.1011	0.0914	0.0948	0.1167	0.1462	0.1670	0.2860
1.20	0.2211	0.1009	0.0422	0.0303	0.0323	-0.0051	0.0032	0.0249	0.0608	0.0903	0.2338

Data Tables

Table A.9: Performance coefficient of average pod 01 at azimuthing conditions and in puller configuration: propulsor (unit) thrust coefficient, K_{TUnit} .

J	-30°	-20°	-15°	-10°	-5°	0°	5°	10°	15°	20°	30°
0.00	0.4241	0.4554	0.4581	0.4733	0.4713	0.4843	0.4910	0.4690	0.4642	0.4609	0.4178
0.10	0.3773	0.4176	0.4198	0.4449	0.4307	0.4511	0.4537	0.4344	0.4274	0.4205	0.3871
0.20	0.3224	0.3725	0.3809	0.4093	0.3902	0.4095	0.4176	0.3998	0.3888	0.3895	0.3451
0.30	0.2610	0.3181	0.3387	0.3594	0.3512	0.3714	0.3758	0.3624	0.3483	0.3499	0.2995
0.40	0.1913	0.2628	0.2910	0.3223	0.2987	0.3291	0.3309	0.3054	0.3080	0.3017	0.2441
0.50	0.1204	0.2061	0.2354	0.2700	0.2453	0.2816	0.2804	0.2666	0.2661	0.2525	0.1817
0.60	0.0489	0.1460	0.1756	0.2176	0.2050	0.2333	0.2298	0.2164	0.2140	0.1987	0.1194
0.65	0.0205	0.1184	0.1455	0.1870	0.1736	0.2087	0.2048	0.1947	0.1883	0.1723	0.0891
0.70	-0.0126	0.0855	0.1228	0.1532	0.1504	0.1891	0.1776	0.1719	0.1687	0.1440	0.0602
0.75	-0.0510	0.0523	0.0883	0.1242	0.1164	0.1631	0.1491	0.1437	0.1430	0.1154	0.0251
0.80	-0.0835	0.0198	0.0535	0.0974	0.0919	0.1347	0.1252	0.1233	0.1131	0.0914	-0.0114
0.85	-0.1229	-0.0115	0.0175	0.0664	0.0576	0.1090	0.0948	0.0830	0.0819	0.0588	-0.0428
0.90	-0.1532	-0.0385	-0.0178	0.0372	0.0273	0.0857	0.0611	0.0693	0.0547	0.0361	-0.0928
0.95	-0.1855	-0.0837	-0.0442	0.0043	0.0045	0.0619	0.0467	0.0357	0.0258	0.0091	-0.1271
1.00	-0.2215	-0.1193	-0.0818	-0.0368	-0.0324	0.0275	0.0053	0.0169	-0.0090	-0.0183	-0.1708
1.10	-0.2921	-0.1918	-0.1719	-0.1099	-0.1115	-0.0416	-0.0568	-0.0492	-0.0775	-0.0904	-0.2427
1.20	-0.3849	-0.2729	-0.2551	-0.2015	-0.1862	-0.1191	-0.1377	-0.1252	-0.1433	-0.1618	-0.3157

Table A.10: Performance coefficient of average pod 01 at azimuthing conditions and in puller configuration: propulsor (unit) transverse force coefficient, K_{FY} .

J	-30°	-20°	-15°	-10°	-5°	0°	5°	10°	15°	20°	30°
0.00	0.2295	0.1643	0.1154	0.0854	0.0301	-0.0160	-0.0495	-0.0806	-0.1130	-0.1495	-0.1894
0.10	0.2553	0.1822	0.1249	0.0855	0.0344	-0.0177	-0.0506	-0.1029	-0.1274	-0.1713	-0.2311
0.20	0.2768	0.1923	0.1333	0.0930	0.0377	-0.0214	-0.0629	-0.1151	-0.1480	-0.1949	-0.2609
0.30	0.2973	0.2038	0.1461	0.1005	0.0379	-0.0244	-0.0725	-0.1232	-0.1713	-0.2285	-0.3065
0.40	0.3265	0.2113	0.1551	0.1133	0.0404	-0.0259	-0.0861	-0.1342	-0.1956	-0.2638	-0.3366
0.50	0.3644	0.2405	0.1652	0.1185	0.0458	-0.0297	-0.0998	-0.1434	-0.2170	-0.2795	-0.3672
0.60	0.3998	0.2478	0.1739	0.1271	0.0525	-0.0283	-0.1006	-0.1529	-0.2369	-0.3166	-0.3993
0.65	0.4252	0.2733	0.1808	0.1349	0.0535	-0.0266	-0.1041	-0.1559	-0.2568	-0.3443	-0.4183
0.70	0.4499	0.2783	0.1867	0.1384	0.0546	-0.0226	-0.1124	-0.1669	-0.2630	-0.3579	-0.4375
0.75	0.4681	0.3120	0.1981	0.1389	0.0564	-0.0162	-0.1124	-0.1779	-0.2740	-0.3750	-0.4519
0.80	0.4841	0.3204	0.2036	0.1413	0.0605	-0.0214	-0.1167	-0.1884	-0.2850	-0.3910	-0.4714
0.85	0.5003	0.3261	0.2096	0.1471	0.0624	-0.0175	-0.1039	-0.1977	-0.3018	-0.4085	-0.4869
0.90	0.5255	0.3541	0.2205	0.1576	0.0683	-0.0279	-0.1048	-0.2058	-0.3172	-0.4307	-0.5015
0.95	0.5346	0.3633	0.2313	0.1689	0.0721	-0.0216	-0.1100	-0.2162	-0.3311	-0.4333	-0.5115
1.00	0.5437	0.3861	0.2462	0.1765	0.0783	-0.0232	-0.1053	-0.2252	-0.3535	-0.4480	-0.5245
1.10	0.5537	0.4121	0.2815	0.1943	0.0852	-0.0211	-0.1148	-0.2450	-0.3698	-0.4700	-0.5230
1.20	0.5616	0.4293	0.3188	0.2188	0.0979	-0.0135	-0.1244	-0.2672	-0.3828	-0.4974	-0.5321

Data Tables

Table A.11: Performance coefficient of average pod 01 at azimuthing conditions and in puller configuration: propulsor (unit) vertical force coefficient, K_{FZ} .

J	-30°	-20°	-15°	-10°	-5°	0°	5°	10°	15°	20°	30°
0.00	-0.0065	-0.0042	-0.0043	0.0067	-0.0031	-0.0023	-0.0023	0.0036	0.0023	0.0078	-0.0001
0.10	-0.0223	-0.0303	-0.0090	0.0100	0.0028	0.0034	0.0281	0.0204	0.0252	0.0347	0.0356
0.20	-0.0389	-0.0460	-0.0124	0.0175	0.0085	0.0136	0.0431	0.0419	0.0554	0.0556	0.0630
0.30	-0.0577	-0.0644	-0.0173	0.0212	0.0087	0.0318	0.0612	0.0598	0.0837	0.0851	0.0928
0.40	-0.0754	-0.0729	-0.0203	0.0247	0.0142	0.0380	0.0694	0.0772	0.1114	0.1185	0.1246
0.50	-0.0758	-0.0774	-0.0186	0.0326	0.0235	0.0493	0.0833	0.1079	0.1421	0.1495	0.1566
0.60	-0.0830	-0.0821	-0.0214	0.0300	0.0262	0.0594	0.0943	0.1292	0.1727	0.1814	0.1874
0.65	-0.0842	-0.0855	-0.0255	0.0312	0.0272	0.0623	0.0995	0.1348	0.1800	0.2001	0.2107
0.70	-0.0877	-0.0888	-0.0279	0.0272	0.0282	0.0658	0.1078	0.1515	0.1903	0.2185	0.2335
0.75	-0.0852	-0.0916	-0.0255	0.0303	0.0306	0.0730	0.1144	0.1550	0.1986	0.2296	0.2455
0.80	-0.0884	-0.0897	-0.0194	0.0316	0.0341	0.0819	0.1219	0.1770	0.2126	0.2433	0.2512
0.85	-0.0896	-0.0915	-0.0173	0.0349	0.0361	0.0837	0.1295	0.1778	0.2118	0.2483	0.2546
0.90	-0.0824	-0.0849	-0.0178	0.0359	0.0376	0.0787	0.1210	0.1705	0.2163	0.2388	0.2576
0.95	-0.0793	-0.0737	-0.0139	0.0355	0.0412	0.0709	0.1231	0.1699	0.2135	0.2451	0.2651
1.00	-0.0605	-0.0700	-0.0078	0.0370	0.0395	0.0666	0.1161	0.1626	0.2064	0.2343	0.2655
1.10	-0.0156	-0.0474	-0.0011	0.0441	0.0381	0.0506	0.1042	0.1476	0.1984	0.2353	0.2691
1.20	0.0385	-0.0059	0.0165	0.0473	0.0402	0.0270	0.0907	0.1278	0.1906	0.2275	0.2791

Table A.12: Performance coefficient of average pod 01 at azimuthing conditions and in puller configuration: propulsor (unit) axial moment coefficient, K_{MX} .

J	-30°	-20°	-15°	-10°	-5°	0°	5°	10°	15°	20°	30°
0.00	-1.7018	-1.0442	-0.7354	-0.4948	-0.4062	0.1313	0.3598	0.7546	0.8227	1.4903	1.9050
0.10	-2.0053	-1.2931	-0.8558	-0.6151	-0.4660	0.1349	0.4022	0.8514	0.9730	1.5736	2.1932
0.20	-2.1425	-1.3500	-0.9073	-0.6052	-0.4830	0.1388	0.4747	0.9465	1.0750	1.6933	2.3508
0.30	-2.3608	-1.4788	-0.9856	-0.6394	-0.4971	0.1408	0.5373	1.0549	1.2556	1.9091	2.6027
0.40	-2.5198	-1.5891	-1.0244	-0.6789	-0.4976	0.1480	0.5853	1.1867	1.4274	2.1305	2.8265
0.50	-2.7208	-1.7008	-1.0861	-0.6842	-0.4862	0.1424	0.6378	1.2315	1.6057	2.3780	3.1344
0.60	-2.8220	-1.7594	-1.1211	-0.7088	-0.5250	0.1368	0.6793	1.3457	1.7454	2.5665	3.2911
0.65	-2.9153	-1.8852	-1.2314	-0.7604	-0.5467	0.1327	0.6802	1.4019	1.8256	2.6615	3.3625
0.70	-2.9756	-1.9491	-1.2584	-0.8018	-0.5702	0.1305	0.6721	1.4360	1.9017	2.7354	3.4221
0.75	-2.9801	-2.0704	-1.3445	-0.8504	-0.6392	0.1288	0.6864	1.4978	2.0122	2.8555	3.4898
0.80	-3.1106	-2.1950	-1.4747	-0.8969	-0.6825	0.1251	0.6627	1.5654	2.1127	2.9402	3.5146
0.85	-3.1451	-2.2522	-1.6415	-1.0023	-0.7378	0.1199	0.6569	1.6186	2.1797	3.0358	3.5493
0.90	-3.1473	-2.3493	-1.7620	-1.1755	-0.8561	0.1121	0.6747	1.6849	2.2401	3.1196	3.6361
0.95	-3.2262	-2.4513	-1.9326	-1.3215	-0.9536	0.1079	0.6516	1.7597	2.2941	3.1738	3.6923
1.00	-3.3429	-2.5506	-2.0685	-1.3719	-1.1474	0.1019	0.6587	1.8412	2.3808	3.2686	3.7626
1.10	-3.4938	-2.9082	-2.5324	-1.6654	-1.4184	0.0967	0.6976	1.9668	2.5027	3.4038	3.8703
1.20	-3.6369	-3.2669	-2.8702	-1.8810	-1.6709	-0.0025	0.6743	2.0345	2.6098	3.5402	4.0185

Data Tables

Table A.13: Performance coefficient of average pod 01 at azimuthing conditions and in puller configuration: propulsor (unit) transverse moment coefficient, K_{MY} .

<i>J</i>	-30°	-20°	-15°	-10°	-5°	0°	5°	10°	15°	20°	30°
0.00	2.9641	3.3365	3.4910	3.5034	3.5132	3.5602	3.5027	3.4974	3.4387	3.4093	3.2458
0.10	2.6291	2.9089	3.0885	3.1271	3.1852	3.2327	3.2807	3.2491	3.1577	3.1380	2.8821
0.20	2.2557	2.5980	2.8261	2.8921	2.9177	2.9884	3.0606	3.0415	2.9335	2.9170	2.6516
0.30	1.8340	2.2295	2.4954	2.5788	2.5820	2.7076	2.7820	2.8093	2.6775	2.6620	2.3461
0.40	1.3497	1.8699	2.0979	2.2253	2.2595	2.3892	2.4461	2.4397	2.3685	2.3083	2.0223
0.50	0.9512	1.4671	1.7402	1.8737	1.9420	2.0603	2.1152	2.1587	2.0482	2.0171	1.6411
0.60	0.4746	1.0664	1.3314	1.5008	1.5366	1.6976	1.7790	1.8319	1.7281	1.6928	1.2200
0.65	0.2825	0.9320	1.1555	1.2904	1.3649	1.5383	1.6083	1.6723	1.5742	1.5117	1.0268
0.70	0.0577	0.6987	0.9552	1.1023	1.1796	1.3695	1.4233	1.4519	1.3818	1.3153	0.8413
0.75	-0.1538	0.4870	0.7764	0.9148	0.9682	1.2046	1.2484	1.3075	1.2589	1.1334	0.6181
0.80	-0.3797	0.2712	0.5366	0.7289	0.7879	0.9780	1.0365	1.1135	1.0641	0.9386	0.3910
0.85	-0.6400	0.0640	0.3217	0.5236	0.5758	0.7941	0.9031	0.9295	0.8571	0.7970	0.1506
0.90	-0.7684	-0.1243	0.1314	0.3361	0.3943	0.6089	0.6805	0.7345	0.6822	0.6440	-0.1213
0.95	-1.0661	-0.3848	-0.0997	0.1162	0.2015	0.4354	0.5184	0.5485	0.4738	0.4251	-0.3863
1.00	-1.2346	-0.5993	-0.3359	-0.1293	-0.0195	0.2270	0.2908	0.3595	0.2309	0.2299	-0.5682
1.10	-1.6401	-1.0805	-0.8721	-0.6078	-0.4991	-0.2163	-0.1212	-0.1123	-0.1858	-0.1784	-1.0311
1.20	-2.2680	-1.5888	-1.3660	-1.1244	-1.0861	-0.7261	-0.6734	-0.6557	-0.6324	-0.6498	-1.5468

Table A.14: Performance coefficient of average pod 01 at azimuthing conditions and in puller configuration: propulsor (unit) steering moment coefficient, K_{MZ} .

<i>J</i>	-30°	-20°	-15°	-10°	-5°	0°	5°	10°	15°	20°	30°
0.00	-0.0192	-0.0280	-0.0229	-0.0164	-0.0154	-0.0164	-0.0015	-0.0095	-0.0106	-0.0029	-0.0184
0.10	-0.0085	-0.0023	-0.0083	-0.0031	-0.0100	-0.0170	-0.0037	-0.0131	-0.0241	-0.0266	-0.0333
0.20	0.0193	0.0151	0.0052	0.0071	-0.0043	-0.0121	-0.0089	-0.0223	-0.0294	-0.0375	-0.0498
0.30	0.0465	0.0365	0.0215	0.0181	0.0053	-0.0091	-0.0137	-0.0308	-0.0388	-0.0588	-0.0719
0.40	0.0726	0.0595	0.0447	0.0333	0.0028	-0.0117	-0.0223	-0.0364	-0.0494	-0.0706	-0.0901
0.50	0.0966	0.0811	0.0605	0.0383	0.0091	-0.0081	-0.0252	-0.0471	-0.0617	-0.0859	-0.1144
0.60	0.1177	0.0961	0.0728	0.0494	0.0129	-0.0056	-0.0315	-0.0543	-0.0752	-0.0974	-0.1314
0.65	0.1338	0.1073	0.0749	0.0559	0.0159	-0.0085	-0.0364	-0.0610	-0.0820	-0.0927	-0.1434
0.70	0.1374	0.1129	0.0850	0.0621	0.0214	-0.0090	-0.0374	-0.0636	-0.0895	-0.1070	-0.1493
0.75	0.1593	0.1192	0.0885	0.0670	0.0269	-0.0119	-0.0431	-0.0628	-0.0963	-0.0995	-0.1593
0.80	0.1715	0.1273	0.0986	0.0707	0.0315	-0.0158	-0.0456	-0.0633	-0.1020	-0.1106	-0.1773
0.85	0.1804	0.1337	0.1034	0.0731	0.0341	-0.0165	-0.0488	-0.0702	-0.1064	-0.1130	-0.1948
0.90	0.1986	0.1468	0.1073	0.0786	0.0338	-0.0184	-0.0509	-0.0795	-0.1141	-0.1296	-0.2057
0.95	0.2105	0.1606	0.1177	0.0831	0.0379	-0.0183	-0.0542	-0.0848	-0.1260	-0.1456	-0.2248
1.00	0.2324	0.1700	0.1223	0.0864	0.0401	-0.0175	-0.0548	-0.0876	-0.1307	-0.1496	-0.2366
1.10	0.2617	0.1818	0.1314	0.0884	0.0420	-0.0181	-0.0631	-0.0928	-0.1363	-0.1732	-0.2581
1.20	0.3161	0.2041	0.1486	0.0943	0.0424	-0.0235	-0.0672	-0.1059	-0.1462	-0.1916	-0.2921

Data Tables

Table A.15: Performance coefficient of average pod 01 at azimuthing conditions and in pusher configuration: propeller thrust coefficient, K_{TProp} .

<i>J</i>	-30°	-20°	-15°	-10°	-5°	0°	5°	10°	15°	20°	30°
0.00	0.4640	0.4621	0.4550	0.4692	0.4583	0.4609	0.4583	0.4867	0.4706	0.4762	0.4892
0.10	0.4047	0.4132	0.4103	0.4209	0.4172	0.4310	0.4371	0.4557	0.4468	0.4514	0.4756
0.20	0.3611	0.3731	0.3679	0.3805	0.3772	0.3938	0.4078	0.4163	0.4211	0.4287	0.4544
0.30	0.3074	0.3201	0.3226	0.3339	0.3364	0.3512	0.3708	0.3792	0.3888	0.4053	0.4376
0.40	0.2547	0.2669	0.2765	0.2839	0.2889	0.3089	0.3330	0.3461	0.3528	0.3843	0.4272
0.50	0.2093	0.2221	0.2281	0.2383	0.2520	0.2660	0.2906	0.3090	0.3175	0.3557	0.3970
0.60	0.1681	0.1794	0.1858	0.1978	0.2121	0.2342	0.2560	0.2746	0.2857	0.3115	0.3716
0.65	0.1458	0.1619	0.1655	0.1776	0.1916	0.2159	0.2405	0.2559	0.2680	0.2917	0.3563
0.70	0.1276	0.1379	0.1483	0.1593	0.1674	0.1940	0.2185	0.2356	0.2456	0.2723	0.3388
0.75	0.1085	0.1177	0.1294	0.1413	0.1462	0.1720	0.1997	0.2162	0.2270	0.2535	0.3323
0.80	0.0966	0.1029	0.1087	0.1165	0.1279	0.1513	0.1773	0.1979	0.2088	0.2306	0.3151
0.85	0.0762	0.0819	0.0929	0.0956	0.1057	0.1310	0.1557	0.1794	0.1878	0.2130	0.2902
0.90	0.0589	0.0659	0.0715	0.0746	0.0863	0.1086	0.1374	0.1597	0.1704	0.1913	0.2768
0.95	0.0369	0.0500	0.0532	0.0514	0.0621	0.0876	0.1132	0.1400	0.1516	0.1791	0.2600
1.00	0.0235	0.0263	0.0335	0.0293	0.0427	0.0662	0.0925	0.1132	0.1296	0.1543	0.2393
1.10	-0.0190	-0.0208	-0.0124	-0.0133	-0.0065	0.0201	0.0494	0.0700	0.0818	0.1191	0.1817
1.20	-0.0746	-0.0659	-0.0640	-0.0684	-0.0587	-0.0373	0.0013	0.0193	0.0409	0.0690	0.1192

Table A.16: Performance coefficient of average pod 01 at azimuthing conditions and in pusher configuration: propeller torque coefficient, $10K_Q$.

<i>J</i>	-30°	-20°	-15°	-10°	-5°	0°	5°	10°	15°	20°	30°
0.00	0.6607	0.6519	0.6494	0.6644	0.6452	0.6512	0.6431	0.6724	0.6771	0.6729	0.6785
0.10	0.5940	0.5919	0.5985	0.6027	0.6041	0.6153	0.6371	0.6271	0.6401	0.6370	0.6545
0.20	0.5430	0.5501	0.5474	0.5541	0.5546	0.5678	0.5969	0.5913	0.6067	0.6037	0.6271
0.30	0.4790	0.4892	0.4910	0.4986	0.5018	0.5139	0.5523	0.5424	0.5594	0.5697	0.5973
0.40	0.4188	0.4257	0.4364	0.4388	0.4449	0.4637	0.4926	0.4989	0.5196	0.5398	0.5679
0.50	0.3640	0.3685	0.3812	0.3857	0.3974	0.4096	0.4379	0.4563	0.4741	0.5011	0.5327
0.60	0.3079	0.3146	0.3263	0.3297	0.3492	0.3738	0.4004	0.4146	0.4322	0.4534	0.4886
0.65	0.2801	0.2879	0.3010	0.3048	0.3229	0.3433	0.3742	0.3876	0.4082	0.4289	0.4642
0.70	0.2493	0.2607	0.2745	0.2829	0.2945	0.3196	0.3505	0.3651	0.3848	0.4043	0.4376
0.75	0.2191	0.2331	0.2479	0.2570	0.2659	0.2932	0.3270	0.3403	0.3649	0.3839	0.4180
0.80	0.1993	0.2069	0.2189	0.2291	0.2393	0.2671	0.2978	0.3200	0.3360	0.3563	0.4044
0.85	0.1712	0.1819	0.1969	0.1977	0.2067	0.2424	0.2778	0.2984	0.3146	0.3392	0.3758
0.90	0.1410	0.1551	0.1715	0.1704	0.1816	0.2142	0.2572	0.2717	0.2959	0.3125	0.3518
0.95	0.1057	0.1305	0.1403	0.1364	0.1497	0.1847	0.2256	0.2511	0.2718	0.2943	0.3339
1.00	0.0817	0.1007	0.1109	0.1054	0.1191	0.1543	0.1994	0.2165	0.2441	0.2667	0.3136
1.10	0.0084	0.0183	0.0421	0.0384	0.0530	0.0849	0.1394	0.1571	0.1924	0.2119	0.2725
1.20	-0.0828	-0.0437	-0.0375	-0.0459	-0.0279	0.0102	0.0741	0.0885	0.1304	0.1606	0.2204

Data Tables

Table A.17: Performance coefficient of average pod 01 at azimuthing conditions and in pusher configuration: propulsor (unit) thrust coefficient, K_{TUnit} .

J	-30°	-20°	-15°	-10°	-5°	0°	5°	10°	15°	20°	30°
0.00	0.3897	0.4117	0.4245	0.4398	0.4461	0.4516	0.4454	0.4542	0.4423	0.4154	0.3873
0.10	0.3326	0.3669	0.3800	0.3956	0.4042	0.4157	0.4141	0.4155	0.4106	0.3846	0.3394
0.20	0.2812	0.3154	0.3331	0.3490	0.3592	0.3780	0.3778	0.3765	0.3734	0.3498	0.2922
0.30	0.2267	0.2657	0.2866	0.2976	0.3141	0.3309	0.3350	0.3332	0.3336	0.3153	0.2451
0.40	0.1660	0.2129	0.2416	0.2522	0.2694	0.2853	0.2930	0.2893	0.2875	0.2737	0.1957
0.50	0.0971	0.1700	0.1903	0.2021	0.2281	0.2432	0.2448	0.2431	0.2415	0.2290	0.1494
0.60	0.0201	0.1163	0.1418	0.1570	0.1830	0.1948	0.2048	0.2032	0.2005	0.1836	0.0894
0.65	-0.0179	0.0840	0.1126	0.1343	0.1576	0.1708	0.1791	0.1781	0.1758	0.1506	0.0555
0.70	-0.0516	0.0572	0.0905	0.1145	0.1320	0.1494	0.1581	0.1570	0.1554	0.1310	0.0218
0.75	-0.0843	0.0305	0.0682	0.0902	0.1081	0.1333	0.1339	0.1357	0.1362	0.1048	-0.0078
0.80	-0.1221	0.0009	0.0405	0.0594	0.0818	0.1084	0.1160	0.1167	0.1129	0.0800	-0.0481
0.85	-0.1545	-0.0220	0.0181	0.0372	0.0537	0.0858	0.0937	0.0894	0.0876	0.0570	-0.0862
0.90	-0.2017	-0.0511	-0.0151	0.0067	0.0294	0.0661	0.0694	0.0651	0.0641	0.0312	-0.1282
0.95	-0.2432	-0.0848	-0.0418	-0.0237	-0.0022	0.0392	0.0441	0.0414	0.0425	0.0081	-0.1612
1.00	-0.2780	-0.1193	-0.0775	-0.0571	-0.0320	0.0192	0.0243	0.0109	0.0137	-0.0243	-0.1995
1.10	-0.3667	-0.2045	-0.1551	-0.1201	-0.0912	-0.0396	-0.0312	-0.0408	-0.0395	-0.0916	-0.2929
1.20	-0.4504	-0.2836	-0.2290	-0.1979	-0.1634	-0.1001	-0.0856	-0.0966	-0.0910	-0.1489	-0.4161

Table A.18: Performance coefficient of average pod 01 at azimuthing conditions and in pusher configuration: propulsor (unit) transverse force coefficient, K_{FY} .

J	-30°	-20°	-15°	-10°	-5°	0°	5°	10°	15°	20°	30°
0.00	-0.2704	-0.1975	-0.1364	-0.0954	-0.0643	0.0055	0.0656	0.1098	0.1506	0.2092	0.2881
0.10	-0.2752	-0.1898	-0.1286	-0.0970	-0.0667	0.0069	0.0762	0.1160	0.1688	0.2210	0.3087
0.20	-0.2739	-0.1890	-0.1350	-0.0978	-0.0671	0.0051	0.0784	0.1214	0.1697	0.2286	0.3250
0.30	-0.2750	-0.1976	-0.1315	-0.1010	-0.0670	0.0031	0.0802	0.1212	0.1763	0.2423	0.3485
0.40	-0.2925	-0.2141	-0.1465	-0.1162	-0.0808	0.0033	0.0894	0.1334	0.1941	0.2658	0.3766
0.50	-0.3099	-0.2364	-0.1644	-0.1328	-0.0789	0.0029	0.0954	0.1526	0.2071	0.2967	0.4021
0.60	-0.3338	-0.2567	-0.1850	-0.1403	-0.0920	0.0030	0.1100	0.1741	0.2365	0.3221	0.4382
0.65	-0.3479	-0.2716	-0.2009	-0.1454	-0.0945	0.0073	0.1101	0.1783	0.2492	0.3409	0.4571
0.70	-0.3634	-0.2876	-0.2047	-0.1544	-0.1060	0.0049	0.1206	0.1845	0.2627	0.3510	0.4723
0.75	-0.3756	-0.3063	-0.2296	-0.1606	-0.1032	-0.0025	0.1327	0.2018	0.2790	0.3696	0.4830
0.80	-0.3958	-0.3282	-0.2436	-0.1711	-0.1092	0.0013	0.1397	0.2178	0.2980	0.3766	0.4969
0.85	-0.4180	-0.3535	-0.2618	-0.1833	-0.1128	0.0044	0.1428	0.2307	0.3161	0.4043	0.5109
0.90	-0.4492	-0.3751	-0.2870	-0.1962	-0.1226	0.0020	0.1586	0.2492	0.3395	0.4290	0.5277
0.95	-0.4747	-0.4005	-0.3094	-0.2168	-0.1340	0.0064	0.1645	0.2564	0.3638	0.4776	0.5527
1.00	-0.5086	-0.4336	-0.3260	-0.2314	-0.1440	0.0001	0.1766	0.2720	0.3934	0.4983	0.5935
1.10	-0.5687	-0.4957	-0.3760	-0.2666	-0.1721	0.0007	0.1929	0.3158	0.4355	0.5675	0.6488
1.20	-0.6293	-0.5587	-0.4144	-0.3023	-0.1998	0.0151	0.2069	0.3496	0.5081	0.7062	0.7451

Data Tables

Table A.19: Performance coefficient of average pod 01 at azimuthing conditions and in pusher configuration: propulsor (unit) vertical force coefficient, K_{FZ} .

J	-30°	-20°	-15°	-10°	-5°	0°	5°	10°	15°	20°	30°
0.00	-0.0708	-0.0326	-0.0005	0.0053	0.0148	0.0268	0.0143	0.0006	0.0256	0.0420	0.0580
0.10	-0.0756	-0.0443	-0.0246	-0.0206	-0.0008	0.0048	0.0001	-0.0043	0.0135	0.0488	0.0778
0.20	-0.0864	-0.0567	-0.0474	-0.0355	-0.0347	-0.0176	-0.0127	-0.0075	0.0200	0.0587	0.0969
0.30	-0.1012	-0.0777	-0.0656	-0.0577	-0.0525	-0.0373	-0.0277	-0.0172	0.0095	0.0630	0.1232
0.40	-0.1339	-0.1124	-0.0937	-0.0886	-0.0612	-0.0478	-0.0372	-0.0272	0.0085	0.0739	0.1339
0.50	-0.1690	-0.1441	-0.1241	-0.1215	-0.0859	-0.0651	-0.0506	-0.0249	0.0145	0.0775	0.1534
0.60	-0.2124	-0.1761	-0.1508	-0.1444	-0.0933	-0.0781	-0.0628	-0.0266	0.0170	0.0814	0.1615
0.65	-0.2196	-0.1959	-0.1652	-0.1626	-0.1101	-0.0894	-0.0757	-0.0227	0.0188	0.0805	0.1749
0.70	-0.2259	-0.2147	-0.1849	-0.1662	-0.1091	-0.1012	-0.0865	-0.0331	0.0159	0.0871	0.1864
0.75	-0.2407	-0.2333	-0.1913	-0.1718	-0.1271	-0.1049	-0.0940	-0.0308	0.0224	0.0930	0.1950
0.80	-0.2665	-0.2611	-0.2137	-0.1784	-0.1389	-0.1200	-0.0985	-0.0223	0.0254	0.0943	0.2036
0.85	-0.2769	-0.2796	-0.2368	-0.1850	-0.1496	-0.1316	-0.1033	-0.0198	0.0274	0.1023	0.2142
0.90	-0.2988	-0.3048	-0.2519	-0.1902	-0.1591	-0.1373	-0.1146	-0.0341	0.0290	0.1071	0.2148
0.95	-0.3164	-0.3405	-0.2769	-0.2019	-0.1770	-0.1470	-0.1038	-0.0398	0.0295	0.1019	0.2068
1.00	-0.3597	-0.3580	-0.2904	-0.2134	-0.1782	-0.1492	-0.1189	-0.0426	0.0298	0.0985	0.1936
1.10	-0.4403	-0.4149	-0.3164	-0.2301	-0.2018	-0.1781	-0.1178	-0.0461	0.0295	0.0933	0.1827
1.20	-0.5167	-0.4727	-0.3498	-0.2406	-0.2194	-0.2025	-0.1294	-0.0592	0.0233	0.0785	0.1371

Table A.20: Performance coefficient of average pod 01 at azimuthing conditions and in pusher configuration: propulsor (unit) axial moment coefficient, K_{MX} .

J	-30°	-20°	-15°	-10°	-5°	0°	5°	10°	15°	20°	30°
0.00	1.7113	1.1370	0.6530	0.5016	0.3304	-0.1162	-0.5408	-0.7471	-0.9503	-1.3560	-1.6356
0.10	1.6187	1.0944	0.7433	0.5227	0.3381	-0.1054	-0.5433	-0.7765	-0.9886	-1.4211	-1.8664
0.20	1.6048	1.0878	0.7707	0.5270	0.3643	-0.0857	-0.5458	-0.8005	-1.0114	-1.4607	-2.0811
0.30	1.6043	1.1316	0.7831	0.5502	0.3813	-0.0704	-0.5392	-0.7929	-1.0441	-1.5392	-2.2555
0.40	1.7032	1.2315	0.8428	0.6397	0.4135	-0.0747	-0.6178	-0.8521	-1.1408	-1.7095	-2.5070
0.50	1.8500	1.3545	0.9299	0.7364	0.4375	-0.0568	-0.6361	-0.9625	-1.2128	-1.9192	-2.6832
0.60	1.8957	1.4709	1.0370	0.7854	0.4869	-0.0660	-0.6929	-1.0716	-1.3404	-1.9876	-2.9077
0.65	1.9119	1.5586	1.0862	0.8479	0.5323	-0.0774	-0.7404	-1.1040	-1.4545	-2.0791	-2.9438
0.70	1.9678	1.6513	1.1821	0.8475	0.5745	-0.0576	-0.7575	-1.1243	-1.4992	-2.1173	-2.9877
0.75	2.0301	1.7530	1.2969	0.8803	0.6044	-0.0452	-0.8181	-1.2190	-1.5839	-2.2249	-3.0858
0.80	2.2003	1.8827	1.3811	0.9529	0.6194	-0.0359	-0.8390	-1.3092	-1.6870	-2.2517	-3.1897
0.85	2.3162	2.0172	1.4720	1.0005	0.6778	-0.0446	-0.8686	-1.3827	-1.7749	-2.4051	-3.1577
0.90	2.4241	2.1396	1.6107	1.1140	0.7333	-0.0271	-0.9390	-1.4789	-1.9465	-2.5490	-3.2635
0.95	2.5893	2.2942	1.7471	1.1762	0.8101	-0.0421	-0.9507	-1.5172	-2.0392	-2.8212	-3.3432
1.00	2.8016	2.4899	1.8443	1.2410	0.8549	-0.0507	-1.0330	-1.5977	-2.2078	-2.9312	-3.4406
1.10	3.1536	3.1143	2.1319	1.3138	1.0162	-0.0545	-1.1294	-1.8440	-2.4885	-3.2236	-3.6158
1.20	3.6708	3.5101	2.4135	1.5337	1.0956	-0.0708	-1.2003	-2.0253	-2.8913	-3.5262	-3.7539

Data Tables

Table A.21: Performance coefficient of average pod 01 at azimuthing conditions and in pusher configuration: propulsor (unit) transverse moment coefficient, K_{MY} .

J	-30°	-20°	-15°	-10°	-5°	0°	5°	10°	15°	20°	30°
0.00	3.0604	3.1990	3.2529	3.3000	3.3309	3.2475	3.1475	3.1142	3.0711	3.0173	3.1121
0.10	2.6067	2.8125	2.9161	2.9627	2.9771	3.0408	3.0118	3.0017	2.9904	2.8430	2.9225
0.20	2.2020	2.4633	2.5524	2.6271	2.6563	2.7278	2.7722	2.7787	2.7532	2.6215	2.5793
0.30	1.7200	2.0300	2.1870	2.2564	2.3235	2.3801	2.4751	2.4684	2.4719	2.3976	2.1771
0.40	1.2323	1.5997	1.7946	1.8580	1.9188	2.0576	2.1536	2.1819	2.1697	2.1511	1.9085
0.50	0.7324	1.2138	1.3877	1.4533	1.6402	1.7727	1.8240	1.8645	1.8590	1.8581	1.5489
0.60	0.2341	0.8513	1.0728	1.1664	1.3266	1.4690	1.5763	1.6139	1.5950	1.5242	0.9642
0.65	-0.0709	0.6743	0.8134	1.0014	1.1727	1.3262	1.4101	1.4606	1.4453	1.3356	0.7649
0.70	-0.3128	0.5062	0.7452	0.8774	0.9981	1.1964	1.2839	1.3186	1.3005	1.1865	0.5456
0.75	-0.5290	0.3297	0.6007	0.7167	0.8580	1.0153	1.1637	1.1527	1.1382	1.0124	0.3392
0.80	-0.7608	0.1594	0.4233	0.5455	0.6806	0.8644	0.9923	1.0069	1.0043	0.8296	0.0629
0.85	-0.9977	-0.0090	0.3093	0.3868	0.5343	0.7151	0.8102	0.8548	0.8310	0.6951	-0.2663
0.90	-1.2856	-0.1841	0.0851	0.2025	0.4030	0.5549	0.6930	0.6834	0.6542	0.4925	-0.4734
0.95	-1.5734	-0.3655	-0.0244	0.0108	0.2013	0.4152	0.4755	0.5584	0.5213	0.3613	-0.6769
1.00	-1.8022	-0.5918	-0.2013	-0.1556	0.0482	0.2726	0.3410	0.3405	0.3131	0.1537	-0.9328
1.10	-2.3960	-1.0590	-0.6454	-0.5499	-0.3796	-0.1393	-0.0196	-0.0252	0.0029	-0.3233	-1.5522
1.20	-2.9404	-1.4399	-1.0154	-0.9979	-0.7798	-0.5715	-0.3929	-0.4240	-0.2870	-0.6659	-2.3813

Table A.22: Performance coefficient of average pod 01 at azimuthing conditions and in pusher configuration: propulsor (unit) steering moment coefficient, K_{MZ} .

J	-30°	-20°	-15°	-10°	-5°	0°	5°	10°	15°	20°	30°
0.00	-0.0944	-0.0668	-0.0421	-0.0232	-0.0076	0.0109	0.0264	0.0551	0.0674	0.0854	0.1112
0.10	-0.0995	-0.0631	-0.0388	-0.0254	-0.0084	0.0124	0.0313	0.0567	0.0745	0.0937	0.1184
0.20	-0.0996	-0.0651	-0.0438	-0.0281	-0.0117	0.0134	0.0323	0.0646	0.0792	0.0981	0.1289
0.30	-0.1037	-0.0729	-0.0544	-0.0326	-0.0203	0.0100	0.0340	0.0650	0.0861	0.1089	0.1404
0.40	-0.1169	-0.0841	-0.0659	-0.0416	-0.0278	0.0092	0.0419	0.0668	0.0954	0.1243	0.1562
0.50	-0.1285	-0.1043	-0.0751	-0.0518	-0.0306	0.0075	0.0456	0.0790	0.1070	0.1443	0.1688
0.60	-0.1521	-0.1259	-0.0912	-0.0629	-0.0349	0.0087	0.0554	0.0931	0.1236	0.1596	0.1899
0.65	-0.1685	-0.1403	-0.0976	-0.0725	-0.0444	0.0135	0.0603	0.1006	0.1370	0.1768	0.2011
0.70	-0.1823	-0.1547	-0.1090	-0.0783	-0.0428	0.0105	0.0706	0.1059	0.1460	0.1802	0.2106
0.75	-0.2059	-0.1672	-0.1218	-0.0831	-0.0539	0.0113	0.0752	0.1154	0.1553	0.1958	0.2221
0.80	-0.2215	-0.1810	-0.1362	-0.0929	-0.0632	0.0075	0.0808	0.1268	0.1686	0.2025	0.2340
0.85	-0.2441	-0.1951	-0.1446	-0.1005	-0.0684	0.0089	0.0822	0.1372	0.1800	0.2179	0.2469
0.90	-0.2670	-0.2043	-0.1537	-0.1134	-0.0690	0.0072	0.0873	0.1485	0.1944	0.2305	0.2700
0.95	-0.2837	-0.2183	-0.1654	-0.1241	-0.0865	0.0102	0.0933	0.1562	0.2069	0.2520	0.2922
1.00	-0.3110	-0.2320	-0.1763	-0.1341	-0.0898	0.0112	0.0994	0.1705	0.2211	0.2725	0.3100
1.10	-0.3492	-0.2607	-0.2000	-0.1580	-0.1056	0.0133	0.1149	0.1991	0.2524	0.3036	0.3504
1.20	-0.4041	-0.2850	-0.2279	-0.1892	-0.1221	0.0189	0.1327	0.2306	0.2961	0.3420	0.3934

Data Tables

Table A.23: Performance coefficient of the pod with 200 mm diameter propeller at static azimuthing angles and in puller configuration: propeller thrust coefficient, K_{TProp} .

AziAng	J= 0	J= 0.2	J= 0.4	J= 0.6	J= 0.7	J= 0.8	J= 0.9	J= 1	J= 1.1	J= 1.2
-180°	0.4902	0.4906	0.4917	0.3467	0.4387	0.5433				
-175°	0.4903	0.5071	0.4906	0.3643	0.4452	0.5463	0.6764			
-170°	0.4902	0.4671	0.4811	0.3824	0.4353	0.5523	0.6496			
-160°	0.4907	0.4646	0.4652	0.4143	0.4782	0.5834	0.6702			
-150°	0.4908	0.4031	0.4803	0.4450	0.5033	0.5630				
-120°	0.4922	0.4168	0.5743	0.6275	0.6807	0.7697				
-90°	0.4933	0.4506	0.5112	0.5410	0.5735	0.6283				
-60°	0.4928	0.4537	0.4648	0.4609	0.4608	0.4592	0.4602	0.4640	0.4670	0.4709
-45°	0.4904	0.4546	0.4211	0.3848	0.3666	0.3471	0.3291	0.3103	0.2893	0.2690
-30°	0.4893	0.4360	0.3766	0.3134	0.2798	0.2450	0.2109	0.1730	0.1364	0.0928
-20°	0.4888	0.4300	0.3598	0.2848	0.2465	0.2057	0.1659	0.1225	0.0760	0.0230
-15°	0.4881	0.4263	0.3517	0.2725	0.2320	0.1878	0.1449	0.1013	0.0502	-0.0066
-10°	0.4884	0.4256	0.3503	0.2681	0.2242	0.1778	0.1332	0.0836	0.0312	-0.0265
-5°	0.4882	0.4243	0.3463	0.2616	0.2168	0.1677	0.1229	0.0717	0.0162	-0.0445
0°	0.4895	0.4211	0.3423	0.2570	0.2130	0.1668	0.1195	0.0702	0.0163	-0.0422
0°	0.4895	0.4211	0.3423	0.2570	0.2130	0.1668	0.1195	0.0702	0.0163	-0.0422
5°	0.4899	0.4204	0.3448	0.2592	0.2145	0.1659	0.1200	0.0709	0.0167	-0.0421
10°	0.4898	0.4223	0.3456	0.2620	0.2179	0.1709	0.1258	0.0763	0.0226	-0.0371
15°	0.4910	0.4263	0.3496	0.2693	0.2273	0.1825	0.1375	0.0904	0.0381	-0.0194
20°	0.4892	0.4282	0.3545	0.2778	0.2386	0.1960	0.1547	0.1095	0.0627	0.0092
30°	0.4878	0.4343	0.3755	0.3142	0.2809	0.2486	0.2132	0.1771	0.1392	0.1012
45°	0.4838	0.4524	0.4177	0.3835	0.3647	0.3531	0.3345	0.3173	0.2979	0.2780
60°	0.4866	0.4710	0.4685	0.4688	0.4710	0.4798	0.4824	0.4868	0.4958	0.5011
90°	0.4894	0.5113	0.5484	0.6076	0.6657	0.7321				
120°	0.4897	0.5868	0.5514	0.6339	0.7005	0.7561				
150°	0.4921	0.5513	0.4821	0.4469	0.4555	0.5218				
160°	0.4918	0.5130	0.4733	0.3978	0.4391	0.5340	0.6624			
170°	0.4905	0.5133	0.4779	0.3639	0.4375	0.5514				
175°	0.4906	0.5120	0.4488	0.3595	0.4517	0.5629				
180°	0.4902	0.4906	0.4917	0.3467	0.4387	0.5433				

Data Tables

Table A.24: Performance coefficient of the pod with 200 mm diameter propeller at static azimuthing angles and in puller configuration: propeller torque coefficient, $10K_Q$.

AziAng	J= 0	J= 0.2	J= 0.4	J= 0.6	J= 0.7	J= 0.8	J= 0.9	J= 1	J= 1.1	J= 1.2
-180°	0.6836	0.6835	0.6861	0.5035	0.6142	0.7432				
-175°	0.6833	0.7040	0.6806	0.5231	0.6246	0.7469	0.8993			
-170°	0.6836	0.6534	0.6693	0.5468	0.6137	0.7521	0.8649			
-160°	0.6837	0.6506	0.6492	0.5830	0.6619	0.7847	0.8821			
-150°	0.6829	0.5706	0.6754	0.6101	0.6890	0.7593				
-120°	0.6839	0.5878	0.7981	0.8694	0.9406	1.0666				
-90°	0.6864	0.6300	0.7083	0.7322	0.7675	0.8347				
-60°	0.6878	0.6393	0.6539	0.6474	0.6454	0.6429	0.6418	0.6434	0.6453	0.6472
-45°	0.6822	0.6393	0.6033	0.5626	0.5387	0.5098	0.4853	0.4594	0.4298	0.3992
-30°	0.6837	0.6200	0.5529	0.4786	0.4368	0.3912	0.3455	0.2941	0.2411	0.1774
-20°	0.6829	0.6125	0.5333	0.4446	0.3960	0.3423	0.2884	0.2279	0.1614	0.0834
-15°	0.6804	0.6076	0.5237	0.4321	0.3803	0.3195	0.2612	0.1999	0.1273	0.0430
-10°	0.6814	0.6076	0.5216	0.4233	0.3671	0.3055	0.2453	0.1760	0.1001	0.0140
-5°	0.6814	0.6066	0.5174	0.4160	0.3579	0.2915	0.2306	0.1591	0.0777	-0.0127
0°	0.6831	0.6035	0.5136	0.4111	0.3550	0.2907	0.2267	0.1571	0.0771	-0.0120
0°	0.6831	0.6035	0.5136	0.4111	0.3550	0.2907	0.2267	0.1571	0.0771	-0.0120
5°	0.6833	0.6034	0.5169	0.4148	0.3571	0.2889	0.2266	0.1573	0.0775	-0.0104
10°	0.6834	0.6039	0.5163	0.4157	0.3586	0.2959	0.2347	0.1658	0.0872	-0.0015
15°	0.6854	0.6089	0.5217	0.4254	0.3713	0.3124	0.2515	0.1854	0.1099	0.0239
20°	0.6830	0.6111	0.5277	0.4359	0.3859	0.3296	0.2731	0.2102	0.1426	0.0643
30°	0.6818	0.6226	0.5555	0.4826	0.4411	0.3966	0.3493	0.3001	0.2457	0.1904
45°	0.6736	0.6388	0.5994	0.5595	0.5394	0.5218	0.4979	0.4746	0.4496	0.4221
60°	0.6811	0.6623	0.6608	0.6606	0.6618	0.6715	0.6734	0.6776	0.6880	0.6941
90°	0.6812	0.7144	0.7640	0.8288	0.8999	0.9819				
120°	0.6805	0.8062	0.7617	0.8753	0.9691	1.0385				
150°	0.6835	0.7641	0.6652	0.6204	0.6268	0.7019				
160°	0.6854	0.7110	0.6583	0.5622	0.6110	0.7247	0.8709			
170°	0.6838	0.7119	0.6667	0.5234	0.6130	0.7505				
175°	0.6844	0.7135	0.6298	0.5169	0.6328	0.7656				
180°	0.6836	0.6835	0.6861	0.5035	0.6142	0.7432				

Data Tables

Table A.25: Performance coefficient of the pod with 200 mm diameter propeller at static azimuthing angles and in puller configuration: propulsor (unit) thrust coefficient, K_{TUnit} .

AziAng	J= 0	J= 0.2	J= 0.4	J= 0.6	J= 0.7	J= 0.8	J= 0.9	J= 1	J= 1.1	J= 1.2
-180°	-0.4580	-0.4652	-0.4649	-0.3760	-0.4458	-0.5399				
-175°	-0.4575	-0.4754	-0.4605	-0.3976	-0.4558	-0.5457	-0.6676			
-170°	-0.4529	-0.4456	-0.4495	-0.4113	-0.4476	-0.5516	-0.6409			
-160°	-0.4328	-0.4303	-0.4284	-0.4343	-0.4908	-0.5895	-0.6642			
-150°	-0.3988	-0.3740	-0.4386	-0.4743	-0.5375	-0.6171				
-120°	-0.2327	-0.2945	-0.4050	-0.4731	-0.5412	-0.6436				
-90°	0.0030	-0.1234	-0.2349	-0.4047	-0.4917	-0.6110				
-60°	0.2315	0.1083	-0.0038	-0.1624	-0.2475	-0.3376	-0.4245	-0.5129	-0.6108	-0.6765
-45°	0.3200	0.2175	0.1041	-0.0193	-0.0914	-0.1657	-0.2408	-0.3122	-0.3786	-0.4509
-30°	0.3971	0.3079	0.2111	0.1139	0.0605	0.0037	-0.0561	-0.1152	-0.1739	-0.2391
-20°	0.4257	0.3431	0.2532	0.1603	0.1127	0.0615	0.0118	-0.0422	-0.0999	-0.1648
-15°	0.4351	0.3582	0.2680	0.1791	0.1342	0.0862	0.0384	-0.0117	-0.0693	-0.1337
-10°	0.4493	0.3726	0.2879	0.2025	0.1558	0.1079	0.0610	0.0086	-0.0473	-0.1076
-5°	0.4557	0.3840	0.3006	0.2156	0.1704	0.1204	0.0742	0.0211	-0.0357	-0.0971
0°	0.4572	0.3861	0.3035	0.2178	0.1737	0.1263	0.0784	0.0275	-0.0273	-0.0872
0°	0.4572	0.3861	0.3035	0.2178	0.1737	0.1263	0.0784	0.0275	-0.0273	-0.0872
5°	0.4572	0.3846	0.3060	0.2194	0.1741	0.1241	0.0770	0.0282	-0.0284	-0.0878
10°	0.4532	0.3826	0.3036	0.2185	0.1725	0.1231	0.0750	0.0224	-0.0355	-0.0982
15°	0.4464	0.3770	0.2956	0.2107	0.1648	0.1154	0.0660	0.0139	-0.0449	-0.1083
20°	0.4337	0.3627	0.2809	0.1957	0.1495	0.0990	0.0506	-0.0024	-0.0579	-0.1214
30°	0.3948	0.3144	0.2314	0.1390	0.0876	0.0317	-0.0232	-0.0806	-0.1408	-0.2140
45°	0.3226	0.2283	0.1330	0.0257	-0.0374	-0.1044	-0.1733	-0.2391	-0.3100	-0.3864
60°	0.2256	0.1076	0.0028	-0.1239	-0.2022	-0.2802	-0.3635	-0.4418	-0.5354	-0.6343
90°	-0.0015	-0.1772	-0.2879	-0.4550	-0.5559	-0.6587				
120°	-0.2232	-0.3941	-0.4338	-0.5105	-0.5767	-0.6461				
150°	-0.3968	-0.4782	-0.4546	-0.4793	-0.5262	-0.5871				
160°	-0.4317	-0.4583	-0.4604	-0.4445	-0.4803	-0.5493	-0.6544			
170°	-0.4508	-0.4742	-0.4474	-0.4040	-0.4515	-0.5473				
175°	-0.4559	-0.4820	-0.4553	-0.3964	-0.4605	-0.5581				
180°	-0.4580	-0.4652	-0.4649	-0.3760	-0.4458	-0.5399				

Data Tables

Table A.26: Performance coefficient of the pod with 200 mm diameter propeller at static azimuthing angles and in puller configuration: propulsor (unit) transverse force coefficient, K_{FY} .

AziAng	J= 0	J= 0.2	J= 0.4	J= 0.6	J= 0.7	J= 0.8	J= 0.9	J= 1	J= 1.1	J= 1.2
-180°	-0.0070	-0.0046	0.0069	0.0178	-0.0035	-0.0192				
-175°	0.0226	0.0414	0.0452	0.0084	-0.0079	-0.0145	-0.0158			
-170°	0.0741	0.0673	0.0792	0.0386	-0.0001	-0.0020	-0.0027			
-160°	0.1544	0.1378	0.1555	0.0835	0.0407	0.0138	0.0176			
-150°	0.2244	0.1711	0.2420	0.1089	0.1096	0.0608				
-120°	0.3919	0.3143	0.4494	0.4677	0.4860	0.5148				
-90°	0.4542	0.4315	0.5228	0.5695	0.6112	0.6916				
-60°	0.3930	0.4117	0.4928	0.5991	0.6649	0.7405	0.8060	0.8758	0.9490	1.0051
-45°	0.3210	0.3562	0.4217	0.5108	0.5744	0.6374	0.7029	0.7567	0.7986	0.8450
-30°	0.2217	0.2508	0.2932	0.3525	0.3893	0.4305	0.4807	0.5099	0.5401	0.5769
-20°	0.1622	0.1813	0.2010	0.2372	0.2594	0.2868	0.3127	0.3376	0.3688	0.4006
-15°	0.1253	0.1374	0.1479	0.1685	0.1848	0.2020	0.2210	0.2460	0.2750	0.3130
-10°	0.0843	0.0943	0.0944	0.0982	0.1102	0.1212	0.1360	0.1553	0.1817	0.2075
-5°	0.0342	0.0352	0.0278	0.0218	0.0242	0.0275	0.0338	0.0486	0.0631	0.0821
0°	-0.0039	-0.0118	-0.0206	-0.0275	-0.0286	-0.0280	-0.0240	-0.0179	-0.0047	0.0075
0°	-0.0039	-0.0118	-0.0206	-0.0275	-0.0286	-0.0280	-0.0240	-0.0179	-0.0047	0.0075
5°	-0.0321	-0.0467	-0.0577	-0.0627	-0.0655	-0.0680	-0.0672	-0.0618	-0.0563	-0.0467
10°	-0.0689	-0.0930	-0.1140	-0.1262	-0.1324	-0.1399	-0.1439	-0.1474	-0.1484	-0.1441
15°	-0.1086	-0.1407	-0.1691	-0.1862	-0.1948	-0.2116	-0.2260	-0.2378	-0.2500	-0.2546
20°	-0.1479	-0.1877	-0.2239	-0.2519	-0.2660	-0.2836	-0.3025	-0.3194	-0.3373	-0.3522
30°	-0.2297	-0.2849	-0.3427	-0.3817	-0.4084	-0.4434	-0.4759	-0.5058	-0.5401	-0.5491
45°	-0.3157	-0.3986	-0.4561	-0.5116	-0.5419	-0.5288	-0.5525	-0.5736	-0.5964	-0.6250
60°	-0.3904	-0.4779	-0.5464	-0.6258	-0.6700	-0.6806	-0.7177	-0.7476	-0.7896	-0.8329
90°	-0.4528	-0.5198	-0.5612	-0.6249	-0.6782	-0.7369				
120°	-0.3937	-0.4301	-0.4054	-0.4421	-0.4647	-0.4869				
150°	-0.2269	-0.2288	-0.2256	-0.1355	-0.0617	-0.0425				
160°	-0.1560	-0.1577	-0.1496	-0.0582	-0.0141	-0.0168	-0.0392			
170°	-0.0822	-0.0864	-0.0779	-0.0162	-0.0069	-0.0228				
175°	-0.0424	-0.0471	-0.0394	-0.0077	-0.0073	-0.0235				
180°	-0.0070	-0.0046	0.0069	0.0178	-0.0035	-0.0192				

Data Tables

Table A.27: Performance coefficient of the pod with 200 mm diameter propeller at static azimuthing angles and in puller configuration: propulsor (unit) vertical force coefficient, K_{FZ} .

AziAng	J= 0	J= 0.2	J= 0.4	J= 0.6	J= 0.7	J= 0.8	J= 0.9	J= 1	J= 1.1	J= 1.2
-180°	0.0052	0.0192	0.0310	-0.0224	-0.0313	-0.0302				
-175°	0.0056	0.0144	0.0312	-0.0172	-0.0359	-0.0432	-0.0407			
-170°	0.0052	0.0323	0.0325	-0.0211	-0.0438	-0.0510	-0.0500			
-160°	0.0055	0.0400	-0.0114	-0.0326	-0.0570	-0.0503	-0.0475			
-150°	0.0069	0.0551	-0.0189	-0.0222	-0.0449	-0.0515				
-120°	0.0077	0.0846	-0.0020	0.0171	0.0361	0.0779				
-90°	0.0067	0.1148	0.1812	0.1936	0.2203	0.2621				
-60°	0.0030	0.1119	0.1972	0.2852	0.3252	0.3612	0.4062	0.4408	0.4729	0.4888
-45°	0.0005	0.0823	0.1576	0.2216	0.2515	0.2812	0.3065	0.3267	0.3314	0.3330
-30°	0.0028	0.0615	0.1127	0.1460	0.1599	0.1713	0.1811	0.1831	0.1846	0.1815
-20°	0.0030	0.0478	0.0876	0.1100	0.1168	0.1216	0.1224	0.1206	0.1151	0.1027
-15°	0.0042	0.0402	0.0720	0.0878	0.0919	0.0934	0.0916	0.0888	0.0790	0.0645
-10°	0.0021	0.0328	0.0551	0.0632	0.0661	0.0660	0.0641	0.0595	0.0529	0.0422
-5°	0.0013	0.0205	0.0317	0.0340	0.0350	0.0356	0.0362	0.0375	0.0362	0.0322
0°	0.0031	0.0115	0.0168	0.0183	0.0212	0.0259	0.0308	0.0360	0.0431	0.0499
0°	0.0031	0.0115	0.0168	0.0183	0.0212	0.0259	0.0308	0.0360	0.0431	0.0499
5°	0.0015	0.0064	0.0077	0.0102	0.0150	0.0224	0.0313	0.0448	0.0561	0.0705
10°	0.0023	-0.0012	-0.0036	0.0008	0.0087	0.0217	0.0357	0.0522	0.0731	0.0960
15°	0.0019	-0.0082	-0.0129	-0.0071	0.0024	0.0171	0.0351	0.0587	0.0869	0.1187
20°	0.0035	-0.0147	-0.0220	-0.0140	-0.0035	0.0138	0.0361	0.0642	0.0960	0.1361
30°	0.0029	-0.0207	-0.0351	-0.0233	-0.0091	0.0151	0.0469	0.0878	0.1345	0.1884
45°	0.0032	-0.0358	-0.0390	-0.0196	0.0008	0.0543	0.0978	0.1492	0.2065	0.2696
60°	0.0060	-0.0338	-0.0328	-0.0153	0.0112	0.0780	0.1239	0.1735	0.2338	0.3086
90°	0.0019	-0.0251	-0.0125	0.0321	0.0623	0.0812				
120°	0.0022	-0.0074	0.0052	0.0333	0.0863	0.1418				
150°	0.0054	-0.0088	0.0203	0.0203	0.0276	0.0631				
160°	0.0048	0.0095	0.0301	-0.0055	0.0066	0.0273	0.0350			
170°	0.0051	0.0132	0.0282	-0.0085	-0.0082	-0.0074				
175°	0.0076	0.0144	0.0188	-0.0131	-0.0202	-0.0218				
180°	0.0052	0.0192	0.0310	-0.0224	-0.0313	-0.0302				

Data Tables

Table A.28: Performance coefficient of the pod with 200 mm diameter propeller at static azimuthing angles and in puller configuration: propulsor (unit) axial moment coefficient, K_{MX} .

AziAng	J= 0	J= 0.2	J= 0.4	J= 0.6	J= 0.7	J= 0.8	J= 0.9	J= 1	J= 1.1	J= 1.2
-180°	-0.0589	-0.0567	-0.0697	-0.0674	-0.0562	-0.0471				
-175°	-0.0964	-0.1186	-0.1183	-0.0594	-0.0606	-0.0672	-0.0818			
-170°	-0.1611	-0.1425	-0.1611	-0.1107	-0.0779	-0.0937	-0.1076			
-160°	-0.2603	-0.2284	-0.2518	-0.1826	-0.1532	-0.1427	-0.1659			
-150°	-0.3445	-0.2512	-0.3731	-0.2310	-0.2490	-0.2171				
-120°	-0.5306	-0.4010	-0.6517	-0.6865	-0.7213	-0.7810				
-90°	-0.5748	-0.5212	-0.5788	-0.6246	-0.6693	-0.7562				
-60°	-0.4634	-0.4647	-0.5235	-0.6230	-0.6874	-0.7605	-0.8256	-0.8896	-0.9559	-1.0083
-45°	-0.3593	-0.3798	-0.4346	-0.5168	-0.5774	-0.6404	-0.7067	-0.7624	-0.8015	-0.8458
-30°	-0.2223	-0.2461	-0.2835	-0.3364	-0.3719	-0.4126	-0.4638	-0.4988	-0.5353	-0.5782
-20°	-0.1431	-0.1601	-0.1792	-0.2148	-0.2375	-0.2661	-0.2944	-0.3229	-0.3588	-0.3970
-15°	-0.0950	-0.1066	-0.1187	-0.1414	-0.1596	-0.1796	-0.2020	-0.2309	-0.2648	-0.3077
-10°	-0.0412	-0.0535	-0.0571	-0.0662	-0.0820	-0.0972	-0.1164	-0.1412	-0.1733	-0.2061
-5°	0.0237	0.0191	0.0197	0.0168	0.0088	-0.0009	-0.0138	-0.0361	-0.0590	-0.0874
0°	0.0725	0.0759	0.0769	0.0724	0.0673	0.0599	0.0483	0.0337	0.0114	-0.0118
0°	0.0725	0.0759	0.0769	0.0724	0.0673	0.0599	0.0483	0.0337	0.0114	-0.0118
5°	0.1083	0.1175	0.1193	0.1128	0.1085	0.1024	0.0939	0.0805	0.0654	0.0450
10°	0.1548	0.1737	0.1841	0.1825	0.1807	0.1796	0.1754	0.1696	0.1605	0.1449
15°	0.2042	0.2310	0.2491	0.2526	0.2535	0.2615	0.2661	0.2675	0.2671	0.2579
20°	0.2516	0.2883	0.3158	0.3318	0.3385	0.3476	0.3564	0.3620	0.3675	0.3680
30°	0.3486	0.4086	0.4656	0.5014	0.5233	0.5526	0.5767	0.5963	0.6196	0.6136
45°	0.4499	0.5521	0.6229	0.6864	0.7178	0.6918	0.7142	0.7344	0.7552	0.7800
60°	0.5326	0.6546	0.7484	0.8487	0.9028	0.9092	0.9599	1.0041	1.0621	1.1170
90°	0.5739	0.6948	0.7498	0.8312	0.9013	0.9818				
120°	0.4651	0.5402	0.5231	0.5184	0.5298	0.5437				
150°	0.2287	0.2499	0.2417	0.1288	0.0540	0.0271				
160°	0.1340	0.1445	0.1374	0.0381	-0.0120	-0.0156	0.0026			
170°	0.0378	0.0447	0.0434	-0.0167	-0.0344	-0.0272				
175°	-0.0133	-0.0050	-0.0062	-0.0338	-0.0441	-0.0396				
180°	-0.0589	-0.0567	-0.0697	-0.0674	-0.0562	-0.0471				

Data Tables

Table A.29: Performance coefficient of the pod with 200 mm diameter propeller at static azimuthing angles and in puller configuration: propulsor (unit) transverse moment coefficient, K_{MY} .

AziAng	J= 0	J= 0.2	J= 0.4	J= 0.6	J= 0.7	J= 0.8	J= 0.9	J= 1	J= 1.1	J= 1.2
-180°	-0.5794	-0.6035	-0.6072	-0.4668	-0.5541	-0.6701				
-175°	-0.5738	-0.6108	-0.5947	-0.4891	-0.5652	-0.6785	-0.8277			
-170°	-0.5593	-0.5612	-0.5707	-0.5098	-0.5560	-0.6895	-0.8000			
-160°	-0.5213	-0.5289	-0.5175	-0.5321	-0.6049	-0.7200	-0.8152			
-150°	-0.4672	-0.4337	-0.5418	-0.5642	-0.6446	-0.7470				
-120°	-0.2286	-0.3010	-0.4394	-0.4986	-0.5578	-0.6673				
-90°	0.0796	-0.0740	-0.1955	-0.3657	-0.4521	-0.5738				
-60°	0.3591	0.2005	0.0589	-0.1165	-0.2087	-0.3072	-0.3998	-0.4988	-0.6040	-0.6809
-45°	0.4612	0.3189	0.1756	0.0314	-0.0484	-0.1285	-0.2084	-0.2848	-0.3620	-0.4442
-30°	0.5416	0.4176	0.2900	0.1680	0.1052	0.0403	-0.0248	-0.0913	-0.1551	-0.2252
-20°	0.5669	0.4539	0.3351	0.2159	0.1580	0.0972	0.0391	-0.0224	-0.0863	-0.1576
-15°	0.5728	0.4686	0.3503	0.2352	0.1788	0.1195	0.0617	0.0028	-0.0632	-0.1363
-10°	0.5847	0.4819	0.3709	0.2586	0.1993	0.1390	0.0809	0.0172	-0.0495	-0.1209
-5°	0.5838	0.4908	0.3831	0.2728	0.2146	0.1504	0.0923	0.0261	-0.0438	-0.1198
0°	0.5803	0.4888	0.3851	0.2764	0.2205	0.1607	0.0996	0.0346	-0.0350	-0.1108
0°	0.5803	0.4888	0.3851	0.2764	0.2205	0.1607	0.0996	0.0346	-0.0350	-0.1108
5°	0.5750	0.4852	0.3873	0.2803	0.2236	0.1615	0.1014	0.0385	-0.0332	-0.1097
10°	0.5642	0.4784	0.3851	0.2825	0.2258	0.1646	0.1035	0.0365	-0.0378	-0.1200
15°	0.5488	0.4681	0.3764	0.2772	0.2219	0.1613	0.0992	0.0322	-0.0433	-0.1268
20°	0.5252	0.4476	0.3595	0.2628	0.2081	0.1473	0.0872	0.0201	-0.0509	-0.1335
30°	0.4623	0.3837	0.2995	0.1989	0.1413	0.0805	0.0190	-0.0467	-0.1178	-0.2091
45°	0.3569	0.2664	0.1700	0.0579	-0.0101	-0.0895	-0.1633	-0.2331	-0.3091	-0.3925
60°	0.2217	0.1031	-0.0103	-0.1423	-0.2250	-0.3091	-0.3929	-0.4711	-0.5644	-0.6645
90°	-0.0787	-0.2789	-0.4069	-0.6016	-0.7179	-0.8350				
120°	-0.3490	-0.5705	-0.6232	-0.6805	-0.7522	-0.8217				
150°	-0.5388	-0.6699	-0.6190	-0.5795	-0.6237	-0.6979				
160°	-0.5706	-0.6233	-0.6195	-0.5342	-0.5827	-0.6727	-0.8025			
170°	-0.5831	-0.6319	-0.6058	-0.4894	-0.5566	-0.6794				
175°	-0.5833	-0.6363	-0.5865	-0.4839	-0.5715	-0.6916				
180°	-0.5794	-0.6035	-0.6072	-0.4668	-0.5541	-0.6701				

Data Tables

Table A.30: Performance coefficient of the pod with 200 mm diameter propeller at static azimuthing angles and in puller configuration: propulsor (unit) vertical force coefficient, K_{MZ} .

AziAng	J= 0	J= 0.2	J= 0.4	J= 0.6	J= 0.7	J= 0.8	J= 0.9	J= 1	J= 1.1	J= 1.2
-180°	-0.0161	-0.0144	-0.0039	0.0041	0.0122	0.0170				
-175°	-0.0158	-0.0117	0.0014	-0.0009	0.0075	0.0093	0.0062			
-170°	-0.0159	-0.0046	0.0132	-0.0104	0.0026	0.0021	-0.0003			
-160°	-0.0156	0.0073	0.0252	-0.0193	-0.0096	-0.0125	-0.0203			
-150°	-0.0149	0.0247	0.0334	-0.0309	-0.0199	-0.0164				
-120°	-0.0120	0.0499	0.0831	0.0667	0.0504	0.0466				
-90°	-0.0114	0.0599	0.1380	0.1924	0.2121	0.2521				
-60°	-0.0128	0.0569	0.1108	0.1778	0.2187	0.2609	0.2986	0.3447	0.3906	0.4257
-45°	-0.0151	0.0373	0.0941	0.1556	0.1902	0.2254	0.2611	0.2998	0.3410	0.3837
-30°	-0.0155	0.0216	0.0638	0.1137	0.1406	0.1690	0.1980	0.2268	0.2591	0.2950
-20°	-0.0144	0.0116	0.0442	0.0820	0.1012	0.1234	0.1479	0.1732	0.2010	0.2320
-15°	-0.0149	0.0050	0.0314	0.0624	0.0783	0.0963	0.1161	0.1365	0.1598	0.1865
-10°	-0.0156	-0.0014	0.0192	0.0400	0.0537	0.0672	0.0811	0.0966	0.1155	0.1342
-5°	-0.0168	-0.0104	-0.0007	0.0102	0.0159	0.0226	0.0299	0.0408	0.0508	0.0619
0°	-0.0166	-0.0176	-0.0156	-0.0145	-0.0137	-0.0128	-0.0102	-0.0081	-0.0042	-0.0001
0°	-0.0166	-0.0176	-0.0156	-0.0145	-0.0137	-0.0128	-0.0102	-0.0081	-0.0042	-0.0001
5°	-0.0176	-0.0222	-0.0264	-0.0324	-0.0348	-0.0371	-0.0388	-0.0401	-0.0399	-0.0384
10°	-0.0172	-0.0296	-0.0427	-0.0581	-0.0655	-0.0726	-0.0786	-0.0849	-0.0913	-0.0964
15°	-0.0170	-0.0368	-0.0578	-0.0819	-0.0926	-0.1046	-0.1162	-0.1290	-0.1422	-0.1539
20°	-0.0171	-0.0436	-0.0731	-0.1042	-0.1189	-0.1360	-0.1521	-0.1698	-0.1876	-0.2076
30°	-0.0173	-0.0596	-0.1004	-0.1412	-0.1624	-0.1874	-0.2129	-0.2381	-0.2687	-0.2897
45°	-0.0217	-0.0759	-0.1243	-0.1725	-0.1960	-0.2064	-0.2344	-0.2623	-0.2909	-0.3216
60°	-0.0208	-0.0898	-0.1446	-0.2035	-0.2356	-0.2581	-0.2929	-0.3238	-0.3574	-0.3906
90°	-0.0228	-0.1040	-0.1399	-0.2131	-0.2430	-0.2703				
120°	-0.0201	-0.0875	-0.0987	-0.0812	-0.0873	-0.0970				
150°	-0.0177	-0.0555	-0.0045	0.0108	0.0150	0.0199				
160°	-0.0169	-0.0325	-0.0177	0.0053	0.0149	0.0216	0.0357			
170°	-0.0171	-0.0195	-0.0115	0.0010	0.0176	0.0248				
175°	-0.0160	-0.0146	-0.0039	0.0031	0.0163	0.0179				
180°	-0.0161	-0.0144	-0.0039	0.0041	0.0122	0.0170				

APPENDIX

B

**UNCERTAINTY
DATA**

Uncertainty Data

B.1 Bias and Precision Estimates for NSERC Pod Measurements

Table B.1: Bias and precision limits for a list of performance coefficients for the NSERC podded propulsor unit.

Variable	Bias Error	Bias Limit	Precision error	Precision Limit
Temp	Calibration	+/- 0.2000 °C	Fossilized into for Temp	Scale +/- 0.0005 °C Range +/- 0.2 °C
	Temp related Errors	+/- 0.0441 Kg/m ³	Overall Limit	+/- 0.0940 Kg/m ³
Density	Density Equation related errors	+/- 0.0830 Kg/m ³		
Propeller Diameter	CNC Machining Errors	+/- 0.0001 m	Overall Limit	+/- 0.0001 m
	Hand Polishing Errors	+/- 0.0001 m		
Azimuthing angle	CNC Machining Errors	+/- 0.0002 rad	Overall Limit	+/- 0.6920 Deg
	Hand Polishing Errors	+/- 0.0020 rad		
	Hole Allowance	+/- 0.0081 rad		
	Equipment Align	+/- 0.0087 rad		
Shaft Speed	Tachometer Reading Error	+/- 0.0080 rps		J=0.0 +/- 0.0117 rps
	A/D Error	+/- 0.0079 rps	Overall Limit	J=0.1 +/- 0.0162 rps
	Curve Fit Error	+/- 0.0320 rps		J=0.2 +/- 0.0159 rps
	Static Zero Error	+/- 0.0241 rps		J=0.3 +/- 0.0164 rps
	A/D Error	+/- 0.0079 rps		J=0.4 +/- 0.0179 rps
				J=0.5 +/- 0.0153 rps
				J=0.6 +/- 0.0161 rps
				J=0.7 +/- 0.0148 rps
				J=0.8 +/- 0.0171 rps
				J=0.9 +/- 0.0179 rps
				J=1.0 +/- 0.0180 rps
				J=1.1 +/- 0.0170 rps
				J=1.2 +/- 0.0162 rps

Uncertainty Data

Table B.1: Bias and precision limits for a list of performance coefficients for the NSERC podded propulsor unit continued.

Variable	Bias Error		Bias Limit		Precision error		Precision Limit		
Advance Speed					Overall Limit +/- 0.0154 m/s	J=0.0	+/-	0.0001	m/s
						J=0.1	+/-	0.0007	m/s
						J=0.2	+/-	0.0001	m/s
						J=0.3	+/-	0.0004	m/s
						J=0.4	+/-	0.0002	m/s
						J=0.5	+/-	0.0003	m/s
						J=0.6	+/-	0.0001	m/s
						J=0.7	+/-	0.0002	m/s
						J=0.8	+/-	0.0000	m/s
						J=0.9	+/-	0.0001	m/s
						J=1.0	+/-	0.0001	m/s
						J=1.1	+/-	0.0005	m/s
J=1.2	+/-	0.0008	m/s						
Propeller Thrust					Overall Limit +/- 2.2159 N	J=0.0	+/-	0.6637	N
						J=0.1	+/-	0.6103	N
						J=0.2	+/-	0.5816	N
						J=0.3	+/-	0.6257	N
						J=0.4	+/-	0.4550	N
						J=0.5	+/-	0.5926	N
						J=0.6	+/-	0.4777	N
						J=0.7	+/-	0.5115	N
						J=0.8	+/-	0.4524	N
						J=0.9	+/-	0.5037	N
						J=1.0	+/-	0.4450	N
						J=1.1	+/-	0.4253	N
J=1.2	+/-	0.3504	N						
Propeller Torque					Overall Limit +/- 0.0662 Nm	J=0.0	+/-	0.0302	Nm
						J=0.1	+/-	0.0388	Nm
						J=0.2	+/-	0.0309	Nm
						J=0.3	+/-	0.0266	Nm
						J=0.4	+/-	0.0563	Nm
						J=0.5	+/-	0.0335	Nm
						J=0.6	+/-	0.0449	Nm
						J=0.7	+/-	0.0491	Nm
						J=0.8	+/-	0.0514	Nm
						J=0.9	+/-	0.0411	Nm
						J=1.0	+/-	0.0452	Nm
						J=1.1	+/-	0.0436	Nm
J=1.2	+/-	0.0518	Nm						

Uncertainty Data

Table B.1: Bias and precision limits for a list of performance coefficients for the NSERC podded propulsor unit continued.

Variable				Bias Error				Bias Limit				Precision error				Precision Limit
Unit Thrust	Overall Limit															
					J=0.0	+/-	1.8539	N					J=0.0	+/-	1.9993	N
					J=0.1	+/-	1.8522	N					J=0.1	+/-	2.1195	N
					J=0.2	+/-	1.8504	N					J=0.2	+/-	2.3606	N
	Weights Error	+/-	0.0014	N	J=0.3	+/-	1.8489	N					J=0.3	+/-	2.6865	N
	Load Angle Error	+/-	0.0114	N	J=0.4	+/-	1.8457	N					J=0.4	+/-	2.4823	N
	Load Cell Align	+/-	0.0114	N	J=0.5	+/-	1.8429	N					J=0.5	+/-	2.4893	N
	Static Zero Error	+/-	0.0356	N	J=0.6	+/-	1.8402	N					J=0.6	+/-	1.5086	N
	A/D Card Error	+/-	0.2014	N	J=0.7	+/-	1.8397	N					J=0.7	+/-	1.1774	N
	Curve Fit Error	+/-	1.7122	N	J=0.8	+/-	1.8358	N					J=0.8	+/-	1.6636	N
	Equipment Align	+/-	0.0114	N	J=0.9	+/-	1.8347	N					J=0.9	+/-	1.6593	N
	Load Cell Align	+/-	0.0005	N	J=1.0	+/-	1.8315	N					J=1.0	+/-	1.4108	N
	Static Zero Error	+/-	0.0356	N	J=1.1	+/-	1.8287	N					J=1.1	+/-	1.7319	N
	A/D Card Error	+/-	0.6041	N	J=1.2	+/-	1.8275	N					J=1.2	+/-	1.4044	N
Side Force	Overall Limit															
					J=0.0	+/-	0.7109	N					J=0.0	+/-	1.6356	N
					J=0.1	+/-	0.7100	N					J=0.1	+/-	1.3660	N
					J=0.2	+/-	0.7090	N					J=0.2	+/-	1.8935	N
	Weights Error	+/-	0.0014	N	J=0.3	+/-	0.7082	N					J=0.3	+/-	1.6951	N
	Load Angle Error	+/-	0.0114	N	J=0.4	+/-	0.7065	N					J=0.4	+/-	2.3155	N
	Load Cell Align	+/-	0.0114	N	J=0.5	+/-	0.7051	N					J=0.5	+/-	1.7913	N
	Static Zero Error	+/-	0.0356	N	J=0.6	+/-	0.7037	N					J=0.6	+/-	1.5143	N
	A/D Card Error	+/-	0.2014	N	J=0.7	+/-	0.7034	N					J=0.7	+/-	1.6067	N
	Curve Fit Error	+/-	0.3113	N	J=0.8	+/-	0.7014	N					J=0.8	+/-	1.6380	N
	Equipment Align	+/-	0.0114	N	J=0.9	+/-	0.7008	N					J=0.9	+/-	1.6606	N
	Load Cell Align	+/-	0.0005	N	J=1.0	+/-	0.6993	N					J=1.0	+/-	1.4291	N
	Static Zero Error	+/-	0.0356	N	J=1.1	+/-	0.6979	N					J=1.1	+/-	2.1846	N
	A/D Card Error	+/-	0.6041	N	J=1.2	+/-	0.6973	N					J=1.2	+/-	1.8557	N

Uncertainty Data

Table B.1: Bias and precision limits for a list of performance coefficients for the NSERC podded propulsor unit continued.

Variable				Bias Error				Bias Limit				Precision error				Precision Limit
Vertical Force	Overall Limit															
					J=0.0	+/-	2.7745	N					J=0.0	+/-	3.0326	N
					J=0.1	+/-	2.7620	N					J=0.1	+/-	3.1700	N
					J=0.2	+/-	2.7489	N					J=0.2	+/-	3.0945	N
	Weights Error	+/-	0.0014	N	J=0.3	+/-	2.7376	N					J=0.3	+/-	2.9514	N
	Load Angle Error	+/-	0.0114	N	J=0.4	+/-	2.7140	N					J=0.4	+/-	3.1975	N
	Load Cell Align	+/-	0.0114	N	J=0.5	+/-	2.6934	N					J=0.5	+/-	3.0613	N
	Static Zero Error	+/-	0.0356	N	J=0.6	+/-	2.6738	N					J=0.6	+/-	3.0220	N
	A/D Card Error	+/-	0.2014	N	J=0.7	+/-	2.6695	N					J=0.7	+/-	3.0098	N
	Curve Fit Error	+/-	2.6999	N	J=0.8	+/-	2.6414	N					J=0.8	+/-	3.1242	N
	Equipment Align	+/-	0.0114	N	J=0.9	+/-	2.6327	N					J=0.9	+/-	3.0497	N
	Load Cell Align	+/-	0.0005	N	J=1.0	+/-	2.6095	N					J=1.0	+/-	3.0931	N
	Static Zero Error	+/-	0.0356	N	J=1.1	+/-	2.5889	N					J=1.1	+/-	3.1568	N
A/D Card Error	+/-	0.6041	N	J=1.2	+/-	2.5802	N					J=1.2	+/-	2.9550	N	
Axial Moment	Overall Limit															
					J=0.0	+/-	0.4751					J=0.0	+/-	1.9516	Nm	
					J=0.1	+/-	0.4716					J=0.1	+/-	1.6544	Nm	
					J=0.2	+/-	0.4680					J=0.2	+/-	1.6660	Nm	
	Calibration Error	+/-	0.0081	Nm	J=0.3	+/-	0.4648					J=0.3	+/-	1.8176	Nm	
	Static Zero Error	+/-	0.0217	Nm	J=0.4	+/-	0.4582					J=0.4	+/-	1.8676	Nm	
	A/D Card Error	+/-	0.0098	Nm	J=0.5	+/-	0.4525					J=0.5	+/-	2.1911	Nm	
	Curve Fit Error	+/-	-0.4743	Nm	J=0.6	+/-	0.4470	Nm					J=0.6	+/-	1.6241	Nm
	Equipment Align	+/-	0.0005	Nm	J=0.7	+/-	0.4458					J=0.7	+/-	1.5967	Nm	
	Static Zero Error	+/-	0.0087	Nm	J=0.8	+/-	0.4379					J=0.8	+/-	1.7481	Nm	
	A/D Card Error	+/-	0.0098	Nm	J=0.9	+/-	0.4355					J=0.9	+/-	1.5054	Nm	
					J=1.0	+/-	0.4290					J=1.0	+/-	1.8073	Nm	
					J=1.1	+/-	0.4232					J=1.1	+/-	1.9409	Nm	
				J=1.2	+/-	0.4208					J=1.2	+/-	1.8763	Nm		

Uncertainty Data

Table B.1: Bias and precision limits for a list of performance coefficients for the NSERC podded propulsor unit continued.

Variable	Bias Error		Bias Limit		Precision error		Precision Limit					
Vertical Moment	Overall Limit											
				<i>J</i> =0.0	+/-	2.7313		<i>J</i> =0.0	+/-	5.6957	Nm	
				<i>J</i> =0.1	+/-	2.7293		<i>J</i> =0.1	+/-	6.2242	Nm	
				<i>J</i> =0.2	+/-	2.7273		<i>J</i> =0.2	+/-	7.0426	Nm	
	Calibration Error	+/-	0.0202	Nm	<i>J</i> =0.3	+/-	2.7255		<i>J</i> =0.3	+/-	6.2363	Nm
	Static Zero Error	+/-	0.9536	Nm	<i>J</i> =0.4	+/-	2.7218		<i>J</i> =0.4	+/-	5.8257	Nm
	A/D Card Error	+/-	1.0742	Nm	<i>J</i> =0.5	+/-	2.7185		<i>J</i> =0.5	+/-	5.2986	Nm
	Curve Fit Error	+/-	-1.8257	Nm	<i>J</i> =0.6	+/-	2.7154	Nm	<i>J</i> =0.6	+/-	6.0425	Nm
	Equipment Align	+/-	0.0005	Nm	<i>J</i> =0.7	+/-	2.7148		<i>J</i> =0.7	+/-	7.0244	Nm
	Static Zero Error	+/-	0.9536	Nm	<i>J</i> =0.8	+/-	2.7103		<i>J</i> =0.8	+/-	5.9199	Nm
	A/D Card Error	+/-	1.0742	Nm	<i>J</i> =0.9	+/-	2.7090		<i>J</i> =0.9	+/-	5.6377	Nm
				<i>J</i> =1.0	+/-	2.7053		<i>J</i> =1.0	+/-	6.4502	Nm	
				<i>J</i> =1.1	+/-	2.7021		<i>J</i> =1.1	+/-	3.7839	Nm	
				<i>J</i> =1.2	+/-	2.7007		<i>J</i> =1.2	+/-	4.0284	Nm	
Vertical Moment	Overall Limit											
				<i>J</i> =0.0	+/-	1.0195		<i>J</i> =0.0	+/-	0.5684	Nm	
				<i>J</i> =0.1	+/-	1.0195		<i>J</i> =0.1	+/-	0.5989	Nm	
				<i>J</i> =0.2	+/-	1.0195		<i>J</i> =0.2	+/-	0.4748	Nm	
	Calibration Error	+/-	0.0081	Nm	<i>J</i> =0.3	+/-	1.0195		<i>J</i> =0.3	+/-	0.4422	Nm
	Static Zero Error	+/-	0.0037	Nm	<i>J</i> =0.4	+/-	1.0195		<i>J</i> =0.4	+/-	0.5594	Nm
	A/D Card Error	+/-	0.0042	Nm	<i>J</i> =0.5	+/-	1.0195		<i>J</i> =0.5	+/-	0.5172	Nm
	Curve Fit Error	+/-	-1.0195	Nm	<i>J</i> =0.6	+/-	1.0195	Nm	<i>J</i> =0.6	+/-	0.5931	Nm
	Equipment Align	+/-	0.0005	Nm	<i>J</i> =0.7	+/-	1.0195		<i>J</i> =0.7	+/-	0.6466	Nm
	Static Zero Error	+/-	0.0037	Nm	<i>J</i> =0.8	+/-	1.0195		<i>J</i> =0.8	+/-	0.6527	Nm
	A/D Card Error	+/-	0.0042	Nm	<i>J</i> =0.9	+/-	1.0195		<i>J</i> =0.9	+/-	0.5779	Nm
				<i>J</i> =1.0	+/-	1.0195		<i>J</i> =1.0	+/-	0.5629	Nm	
				<i>J</i> =1.1	+/-	1.0195		<i>J</i> =1.1	+/-	0.6511	Nm	
				<i>J</i> =1.2	+/-	1.0195		<i>J</i> =1.2	+/-	0.7027	Nm	

Uncertainty Data

B.2 Bias and Precision Estimates for IOT Pod Measurements

Table B.2: Bias and precision limits of a list of performance coefficients for the IOT podded propulsor unit.

Variable	Bias Error	Bias Limit	Precision error	Precision Limit
Temp	Calibration	+/- 0.2000 °C	Fossilized into for Temp	+/- 0.0707 °C
				Scale +/- 0.0005 °C Range +/- 0.05 °C
Density	Temp related Errors	+/- 0.0110 Kg/m ³	Overall Limit	+/- 0.0721 Kg/m ³
	Density Equation related errors	+/- 0.0712 Kg/m ³		
Propeller Diameter	CNC Machining Errors	+/- 0.0001 m	Overall Limit	+/- 0.0001 m
	Hnad Polishing Errors	+/- 0.0001 m		
Azimuthing angle	CNC Machining Errors	+/- 0.0002 rad	Overall Limit	+/- 0.6920 Deg
	Hnad Polishing Errors	+/- 0.0020 rad		
	Hole Allowance	+/- 0.0081 rad		
	Equipment Allign	+/- 0.0087 rad		
Shaft Speed	Techometer Reading Error	+/- 0.0083 rps		J=0.0 +/- 1.90E-05 rps
	A/D Error	+/- 0.0079 rps	Overall Limit	J=0.2 +/- 1.97E-05 rps
	Curve Fit Error	+/- 0.0320 rps		J=0.4 +/- 2.54E-05 rps
	Static Zero Error	+/- 0.0241 rps		J=0.6 +/- 2.24E-05 rps
	A/D Error	+/- 0.0079 rps		J=0.7 +/- 1.81E-05 rps
				J=0.8 +/- 2.55E-05 rps
				J=0.9 +/- 1.11E-05 rps
				J=1.0 +/- 7.92E-06 rps
				J=1.1 +/- 2.60E-05 rps
				J=1.2 +/- 1.90E-05 rps

Uncertainty Data

Table B.2: Bias and precision limits of a list of performance coefficients for the IOT podded propulsor unit continued.

Variable	Bias Error	Bias Limit	Precision error	Precision Limit
Advance Speed	Calibration Error	+/- 0.0050 m/s		J=0.0 +/- 0.0001 m/s
	A/D Error	+/- 0.0010 m/s		J=0.2 +/- 0.0002 m/s
	Wheel Dia Error	+/- 0.0001 m/s		J=0.4 +/- 0.0001 m/s
	Tide Error	+/- 0.0010 m/s		J=0.6 +/- 0.0001 m/s
	Curve Fit Error	+/- 0.0002 m/s		J=0.7 +/- 0.0002 m/s
	A/D Error	+/- 0.0010 m/s		J=0.8 +/- 0.0001 m/s
	Static Zero Error	+/- 0.0024 m/s		J=0.9 +/- 0.0001 m/s
			Overall Limit +/- 0.0058 m/s	J=1.0 +/- 0.0001 m/s
				J=1.1 +/- 0.0001 m/s
				J=1.2 +/- 0.0002 m/s
Propeller Thrust	Weights Error	+/- 0.0010 N		J=0.0 +/- 0.4019 N
	Load Angle Error	+/- 0.0069 N		J=0.2 +/- 0.4019 N
	Load Cell Align	+/- 0.0003 N		J=0.4 +/- 0.4019 N
	Static Zero Error	+/- 0.0354 N		J=0.6 +/- 0.4019 N
	A/D Card Error	+/- 0.6004 N		J=0.7 +/- 0.4019 N
	Curve Fit Error	+/- 4.1720 N	Overall Limit +/- 4.2578 N	J=0.8 +/- 0.4019 N
	Equipment Align	+/- 0.0069 N		J=0.9 +/- 0.4019 N
	Load Cell Align	+/- 0.0003 N		J=1.0 +/- 0.4019 N
	Static Zero Error	+/- 0.0354 N		J=1.1 +/- 0.4019 N
	A/D Card Error	+/- 0.6004 N		J=1.2 +/- 0.4019 N
Propeller Torque	Calibration Error	+/- 0.0104 Nm		J=0.0 +/- 0.0108 Nm
	Static Zero Error	+/- 0.0217 Nm		J=0.2 +/- 0.0108 Nm
	A/D Card Error	+/- 0.0171 Nm		J=0.4 +/- 0.0108 Nm
	Curve Fit Error	+/- 0.0596 Nm		J=0.6 +/- 0.0108 Nm
	Equipment Align	+/- 0.0005 Nm		J=0.7 +/- 0.0108 Nm
	Static Zero Error	+/- 0.0152 Nm		J=0.8 +/- 0.0108 Nm
	A/D Card Error	+/- 0.0171 Nm		J=0.9 +/- 0.0108 Nm
			Overall Limit +/- 0.0703 Nm	J=1.0 +/- 0.0108 Nm
				J=1.1 +/- 0.0108 Nm
				J=1.2 +/- 0.0108 Nm

Uncertainty Data

Table B.2: Bias and precision limits of a list of performance coefficients for the IOT podded propulsor unit continued.

Variable	Bias Error		Bias Limit		Precision error		Precision Limit	
				Overall Limit				
Vertical Force	Weights Error	+/- 0.0030	N	J=0.0	+/- 4.7301	J=0.0	+/- 0.2340	N
	Load Angle Error	+/- 0.0069	N	J=0.1	+/- 4.0175	J=0.2	+/- 0.2340	N
	Load Cell Align	+/- 0.0069	N	J=0.2	+/- 3.1933	J=0.4	+/- 0.2340	N
	Static Zero Error	+/- 0.0026	N	J=0.3	+/- 2.4086	J=0.6	+/- 0.2340	N
	A/D Card Error	+/- 0.0146	N	J=0.4	+/- 1.9033	J=0.7	+/- 0.2340	N
	Curve Fit Error	+/- 2.6999	N	J=0.5	+/- 1.3536	J=0.8	+/- 0.2340	N
	Equipment Align	+/- 0.0069	N	J=0.6	+/- 0.7220	J=0.9	+/- 0.2340	N
	Load Cell Align	+/- 0.0003	N	J=0.7	+/- 0.0521	J=1.0	+/- 0.2340	N
	Static Zero Error	+/- 0.0026	N	J=0.8	+/- 0.8571	J=1.1	+/- 0.2340	N
	A/D Card Error	+/- 0.0438	N	J=0.9	+/- 1.7699	J=1.2	+/- 0.2340	N
				Overall Limit				
Axial Moment				J=0.0	+/- 0.0230	J=0.0	+/- 0.0542	Nm
				J=0.1	+/- 0.0225	J=0.2	+/- 0.0542	Nm
				J=0.2	+/- 0.0220	J=0.4	+/- 0.0542	Nm
	Calibration Error	+/- 0.0036	Nm	J=0.3	+/- 0.0216	J=0.6	+/- 0.0542	Nm
	Static Zero Error	+/- 0.0097	Nm	J=0.4	+/- 0.0214	J=0.7	+/- 0.0542	Nm
	A/D Card Error	+/- 0.0110	Nm	J=0.5	+/- 0.0212	J=0.8	+/- 0.0542	Nm
	Curve Fit Error	+/- -0.0064	Nm	J=0.6	+/- 0.0211	J=0.9	+/- 0.0542	Nm
	Equipment Align	+/- 0.0014	Nm	J=0.7	+/- 0.0211	J=1.0	+/- 0.0542	Nm
	Static Zero Error	+/- 0.0097	Nm	J=0.8	+/- 0.0211	J=1.1	+/- 0.0542	Nm
	A/D Card Error	+/- 0.0110	Nm	J=0.9	+/- 0.0213	J=1.2	+/- 0.0542	Nm

Uncertainty Data

Table B.2: Bias and precision limits of a list of performance coefficients for the IOT podded propulsor unit continued.

Variable	Bias Error		Bias Limit		Precision error		Precision Limit		
Vertical Moment			Overall Limit						
			<i>J</i> =0.0	+/-	0.1821	<i>J</i> =0.0	+/-	0.0543 Nm	
			<i>J</i> =0.1	+/-	0.1552	<i>J</i> =0.2	+/-	0.0543 Nm	
			<i>J</i> =0.2	+/-	0.1241	<i>J</i> =0.4	+/-	0.0543 Nm	
	Calibration Error	+/-	0.0088 Nm	<i>J</i> =0.3	+/-	0.0947	<i>J</i> =0.6	+/-	0.0543 Nm
	Static Zero Error	+/-	0.0097 Nm	<i>J</i> =0.4	+/-	0.0761	<i>J</i> =0.7	+/-	0.0543 Nm
	A/D Card Error	+/-	0.0110 Nm	<i>J</i> =0.5	+/-	0.0564	<i>J</i> =0.8	+/-	0.0543 Nm
	Curve Fit Error	+/-	0.1278 Nm	<i>J</i> =0.6	+/-	0.0356 Nm	<i>J</i> =0.9	+/-	0.0543 Nm
	Equipment Align	+/-	0.0014 Nm	<i>J</i> =0.7	+/-	0.0226	<i>J</i> =1.0	+/-	0.0543 Nm
	Static Zero Error	+/-	0.0097 Nm	<i>J</i> =0.8	+/-	0.0397	<i>J</i> =1.1	+/-	0.0543 Nm
A/D Card Error	+/-	0.0110 Nm	<i>J</i> =0.9	+/-	0.0713	<i>J</i> =1.2	+/-	0.0543 Nm	
Vertical Moment			Overall Limit						
			<i>J</i> =0.0	+/-	0.0215	<i>J</i> =0.0	+/-	0.0572 Nm	
			<i>J</i> =0.1	+/-	0.0214	<i>J</i> =0.2	+/-	0.0572 Nm	
			<i>J</i> =0.2	+/-	0.0213	<i>J</i> =0.4	+/-	0.0572 Nm	
	Calibration Error	+/-	0.0036 Nm	<i>J</i> =0.3	+/-	0.0212	<i>J</i> =0.6	+/-	0.0572 Nm
	Static Zero Error	+/-	0.0097 Nm	<i>J</i> =0.4	+/-	0.0211	<i>J</i> =0.7	+/-	0.0572 Nm
	A/D Card Error	+/-	0.0110 Nm	<i>J</i> =0.5	+/-	0.0211	<i>J</i> =0.8	+/-	0.0572 Nm
	Curve Fit Error	+/-	-1.0195 Nm	<i>J</i> =0.6	+/-	0.0211 Nm	<i>J</i> =0.9	+/-	0.0572 Nm
	Equipment Align	+/-	0.0014 Nm	<i>J</i> =0.7	+/-	0.0211	<i>J</i> =1.0	+/-	0.0572 Nm
	Static Zero Error	+/-	0.0097 Nm	<i>J</i> =0.8	+/-	0.0211	<i>J</i> =1.1	+/-	0.0572 Nm
A/D Card Error	+/-	0.0110 Nm	<i>J</i> =0.9	+/-	0.0211	<i>J</i> =1.2	+/-	0.0572 Nm	

APPENDIX

C

**DOE
TECHNIQUE**

C-1 Design of Experiment Technique

This section presents a brief introduction to the statistical design of experiments or DOE method, which was used to study the hydrodynamic performance of podded propulsors at varied geometry.

Engineers in general carry out a fair amount of physical experimentation in the laboratory and on the computer using a variety of numerical models. Experiments are carried out to 1) evaluate and compare basic design configurations, 2) evaluate material alternatives, 3) select design parameters so that the design will work well under a wide variety of field conditions (robust design), and 4) determine the key design parameters that impact performance. As with most engineering problems, time and budget are often limited. Hence, it is necessary to gain as much information as possible from an experimental program and do so as efficiently as possible.

In engineering, one often-used approach is the best-guess (with engineering judgment) approach. Another strategy of experimentation that is prevalent in practice is the one-factor-at-a-time or OFAT approach. The OFAT method was once considered the standard, systematic, and accepted method of scientific experimentation. Both of these methods have been shown to be inefficient and in fact can be disastrous (Montgomery, 2005). These methods of experimentation became outdated in the early 1920s when Ronald A. Fisher discovered much more efficient methods of experimentation based on factorial designs. This class of experimental designs includes the general factorial, two-level factorial, fractional factorial, and response surface designs among others. These

DOE Technique

statistically based experimental design methods are now simply called design of experiment methods or DOE methods. A recent application of DOE methods in ocean engineering can be found in Hawkins and Lye (2006), among others.

Basically, DOE is a methodology for systematically applying statistics to experimentation. DOE lets experimenters develop a mathematical model that predicts how input variables *interact* to create output variables or responses in a process or system. DOE can be used for a wide range of experiments for various purposes including nearly all fields of engineering and science and even in marketing studies. The use of statistics is important in DOE but not necessary. In general, by using DOE, one can:

- ✓ learn about the process being investigated;
- ✓ screen important factors;
- ✓ determine whether factors interact;
- ✓ build a mathematical model for prediction; and
- ✓ optimize the response(s), if required.

DOE methods are also very useful as a strategy for building mechanistic models, and they have the additional advantage that no complicated calculations are needed to analyze the data produced from the designed experiment. It has now been recognized that the factorial-based DOE is the correct and the most efficient method of conducting multi-factored experiments; they allow a large number of factors to be investigated in few experimental runs. The efficiency stems from using settings of the independent factors that are completely uncorrelated with each other. That is, the experimental designs are orthogonal. The consequence of the orthogonal design is that the main effect of each

experiment factor, and also the interactions between factors, can be estimated independent of the other effects. As stated earlier, many industries have recognized this fact and design of experiment methodologies is a key component of the Six-Sigma quality program used by many major corporations. Yet it is surprising that after about 90 years since the invention of modern experimental design it is still not widely taught in schools of engineering or science in our universities (Box 2006). The wide variety of experimental designs and their statistical details can be found in many excellent texts including Montgomery (2005), Myers and Montgomery (2002), Ryan (2007), Antony (2006), Box *et al.* (2006), among others.

A two-level full factorial design is usually denoted as a 2^k factorial design, which is basically an experimental technique involving k factors, each of which has two-levels (low and high). Such a multi-factor two-level experiment means that the number of treatment combinations to get complete results is equal to 2^k . For complex systems, the factorial design often ends up with a more complex analysis, which shows more influence of two or more geometric parameters together on the result than just one of the parameters individually. In most of the cases it is the interactions of two factors (called two-factor interaction), which are more important than three-, or more factor interaction. For example, consider a process that is dependent on three factors A, B and C. In the analysis of a two-factorial design, it is more likely that the interaction effects AB or BC or AC will be more significant than the interaction effects ABC in the output of the process.

In the current study of pod geometry, a two-level full factorial design of experiment technique is adopted to study five parameters. There were 32 different combinations of factors (2^k , here k is the number of independent parameters which equals 5). That means 32 pods had to be manufactured. If the tests were to run at a variety of advance speeds for each of the pods, the number of runs would have been huge with additional time requirement for subsequent analyses. One way of limiting the growth of this test series is to use experience to eliminate certain combinations of factors from the analysis. The Fractional Factorial Design (FFD) of the 2^k analysis is denoted 2^{k-p} where the k is the number of factors and p is the reduction. Therefore, if a 2^5 factorial design requires 32 runs then a 2^{5-1} factorial design requires 2^4 or 16 runs (Montgomery 2005, Chapter 11 and Lye 2002). This is called the “half fractional factorial design”. Using this technique, it can be logically assumed that the effects of certain combinations of factors are negligible. Usually a relationship is set up between factors e.g. $E=ABCD$ for a five factor FFD design. This relationship is called an “alias” and the components cannot be differentiated. This helps to reduce the number of combinations. This relationship means a change in the output of the process due to E could actually be caused by $ABCD$, but since $ABCD$ is a four-factor interaction and is being ignored, the response is considered to be that of E . This still maintains the integrity of the factorial design since it is very unlikely that the interaction effect $ABCD$ is significant. All factors and combinations tested have an alias in a fractional design, however the design process ensures that the factors are not correlated (Montgomery 2005, Chapter 11). Table C-1 shows the factorial effects aliases for the fractional factorial design matrix for the pod series. As shown in the table, the single factors are aliased with three factor interactions, which are usually insignificant. The two

DOE Technique

factor interactions AD and AE are aliased with the two factor interactions BE and BD, respectively. If these two interaction factors significantly change the output, it is impossible to differentiate (AD or BE, AE or BD) which two factor interactions are significant. In fractional factorial design, it is impossible to differentiate the alias terms.

Table C-1. Factorial effect aliases in the 16 pods series design (used in fractional factorial design).

[Estimated Terms]	Aliased Terms
[A]	A + BDE
[B]	B + ADE
[C]	C
[D]	D + ABE
[E]	E + ABD
[AB]	AB + DE
[AC]	AC
[AD]	AD + BE
[AE]	AE + BD
[BC]	BC
[CD]	CD
[CE]	CE
[ABC]	ABC + CDE
[ACD]	ACD + BCE
[ACE]	ACE + BCD

The DOE technique such as FFD is particularly useful in experiments where a number of factors may affect the outcome. The joint (interaction) effects on the result can be studied. In order to design experiments economically, the factors that have the most significant effect on the outcome can be determined using a FFD design and then, once those factors are identified, a more limited but relevant one-factor series can be designed to test the effects of the significant factors.



